

University of Groningen

Development and preclinical evaluation of radioligands for the PET studies of cerebral adenosine A1 and A2A receptors

Shivashankar, Shivashankar

IMPORTANT NOTE: You are advised to consult the publisher's version (publisher's PDF) if you wish to cite from it. Please check the document version below.

Document Version

Publisher's PDF, also known as Version of record

Publication date:

2014

[Link to publication in University of Groningen/UMCG research database](#)

Citation for published version (APA):

Shivashankar, S. (2014). *Development and preclinical evaluation of radioligands for the PET studies of cerebral adenosine A1 and A2A receptors*. [S.n.].

Copyright

Other than for strictly personal use, it is not permitted to download or to forward/distribute the text or part of it without the consent of the author(s) and/or copyright holder(s), unless the work is under an open content license (like Creative Commons).

The publication may also be distributed here under the terms of Article 25fa of the Dutch Copyright Act, indicated by the "Taverne" license. More information can be found on the University of Groningen website: <https://www.rug.nl/library/open-access/self-archiving-pure/taverne-amendment>.

Take-down policy

If you believe that this document breaches copyright please contact us providing details, and we will remove access to the work immediately and investigate your claim.

Downloaded from the University of Groningen/UMCG research database (Pure): <http://www.rug.nl/research/portal>. For technical reasons the number of authors shown on this cover page is limited to 10 maximum.

**Development and Preclinical
Evaluation of Radioligands for the
PET Studies of Cerebral Adenosine
A1 and A2A Receptors**

Shivashankar

Printing of this thesis was financially supported by:

Graduate School for Drug Exploration University of Groningen



University Medical Center Groningen



IBA RadioPharma Solutions



IDB Holland BV



Von Gahlen Netherland B.V.



And

Foundation Trace 2000

Cover design: Manoj Kumar Yadava

Printed by: CPI-Koninklijke Wöhrmann, Zutphen

©2014, Shivashankar. All rights reserved.

No part of this publication may be reproduced, stored in a retrieval system, or transmitted in any form or by any means, mechanically, by photocopying, recording, or otherwise, without permission of the author.

ISBN: 978-90-367-7226-6 (hardcopy)

978-90-367-7225-9 (electronic version)



university of
 groningen

Development and preclinical evaluation of radioligands for the PET studies of cerebral adenosine A₁ and A_{2A} receptors

PhD thesis

to obtain the degree of PhD at the
 University of Groningen
 on the authority of the
 Rector Magnificus Prof. E. Sterken
 and in accordance with
 the decision by the College of Deans.

This thesis will be defended in public on

Monday 15 September 2014 at 11.00 hours

by

Shivashankar

born on 20 June 1979
 in Sirwar, India

Supervisors

Prof. P.H. Elsinga

Prof. R.A.J.O. Dierckx

Co-supervisor

Dr. A. van Waarde

Assessment committee

Prof. F. De Vos

Prof. J. Booij

Prof. K.L. Leenders

Dedicated to my family and friends

Paranymphs: Chantal Kwizera

Tushar Tomar

TABLE OF CONTENTS

Chapter 1	General Introduction	9
Chapter 2	Adenosine A _{2A} Receptor Antagonists as Positron Emission Tomography (PET) Tracers <i>Curr. Med. Chem.</i> 2014 ;21(3):312-328.	33
Chapter 3	Development of [¹⁸ F]-Labeled Pyrazolo[4,3- <i>e</i>]-1,2,4-triazolo[1,5- <i>c</i>]pyrimidine (SCH442416) Analogs for the Imaging of Cerebral Adenosine A _{2A} Receptors with Positron Emission Tomography <i>J. Med. Chem.</i> 2014 (Epub ahead of publication)	85
Chapter 4	Synthesis and Preclinical Evaluation of 2-(2-Furanyl)-7-[2-[4-[4-(2-[¹¹ C]methoxyethoxy)phenyl]-1-piperazinyl]ethyl]7 <i>H</i> -pyrazolo[4,3- <i>e</i>][1,2,4]triazolo[1,5- <i>c</i>]pyrimidine-5-amine ([¹¹ C]Preladenant) as a PET Tracer for the Imaging of Cerebral Adenosine A _{2A} Receptors (Under revision by <i>J. Med. Chem.</i>)	135
Chapter 5	Small-Animal PET to Study Adenosine A ₁ and A _{2A} Receptor Agonist-Induced Changes of Blood Brain Barrier Permeability	161
Chapter 6	Small-Animal PET Study of Adenosine A ₁ Receptors in Rat Brain: Blocking Receptors and Raising Extracellular Adenosine <i>J Nucl Med</i> 2011 ; 52:1293–1300	179
Chapter 7	English Summary	205
Chapter 8	Future Perspectives	213
Chapter 9	Nederlandse Samenvatting	225
	Acknowledgements	233



General Introduction

1

Adenosine, an endogenous signaling substance, is a purine ribonucleoside composed of adenine (purine base) and ribose (sugar molecule).¹ It functions as cytoprotectant and neuromodulator in response to stress to an organ or tissue under both physiological and pathological conditions.² In the brain, adenosine plays an important role in the regulation of both neuronal and glial cell functions. Furthermore, it counteracts glutamate excitotoxicity and cytokine-induced apoptosis.³ Its actions are mediated through activation of four subtypes of G-protein coupled adenosine receptors (ARs) namely A_1 , A_{2A} , A_{2B} and A_3 .²

Adenosine A_1 receptors (A_1 Rs) and adenosine A_3 receptors (A_3 Rs) are G-protein coupled binding sites for adenosine which inhibit adenylyl cyclase, whereas adenosine A_{2A} receptors (A_{2A} Rs) and adenosine A_{2B} receptors (A_{2B} Rs) stimulate adenylyl cyclase via G_s proteins and hence the formation of the second messenger, cyclic adenosine monophosphate (cAMP).⁴ The subtypes differ in size (A_1 , A_{2A} , A_{2B} and A_3 consist of 326, 409, 328 and 318 amino acids, respectively) and they exhibit unique tissue distributions.⁵

In the last 30 years, the most extensively studied AR subtypes are the biochemically and pharmacologically well-characterized high affinity A_1 Rs and A_{2A} Rs. Adenosine activates these receptors in nanomolar concentrations.² A_1 Rs are widely distributed in the human brain, the highest densities being found in the hippocampus, cerebral cortex, thalamic nuclei and dorsal horn of spinal cord; whereas A_{2A} Rs are highly expressed in the dopamine-rich regions of the brain and highest levels of expression occur in the striatum (caudate-putamen, nucleus accumbens and olfactory tubercle), globus pallidus and substantia nigra.⁶⁻⁹ Lower levels of A_{2A} Rs occur in the hippocampus, cerebral cortex, amygdala, cerebellum, brainstem and hypothalamus.¹⁰⁻¹³

A_1 R is strongly neuromodulatory and may initiate the neuroprotective effects of ischemic preconditioning. A_1 R activation results in protection of neurons and myocardial cells during periods

of hypoxic and cerebral (and cardiac) ischemia. A₁R agonists are neuroprotective in an animal model of Parkinson's disease (PD, MPTP mice) where they attenuate neuroinflammation and dopamine neurodegeneration.¹⁴ Activation of A₁Rs (i.e., by A₁R agonists) increases sleep, inhibits seizures, reduces anxiety and promotes neuroprotection. On the other hand, A₁R antagonists are anxiolytics, beneficial in the treatment of cognitive disorders, cardiac arrhythmia, asthma or other respiratory disorders and are therapeutic drugs for kidney protection.¹⁵ A_{2A}R agonists are implicated in tissue repair which involves a series of coordinated and overlapping phases like inflammation, wound healing, angiogenesis and tissue reorganization.¹⁶⁻¹⁸ The vasodilating effect of A_{2A}R agonists (adenosine, regadenoson) has been fully validated (see Figure 1). In clinical practice, adenosine is used for the treatment of paroxysmal supraventricular tachycardia and as a pharmacological stressor in (radionuclide) myocardial perfusion imaging. In addition, regadenoson (Brand name: Rapiscan), is currently also marketed for use as a pharmacologic stress agent in (radionuclide) myocardial perfusion imaging.¹⁹ Regadenoson has a relatively low affinity ($K_i \approx 1.3 \mu\text{M}$) for the A_{2A}Rs.^{3,20}

A_{2A}R antagonists can be used for the treatment of motor dysfunctions and impede the neurodegenerative process in disorders such as PD. A_{2A}R antagonists may also be beneficial in the treatment of ischemic stroke and as anti-fibrotic agents.²¹ Caffeine and theophylline (xanthine analogs, Figure 1) are the prototypical antagonists of ARs.³

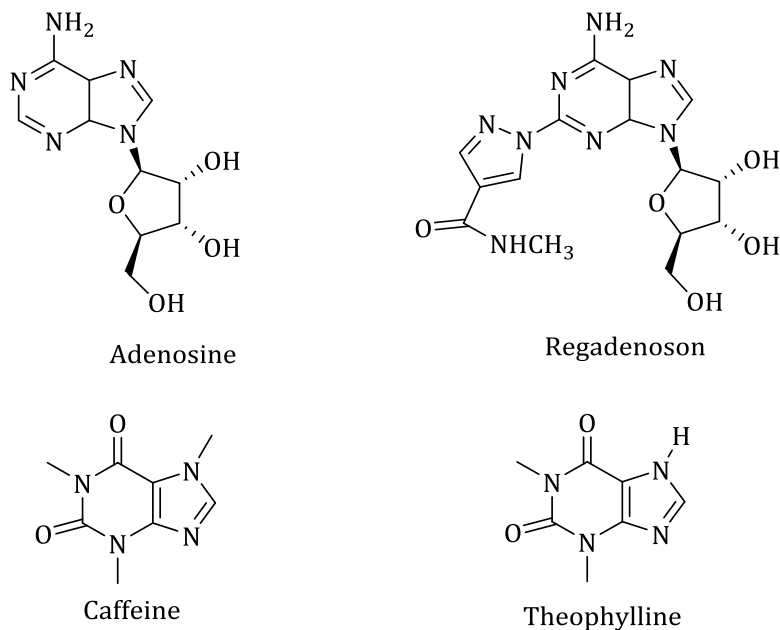


Figure 1. Structures of some AR agonists and antagonists

Sources and Fate of Extracellular Adenosine

Figure 2 shows the pathways for formation and removal of extra- and intracellular adenosine. It displays key enzymes involved in adenosine metabolism, besides receptors and transduction mechanisms involved in adenosinergic signaling. Extracellular adenosine may arise from either intracellular adenosine, which can pass the cell membrane via equilibrative nucleotide transporters (ENT) or from the breakdown of cytosolic or released adenine nucleotides, such as adenosine triphosphate (ATP), adenosine diphosphate (ADP), adenosine monophosphate (AMP) and to a lesser extent cyclic AMP.¹⁵

Several enzymes like ectonucleoside triphosphate diphosphohydrolase family (E-NTPDases), phosphodiesterase (PDE), ecto-5'-nucleotidase (CD73) and alkaline phosphatases (ALPs) are involved in the formation of extracellular adenosine. Purine nucleotides (ATP and ADP) are dephosphorylated to 5'-AMP

by E-NTPDases. Further dephosphorylation of 5'-AMP by CD73 and ALPs results in extracellular adenosine.²² The critical and rate-limiting step is the conversion of AMP to adenosine, carried out by CD73 (Figure 2). Overexpression of CD73 has been proposed to protect organs and tissues under stress by the formation of adenosine.³

Intracellular adenosine formation occurs mainly by AMP dephosphorylation. This reaction is catalyzed by cytosolic-5'-nucleotidases. Another source of intracellular adenosine is the hydrolysis of S-adenosylhomocysteine (SAH) by the enzyme SAH hydrolase (Figure 2).²²

In response to stress, hypoxia, cellular death, inflammatory stimuli and increased alkaline phosphatase activity, adenine nucleotides are rapidly dephosphorylated by the combined actions of adenylate cyclase (AC), PDE, ALPs, ecto- and cytosolic nucleotidases resulting in formation of intra- and extracellular adenosine (Figure 2).^{23, 24}

Metabolism of extracellular adenosine to inosine is mediated by adenosine deaminase (ADA). Inosine is converted to hypoxanthine by the action of purine nucleoside phosphorylase (PNP). Hypoxanthine can then enter the xanthine oxidase (XO) pathway to form xanthine and uric acid.²¹ (Figure 2). In the brain, the SAH pathway of adenosine inactivation is negligible. Under normal physiological conditions, the major route of adenosine metabolism is phosphorylation of adenosine to AMP by adenosine kinase (AK).¹⁵

Extracellular adenosine can interact with adenosine receptors (AR) that are coupled to G-proteins resulting in multiple physiological effects via the second messenger, cAMP (Figure 2).²⁴

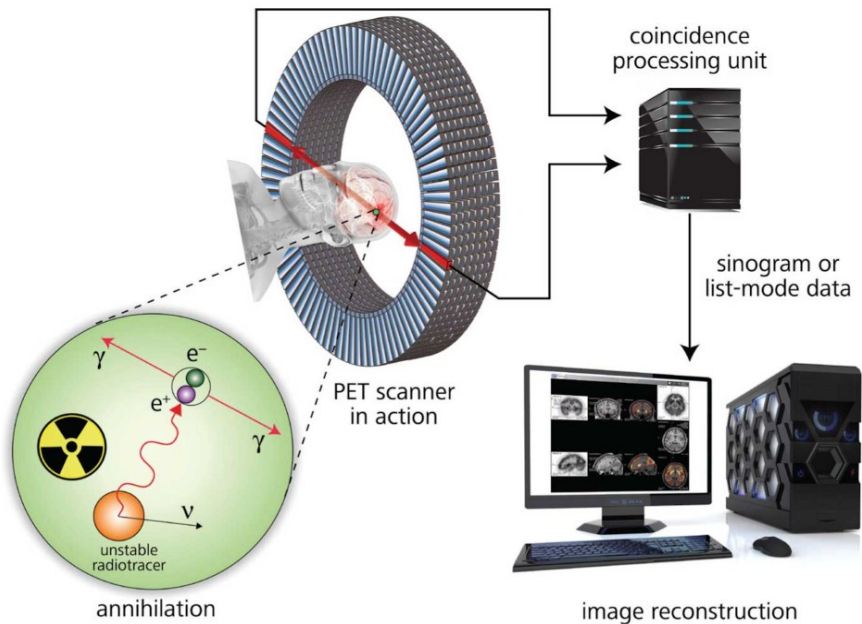
Positron Emission Tomography

Positron Emission Tomography (PET) is a noninvasive nuclear medicine imaging technique capable of measuring metabolic and functional processes *in vivo* in a quantitative manner.²⁵ A cyclotron produces positron-emitting radionuclides that are incorporated into a biologically interesting molecule with desired physiological properties. Upon administration of very small amounts (in pico- or nanomole) of the resulting radiotracer to the subject (patient, volunteer or experimental animal) it distributes throughout the body.²⁶ The radioactive nuclides of the radiotracer undergo decay and emit positrons. A positron (β^+) is the anti-particle of an electron i.e., the positron has the same mass as the electron but opposite charge, and both particles interact. This interaction results in annihilation of both particles under the emission of two photons. During this process, the mass of both particles is converted to energy (E) according to the formula $E = mc^2$, where c is the speed of light. The emitted photons have energy of 511 keV and move in opposite directions from the annihilation site (i.e., 180° opposite).²⁷ The emitted photons are detected simultaneously by the photomultiplier-scintillator combinations positioned on opposite sides of the subject (coincidence detection).²⁸ The data from the detectors are analyzed, integrated and reconstructed by means of a computer to create a 3D image of the radioactivity distribution in the body (Figure 3).²⁶

Radionuclides used in PET scanning are typically isotopes with short half-lives such as carbon-11 (~20 min), nitrogen-13 (~10 min), oxygen-15 (~2 min), fluorine-18 (~110 min) or rubidium-82 (~1.27 min).²⁹ Nowadays, other isotopes such as gallium-68 (68 min), zirconium-89 (78.41 h), scandium-44 (3.97 h), terbium-152 (17.5 h) and copper-64 (12.7 h) are applied as well.²⁷ Most radionuclides have been produced on-site using a cyclotron.²⁹ PET displays several unique properties such as high sensitivity (by approximately two-to-three orders of magnitude over SPECT), low radiation dose, the possibility to correct images for attenuation and scatter of the

radiation. In addition, biologically active compounds for example drugs can be radiolabelled which can be used as tracers to monitor the pharmacokinetics of the nonradioactive compounds.

In addition to a high degree of target selectivity, appropriate combination of lipophilicity, molecular weight and affinity is important in the development of PET tracers.³⁰ For a compound to cross the blood-brain-barrier (BBB), relatively small molecular weight (400 to 500 Da) and moderate lipophilicity (approximate range of logP is 2 to 3.5) are optimal.³⁰⁻³² So, in practice only [¹¹C] and [¹⁸F] radioisotopes are used in brain studies. High lipophilicity causes unacceptable binding to plasma proteins thereby decreasing the free drug concentration available to pass the BBB or binding to lipid bilayers resulting in high levels of nonspecific binding in brain.³⁰ Low lipophilicity decreases the penetration of PET agents across the BBB. In addition, the tracer's affinity must balance the opposing goals of tight binding and fast washout from the brain. With tight binding tracers (for example [¹⁸F] haloperidol- as dopamine D₂/D₃ antagonist tracer) washout rate cannot be determined within the time frame of a PET study and hence critical kinetic data (off rate) are unavailable to calculate receptor densities in the brain.³⁰ Furthermore, easy and quick (within 3 half-lives) incorporation of radionuclides into appropriate precursor molecules is necessary because of the rapid decay of the radioisotopes.²⁷ Finally, formation of lipophilic radioactive metabolites should be negligible for an ideal brain PET tracer because the presence of radiometabolites in the target tissue would impede quantification of PET data with kinetic models.^{30, 33} Careful selection of the most appropriate position of the radionuclide in a molecule is very important to avoid formation of possible interfering radiometabolites.³³ PET can be used to assess changes of regional AR densities in living subjects and the dose-dependent occupancy of the receptor population by therapeutic drugs.¹⁵



Adapted from Espinosa *et al.*

Figure 3. Principle of Positron Emission of Tomography (PET)³⁴

Radioligands for A₁R Imaging

Several PET ligands for A₁R imaging have been developed and evaluated in both experimental animals and humans. All these compounds (xanthine and nonxanthine A₁R antagonists and agonists) bind with nanomolar affinity to A₁R (Table 1).¹⁵ The widely used tracers, [¹¹C]MPDX and [¹⁸F]CPFPX are applied for quantitative measurement of cerebral A₁R in humans. Because of the relatively long physical half-life, [¹⁸F]CPFPX can be distributed to remote imaging centers distant from the cyclotrons which synthesized the radionuclide. However, the radiation burden of [¹⁸F]CPFPX (300 MBq) is greater than that of [¹¹C]MPDX (300 MBq): 5.3 mSv vs 1.05 mSv, respectively.^[35, Ishiwata's unpublished data] Thus, repeated PET studies in the same subject within a short time frame are only possible with [¹¹C]MPDX. Another advantage of [¹¹C]MPDX over [¹⁸F]CPFPX is its *in vivo* stability (89 % vs 25 % at 10 min).

The nonxanthine structures were proposed to address xanthine tracer problems like nonspecific binding and poor water solubility. However, the first reported nonxanthine tracer, [^{11}C]FR194921, did not produce better results in experimental animals than [^{11}C]MPDX or [^{18}F]CPFPX.³⁶

Table 1. Development of Radioligands for PET Imaging of A₁R

Ligand	A ₁ R affinity	Studies performed	Findings
<i>Xanthines</i>			
[^{11}C]KF15372 (8-Dicyclopropylmethyl-3-propylxanthine)	3.0 nM (K _i)	Biodistribution study in mice	About 57% specific binding (to A ₁ R not A ₂ R) Tracer distribution in brain reflects regional A ₁ R density
		<i>Ex vivo</i> autoradiography (ARG) in mice/rats	Decreased binding in superior colliculus after unilateral eye removal
		PET study in anesthetized monkeys	Tracer distribution in brain reflects regional A ₁ R density About 50% reduction in uptake after treatment with "cold" KF15372
[^{11}C]EPDX (2-Ethyl-8-dicyclopropylmethyl-3-propylxanthine)	1.7 nM (K _i)	Biodistribution study in mice	About 50% specific binding (to A ₁ R not A ₂ R)
[^{11}C]MPDX (8-Dicyclopropylmethyl-1-methyl-3-propylxanthine)	4.2 nM (K _i)	Biodistribution study in mice	Initial brain uptake higher than EPDX and KF15372 but faster washout Dosimetry data indicate acceptable radiation dose in human studies

	Metabolite analysis in mice	Metabolites appear in plasma but brain activity is mainly parent at 30 min
	<i>Ex vivo</i> ARG (rats)	Decreased binding in superior colliculus after unilateral eye removal About 55% specific binding (to A ₁ R not A ₂ R) In animal model of dystonia, tracer binding in hippocampus is decreased
	Radiochemical synthesis improved	
	PET study in anesthetized cats	Distribution volume of tracer in brain reflects regional A ₁ R density Bound tracer can be displaced by an excess of cold A ₁ R antagonist In a cat model of stroke, losses of A ₁ R can be detected in ischemic areas The magnitude of these losses indicates severity of the insult and predicts subsequent complications (including mortality)
	PET study in anesthetized monkey	Good brain uptake, distribution reflects regional A ₁ R density
	Human PET study (healthy volunteers)	Tracer distribution in brain reflects regional A ₁ R density Pattern differs from that of a flow tracer or a glucose analog Distribution volume

			(Logan plot) or binding potential (compartment model analysis) can be used for quantification purposes
[¹⁸ F]CPFPX (8-Cyclopentyl-3-[3-fluoropropyl]-1-propyl-xanthine)	0.6–1.4 nM (K _d mouse, pig, human) 4.4 nM (K _d Rat)	Biodistribution study in mice	Distribution in brain reflects regional A ₁ R density
		Metabolite analysis in mice	Metabolites appear in plasma but brain activity is mainly parent at 60 min
		<i>Ex vivo</i> ARG (rats)	About 70% of brain uptake is specific (to A ₁ R) and reversible
		Animal PET study in rats	Tracer distribution in brain reflects regional A ₁ R density (>90% specific) Brain well-visualized, bound tracer can be displaced by A ₁ R antagonist
		Human PET study (healthy volunteers)	Tracer distribution in brain reflects regional A ₁ R density Tracer kinetics in human brain is appropriate for quantitative imaging Distribution volume (Logan plot) or binding potential (compartment model analysis) can be used for quantification purposes Simplified study protocols are possible (venous rather than arterial blood sampling, bolus-infusion or single bolus administration of

			<p>the tracer) Short scanning protocols (60 min) are possible in humans Bound tracer can be displaced by cold CFPX in all brain regions Noninvasive procedure (reference tissue model) is suitable for quantification of A₁R in human brain</p>
		Metabolite study (liver microsomes)	Tracer is metabolized by cytochrome CYP1A2 Its metabolism can be inhibited by therapeutic drugs like fluvoxamine
[¹³¹ I]CPIPX ^a (8-Cyclopentyl-3-[(<i>E</i>)-3-iodoprop-2-en-1-yl]-1-propylxanthine)	0.8–7.9 nM (K _d rat, pig cortex)	<i>Ex vivo</i> ARG (rats)	Tracer binding is largely nonspecific Thus, this ligand is not suitable for imaging purposes Iodine radiolabeling results also in loss of selectivity for the A ₁ R
Nonxanthines			
[¹¹ C]FR194921 (2-(1-methyl-4-piperidinyl)-6-(2-phenylpyrazolo[1,5-a]pyridin-3-yl)-3(2H)-pyridazinone)	2.9 nM (K _i)	<i>Ex vivo</i> ARG (rats)	Tracer distribution in brain reflects regional A ₁ R density. About 50% specific binding (to A ₁ R not A ₂ R).

		PET study in conscious monkeys	Brain well-visualized, tracer accumulates in cortex, striatum and thalamus.
Agonists			
5-O-(methyl[⁷⁵ Se]seleno)-N6-cyclopentyladenosine	0.9 nM (K _i) (pig cortex)	Radiochemical synthesis described	No <i>in vivo</i> data reported
5'-N-(2-[¹⁸ F]fluoroethyl)-carboxamidoadenosine	Nanomolar range	Radiochemical synthesis described	No <i>in vivo</i> data reported May bind not only to A ₁ R but also to other AR subtypes

^aThis compound was prepared for Single Photon Emission Computed Tomography (SPECT) rather than PET imaging. This table is adapted from Paul *et al.*, *Curr Med Chem.* **2011**;18(31):4820–4235.

Radioligands for A_{2A}R Imaging

The adenosine A_{2A} receptor (A_{2A}R) is highly concentrated in the striatum, and a potential therapeutic target for neurological disorders like PD, Alzheimer's and Huntington's disease. High affinity and selective radiolabeled A_{2A}R antagonists can be important research and diagnostic tools for PD. Chapter 2 presents an overview of current PET tracers for A_{2A}R and their biological evaluation in rodents, nonhuman primates and humans. Several A_{2A}R antagonists (both xanthine and nonxanthine derivatives) have been evaluated in many studies in experimental animals and in some studies in humans. Besides KF17837 and several related xanthine analogs, nonxanthine SCH442416 and its fluorinated derivative have been radiolabelled with positron emitters. [¹¹C]TMSX (a xanthine tracer) and [¹¹C]SCH442416 have been employed for studies in humans.²

All xanthine tracers suffer from several disadvantages like photoisomerization, extrastriatal binding, low selectivity over other AR subtypes. To overcome the problems associated with xanthine-like structures, nonxanthine compounds were proposed. Initial results indicated that [^{11}C]SCH442416 and its [^{18}F]fluoroethyl SCH442416 are promising tracers for mapping cerebral A_{2A} Rs. However, more studies in rodents and humans are needed to determine their usefulness.² Please refer to chapter 2 for a detailed discussion of A_{2A} R imaging.

Summary

Adenosine is released to either reduce the energy demand or increase the energy supply to an organ or tissue which is damaged or stressed and thereby elicits cytoprotective effects.³ ARs are ubiquitous in the body and play a central role in tissue protection and regeneration.³⁷ The development of high affinity and subtype selective synthetic agonists and antagonists of ARs has been the subject of medicinal chemistry for more than 35 years. The nonradioactive adenosine agonist, regadenoson, has been approved for myocardial perfusion imaging and positron-emitting adenosine antagonists are in development for diagnostic use.³ PET using the A_1 R tracers [^{11}C]MPDX and [^{18}F]CPFPX could be applied to evaluate changes of adenosine receptor (A_1 R) availability in humans with neurological and psychiatric disorders.²⁵ Further characterization of [^{11}C]SCH442416 and its derivative [^{18}F]fluoroethylSCH442416 in animal models of human diseases and in humans is required. However, continued efforts for seeking high-affinity and selective ligands in medicinal chemistry may yield better radioligands for A_{2A} R visualization and quantification in the near future.²

Aim of the Thesis and Survey of Its Contents

Because of the clinical importance of A_1 Rs and A_{2A} Rs, the development of high affinity and subtype selective radioligands for mapping AR density is urgently needed. This thesis has dual objectives. The first objective is to develop A_{2A} R tracers with a good

kinetic profile and larger target-to-nontarget ratios than existing radiotracers such as [^{11}C]SCH442416 (striatum/cerebellum ratio 4.6 at the time of its maximum uptake), higher absolute brain uptake values (SUV) in experimental animals. Second objective of the thesis is further *in vivo* characterization of positron-emitting radioligands for AR under several physiological conditions or during pharmacological challenges.

Chapter 1 is a general introduction with literature review concerning PET imaging of $A_1\text{R}$ and $A_{2A}\text{Rs}$ and their role in health and disease.

Chapter 2 reviews current radioligands for PET imaging of $A_{2A}\text{R}$. In addition, potential drug candidates for radiolabeling and molecular imaging of $A_{2A}\text{R}$ expression are discussed.

In **Chapter 3**, development of high affinity and selective SCH442416 analogs as *in vivo* probes for $A_{2A}\text{R}$ using PET is described. Our aim was to optimize the length of the fluoroalkyl chain which could affect both $A_{2A}\text{R}$ affinity and selectivity. We have prepared the ^{18}F -labeled fluoropropyl derivative of SCH442416 ([^{18}F]FPSCH) and compared its kinetics and biodistribution in healthy rats with those of [^{18}F]FESCH and [^{11}C]SCH442416.

Our continued search for more pronounced $A_{2A}\text{R}$ -selectivity resulted in the development of a novel high affinity $A_{2A}\text{R}$ ligand, [^{11}C]SCH420814 (^{11}C Preladenant). Radiosynthesis, *in vitro* ARG experiments, *in vitro* stability test in saline, PBS, rat and human plasma, metabolite analysis and a validation study in healthy rats were carried out. The results of these experiments are discussed in **chapter 4**.

Chapter 5 aimed to answer the question whether transient opening of the blood-brain barrier (BBB) after treatment of animals with adenosine receptor agonists can be detected with hydrophilic radiotracers and PET. Such tracers do not pass the intact barrier, but may pass after BBB opening. An $A_1\text{R}$ agonist (N^6 -

Cyclopentyladenosine, CPA) and an A_{2A}R agonist (regadenoson or CVT-3146, brand name Rapiscan) were applied to study their effect on BBB permeability. The hydrophilic tracer [¹¹C]CH₃-AMD3465 (CXCR4 ligand) was tried as PET tracer. Moreover, the outcome of the PET assay was compared with results of a widely used and generally accepted assay for BBB permeability, the Evans Blue assay.

The aim of the study described in **chapter 6** was to determine whether competition between adenosine and [¹¹C]MPDX for binding to A₁R could be assessed with PET. We have investigated the effect of extracellular adenosine (levels raised with ethanol and the adenosine kinase inhibitor ABT-702) on the cerebral binding of [¹¹C]MPDX.

Chapter 7 summarizes the findings reported in this thesis and **chapter 8** is a description of future perspectives.

References

1. Estrela, A. B.; Abraham, W. R. Adenosine in the inflamed gut: A Janus faced compound. *Curr. Med. Chem.* **2011**, *18*, 2791–2815.
2. Khanapur, S.; van Waarde, A.; Ishiwata, K.; Leenders, K. L.; Dierckx, R. A.; Elsinga, P. H. Adenosine A_{2A} receptor antagonists as Positron Emission Tomography (PET) tracers. *Curr. Med. Chem.* **2014**, *21*, 312–328.
3. Jacobson, K. A. Introduction to adenosine receptors as therapeutic targets. *Handb. Exp. Pharmacol.* **2009**, *193*, 1–24.
4. Ralevic, V.; Burnstock, G. Receptors for purines and pyrimidines. *Pharmacol. Rev.* **1998**, *50*, 413–492.
5. Ben, D.; Lambertucci, C.; Vittori, S.; Volpini, R.; Cristalli, G. GPCRs as therapeutic targets: A view on adenosine receptors structure and functions, and molecular modeling support. *J. Iran. Chem. Soc.* **2005**, *2*, 176–188.
6. Fastbom, J.; Pazos, A.; Palacios, J. M. The distribution of adenosine A₁ receptors and 5'-nucleotidase in the brain of some commonly used experimental animals. *Neuroscience* **1987**, *22*, 813–826.

7. Martinez-Mir, M. I.; Probst, A.; Palacios, J. M. Adenosine A₂ receptors: Selective localization in the human basal ganglia and alterations with disease. *Neuroscience* **1991**, *42*, 697–706.
8. Ji, X. D.; Stiles, G. L.; van Galen, P. J.; Jacobson, K. A. Characterization of human striatal A₂-adenosine receptors using radioligand binding and photoaffinity labeling. *J. Recept. Res.* **1992**, *12*, 149–169.
9. Parkinson, F. E.; Fredholm, B. B. Autoradiographic evidence for G-protein coupled A₂-receptors in rat neostriatum using [3H]-CGS 21680 as a ligand. *Naunyn-Schmiedeberg's Arch. Pharmacol.* **1990**, *342*, 85–89.
10. Lindstrom, K.; Ongini, E.; Fredholm, B. B. The selective adenosine A_{2A} receptor antagonist SCH 58261 discriminates between two different binding sites for [3H]-CGS 21680 in the rat brain. *Naunyn-Schmiedeberg's Arch. Pharmacol.* **1996**, *354*, 539–541.
11. Ongini, E.; Fredholm, B. B. Pharmacology of adenosine A_{2A} receptors. *Trends Pharmacol. Sci.* **1996**, *17*, 364–372.
12. Fredholm, B. B.; Ijzerman, A. P.; Jacobson, K. A.; Linden, J.; Muller, C. E. International Union of Basic and Clinical Pharmacology. LXXXI. Nomenclature and classification of adenosine receptors: An update. *Pharmacol. Rev.* **2011**, *63*, 1–34.
13. Cunha, R. A.; Johansson, B.; Constantino, M. D.; Sebastiao, A. M.; Fredholm, B. B. Evidence for high-affinity binding sites for the adenosine A_{2A} receptor agonist [3H] CGS 21680 in the rat hippocampus and cerebral cortex that are different from striatal A_{2A} receptors. *Naunyn-Schmiedeberg's Arch. Pharmacol.* **1996**, *353*, 261–271.
14. Liu, H.; Zhang, W.; Luo, X.; Ye, Y.; Zhu, X. Paeoniflorin attenuates neuroinflammation and dopaminergic neurodegeneration in the MPTP model of Parkinson's disease by activation of adenosine A₁ receptor. *Br. J. Pharmacol.* **2006**, *148*, 314–325.

15. Paul, S.; Elsinga, P. H.; Ishiwata, K.; Dierckx, R. A.; van Waarde, A. Adenosine A(1) receptors in the central nervous system: Their functions in health and disease, and possible elucidation by PET imaging. *Curr. Med.Chem.* **2011**, *18*, 4820–4835.
16. Macedo, L.; Pinhal-Enfield, G.; Alshits, V.; Elson, G.; Cronstein, B. N.; Leibovich, S. J. Wound healing is impaired in MyD88-deficient mice: a role for MyD88 in the regulation of wound healing by adenosine A2A receptors. *Am. J. Pathol.* **2007**, *171*, 1774–1788.
17. Feoktistov, I.; Biaggioni, I.; Cronstein, B. N. Adenosine receptors in wound healing, fibrosis and angiogenesis. *Handb. Exp. Pharmacol.* **2009**, *193*, 383–397.
18. Blackburn, M. R.; Vance, C. O.; Morschl, E.; Wilson, C. N. Adenosine receptors and inflammation. *Handb. Exp. Pharmacol.* **2009**, *193*, 215–269.
19. de Lera Ruiz, M.; Lim, Y. H.; Zheng, J. Adenosine A2A receptor as a drug discovery target. *J. Med. Chem.* **2014**, *57*, 3623–3650.
20. Gao, Z.; Li, Z.; Baker, S. P.; Lasley, R. D.; Meyer, S.; Elzein, E.; Palle, V.; Zablocki, J. A.; Blackburn, B.; Belardinelli, L. Novel short-acting A2A adenosine receptor agonists for coronary vasodilation: inverse relationship between affinity and duration of action of A2A agonists. *J. Pharmacol. Exp. Ther.* **2001**, *298*, 209–218.
21. Moro, S.; Gao, Z. G.; Jacobson, K. A.; Spalluto, G. Progress in the pursuit of therapeutic adenosine receptor antagonists. *Med. Res. Rev.* **2006**, *26*, 131–159.
22. Fredholm, B. Adenosine and metabolism—a brief historical note. In *Adenosine—a key link between metabolism and brain activity*; Masino, S., Boison, D., Eds.; Springer New York: 2013; pp 3–19.
23. Ham, J.; Evans, B. A. An emerging role for adenosine and its receptors in bone homeostasis. *Front. Endocrinol. (Lausanne)* **2012**, *3*, 113.

24. Wilson, C. N.; Nadeem, A.; Spina, D.; Brown, R.; Page, C. P.; Mustafa, S. J. Adenosine receptors and asthma. *Handb. Exp. Pharmacol.* **2009**, (193):329–362.
25. Ishiwata, K.; Kimura, Y.; De Vries, Erik F. J.; Elsinga, P. H. PET Tracers for Mapping Adenosine Receptors as Probes for Diagnosis of CNS Disorders. *Cent. Nerv. Syst. Agents Med. Chem.* **2007**, 7, 57–77.
26. Ronald Boellaard PET imaging instrumentation and principles of PET protocol optimisation. In *Principles and practice of PET/CT Part1: A Technologist's Guide*; Peter Hogg, G. T., Ed.; European Association of Nuclear Medicine: Vienna, Austria, 2010; pp 38.
27. Antunes, I. F. General Introduction In Development and evaluation of PET tracers for imaging beta-glucuronidase activity in cancer and inflammation; University Medical Center, University of Groningen, Groningen, The Netherlands: 2011;pp 8–9.
28. van Waarde, A. *Introduction on PET: Description of Basics and Principles*; Asian Scientist Publishing Pte. Ltd: Singapore, 2013; Vol. 7851(Chapter 01), pp 1–13.
29. contributors, W. Positron emission tomography. 2013 (accessed August, 2014).
30. Fujita, M.; Innis, R. B. *In vivo* molecular imaging: Ligand development and research applications. In *Neuropsychopharmacology: The Fifth Generation Of Progress*; Davis, K. , Charney, D. , Coyle, J., Nemeroff, C. , Eds.; Lippincott, Williams, & Wilkins: Philadelphia, PA, 2002; pp 411–425.
31. Leopoldo, M.; Lacivita, E.; De Giorgio, P.; Contino, M.; Berardi, F.; Perrone, R. Design, synthesis, and binding affinities of potential positron emission tomography (PET) ligands with

- optimal lipophilicity for brain imaging of the dopamine D3 receptor. Part II. *Bioorg. Med. Chem.* **2009**, *17*, 758–766.
32. Pike, V. W. PET radiotracers: Crossing the blood-brain barrier and surviving metabolism. *Trends Pharmacol. Sci.* **2009**, *30*, 431–440.
33. Amini, N.; Nakao, R.; Schou, M.; Halldin, C. Identification of PET radiometabolites by cytochrome P450, UHPLC/Q-ToF-MS and fast radio-LC: Applied to the PET radioligands [11C]flumazenil, [18F]FE-PE2I, and [11C]PBR28. *Anal. Bioanal. Chem.* **2013**, *405*, 1303–1310.
34. Espinosa M, Jiménez JC, Galliker B, Steinbach A, Wille A Radio IC for Quality Control in PET Diagnostics. <http://www.sepscience.com/Sectors/Pharma/Articles/429-/Radio-IC-for-Quality-Control-in-PET-Diagnostics?pageNo=1> (accessed February, 2014).
35. Herzog, H.; Elmenhorst, D.; Winz, O.; Bauer, A. Biodistribution and radiation dosimetry of the A1 adenosine receptor ligand 18F-CPFPX determined from human whole-body PET. *Eur. J. Nucl. Med. Mol. Imaging* **2008**, *35*, 1499–1506.
36. Matsuya, T.; Takamatsu, H.; Murakami, Y.; Noda, A.; Ichise, R.; Awaga, Y.; Nishimura, S. Synthesis and evaluation of [11C]FR194921 as a nonxanthine-type PET tracer for adenosine A1 receptors in the brain. *Nucl. Med. Biol.* **2005**, *32*, 837–844.
37. Linden, J. Adenosine in Tissue Protection and Tissue Regeneration. *Molecular Pharmacology* **2005**, *67*, 1385–1387.



Adenosine A_{2A} Receptor Antagonists as Positron Emission Tomography (PET) Tracers

Shivashankar Khanapur^{*,†}, Aren van Waarde[†], Kiichi Ishiwata[‡], Klaus. L. Leenders^{||}, Rudi A.J.O. Dierckx^{†,§}, Philip H. Elsinga^{†,§}.

[†]Nuclear Medicine and Molecular Imaging, University Medical Center Groningen, University of Groningen, Groningen, The Netherlands

[‡]Positron Medical Center, Tokyo Metropolitan Institute of Gerontology, Tokyo, Japan

[§]Department of Nuclear Medicine, University Hospital Ghent, Ghent, Belgium; and

^{||}Department of Neurology, University Medical Center Groningen, University of Groningen, Groningen, The Netherlands.

* Corresponding author

Curr. Med. Chem. 2014; 21(3):312-328.

2

Abstract

The adenosine A_{2A} receptor (A_{2A}R) is highly concentrated in the striatum, and a therapeutic target for Parkinson's disorder (PD) and Huntington's disease. High affinity and selective radiolabeled A_{2A}R antagonists can be important research and diagnostic tools for PD. Positron Emission Tomography (PET) can play an important role by measuring radiolabeled A_{2A} antagonists noninvasively in the brain. However, till date no complete review on A_{2A}R PET ligands is available. The present article has been therefore focused on available PET tracers for A_{2A}R and their detailed biological evaluation in rodents, nonhuman primates and humans. Drug design and development by molecular modeling is discussed including new lead structures that are potential candidates for radiolabeling and mapping of cerebral A_{2A}Rs is discussed in the present article. A brief overview of functions of adenosine in health and disease, including the relevance of A_{2A}R for PD has also been presented.

Introduction

Adenosine, an endogenous ligand, functions as a cytoprotective and neuromodulator in response to stress to an organ or tissue under both physiological and pathophysiological conditions. It elicits intracellular signaling cascades through four subtypes of G-protein coupled adenosine receptors (ARs) namely A₁, A_{2A}, A_{2B} and A₃ (A₁R, A_{2A}R, A_{2B}R and A₃R, respectively).¹⁻⁴

Cytoprotective mechanisms may be indicated by increased blood supply (vasodilatation or angiogenesis), cerebral and cardiac preconditioning and / or suppression of inflammation.⁵ Adenosine is believed to play an important role in promoting sleep and suppressing arousal, cognition and memory, neuronal damage and degeneration as well as neuronal maturation.^{5, 6} Furthermore, adenosine is a local modulator for several neurotransmitters and counteracts glutamate excitatory effects. As a result, ARs are promising targets for investigation and treatment of cerebral and cardiac diseases, ischemic renal injury, endocrine, pain and sleep disorders, immune and inflammatory disorders and cancers.⁶⁻¹⁰

In the last two decades, the most extensively studied adenosine receptor (AR) subtypes are high affinity adenosine A₁ receptors (A₁Rs) and adenosine A_{2A} receptors (A_{2A}Rs), because adenosine activates these receptors in nanomolar concentrations. These subtypes are well-characterized biochemically and pharmacologically.^{11, 12} The high affinity A_{2A} subtype, when coupled with G-proteins, exhibits a lower affinity to adenosine. Activation of A_{2A}R assists neuronal function of neurotropic receptors like tropomyosin-related kinase B (TrkB) receptors and enhances neuronal communication.¹³ A_{2A}Rs stimulate adenylyl cyclase activity via G_s proteins.¹⁴ They can also activate potassium channels but inactivate Ca²⁺ channels, modulate the activities of phospholipases C, D, and A₂ and upregulate mitogen-activated protein kinases and inflammatory cytokines like IL-1 β .¹⁴

The regional distribution of A_{2A}R within the human brain is more restricted than that of A₁Rs. A_{2A}Rs are abundantly expressed in the basal ganglia and highest levels of expression occur in the substantia nigra [striatum maximum receptor density (B_{max}) 313 ± 10 fmol / mg protein]¹⁵, nucleus accumbens and olfactory tubercle whereas A₁Rs are highly expressed in the cerebral cortex, cerebellum, hippocampus and dorsal horn of spinal cord.¹⁶ Lower densities of A_{2A}Rs occur in the amygdala, cerebellum, brainstem and hypothalamus.¹⁷⁻¹⁹ A_{2A}Rs are implicated in several cerebral diseases such as Parkinson's disease (PD), Huntington's disease, Alzheimer's disease, attention deficit hyperactivity and panic disorders, schizophrenia, pain and sleep disorders. Also, A_{2A}Rs play an important role in cardiac diseases, immune and inflammatory disorders and ischemic kidney injury.^{7-10, 20}

Symptomatic dopaminergic replacement strategy using L-3,4-dihydroxyphenyl alanine (L-DOPA) and dopamine agonists is the current therapy for PD.^{21, 22} However, with disease progression the therapy suffers from several limitations like negligible effects on nonmotor symptoms, reduced effectivity in reverting motor impairment, unwanted side effects like dyskinesia, motor fluctuations and neuropsychiatric complications and importantly, fails to delay disease progression.²³⁻²⁶ A_{2A}Rs are mainly restricted to the indirect striatal output function [i.e., GABAergic neurons projecting to the globus pallidus (GP), pars externa] and are colocalized with dopamine D₂ receptors (D₂Rs) in the striatum. Along with D₂Rs, blockade of A_{2A}Rs dampens the hyperactivity of the indirect dopamine pathway observed during PD, restores correct movement execution and suppresses the neurodegenerative process and hence has raised a lot of interest due to unmet medical needs of PD.²⁶ Colocalization and synergistic interaction between A_{2A}R and metabotropic glutamate subtype 5 (mGlu5) receptor make A_{2A}Rs an important target for the therapy of PD.^{27, 28} Heteromeric forms like A₁/A_{2A}, D₃/A_{2A} and cannabinoid CB₁/A_{2A} have all been observed.^{29, 30} In addition, evidence for heterotrimers like CB₁/A_{2A}/D₂, A_{2A}/D₂/mGlu5 was also reported.^{29, 31} Apart from its central location, A_{2A}Rs

present in peripheral organs like heart, kidney, liver, muscle and lung.³² In heart, adenosine is an important mediator in cardioprotective action.^{5, 32} Myocardial protection action of adenosine is mediated mainly through A₁R and A_{2A}R. Activation of A_{2A}Rs causes coronary vasodilatation,³³ increases myocardial contractibility³⁴, relaxes smooth muscle and inhibits cytokine production, increases coronary blood flow and inhibits platelet aggregation.⁵ A_{2A}Rs via the action of adenosine help in regulation of physiological functions of skeletal muscle like glucose uptake, blood flow and contractile force.³⁵

Positron emission tomography (PET) can contribute important information in drug development resulting in a more rapid evaluation of novel compounds. High affinity and selective radiolabeled A_{2A}R antagonists can be used to assess changes of A_{2A}R density during the progression of disease and the affect of therapy on such changes. Moreover, A_{2A}R ligands can be employed to assess occupancy of the receptor population by therapeutic drugs in the human brain, which will allow correlation of receptor occupancy and therapeutic effects.^{36, 37} PET is a noninvasive technique allowing studies of physiological processes in the brain of normal individuals and patients with neurologic illness.³ Furthermore, PET can help to increase diagnostic specificity for dopamine-deficient parkinsonian syndromes and justify management decisions at initial stages of disease. Along with single photon emission computed tomography (SPECT) and proton magnetic resonance spectroscopy, ¹⁸F-DOPA PET is useful in discriminating atypical parkinsonian disorders (multiple system atrophy, progressive supranuclear palsy and corticobasal degeneration) from idiopathic PD with up to 80 % specificity.³⁸

On the basis of these considerations, several A_{2A}R antagonists (both xanthine and nonxanthine derivatives) have been produced and some of them are being tested as treatment for PD in several clinical trials as well as in preclinical studies.^{35,39-50} Moreover, some of these chemical structures allow easy incorporation of radionuclides.

Besides KF17837 and several related xanthine analogs, nonxanthine SCH442416 and its fluorinated derivative have been evaluated as PET ligands. In clinical studies, only one xanthine ($[^{11}\text{C}]\text{TMSX} = [^{11}\text{C}]\text{KF18446}$) and a nonxanthine derivative ($[^{11}\text{C}]\text{SCH442416}$) have been employed.³

Adenosine antagonists and their PET tracers have been the topic of many reviews.^{2,3,21,51-59} These reviews have provided a discussion on adenosine functions in health and disease, PET tracers for mapping adenosine receptors (mainly A₁R) and the development of potential novel radioligands. However, to date no comprehensive review on PET ligands for A_{2A}R is available. The major goals of the current chapter is three-fold: 1) to present an overview of A_{2A}R antagonists used as PET tracers, 2) to summarize preclinical and clinical A_{2A}R imaging data, and 3) to highlight the design and development of new lead compounds as potential tracers for mapping of A_{2A}Rs.

A_{2A}R PET Tracers

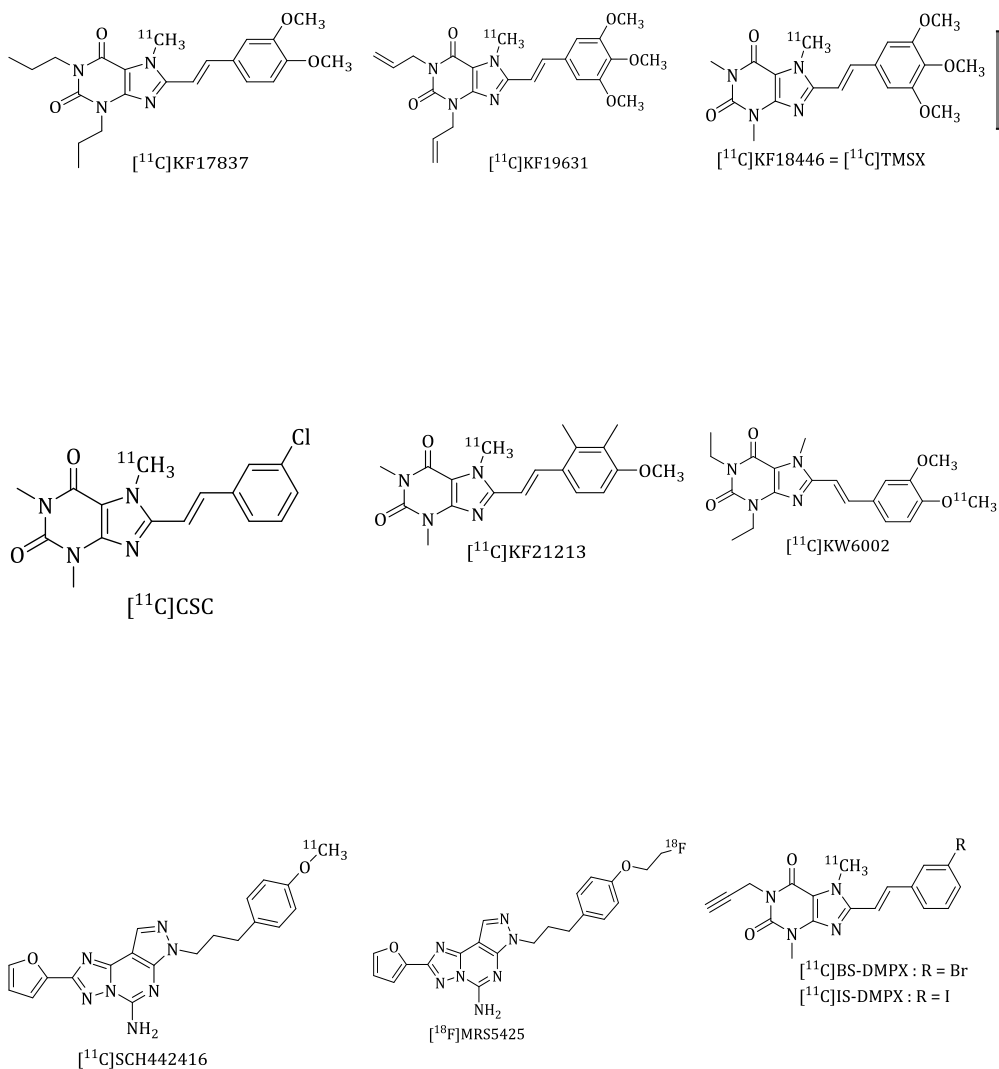
A_{2A}R antagonist PET tracers (Figure 1) are divided into two classes.

1. Xanthine PET tracers
2. Nonxanthine PET tracers

Xanthine Ligands

All xanthine type radioligands were synthesized either by N- or O-methylation of the corresponding desmethyl compounds using primarily $[^{11}\text{C}]\text{CH}_3\text{I}$ with sufficient radiochemical yields suitable for routine use⁶⁰⁻⁶⁴ (Table 1). In one of the radioligand syntheses, the more reactive methylating agent $[^{11}\text{C}]\text{CH}_3\text{OTf}$ has been used to achieve high radiochemical yield. However, reaction temperature, time and specific activity were not mentioned in the literature.⁶⁵ All xanthine analogues suffer from a serious photoisomerization problem (Figure 1). The styryl group in the xanthine scaffold is isomerized to form a stable equilibrium mixture of E-isomer and Z-isomer in the presence of light. Therefore in experimental and

clinical studies, all procedures should be carefully carried out under dim light.³



2

Figure 1. Current PET tracers for the adenosine A_{2A} receptors

Table 1. Radiochemical Synthesis of Xanthine Analogs

Radio tracers	Methylating agent	Precursor (mg)	DMF (mL)	Base	Reaction temperature (°C)	Reaction time (min)	RCY # (%)	S. A.# (GBq/ μ mol)	Ref #
[¹¹ C]KF17837	[¹¹ C]CH ₃ I	0.5	0.25	5 mg CS ₂ CO ₃	120	1	19-48	37-64	60
[¹¹ C]CSC	[¹¹ C]CH ₃ I	1	0.4	10 mg K ₂ CO ₃	60	10	44	1.8-5.5	63
[¹¹ C]KF21213	[¹¹ C]CH ₃ I	0.5	0.25	5 mg CS ₂ CO ₃	120	3	31-62	43±9	66
[¹¹ C]TMSX	[¹¹ C]CH ₃ I	0.5	0.25	5-10 mg CS ₂ CO ₃	120	3	25-46	10-72	61
[¹¹ C]KF19631	[¹¹ C]CH ₃ I	0.5	0.25	5 mg CS ₂ CO ₃	120	1-5	25-46	10-72	61
[¹¹ C]KW6002	[¹¹ C]CH ₃ I	3	0.4	20 μ l, 5MNaOH	100	6	1.1-2.2*	-	64

* Radiochemical yield in GBq on each automated synthesis run and no specific activity data available

RCY = Radiochemical yield, S.A = Specific activity, Ref = References, RT = Room temperature.

In Vitro and Preclinical Studies

Researchers earlier emphasized the selectivity of KF17837 towards A_{2A}R.⁶⁷ However, in a later study its specificity for A_{2A}R was questioned because in dilute solution this styrylxanthine undergoes photoisomerisation to the less active Z-isomer (82 %) ⁶⁸. The Z-isomer has about 860-fold lower affinity (K_i value, 860 ± 120 nM) for the A_{2A}R than the E-isomer (1.0 ± 0.1 nM).^{60, 68}

Suzuki and coworkers developed the xanthine compound KF17837^{69, 70} and two other groups successfully labeled its desmethyl precursor with carbon-11 by N-methylation reaction using [¹¹C]methyl iodide (Table 1). Radiosynthesis was carried out under dim light in an amber glass vial, which preserved the E-isomer over the entire period of study.^{60, 62} Biodistribution studies showed highest radioactivity uptake [13 % injected dose per gram (% ID / g)] in the heart at 5 min after injection of [¹¹C]KF17837 in normal healthy mice but falling gradually thereafter. A high and saturable uptake of tracer by the mouse heart confirmed its usefulness for mapping myocardial adenosine receptors.⁶⁰ Similar results were observed with a dynamic PET scanning of the heart in rabbits.⁷¹ Regional brain distribution showed a higher uptake in striatum than in other regions (striatum / cerebellum ratio approximately 2.0 at 60 min). The compound's affinity for A_{2A}R-rich striatum was confirmed by carrier KF17837 coinjection and by sequential PET studies in the same rats using D₂R ligand [¹¹C]N-methylspiperone. A 68 % reduction radioactivity in striatum, 30 min after carrier injection, and accumulation [¹¹C]KF17837 in the same brain regions as [¹¹C]N-methylspiperone indicate specific binding of [¹¹C]KF17837 in the striatum⁶⁰(Table 2).

Later studies were aimed at evaluation of [¹¹C]KF17837 as a central nervous system (CNS) tracer in rodents and monkey.⁷² *In vitro* autoradiography (ARG) experiments in rats showed 2.3 – 3.0 times higher striatal uptake than in other brain regions. On contrary, results from a regional brain distribution study in mice, an *ex vivo* ARG study in rats and a PET study in a monkey suggested only slightly higher uptake in the striatum than in other brain regions(1.1

- 1.5 times) (Table 2). Authors hypothesized that the *in vivo* receptor binding sites of xanthine type antagonists may be different from those of nonxanthine type A₂AR ligands as *in vivo* uptake of [¹¹C]KF17837 was not significantly decreased in a blocking study using subtype selective nonxanthine analogues such as SCH58621 or ZM241385.⁷⁵ Their data indicated nonspecific binding and the presence of unknown but specific binding sites for [¹¹C]KF17837 in the cortex and cerebellum. In this study no clear conclusion was reached concerning its potential to bind adenosine A_{2B} receptor (A_{2B}R) because at the time of the study there was no subtype selective A_{2B}R ligand. However, a weak A_{2B} antagonist, alloxazine, did not reduce [¹¹C]KF17837 uptake in the brain.⁷²

In addition, another group evaluated [¹¹C]KF17837 in monkey by PET examination. PET biodistribution studies using 3-D mode of data acquisition was used to express radioactivity retention in the striatum, cerebellum, and cerebral cortex (1.1, 1.0, and 0.8, respectively). Radioactive accumulation was significantly different from the known relative A₂AR densities in these regions⁷³⁻⁷⁵ (Table 2). The ligand has limited usefulness for mapping the cerebral A₂AR because of its limited diffusion through the blood-brain-barrier (BBB) and high nonspecific binding. However, radiotracer uptake in the heart was rapid (maximum reached at 2 – 4 min post injection). In a saturation binding experiment, there was an indication of competition between the labeled and unlabeled drugs for the same receptor binding sites in heart. Hence, authors suggested further investigation to establish the specificity of the interaction of this tracer with myocardial A₂ARs and other potent and selective A₂AR antagonists (ZM241385 and SCH58261) could be considered as ligands for *in vivo* PET studies.⁶² In conclusion, both groups clearly demonstrated limited suitability of [¹¹C]KF17837 for A₂AR quantification because of its low brain penetration and high degree of nonspecific binding (Table 2). Apparently, investigated time is not an ideal point for comparing *in vitro* and *in vivo* studies as shown in Table 2.

Table 2. Summary of Striatal Uptake of [¹¹C]KF17837

Species	Regional brain distribution (% ID / g)		<i>In vitro</i> ARG ^a (% ID / g)	<i>Ex vivo</i> ARG ^a (% ID / g)	Ref
	striatum-to-cerebellum	striatum-to-cortex			
Mouse	1.1 – 1.2 (15 min)	1.2 – 1.5 (15 min)	–	–	60
	1.2 (30 min)	1.4 (30 min)	–	–	72
Rat	–	–	2.3 – 3.0	1.2 – 1.5 (15 min)	72
Female Rhesus monkey (n=1)	1.32 (30 min)	1.38 (30 min)	–	–	72
Male Cynomolgus monkey (n=2)**	1.05 - 1.1 (20 min)	1.3 - 1.4 (20 min)	–	–	62

^aARG, autoradiography

^bRadioactivity uptake was expressed by PET biodistribution study using 3-D mode acquisition.

A comprehensive comparison of four xanthine PET tracers (carbon-11 labeled KF17837, KF19631, TMSX and CSC) was made in order to search for a selective A_{2A}R ligand.⁶¹ [¹¹C]CSC had similar characteristics as [¹¹C]KF17837, but [¹¹C]CSC showed higher uptake in the lung and small intestine and it was cleared more rapidly. Another study described in detail optimization of the radiochemical synthesis of [¹¹C]CSC.⁶³ Also, significant [¹¹C]CSC accumulation in the lung was detected whereas autoradiographic investigations indicated uptake in the striatum, consistent with observations by Ishiwata *et al.*⁶¹ Dynamic PET scans in rabbits showed rapid uptake

of the radiotracer in the brain in less than 2 min after injection. An *in vivo* competition study with cold CSC suggested that [¹¹C]CSC binds specifically to A_{2A}R in the rabbit brain.⁶³ However, the tracer's rapid clearance, different distribution pattern from other xanthine PET tracers (i.e., high uptake in small intestine and lungs) and low affinity made it unsuitable as a PET tracer for A_{2A}R.

Wang and coworkers continued their work in search for A_{2A}R tracers with high affinity and selectivity and found KF21213 with higher selectivity for A_{2A}R than KF17837 or KF18446.⁶⁶ An *in vitro* study showed that K_i values of KF21213 were 3.0 nM for A_{2A}R and >10,000 nM for A₁R whereas for KF18446 they were 5.9 nM for A_{2A}R and 1600 nM for A₁R (Table 3). In mice, regional brain distribution data of [¹¹C]KF21213 suggested a high striatal uptake for the first 15 min followed by a gradual decrease. A very low uptake was seen in the cortex and cerebellum. As a result of this, high striatum-to-cortex (8.6 ± 1.6) and striatum-to-cerebellum (10.5 ± 2.1) uptake ratios were found at 60 min post injection. On the other hand, the uptake of [¹¹C]TMSX was higher in all three regions of brain but decreased more rapidly with time such that the striatum-to-cortex ratio was 2.8 ± 0.5 and striatum-to-cerebellum ratio was 2.7 ± 0.5 at 15 min. Coinjection of cold KF21213 and three other A_{2A} antagonists (KF17837, KF18446 and SCH58261), but not the A₁R antagonist KF15372, effectively blocked uptake of [¹¹C]KF21213 especially in the striatum. However, no significant effect was seen in the cortex and cerebellum. *Ex vivo* ARG showed a high uptake in the caudate-putamen, GP and olfactory tubercle and good uptake ratios of striatum-to-cortex (4.0 ± 0.4) and striatum-to-cerebellum (3.7 ± 0.4) at 15 min post tracer injection. A PET study in rats indicated high striatal retention of [¹¹C]KF21213 at 5 min followed by a gradual decrease whereas [¹¹C]TMSX cleared more rapidly.⁶⁶ However, its low BBB penetration, signal-to-noise ratio and poor water solubility made it not a very practical tracer for PET studies of the CNS.

In search for more pronounced A_{2A}R-selectivity, ¹¹C-labeled iodinated and brominated xanthine analogs were synthesized and

evaluated for their capability of detecting A_{2A}R changes in brain. *In vitro* binding assays showed that both IS-DMPX and BS-DMPX had high affinity and selectivity for A_{2A}R (Table 3). However, because of their low *in vivo* uptake ratios of striatum to other brain regions and high nonspecific binding they were judged unsuitable for mapping cerebral A_{2A}Rs.⁷⁶

In another PET study, the xanthine-type radioligand [¹¹C]KW6002 was reported. High striatal uptake [Standard uptake value (SUV) = 3.3] and low uptake in frontal cortex (SUV = 1.7) reflects specific binding.^{46, 64} In a blocking study, specificity and selectivity of tracer was confirmed. However, extrastriatal regions like cerebellum and superior colliculi uptake can be seen where a low A_{2A}R density was reported.^{46, 64} Saturation binding study with A₁R antagonist KF15372, nonxanthine type A_{2A}R antagonist ZM241385⁶⁴ and A_{2B} selective antagonist MRS1745⁴⁶ failed to solve the nature of extrastriatal binding. In rats, specific *in vivo* binding of [¹¹C]KW6002 to A_{2A}R could not be observed and thus the compound does not appear to be a good PET tracer. Further study concerning its *in vivo* selectivity is warranted. In general, [¹¹C]KW6002 has shown similar *in vivo* properties as [¹¹C]KF17837.⁶⁴ All xanthine A_{2A} antagonists e.g., [¹¹C]KF17837, [¹¹C]TMSX, [¹¹C]KF21213, [¹¹C]KF19631 and [¹¹C]KW6002 seem to interact with multiple binding sites and undefined binding sites are responsible for extrastriatal retention of radioactivity.^{46, 64, 66, 72, 77}

[¹¹C]TMSX showed more desirable properties for mapping A_{2A}R such as high retention in the rat brain and especially in the striatum (ratio of striatum uptake to other brain regions was up to 3.2). Additionally, [¹¹C]TMSX- PET imaging of monkey brain showed 10 fold higher striatal uptake at 5–10 min than [¹¹C]KF17837 but indicated a rapid washout pattern. However, uptake ratios of [¹¹C]TMSX [striatum: cortex: cerebellum (1.0: 1.56: 1.46, respectively) at 60 min] in the monkey brain were slightly better than those of [¹¹C]KF17837. An *in vivo* saturation binding experiment also suggested superiority of [¹¹C]TMSX over other KF compounds.⁶¹

Promising preliminary results stimulated further characterization of [¹¹C]TMSX by *in vitro* ARG and *in vivo* biodistribution experiments.⁷⁷ The binding characteristics of [¹¹C]TMSX (*in vitro* ARG) were slightly better than those of reference standard [³H]CGS21680. Nonspecific binding of [¹¹C]TMSX in the striatum was less than 10 % of the total uptake and striatum-to-cortex ratio was 5.0 whereas related values for [³H]CGS21680 were estimated as 19 % and 4.6. TMSX had a very low affinity for 13 other neuroreceptors like dopamine D₁ and D₂; histamine H₁ and H₂, nicotine acetylcholine in binding assays. *In vitro* blocking study with various A_{2A}R and A₁R antagonists indicated K_d values for [¹¹C]TMSX of 9.6 nM in the striatum and 16.4 nM in the cerebral cortex. Also, all antagonists significantly reduced the binding of [¹¹C]TMSX in the striatum and cortex but stronger effects were seen in the striatum. The *in vitro* ARG experiments suggested that xanthine ligands interact with unknown binding sites in the cortex and hippocampus that are different from known A_{2A}R binding sites. Fredholm and coworkers also measured binding sites of an A_{2A}R radioligand in the hippocampus and cerebral cortex.^{17, 73} However, the *in vivo* results were remarkably different from those obtained *in vitro*. In an *in vivo* blocking study, striatal uptake was reduced by all four xanthine-type A_{2A} antagonists (KF17837 > KF19631 > TMSX > CSC), consistent with the *in vitro* result whereas nonselective AR antagonists (DMPX and XAC) and an A₁R antagonist (KF15372) did not block tracer uptake in any region of the brain. However, SCH58621 significantly blocked striatal but not cerebellar or cortical uptake whereas three other nonxanthine antagonists (ZM241385, CP-66713, and ZD9255) did not reduce uptake in any brain region, suggesting that nonxanthine ligands may have other blocking effects than xanthine ligands.⁷⁷ Hence, these findings suggested that ligands can have multiple binding sites and undefined binding sites may be involved in the cerebral uptake of [¹¹C]TMSX.

GP plays an important role in the pathophysiology of neurologic disorders like PD and Huntington's disease. Thus far there are no tracers for imaging the pallidal terminals projecting from the striatum. For these reasons, Ishiwata *et al.* performed *ex vivo* ARG of

the GP in the rat brain, using [¹¹C]TMSX.⁷⁸ The highest uptake was found for [¹¹C]SCH23390 [dopamine D₁ receptor (D₁R)] followed by [¹⁸F]FDG (Fluorodeoxyglucose), [¹¹C]TMSX (A_{2A}R) and [¹¹C]raclopride (D₂R). Receptor-specific uptake in the GP was found for [¹¹C]TMSX and [¹¹C]SCH23390 but was negligible for [¹¹C]raclopride. GP-to- striatum uptake ratio is helpful in evaluating the contrast of the image. These ratios were ≈ 0.6 for [¹¹C]TMSX and FDG, twice as large as those for [¹¹C]SCH23390. These results suggested that D₁R and D₂R receptor ligands are not suitable for imaging GP. Authors suggested using PET-MRI coregistration or a high-resolution PET scanner to prove clear visualization of the GP by these tracers. Intra-striatal injection of quinolinic acid significantly reduced the uptake of [¹¹C]TMSX in the striatum and GP, suggesting the degeneration of A_{2A}R-expressing neurons and hence, specific uptake of [¹¹C]TMSX.⁷⁸

On the basis of the previous promising results, extensive preclinical studies (stability test, internal dosimetry data for human organs and toxicological data) were carried out to establish [¹¹C]TMSX as a radioligand for imaging human A_{2A}R.⁷⁹ Theophylline challenge in mice resulted in a decrease of tracer uptake in the striatum, as theophylline is a nonsubtype-selective adenosine antagonist. This suggested that [¹¹C]TMSX-PET scan data should be interpreted with caution in patients who received theophylline. [¹¹C]TMSX was metabolically stable as about 80 % and >98 % of radioactivity in plasma and striatum represented intact tracer at 30 min post injection. From the mouse data of tissue radioactivity distribution, absorbed doses of [¹¹C]TMSX for human adults were estimated. The radiation absorbed doses in the brain (0.09 μ Gy / MBq) and heart (0.31 μ Gy / MBq) were very low. In rodents, neither mortality nor any other abnormality was found in an acute toxicity study, which was evaluated after single intraperitoneal administration of TMSX at a dose of 4.77 mg / kg and after intravenous injection of 3.3 – 3.9 μ g / kg over a period of 15 days. An Ames test (with 4 strains of *Salmonella typhimurium*) suggested absence of mutagenic activity.

All these findings encouraged the authors to use [¹¹C]TMSX for the assessment of A_{2A}R in the human brain.⁷⁹

Clinical Studies

A first human study with [¹¹C]TMSX was reported concerning myocardial imaging. The levels of radioactivity in the left ventricular lateral wall, left ventricular anterior wall and interior ventricular septum increased during the first 2.5 min post injection and then gradually decreased with time. Time-activity curves in 3 heart regions and graphical analysis using Logan plot suggested that [¹¹C]TMSX was taken up via a receptor-mediated mechanism. During the 60 min study period, [¹¹C]TMSX was very stable in plasma (more than 90 % unchanged form). These preliminary findings suggested that [¹¹C]TMSX-PET may be useful for myocardial imaging in the diagnosis of ischemia and other myocardial diseases.³⁹ This may be possible in combination with a pharmacologic stress agent like regadenoson (an adenosine derivative) or with a flow tracer.

An additional study evaluated [¹¹C]TMSX for mapping A_{2A}R of skeletal muscle and heart in humans using PET. In humans, the heart was clearly visualized at baseline. Radioactivity in three regions of the heart was in line with the previous result.³⁹ Theophylline (a nonsubtype-selective adenosine antagonist, at a dose of 100 mg / kg) slightly decreased the distribution volume (DV) of [¹¹C]TMSX in the heart (by 18 – 22 %) and muscle (by 10 %) suggesting some specific binding of the tracer.⁴⁰

Using PET, a comparison of A_{2A}R densities in cardiac muscle has been made in both endurance-trained subjects and untrained men at resting state.³⁵ In addition, a group from Japan evaluated receptor functions in the skeletal muscle using PET based on their previous result⁴⁰ whereas a Finnish group recorded the myocardial perfusion effect at rest and during adenosine-induced hyperemia.⁴¹ Higher density of A_{2A}Rs was found in cardiac muscle than in skeletal muscle. Also, higher levels of A_{2A}R were recorded in cardiac and skeletal muscle of endurance-trained subjects than in untrained subjects (DV of [¹¹C]TMSX in heart, 3.6 ± 0.3 vs 3.1 ± 0.4 mL g⁻¹, triceps brachii

muscle 1.7 ± 0.3 vs 1.2 ± 0.2 mL g⁻¹, respectively).³⁵ As a follow-up the interrelation was studied between A_{2A}R density and myocardial blood flow (MBF) in both endurance-trained men and untrained men. Neither difference in A_{2A}R densities between groups nor affiliation of MBF with A_{2A}R density and adenosine-induced hyperemia was found.⁴¹

The effect of age on the distribution of A_{2A}R in the striatum of healthy human subjects has been studied using [¹¹C]TMSX-PET [11 young & 6 elder (3 men and women volunteers)]. There was no significant difference between calculated distribution volume ratio (DVR) of [¹¹C]TMSX in the striatum of young and elderly subjects suggesting distribution of A_{2A}R does not change with age. Also, no gender difference was found in elderly subjects (Females DVR = 1.37 ± 0.10 , males DVR = 1.39 ± 0.06).⁴²

Kinetic modeling was carried out to investigate the behavior of [¹¹C]TMSX in the brain and to examine the usefulness of Logan plot.⁴⁴ In the study, estimation of binding potential (BP) with the Logan plot agreed to the three-compartmental model data with or without metabolite correction and arterial blood sampling. The estimated BP without metabolite correction was only 5 % lower than the values acquired with or without arterial blood sampling in different brain regions.⁴⁴

The cerebral distribution of [¹¹C]TMSX⁴³ was in agreement with the distribution of A_{2A}R known from post mortem studies in humans, rodents and primates.^{3, 20, 74, 75} A two-tissue, three-compartment model was used to measure the distribution of A_{2A}R in the brain (n = 5) using metabolite corrected arterial input function. Specific binding was found to be 62 % in putamen. The BP was largest in the anterior putamen (1.25), posterior putamen (1.20), caudate nucleus (1.05) and thalamus (1.03) followed by the cerebellum, brainstem, posterior cingulate gyrus, occipital, temporal, parietal and frontal lobes.⁴³ [¹¹C]TMSX binding in human thalamus was relatively larger than in the thalamus of other mammals.

Furthermore, using [¹¹C]TMSX-PET, differences between A_{2A}R expression and the dopaminergic system in the striata of drug-naïve PD patients, PD patients with dyskinesia and alterations of these receptor systems after antiparkinsonian therapy were studied.⁴⁵ In order to elucidate the relationship between changes in A_{2A}R density and dopaminergic system in striatum, authors also used other dopaminergic system related tracers like [¹¹C]2β-carbomethoxy-3β-(4-fluorophenyl)tropane ([¹¹C]CFT), a marker for presynaptic dopamine transporter and [¹¹C]raclopride ([¹¹C]RAC), a marker for postsynaptic D₂R. In an early PD patient with right dominant PD symptoms, the left-side [¹¹C]CFT binding was more decreased than the right-side one and the uptake of [¹¹C]RAC was increased bilaterally. In contrast, the [¹¹C]TMSX retention (A_{2A}R density) was decreased on the left side. These observations suggested that the changes in A_{2A}R binding measured with [¹¹C]TMSX were coupled with the asymmetry of the symptoms. The BP of [¹¹C]TMSX was increased in the putamen of PD patients with mild dyskinesia. The study also showed that A_{2A}Rs were significantly increased in bilateral putamen of drug-naïve patients after antiparkinsonian therapy.⁴⁵

KW6002, a very potent, selective and orally active drug has completed clinical trials for the treatment of PD. In spite of extrastriatal *in vivo* binding result obtained in rats⁶⁴, [¹¹C]KW6002 uptake was well characterized in human study by a two-tissue compartmental model with a blood volume component and reversible kinetics were observed during the scan time.⁴⁶ The caudate (3.38) showed the highest BP, followed by putamen (2.90), nucleus accumbens (2.37), cerebellum (2.26), and thalamus (2.19). Oral dose of 20 – 40 mg / day produced >90 % of receptor occupancy in healthy volunteers.⁴⁶ Additional study is required to determine the dose-receptor binding relationship of KW6002 in PD patients.

Table 3. Binding Affinities of Adenosine A_{2A} Receptor Antagonists

Compound	Affinity (K _i , nM)		Selectivity A ₁ / A _{2A}	Ref
	A ₁	A _{2A}		
KF17837	62	1	62	60
KF19631	>10000	3.5	2857	61
KF18446 (= TMSX)	1600	5.9	270	61
CSC	28000	54	520	61
BS-DMPX	2300	7.7	300	76
IS-DMPX	>10000	8.9	>1100	76
KF21213	>10000	3	>3300	66
KW6002	150	2.2	68	64
SCH442416	1800	0.5	3600	80
	1100 (h)**	0.048 (h)**	22916 (h)**	
MRS5425	42.7 ± 0.6 ^a	12.4 ± 0.8 ^a	–	81
Fluoropropyl SCH442416	1000 ± 40 ^c	53.6 ± 25.5 ^c	19	82
SCH58261	549	1.1	499	83

^a% inhibition at 10 μM ^bh = humans

^cValue is expressed as the mean ± SEM

The design and development of new A_{2A}R antagonist PET tracers is a hot research topic since there are still major problems, especially with xanthine PET tracers, including high nonspecific binding, reduced tracer uptake, low signal to noise ratio and barely visible target areas in the brain.^{60, 62–64, 66} Usefulness of all xanthine type PET tracers may be limited due to its photoisomerisation problem, lower specific activity and selectivity towards A_{2A}R. On the basis of these considerations, nonxanthine compounds (Figure 1) were developed and tested in many preclinical and clinical studies for the assessment of cerebral A_{2A}Rs. The following paragraphs are devoted to nonxanthine PET ligands.

Nonxanthine Ligands

Nonxanthine [¹¹C]SCH442416 was synthesized by O-methylation of desmethyl compound using [¹¹C]CH₃I with radiochemical yield of 29

$\pm 7\%$ (decay corrected), radiochemical purity $>96\%$, and specific activity of 55 ± 36 GBq / μmol ($n=18$). Overall synthesis time was about 40 min⁸⁰ (Figure 2).

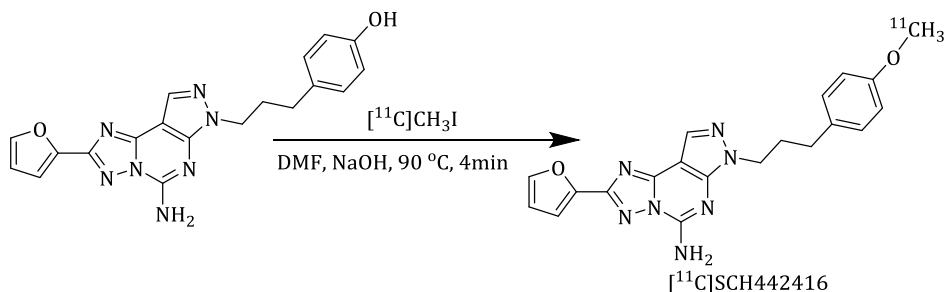


Figure 2. Radiosynthesis of $[^{11}\text{C}]\text{SCH442416}$

A two-pot radiosynthesis method was adopted using the fluorosynthon 2- $[^{18}\text{F}]$ -fluoroethyl- 3,4-dibromobenzenesulfonate. The whole synthesis time including HPLC purification was about 130 min. The radiochemical yield was $15 \pm 4\%$ ($n = 8$) uncorrected for decay and the radiochemical purity was $\geq 98\%$ ⁴⁸ (Figure 3).

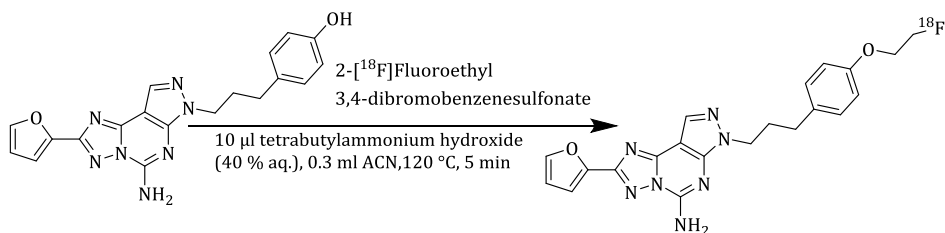


Figure 3. Radiosynthesis of $[^{18}\text{F}]\text{-MRS5425}$

In Vitro and Preclinical Studies

The development of the high affinity and selective novel nonxanthine compound SCH442416 as an *in vivo* probe for $A_{2A}\text{R}$ using PET was reported by Todde *et al.*⁸⁰. In receptor binding studies, SCH442416 showed a very good selectivity for $A_{2A}\text{R}$ as K_i values were 0.048 nM for $A_{2A}\text{R}$, $> 10,000$ nM for A_{2B} and A_3 , and 1,111 nM for A_{1R} (Table 3). Biodistribution studies showed not only radioactive uptake in the adrenal glands and kidneys, where $A_{2A}\text{Rs}$

are highly expressed, but also in highly perfused organs like lung and liver radioactive uptake reached maximum at 5 min post injection in normal healthy rats. [¹¹C]SCH442416 penetrated the BBB easily and was retained in the brain where the maximum uptake was reached at 5 – 15 min after injection. Regional brain distribution showed a high striatal uptake (0.46 % ID / g) whereas tracer levels in the cerebellum (0.10 % ID / g) and cortex (0.10 % ID / g) were lower. Striatum-to-cerebellum ratio was 4.6 ± 0.17 at the time of maximum uptake (at 15 min post injection). Two hydrophilic metabolites were found in plasma extracts [Retention time (t_R) = 4.5 and 2.5 min] with about 40 % of an intact tracer at 60 min. The regional distribution of radioactivity, the good signal-to-noise ratio and low amounts of radioactive metabolites in the brain all suggested that [¹¹C]SCH442416 was the first nonxanthine ligand suitable for mapping of A_{2A}R using PET.⁸⁰

In a later study, [¹¹C]SCH442416 was tested as a new PET tracer for *in vivo* imaging of A_{2A}Rs in rat and monkey brain.⁸⁴ Preadministered A_{2A}R selective (SCH442416, SCH58261 and KW6002) or nonsubtype selective antagonists (caffeine) decreased tracer accumulation in the striatum at 15 min after injection. Caffeine and KW6002 significantly decreased tracer retention (71 % and 68 %, respectively) in the striatum. Interestingly, subtype selective, potent antagonists like SCH442416 and SCH58621 did not yield a good blocking effect. These compounds may pose formulation problems due to poor water solubility. Receptor-specific uptake was confirmed by intrastriatal injection of quinolinic acid. Using PET, serial brain scans were made in a single monkey after injection of 30 MBq of [¹¹C]SCH442416. Rapid uptake of the tracer was observed in 0 - 4 min. Higher uptake in the striatum was noticed during the second frame (2 - 4 min). Striatum-to-cerebellum ratios reached a maximum value of 2.2 at approximately 15 min. BP in the striatum was estimated as 0.74 with the cerebellum as an input function (reference tissue model). These findings suggested suitability of [¹¹C]SCH442416 as an *in vivo* probe for A_{2A}R.⁸⁴

Acute pharmacological interaction of adenosine receptor (A₁-, A_{2A}-, & A_{2B}-R) antagonists with L-DOPA has been investigated.⁴⁷ Neither the A₁R antagonist CPX (5 mg / kg) nor the A_{2B}R antagonist alloxazine (3mg / kg) induced rotational behaviors in 6-hydroxydopamine (6 - OHDA)-lesioned mice after L-DOPA treatment. However, synergistically increased contralateral rotations were seen with the A_{2A}R antagonist SCH58261. In contrast, when used separately, neither SCH58261 (10 mg / kg) nor L-DOPA (2.5 mg / kg) induced rotational behaviors in this PD model. In addition, levels of A_{2A}Rs in 6-OHDA-lesioned mice have been determined with the A_{2A}R specific tracer [¹¹C]SCH442416. No significant differences in striatal uptake were observed between the two groups indicating that 6-OHDA-induced lesions of the dopaminergic system do not affect the *in vivo* binding of the A_{2A}R tracer [¹¹C]SCH442416. This contrasts strongly with reported changes of A_{2A}R mRNA expression in human PD.⁸⁵ Overall, this study suggested a synergistic beneficial role of A_{2A}R antagonists in the reduction of L-DOPA dosage in 6-OHDA-lesioned mouse model.⁴⁷

A_{2A}R occupancy in Rhesus monkeys after administration of various doses of the A₁R and A_{2A}R antagonist ASP5854 has been assessed using [¹¹C]SCH442416 and PET. The amount of receptor occupancy required to inhibit haloperidol-induced catalepsy (0.03 mg / kg, intramuscularly) was also determined.⁸⁶ Receptor occupancy was studied after a intravenous bolus injection of ASP5854 in animals (n = 3) and a dynamic PET scan was performed at 1, 4, and 8 hour after injection of approximately 740 MBq of [¹¹C]SCH442416. Incidence and duration of catalepsy were monitored throughout the study. Catalepsy was scored on the basis of a forced posture test and all experiments were video-recorded. If animals maintained the cataleptic posture then the trial was scored as “onset-positive”; else it was scored “onset-negative”. The anticataleptic effect of ASP5854 was achieved at 85 – 90 % occupancy of A_{2A}Rs. Dose-dependent receptor occupancy 9.0 % (0.001 mg / kg), 50.7 % (0.01 mg / kg), and 87.4 % (0.1 mg / kg) was seen in the caudate nucleus. Bound ASP5854 dissociated slowly from cerebral A_{2A}Rs and hence a single

drug administration provides a long-lasting effect. ASP5854 might be useful for treatment of psychotic patients in combination with antipsychotics like haloperidol. [¹¹C]SCH442416-PET might be a useful tool for estimating the effective doses of A_{2A}R antagonists in humans.⁸⁶

It has been reported that [¹⁸F]-MRS5425 (a [¹⁸F]-fluoroethyl derivative of SCH442416) can map A_{2A}R changes in the rat model of PD (6-OHDA model). Also, precursor synthesis for radiolabelling and a two-pot radiosynthesis of [¹⁸F]-MRS5425 were described.⁴⁸ In anesthetized rats, [¹⁸F]-MRS5425 was intravenously injected and PET data were collected. The % ID / g values in regions of interest were measured in the striatum of normal rats and in rats unilaterally lesioned with 6-OHDA after intravenous administration of saline (baseline), the D₂R agonist quinpirole (1.0 mg / kg) or the D₂R antagonist raclopride (6.0 mg / kg). *In vitro* and *ex vivo* brain ARG showed A_{2A}R specific uptake in the striatum. In addition, *in vivo* biodistribution studies suggested radioactivity in the striatum reached a maximum at 30 and 60 min then dropped slowly. Radioactivity levels in the striatum were two-fold higher than in blood, suggesting suitability of [¹⁸F]-MRS5425 as an *in vivo* probe for mapping A_{2A}Rs. Results of the PET study were comparable to the previous one using [¹¹C]SCH442416 in anesthetized nonhuman primates.⁸⁴ Radioactivity uptake was higher (9 – 12 % in the % ID / g) in the lesioned striatum than in the contralateral intact side due to upregulation of A_{2A}Rs.^{48, 81} Conflicting results (either upregulation or no change of A_{2A}Rs in animal models of PD)^{47, 48} may be related to differences in the experimental setup and / or species differences (rat vs mice).

Clinical Studies

In an important study, A_{2A}R availability in 12 PD patients with and without levodopa-induced dyskinesias (LIDs) and in age-matched healthy controls (n=6) using PET and [¹¹C]SCH442416 was reported.⁴⁹ PD patients with LIDs have elevated striatal A_{2A}R availability (BPs up to 1.67 vs 0.96 of patients without LIDs). However, no correlation was found between severity of dyskinesia

and increased striatal A_{2A}Rs. Also, the increase was not correlated to age, disease duration, levodopa equivalent unit or Hoehn and Yahr staging. Higher A_{2A}R binding was found in the caudate and putamen of PD patients with LIDs with respect to both control group and PD patients without LIDs. Hence, this study suggested A_{2A}R antagonists might be useful for the management of LIDs along with reductions in levodopa dosage. However, to prove the concept, further studies are required in larger groups of patients. [¹¹C]SCH442416-PET might provide a robust and reliable method for *in vivo* investigations of A_{2A}R availability.⁴⁹

[¹¹C]SCH442416 has been employed to assess A_{2A}R occupancy by a therapeutic drug, vipadenant, in the human brain in order to correlate receptor occupancy and therapeutic effect.⁵⁰ The drug crossed the BBB and displaced receptor-bound [¹¹C]SCH442416 in a dose-dependent fashion (2.5 – 100 mg /day for 10 or 11 days). The estimated receptor occupancy of the drug in the brain varied from 74-94 % at the lowest daily dose (2.5 mg)⁵⁰ Unfortunately, negative findings in preclinical toxicology studies led to discontinuation of this drug in July 2010 by Vernalis Plc.⁸⁷ Thus, [¹¹C]SCH442416 might be an excellent tool for measurement of the A_{2A}R occupancy of various compounds (both xanthine and nonxanthine antagonists).

Trends in Medicinal Chemistry Including Molecular Docking of A_{2A}R Antagonists as Potential PET Tracers

Recent developments in medicinal chemistry (both in synthesis and biological evaluation) resulted in the identification of large number of ligands with high affinity and specific binding to the A_{2A}R. Potential candidates for radiolabeling and molecular imaging have been reviewed below.

In the last 20 years, a number of selective A_{2A}R antagonists have been developed and some of them are being evaluated for treatment of PD in several preclinical and clinical studies. As shown above, A_{2A}R antagonists can be divided in two main categories. i) xanthine-type compounds and ii) polyheterocyclic compounds.

The xanthine scaffold present in the most popular compound caffeine represented an important starting point for the development of antagonists for this class of receptors.⁸⁸ Extensive structure-activity relationship studies among the xanthine derivatives have already led to the clinical candidates KW6002 and TMSX, both of which were labeled with carbon-11.^{39, 40, 64} However, there is an increasing interest among researchers in this field (particularly A_{2A}R) to explore other class of compounds (polyheterocyclic compounds) as potential PET antagonists because xanthine-type antagonists seriously suffer from low subtype selectivity and poor physicochemical properties such as photoisomerisation and low water solubility.^{68, 89-91} Attempts have been made to improve water solubility of styrylxanthines such as introduction of polar groups on phenyl ring and prodrug approach with the aim not to compromise on affinity and selectivity (for example, the introduction of the sulfonate group on the phenyl ring of DMPX and MSX-3, a phosphate prodrug of MSX-2) (Figure 4).⁹² All these studies appeal strongly to reconsider the xanthine family for A_{2A}R. Later, tricyclic xanthines and aminopyridopyrimidinedione derivatives (xanthine-adenine hybrid structures) were developed.^{91, 93-96} However, lack of affinity and selectivity made them unsuitable for further development (Figure 4).

Presence of adenine base, a partial adenosine structure, in CGS15943 was an important starting point for the investigation of nonxanthine compounds.⁹² The 2-alkynyl-substituted adenine derivative and 1,2,3-triazole adenine derivative are the most potent compounds of this class exhibiting high A_{2A}R affinity (K_i, 0.95 nM and 4.7 nM, respectively) but moderate selectivity of A_{2A} versus A₁ receptors (Figure 4).^{91, 97} Later, a bioisoster of CGS15943 showing good affinity and enhanced selectivity towards A_{2A}R was reported.⁹⁸ Pyrazolo-triazolo-pyrimidine nucleus was introduced as lead tricyclic molecule to determine A_{2A}R affinity and selectivity. Selected compounds of this class are SCH58621 and SCH442416 (Figure 4). These compounds proved to have very good affinity and selectivity for both rat and human A_{2A}Rs (Table 3). The phenylethyl group of

SCH58621 was substituted with an arylpiperazine ethyl group to obtain a new series of nonxanthines with high potency and selectivity for A_{2A}R. Poor water solubility is also a limiting factor for these nonxanthines.⁹² However, further introduction of ether substituents gave derivatives with high affinity, selectivity and improved water solubility (SCH420814). Synthetic routes to various pyrazolo[4,3-e] [1,2,4]triazolo[1,5-c]pyrimidin-5-amine analogs were described.^{81, 82, 98-101} The methoxy group of SCH442416 was replaced with various conjugates like ester, carboxylic acid, amines, alkyne, fluoropropyl and fluorophore reporter groups. The fluoropropyl derivative of SCH442416 might be useful as a PET ligand after labeling with ¹⁸F because of its good affinity (Table 3) towards A_{2A}R.⁸² Pyrazole of the tricyclic moiety was replaced by an imidazole ring resulting in enhanced potency and selectivity (isomer of SCH420814).¹⁰² Researchers from Jülich synthesized and tested oxazolopyrimidines, derived from the triazolotriazine derivative, ZM241385 and triazoloquinoxalone series as potential PET tracers for imaging brain A_{2A}Rs. *In vitro* ARG experiments indicated high nonspecific binding which conceals specific binding to A_{2A}Rs. In addition, triazoloquinoxaline derivatives lack good selectivity for A_{2A}R over A₁R and have poor water solubility.^{103,104}

ADENOSINE A_{2A} ANTAGONISTS AS PET TRACERS

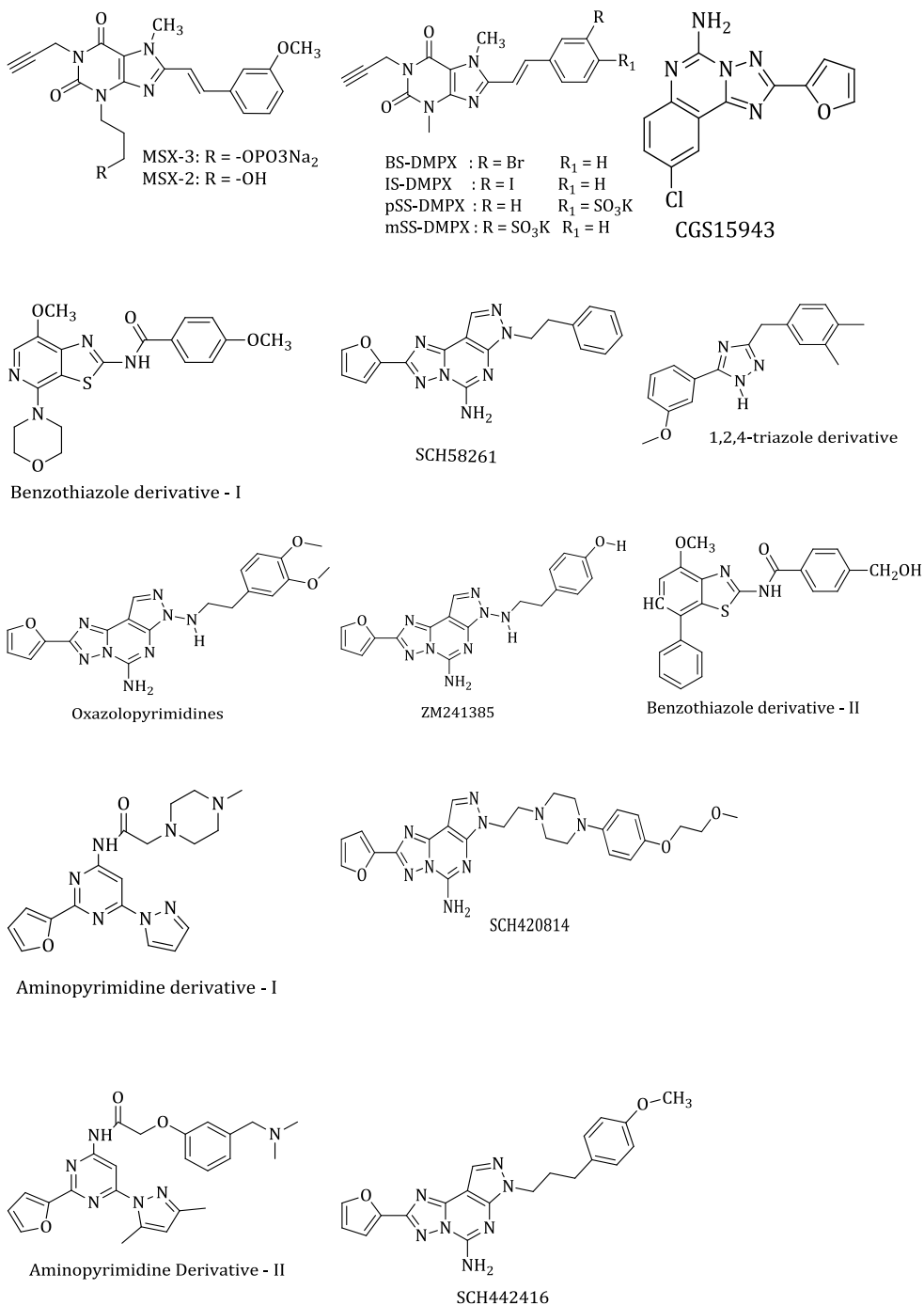


Figure 4. Adenosine A_{2A} receptor antagonists

Many groups described several very potent and highly subtype-selective bicyclic and tricyclic nonxanthine analogs.^{83, 105-107} Unfortunately, all the structures are not amenable to radiolabelling with ¹¹C or ¹⁸F. However, more suitable candidates are: 2-[2-furanyl]-7-phenyl[1,2,4]triazolopyrimidineamine derivatives^{108, 109}, triazolopurinamine analogs⁹⁷, piperazine diamino and triamino derivatives of triazolotriazine, arylpiperazine derivatives of pyrazolotriazolopyrimidines¹⁰¹ and triazolopyrimidine^{91, 106, 109-113} which can be labeled both with ¹¹C (potential radiolabelling position on -NCH₃ or -OCH₃ groups) or ¹⁸F (fluorine atom on aromatic ring). In addition to the above compounds, aminopyrimidine derivatives, benzothiazole, thiazolopyridine and 1,2,4-triazole derivatives have emerged as potential new lead molecules for the development of A_{2A}R antagonists⁹¹ (Table 4).

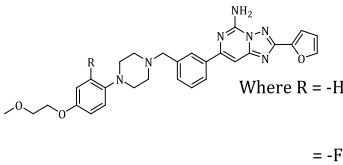
To identify potent potential PET ligands, computer-aided drug design is of great value. Scientists made use of molecular docking software to predict the binding orientation of small molecules to their protein targets. Hence *in silico* docking is useful in rational drug design. Several A_{2A}R antagonists were docked using different software packages and protein data bank (PDB) crystal structures by different groups. A cocrystal structure of the A_{2A}R with the selective antagonist ZM241385 (PDB Identification number: 3EML) has been reported.¹¹⁴ Important characteristic receptor-ligand interactions include H-bond interactions with Asn253 and Glu269 and hydrophobic interaction with Phe168.

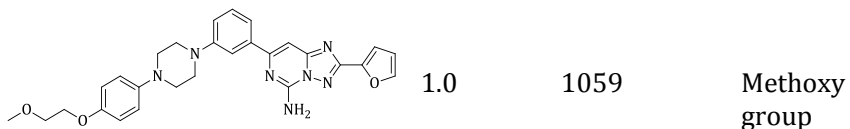
Another study reported docking analysis of structurally diverse A_{2A}R antagonists with the aim to characterize the binding sites of A_{2A}R. They identified five transmembrane helices (TM2, TM3, TM5, TM6, and TM7), which surround the active binding site of all A_{2A}R antagonists.¹¹⁵ These results were consistent with site-directed mutagenesis studies.¹¹⁶ The three most potent xanthine analogs (KW6002, KF17837 and BS-DMPX) were first subjected to a docking study to validate the residues involved in stable binding interactions between antagonists and the receptor. All three xanthine type

antagonists have similar binding mode patterns. Binding energy scores of all nonxanthine analogs were in agreement with receptor affinity (K_i) of the molecules. Moreover, all compounds shared similar $\pi - \pi$ interactions between receptor aromatic residues and antagonists.¹¹⁵ Critical interaction for xanthine analogs was hydrogen-bonding formation between Ser277 of $A_{2A}R$ with the carbonyl group of ligands whereas for nonxanthine compounds the free NH_2 groups and the oxygen in the furan ring are important features for binding to the receptor.¹¹⁵

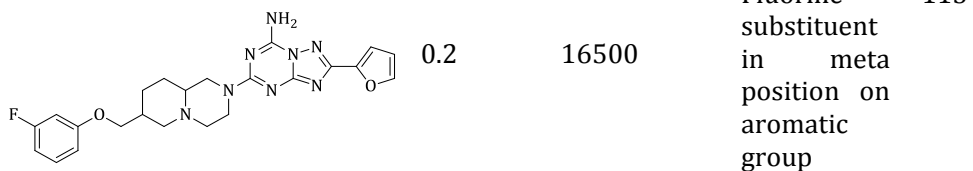
Bidhan *et al.* studied in detail pyrazolotriazolopyrimidine (SCH442416) derivatives by induced fit docking methodology using GLIDE software and they reported the 2-fluoroethyl derivative of SCH442416 as a highly selective PET tracer for $A_{2A}R$.⁸¹ This fluorinated analogue showed a similar binding mode as ZM241385 in the crystal structure whereas key interactions with important amino acids in the active site cavity such as Asn253, Phe168 and Glu169 were maintained.⁸¹ The *in silico* results were fully substantiated with *in vivo* results.⁸¹

Table 4. Development of Novel Medicinal Lead Compounds as Potential PET Tracers

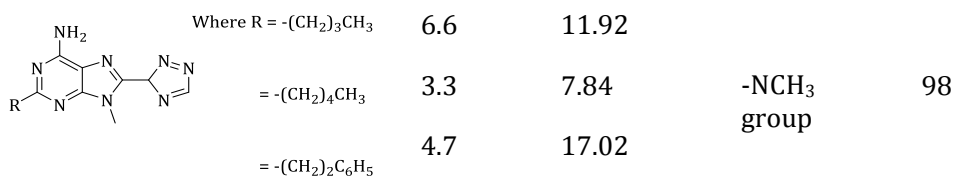
Compounds	$A_{2A}R$ Binding affinity (K_i , nM)	Selectivity (A_1/A_{2A})	Potential position for [^{11}C] or [^{18}F] labelling	Ref
<u>2-[2-(2-Furanyl)-7-phenyl[1,2,4]triazolopyrimidinamine derivatives</u>  Where R = -H = -F	2.8	601	Methoxy group	109
	2.7	642	Methoxy and fluorine atoms	110



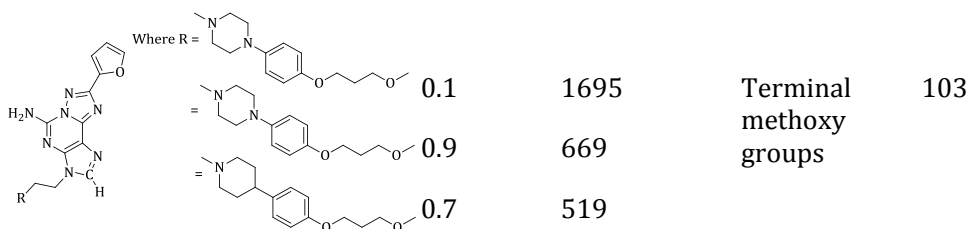
Bicyclic piperazine derivatives of Triazolotriazine



9H-purinyamine analogs

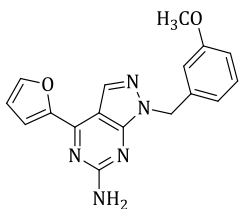


Triazolopurinamine analogs



Pyrazolopyrimidine

92



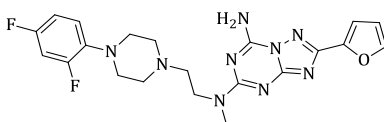
2.0

-

Methoxy group

2

Piperazine derivatives of Triazolotriazine

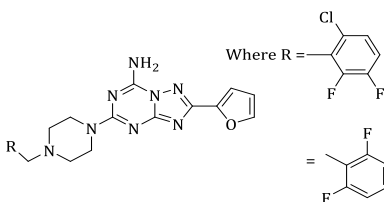


4.0

205

Fluorine atoms on aromatic ring and -NCH₃

111

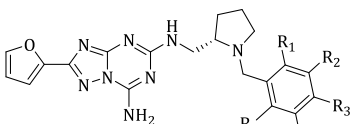


100

Fluorine substituents on aromatic ring

433

Diamino derivatives of triazolotriazines



5

250

Fluorine atoms on benzene ring

112

Where R₁ = R₂ = -F and R₃ = R₄ = R₅ = -H

8

250

R₁ = R₃ = R₄ = -F and R₂ = R₅ = -H

2

800

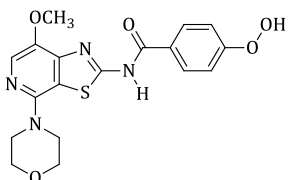
R₁ = R₃ = R₅ = -F and R₂ = -H

4

250

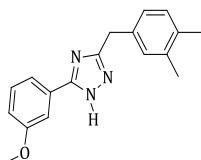
R₂ = R₅ = -F, R₁ = -Cl and R₃ = -H

Thiazolopyridine



3 450 Methoxy group 92

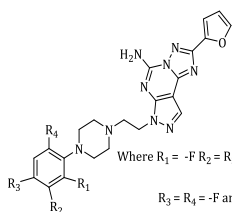
Phenyl substituted triazole



20 69 Methoxy group 92

93

Arylpiperazine derivatives of pyrazolotriazolopyrimidines



Where R₁ = -F R₂ = R₃ = R₄ = -H

R₃ = R₄ = -F and R₁ = R₂ = -H

R₁ = R₂ = R₃ = -F and R₄ = -H

R₁ = R₂ = R₄ = -H and R₃ = -OCH₂CH₂OCH₃

R₁ = R₂ = -H, R₄ = -F and R₃ = -OCH₂CH₂OCH₃

R₁ = R₂ = R₄ = -H, and R₃ = -OCH₂CH₂OCH₃

0.6 894 Fluorine atoms on aromatic ring

0.6 1600

0.6 1498

1.1 1340

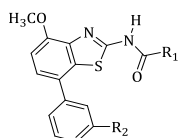
0.4 1736 Methoxy group

0.6 1158

102

118

Benzothiazoles



R₁ = R₂ = -H

R₁ = R₂ = -NH₂

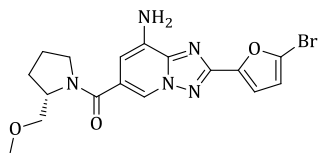
R₁ = R₂ = -NH₂

0.5 - Methoxy group 92

0.8 - 93

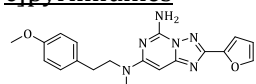
1.0 -

Triazolopyridine

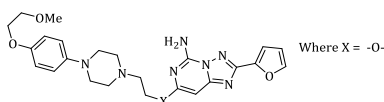


16 65.8 Methoxy group 92

1,2,4-Triazolo[1,5-c]pyrimidines



1.8 473 Methoxy group 118



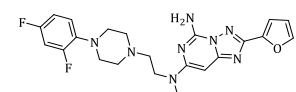
2.8 405

= -S-

1.5 965

= -NCH₃-

1.0 1580



2.5 694

Methoxy group

Methoxy group

Fluorine atoms on benzene ring & -NCH₃

Summary and Future Perspectives

All the xanthine analogs including [¹¹C]TMSX proved to be not very suitable for molecular imaging mainly because of low signal to noise ratio, barely visible receptor density and high degree of nonspecific binding. All xanthine A_{2A} antagonists e.g., [¹¹C]KF17837, [¹¹C]TMSX, [¹¹C]KF21213, [¹¹C]KF19631 and [¹¹C]KW6002 indicated multiple binding sites and undefined binding sites are responsible for extrastriatal retention of radioactivity.^{46,64,66, 72, 77} Through saturation binding experiment, previous studies showed that multiple binding sites and undefined binding sites of xanthine compounds are quite different from those of nonxanthine analogue's binding sites.^{54, 59, 65, 70, 75} Photoisomerisation problem and specific selectivity towards A_{2A}R limits xanthine analogue use.

To overcome all the problems associated with xanthine type compounds, polyheterocyclic compounds were proposed, developed and tested. The regional distribution of radioactivity, the good signal-to-noise ratio and low amounts of radioactive metabolites in the brain all suggested that [¹¹C]SCH442416 was the first nonxanthine ligand being suitable for mapping of A_{2A}R using PET.^{80, 84} However, researchers aim to develop tracers with larger striatum/cerebellum ratios than [¹¹C]SCH442416 and higher absolute values of brain uptake both in experimental animals and humans, which are important for good count statistics. In this regard, [¹⁸F]fluoroethyl SCH442416 derivative was evaluated in 6-OHDA PD rat model.⁴⁸ Preliminary findings indicated that [¹¹C]SCH442416 and its [¹⁸F]fluoroethyl SCH442416 are good tracers for mapping cerebral A_{2A}Rs.^{48, 80, 84}

Some studies performed by the Jülich group^{103, 104} have indicated that A_{2A}R antagonists can be very potent and have appropriate lipophilicity for crossing BBB, yet fail as radiopharmaceuticals because of high nonspecific binding. Furthermore, receptor subtype selectivity plays an important role in PET. It may thus be a challenge to develop PET ligands with better *in vivo* properties than [¹¹C]TMSX or [¹¹C]SCH442416. However, recently, newly developed F-18 labeled SCH442416 derivatives are under consideration mainly because of longer physical half-life (109.8 vs 20.4 min) allowing tracer distribution to remote imaging centers without cyclotron facilities and can achieve longer biodistribution and scanning times.^{81, 82} Aminopyrimidine derivatives, benzothiazole, thiazolopyridine and 1,2,4-triazole derivatives have emerged as potential new lead molecules for the development of A_{2A}R antagonists and PET tracers for both therapeutic and diagnostic applications.⁹¹ Further studies with these compounds and other fluorinated analogues of SCH442416 are warranted. Computer-aided drug design and rapid developments in medicinal chemistry may yield better radioligands for A_{2A}R visualization and quantification in the nearest future.

References

1. Fredholm, B. B.; Abbracchio, M. P.; Burnstock, G.; Daly, J. W.; Harden, T. K.; Jacobson, K. A.; Leff, P.; Williams, M. Nomenclature and classification of purinoceptors. *Pharmacol. Rev.* **1994**, *46*, 143–156.
2. Hess, S. Recent advances in adenosine receptor antagonist research. *Expert Opin. Ther. Patents* **2001**, *11*, 1533–1561.
3. Ishiwata, K.; Kimura, Y.; De Vries, Erik F. J.; Elsinga, P. H. PET Tracers for mapping adenosine receptors as probes for diagnosis of CNS disorders. *Cent. Nerv. Syst. Agents Med. Chem.* **2007**, *7*, 57–77.
4. Palmer, T. M.; Stiles, G. L. Adenosine receptors. *Neuropharmacology* **1995**, *34*, 683–694.
5. Linden, J. Adenosine in tissue protection and tissue regeneration. *Mol. Pharmacol.* **2005**, *67*, 1385–1387.
6. Dunwiddie, T.; Masino, S. The role and regulation of adenosine in the central nervous system. *Annu. Rev. Neurosci.* **2001**, *24*, 31–55.
7. von Lubitz, D. K. Adenosine in the treatment of stroke: yes, maybe, or absolutely not? *Expert Opin. Investig. Drugs* **2001**, *10*, 619–632.
8. Ribeiro, J. A.; Sebastião, A. M.; de Mendonça, A. Adenosine receptors in the nervous system: pathophysiological implications. *Prog. Neurobiol.(N.Y.)* **2002**, *68*, 377–392.
9. Jacobson, K. A.; Gao, Z. Adenosine receptors as therapeutic targets. *Nat Rev Drug Discov* **2006**, *5*, 247–264.
10. El Yacoubi, M.; Costentin, J.; Vaugeois, J. M. Adenosine A2A receptors and depression. *Neurology* **2003**, *61*, S82– S87.

11. Holschbach, M. H.; Olsson, R. A.; Bier, D.; Wutz, W.; Sihver, W.; Schüller, M.; Palm, B.; Coenen, H. H. Synthesis and evaluation of no-carrier-added 8-cyclopentyl-3-(3-[¹⁸F]fluoropropyl)-1-propylxanthine ([¹⁸F]CPFPX): A potent and selective A₁-adenosine receptor antagonist for *in vivo* imaging. *J. Med. Chem.* **2002**, *45*, 5150–5156.
12. Paul, S.; Elsinga, P. H.; Ishiwata, K.; Dierckx, R. A.; van Waarde, A. Adenosine A₁ receptors in the central nervous system: their functions in health and disease, and possible elucidation by PET imaging. *Curr. Med. Chem.* **2011**, *18*, 4820–4835.
13. Sebastião, A. M.; Ribeiro, J. A. Triggering neurotrophic factor actions through adenosine A_{2A} receptor activation: implications for neuroprotection. *Br. J. Pharmacol.* **2009**, *158*, 15–22.
14. Ralevic, V.; Burnstock, G. Receptors for purines and pyrimidines. *Pharmacol. Rev.* **1998**, *50*, 413–492.
15. Ji, X. D.; Stiles, G. L.; van Galen, P. J.; Jacobson, K. A. Characterization of human striatal A₂-adenosine receptors using radioligand binding and photoaffinity labeling. *J. Recept. Res.* **1992**, *12*, 149–169.
16. Goodman, R. R.; Synder, S. H. Autoradiographic localization of adenosine receptors in rat brain using [³H]cyclohexyladenosine. *J. Neurosci.* **1982**, *2*, 1230–1241.
17. Lindstrom, K.; Ongini, E.; Fredholm, B. B. The selective adenosine A_{2A} receptor antagonist SCH 58261 discriminates between two different binding sites for [³H]-CGS 21680 in the rat brain. *Naunyn-Schmiedebergs Arch. Pharmacol.* **1996**, *354*, 539–541.
18. Ongini, E.; Fredholm, B. B. Pharmacology of adenosine A_{2A} receptors. *Trends Pharmacol. Sci.* **1996**, *17*, 364–372.

19. Fredholm, B. B.; IJzerman, A. P.; Jacobson, K. A.; Linden, J.; Muller, C. E. International Union of Basic and Clinical Pharmacology. LXXXI. Nomenclature and classification of adenosine receptors--an update. *Pharmacol. Rev.* **2011**, *63*, 1–34.
20. Moreau, J.; Huber, G. Central adenosine A_{2A} receptors: an overview. *Brain Res. Rev.* **1999**, *31*, 65–82.
21. Horstink, M.; Tolosa, E.; Bonuccelli, U.; Deuschl, G.; Friedman, A.; Kanovsky, P.; Larsen, J. P.; Lees, A.; Oertel, W.; Poewe, W.; Rascol, O.; Sampaio, C. Review of the therapeutic management of Parkinson's disease. Report of a joint task force of the European Federation of Neurological Societies (EFNS) and the Movement Disorder Society-European Section (MDS-ES). Part II: late (complicated) Parkinson's disease. *Eur. J. Neurol.* **2006**, *13*, 1186–1202.
22. Horstink, M.; Tolosa, E.; Bonuccelli, U.; Deuschl, G.; Friedman, A.; Kanovsky, P.; Larsen, J. P.; Lees, A.; Oertel, W.; Poewe, W.; Rascol, O.; Sampaio, C. Review of the therapeutic management of Parkinson's disease. Report of a joint task force of the European Federation of Neurological Societies and the Movement Disorder Society? European Section. Part I: early (uncomplicated) Parkinson's disease. *Eur. J. Neurol.* **2006**, *13*, 1170–1185.
23. Fabbrini, G.; Brotchie, J. M.; Grandas, F.; Nomoto, M.; Goetz, C. G. Levodopa-induced dyskinesias. *Mov. Disord.* **2007**, *22*, 1379–1389; quiz 1523.
24. Jankovic, J. Motor fluctuations and dyskinesias in Parkinson's disease: clinical manifestations. *Mov. Disord.* **2005**, *20 Suppl 11*, S11-6.
25. Jankovic, J.; Stacy, M. Medical management of levodopa-associated motor complications in patients with Parkinson's disease. *CNS Drugs* **2007**, *21*, 677–692.

26. Morelli, M.; Carta, A. R.; Jenner, P. Adenosine A_{2A} receptors and Parkinson's disease. *Handb. Exp. Pharmacol.* **2009**, (193), 589–615.
27. Ferre, S.; Karcz-Kubicha, M.; Hope, B. T.; Popoli, P.; Burgueno, J.; Gutierrez, M. A.; Casado, V.; Fuxe, K.; Goldberg, S. R.; Lluis, C.; Franco, R.; Ciruela, F. Synergistic interaction between adenosine A_{2A} and glutamate mGlu5 receptors: implications for striatal neuronal function. *Proc. Natl. Acad. Sci. U. S. A.* **2002**, 99, 11940–11945.
28. Coccorello, R.; Breyse, N.; Amalric, M. Simultaneous blockade of adenosine A_{2A} and metabotropic glutamate mGlu5 receptors increase their efficacy in reversing Parkinsonian deficits in rats. *Neuropsychopharmacology* **2004**, 29, 1451–1461.
29. Schiffmann, S. N.; Fisone, G.; Moresco, R.; Cunha, R. A.; Ferre, S. Adenosine A_{2A} receptors and basal ganglia physiology. *Prog. Neurobiol.* **2007**, 83, 277–292.
30. Ferré, S.; Goldberg, S. R.; Lluis, C.; Franco, R. Looking for the role of cannabinoid receptor heteromers in striatal function. *Neuropharmacology* **2009**, 56, Supplement 1, 226–234.
31. Marcellino, D.; Carriba, P.; Filip, M.; Borgkvist, A.; Frankowska, M.; Bellido, I.; Tanganelli, S.; Muller, C. E.; Fisone, G.; Lluis, C.; Agnati, L. F.; Franco, R.; Fuxe, K. Antagonistic cannabinoid CB₁/dopamine D₂ receptor interactions in striatal CB₁/D₂ heteromers. A combined neurochemical and behavioral analysis. *Neuropharmacology* **2008**, 54, 815–823.
32. Olah, M. E.; Stiles, G. L. Adenosine receptor subtypes: characterization and therapeutic regulation. *Annu. Rev. Pharmacol. Toxicol.* **1995**, 35, 581–606.
33. Shryock, J. C.; Snowdy, S.; Baraldi, P. G.; Cacciari, B.; Spalluto, G.; Monopoli, A.; Ongini, E.; Baker, S. P.; Belardinelli, L. A_{2A}-

- adenosine receptor reserve for coronary vasodilation. *Circulation* **1998**, *98*, 711–718.
34. Dobson, J. G., Jr; Fenton, R. A. Adenosine A₂ receptor function in rat ventricular myocytes. *Cardiovasc. Res.* **1997**, *34*, 337–347.
35. Mizuno, M.; Kimura, Y.; Tokizawa, K.; Ishii, K.; Oda, K.; Sasaki, T.; Nakamura, Y.; Muraoka, I.; Ishiwata, K. Greater adenosine A_{2A} receptor densities in cardiac and skeletal muscle in endurance-trained men: a [11C]TMSX PET study. *Nucl. Med. Biol.* **2005**, *32*, 831–836.
36. Bauer, A.; Ishiwata, K. Adenosine receptor ligands and PET imaging of the CNS. *Handb. Exp. Pharmacol.* **2009**, *193*, 617–642.
37. Holschbach, M. H.; Olsson, R. A. Applications of adenosine receptor ligands in medical imaging by positron emission tomography. *Curr. Pharm. Des.* **2002**, *8*, 2345–2352.
38. Brooks, D. J. Morphological and functional imaging studies on the diagnosis and progression of Parkinson's disease. *J. Neurol.* **2000**, *247*, II11–II18.
39. Ishiwata, K.; Kawamura, K.; Kimura, Y.; Oda, K.; Ishii, K. Potential of an adenosine A_{2A} receptor antagonist [11C]TMSX for myocardial imaging by positron emission tomography: a first human study. *Ann. Nucl. Med.* **2003**, *17*, 457–462.
40. Ishiwata, K.; Mizuno, M.; Kimura, Y.; Kawamura, K.; Oda, K.; Sasaki, T.; Nakamura, Y.; Muraoka, I.; Ishii, K. Potential of [11C]TMSX for the evaluation of adenosine A_{2A} receptors in the skeletal muscle by positron emission tomography. *Nucl. Med. Biol.* **2004**, *31*, 949–956.
41. Heinonen, I.; Nesterov, S. V.; Liukko, K.; Kemppainen, J.; Någren, K.; Luotolahti, M.; Virsu, P.; Oikonen, V.; Nuutila, P.;

- Kujala, U. M.; Kainulainen, H.; Boushel, R.; Knuuti, J.; Kalliokoski, K. K. Myocardial blood flow and adenosine A_{2A} receptor density in endurance athletes and untrained men. *J. Physiol.* **2008**, *586*, 5193–5202.
42. Mishina, M.; Kimura, Y.; Naganawa, M.; Ishii, K.; Oda, K.; Sakata, M.; Toyohara, J.; Kobayashi, S.; Katayama, Y.; Ishiwata, K. Differential effects of age on human striatal adenosine A_1 and A_{2A} receptors. *Synapse* **2012**, *66*, 832–839.
43. Mishina, M.; Ishiwata, K.; Kimura, Y.; Naganawa, M.; Oda, K.; Kobayashi, S.; Katayama, Y.; Ishii, K. Evaluation of distribution of adenosine A_{2A} receptors in normal human brain measured with [11C]TMSX PET. *Synapse* **2007**, *61*, 778–784.
44. Naganawa, M.; Kimura, Y.; Mishina, M.; Manabe, Y.; Chihara, K.; Oda, K.; Ishii, K.; Ishiwata, K. Quantification of adenosine A_{2A} receptors in the human brain using [11C]TMSX and positron emission tomography. *Eur. J. Nucl. Med. Mol. Imaging* **2007**, *34*, 679–687.
45. Mishina, M.; Ishiwata, K.; Naganawa, M.; Kimura, Y.; Kitamura, S.; Suzuki, M.; Hashimoto, M.; Ishibashi, K.; Oda, K.; Sakata, M.; Hamamoto, M.; Kobayashi, S.; Katayama, Y.; Ishii, K. Adenosine A_{2A} receptors measured with [11C]TMSX PET in the striata of Parkinson's disease patients. *PLoS ONE* **2011**, *6*(2), e17338.
46. Brooks, D. J.; Doder, M.; Osman, S.; Luthra, S. K.; Hirani, E.; Hume, S.; Kase, H.; Kilborn, J.; Martindill, S.; Mori, A. Positron emission tomography analysis of [11C]KW-6002 binding to human and rat adenosine A_{2A} receptors in the brain. *Synapse* **2008**, *62*, 671–681.
47. Matsuya, T.; Takuma, K.; Sato, K.; Asai, M.; Murakami, Y.; Miyoshi, S.; Noda, A.; Nagai, T.; Mizoguchi, H.; Nishimura, S.; Yamada, K. Synergistic effects of adenosine A_{2A} antagonist and L-DOPA on rotational behaviors in 6-hydroxydopamine-

- induced hemi-Parkinsonian mouse model. *J. Pharmacol. Sci.* **2007**, *103*, 329–332.
48. Bhattacharjee, A. K.; Lang, L.; Jacobson, O.; Shinkre, B.; Ma, Y.; Niu, G.; Trenkle, W. C.; Jacobson, K. A.; Chen, X.; Kiesewetter, D. O. Striatal adenosine A_{2A} receptor-mediated positron emission tomographic imaging in 6-hydroxydopamine-lesioned rats using [(18)F]-MRS5425. *Nucl. Med. Biol.* **2011**, *38*, 897–906.
49. Ramlackhansingh, A. F.; Bose, S. K.; Ahmed, I.; Turkheimer, F. E.; Pavese, N.; Brooks, D. J. Adenosine 2A receptor availability in dyskinetic and nondyskinetic patients with Parkinson disease. *Neurology* **2011**, *76*, 1811–1816.
50. Brooks, D. J.; Papapetropoulos, S.; Vandenhende, F.; Tomic, D.; He, P.; Coppel, A.; O'Neill, G. An open-label, positron emission tomography study to assess adenosine A_{2A} brain receptor occupancy of vipadenant (BIIB014) at steady-state levels in healthy male volunteers. *Clin. Neuropharmacol.* **2010**, *33*, 55–60.
51. Burnstock, G. Purinergic signalling and disorders of the central nervous system. *Nat. Rev. Drug Discov.* **2008**, *7*, 575–590.
52. Baraldi, P. G.; Tabrizi, M. A.; Gessi, S.; Borea, P. A. Adenosine receptor antagonists: translating medicinal chemistry and pharmacology into clinical utility. *Chem. Rev.* **2008**, *108*, 238–263.
53. Xu, K.; Bastia, E.; Schwarzschild, M. Therapeutic potential of adenosine A_{2A} receptor antagonists in Parkinson's disease. *Pharmacol. Ther.* **2005**, *105*, 267–310.
54. Hauser, R. A.; Schwarzschild, M. A. Adenosine A_{2A} receptor antagonists for Parkinson's disease: rationale, therapeutic potential and clinical experience. *Drugs Aging* **2005**, *22*, 471–482.

55. Okusa, M. D. A_{2A} adenosine receptor: a novel therapeutic target in renal disease. *Am. J. Physiol. Renal Physiol.* **2002**, *282*, F10-8.
56. Pinna, A.; Wardas, J.; Simola, N.; Morelli, M. New therapies for the treatment of Parkinson's disease: adenosine A_{2A} receptor antagonists. *Life Sci.* **2005**, *77*, 3259–3267.
57. Pinna, A. Novel investigational adenosine A_{2A} receptor antagonists for Parkinson's disease. *Expert Opin. Investig. Drugs* **2009**, *18*, 1619–1631.
58. Press, N. J.; Gessi, S.; Borea, P. A.; Polosa, R. Therapeutic potential of adenosine receptor antagonists and agonists. *Expert Opin. Ther. Pat.* **2007**, *17*, 979–991.
59. Cristalli, G.; Cacciari, B.; Dal Ben, D.; Lambertucci, C.; Moro, S.; Spalluto, G.; Volpini, R. Highlights on the development of A_{2A} adenosine receptor agonists and antagonists. *ChemMedChem* **2007**, *2*, 260–281.
60. Ishiwata, K.; Noguchi, J.; Toyama, H.; Sakiyama, Y.; Koike, N.; Ishii, S.; Oda, K.; Endo, K.; Suzuki, F.; Senda, M. Synthesis and preliminary evaluation of [11C]KF17837, a selective adenosine A_{2A} antagonist. *Appl. Radiat. Isot.* **1996**, *47*, 507–511.
61. Ishiwata, K.; Noguchi, J.; Wakabayashi, S.; Shimada, J.; Ogi, N.; Nariai, T.; Tanaka, A.; Endo, K.; Suzuki, F.; Senda, M. 11C-labeled KF18446: a potential central nervous system adenosine A_{2A} receptor ligand. *J. Nucl. Med.* **2000**, *41*, 345–354.
62. Stone-Elander, S.; Thorell, J.; Eriksson, L.; Fredholm, B. B.; Ingvar, M. In vivo biodistribution of [N-11C-methyl]KF 17837 using 3-D-PET: evaluation as a ligand for the study of adenosine A_{2A} receptors. *Nucl. Med. Biol.* **1997**, *24*, 187–191.

63. Marian, T.; Boros, I.; Lengyel, Z.; Balkay, L.; Horvath, G.; Emri, M.; Sarkadi, E.; Szentmiklosi, A. J.; Fekete, I.; Tron, L. Preparation and primary evaluation of [¹¹C]CSC as a possible tracer for mapping adenosine A_{2A} receptors by PET. *Appl. Radiat. Isot.* **1999**, *50*, 887–893.
64. Hirani, E.; Gillies, J.; Karasawa, A.; Shimada, J.; Kase, H.; Opacka-Juffry, J.; Osman, S.; Luthra, S. K.; Hume, S. P.; Brooks, D. J. Evaluation of [4-O-methyl-(¹¹C)]KW-6002 as a potential PET ligand for mapping central adenosine A_{2A} receptors in rats. *Synapse* **2001**, *42*, 164–176.
65. Kawamura, K.; Ishiwata, K. Improved synthesis of [¹¹C]SA4503, [¹¹C]MPDX and [¹¹C]TMSX by use of [¹¹C]methyl triflate. *Ann. Nucl. Med.* **2004**, *18*, 165–168.
66. Wang, W.; Ishiwata, K.; Nonaka, H.; Ishii, S.; Kiyosawa, M.; Shimada, J.; Suzuki, F.; Senda, M. Carbon-11-labeled KF21213: a highly selective ligand for mapping CNS adenosine A_{2A} receptors with positron emission tomography. *Nucl. Med. Biol.* **2000**, *27*, 541–546.
67. Jacobson, K. A.; Gallo-Rodriguez, C.; Melman, N.; Fischer, B.; Maillard, M.; van Bergen, A.; van Galen, P. J.; Karton, Y. Structure-activity relationships of 8-styrylxanthines as A₂-selective adenosine antagonists. *J. Med. Chem.* **1993**, *36*, 1333–1342.
68. Nonaka, Y.; Shimada, J.; Nonaka, H.; Koike, N.; Aoki, N.; Kobayashi, H.; Kase, H.; Yamaguchi, K.; Suzuki, F. Photoisomerization of a potent and selective adenosine A₂ antagonist, (E)-1,3-Dipropyl-8-(3,4-dimethoxystyryl)-7-methylxanthine. *J. Med. Chem.* **1993**, *36*, 3731–3733.
69. Nonaka, H.; Ichimura, M.; Takeda, M.; Nonaka, Y.; Shimada, J.; Suzuki, F.; Yamaguchi, K.; Kase, H. KF17837 ((E)-8-(3,4-dimethoxystyryl)-1,3-dipropyl-7-methylxanthine) a potent

and selective adenosine A₂ receptor antagonist. *Eur. J. Pharm-Molec. Ph* **1994**, *267*, 335–341.

70. Shimada, J.; Suzuki, F.; Nonaka, H.; Ishii, A.; Ichikawa, S. (E)-1,3-Dialkyl-7-methyl-8-(3,4,5-trimethoxy-styryl)xanthines: Potent and selective adenosine A₂ antagonists [2]. *J. Med. Chem.* **1992**, *35*, 2342–2345.
71. Ishiwata, K.; Sakiyama, Y.; Sakiyama, T.; Shimada, J.; Toyama, H.; Oda, K.; Suzuki, F.; Senda, M. Myocardial adenosine A_{2A} receptor imaging of rabbit by PET with [11C]KF17837. *Ann. Nucl. Med.* **1997**, *11*, 219–225.
72. Noguchi, J.; Ishiwata, K.; Wakabayashi, S.; Nariai, T.; Shumiya, S.; Ishii, S.; Toyama, H.; Endo, K.; Suzuki, F.; Senda, M. Evaluation of carbon-11-labeled KF17837: a potential CNS adenosine A_{2A} receptor ligand. *J. Nucl. Med.* **1998**, *39*, 498–503.
73. Cunha, R. A.; Johansson, B.; Constantino, M. D.; Sebastiao, A. M.; Fredholm, B. B. Evidence for high-affinity binding sites for the adenosine A_{2A} receptor agonist [3H] CGS 21680 in the rat hippocampus and cerebral cortex that are different from striatal A_{2A} receptors. *Naunyn-Schmiedebergs Arch. Pharmacol.* **1996**, *353*, 261–271.
74. Parkinson, F. E.; Fredholm, B. B. Autoradiographic evidence for G-protein coupled A₂-receptors in rat neostriatum using [3H]-CGS 21680 as a ligand. *Naunyn-Schmiedebergs Arch. Pharmacol.* **1990**, *342*, 85–89.
75. Martinez-Mir, M. I.; Probst, A.; Palacios, J. M. Adenosine A₂ receptors: selective localization in the human basal ganglia and alterations with disease. *Neuroscience* **1991**, *42*, 697–706.
76. Ishiwata, K.; Shimada, J.; Wang, W. F.; Harakawa, H.; Ishii, S.; Kiyosawa, M.; Suzuki, F.; Senda, M. Evaluation of iodinated and brominated [11C]styrylxanthine derivatives as in vivo

radioligands mapping adenosine A_{2A} receptor in the central nervous system. *Ann. Nucl. Med.* **2000**, *14*, 247–253.

77. Ishiwata, K.; Ogi, N.; Shimada, J.; Nonaka, H.; Tanaka, A.; Suzuki, F.; Senda, M. Further characterization of a CNS adenosine A_{2A} receptor ligand [11C]KF18446 with in vitro autoradiography and *in vivo* tissue uptake. *Ann. Nucl. Med.* **2000**, *14*, 81–89.
78. Ishiwata, K.; Ogi, N.; Shimada, J.; Wang, W.; Ishii, K.; Tanaka, A.; Suzuki, F.; Senda, M. Search for PET probes for imaging the globus pallidus studied with rat brain *ex vivo* autoradiography. *Ann. Nucl. Med.* **2000**, *14*, 461–466.
79. Ishiwata, K.; Wang, W. F.; Kimura, Y.; Kawamura, K.; Ishii, K. Preclinical studies on [11C]TMSX for mapping adenosine A_{2A} receptors by positron emission tomography. *Ann. Nucl. Med.* **2003**, *17*, 205–211.
80. Todde, S.; Moresco, R. M.; Simonelli, P.; Baraldi, P. G.; Cacciari, B.; Spalluto, G.; Varani, K.; Monopoli, A.; Matarrese, M.; Carpinelli, A.; Magni, F.; Kienle, M. G.; Fazio, F. Design, radiosynthesis, and biodistribution of a new potent and selective ligand for in vivo imaging of the adenosine A_{2A} receptor system using positron emission tomography. *J. Med. Chem.* **2000**, *43*, 4359–4362.
81. Shinkre, B. A.; Kumar, T. S.; Gao, Z. G.; Deflorian, F.; Jacobson, K. A.; Trenkle, W. C. Synthesis and evaluation of 1,2,4-triazolo[1,5-c]pyrimidine derivatives as A_{2A} receptor-selective antagonists. *Bioorg. Med. Chem. Lett.* **2010**, *20*, 5690–5694.
82. Kumar, T. S.; Mishra, S.; Deflorian, F.; Yoo, L. S.; Phan, K.; Kecskes, M.; Szabo, A.; Shinkre, B.; Gao, Z. G.; Trenkle, W.; Jacobson, K. A. Molecular probes for the A_{2A} adenosine receptor based on a pyrazolo[4,3-e][1,2,4]triazolo[1,5-c]pyrimidin-5-amine scaffold. *Bioorg. Med. Chem. Lett.* **2011**, *21*, 2740–2745.

83. Baraldi, P. G.; Cacciari, B.; Romagnoli, R.; Spalluto, G.; Monopoli, A.; Ongini, E.; Varani, K.; Borea, P. A. 7-Substituted 5-amino-2-(2-furyl)pyrazolo[4,3-e]-1,2,4-triazolo[1,5-c]pyrimidines as A_{2A} adenosine receptor antagonists: a study on the importance of modifications at the side chain on the activity and solubility. *J. Med. Chem.* **2002**, *45*, 115–126.
84. Moresco, R. M.; Todde, S.; Belloli, S.; Simonelli, P.; Panzacchi, A.; Rigamonti, M.; Galli-Kienle, M.; Fazio, F. *In vivo* imaging of adenosine A_{2A} receptors in rat and primate brain using [11C]SCH442416. *Eur. J. Nucl. Med. Mol. Imaging* **2005**, *32*, 405–413.
85. Calon, F.; Dridi, M.; Hornykiewicz, O.; Bedard, P. J.; Rajput, A. H.; Di Paolo, T. Increased adenosine A_{2A} receptors in the brain of Parkinson's disease patients with dyskinesias. *Brain* **2004**, *127*, 1075–1084.
86. Mihara, T.; Noda, A.; Arai, H.; Mihara, K.; Iwashita, A.; Murakami, Y.; Matsuya, T.; Miyoshi, S.; Nishimura, S.; Matsuoka, N. Brain adenosine A_{2A} receptor occupancy by a novel A₁/A_{2A} receptor antagonist, ASP5854, in rhesus monkeys: relationship to anticataleptic effect. *J. Nucl. Med.* **2008**, *49*, 1183–1188.
87. Morelli, M.; Blandini, F.; Simola, N.; Hauser, R. A. A_{2A} receptor antagonism and dyskinesia in Parkinson's Disease. *Parkinsons Dis.* **2012**, *2012*, 8.
88. Daly, J. W.; Hide, I.; Muller, C. E.; Shamim, M. Caffeine analogs: structure-activity relationships at adenosine receptors. *Pharmacology* **1991**, *42*, 309–321.
89. Muller, C. E.; Geis, U.; Hipp, J.; Schobert, U.; Frobenius, W.; Pawlowski, M.; Suzuki, F.; Sandoval-Ramirez, J. Synthesis and structure-activity relationships of 3,7-dimethyl-1-propargylxanthine derivatives, A_{2A}-selective adenosine receptor antagonists. *J. Med. Chem.* **1997**, *40*, 4396–4405.

90. Muller, C. E.; Sandoval-Ramirez, J.; Schobert, U.; Geis, U.; Frobenius, W.; Klotz, K. N. 8-(Sulfostryl)xanthines: water-soluble A_{2A}-selective adenosine receptor antagonists. *Bioorg. Med. Chem.* **1998**, *6*, 707–719.
91. Muller, C. E.; Ferre, S. Blocking striatal adenosine A_{2A} receptors: a new strategy for basal ganglia disorders. *Recent. Pat. CNS Drug Discov.* **2007**, *2*, 1–21.
92. Cristalli, G.; Muller, C. E.; Volpini, R. Recent developments in adenosine A_{2A} receptor ligands. *Handb. Exp. Pharmacol.* **2009**, (193), 59–98.
93. Drabczynska, A.; Schumacher, B.; Muller, C. E.; Karolak-Wojciechowska, J.; Michalak, B.; Pekala, E.; Kiec-Kononowicz, K. Impact of the aryl substituent kind and distance from pyrimido[2,1-f]purindiones on the adenosine receptor selectivity and antagonistic properties. *Eur. J. Med. Chem.* **2003**, *38*, 397–402.
94. Weyler, S.; Fulle, F.; Diekmann, M.; Schumacher, B.; Hinz, S.; Klotz, K. N.; Muller, C. E. Improving potency, selectivity, and water solubility of adenosine A₁ receptor antagonists: xanthines modified at position 3 and related pyrimido[1,2,3-cd]purinediones. *ChemMedChem* **2006**, *1*, 891–902.
95. Muller, C. E. Medicinal chemistry of adenosine A₃ receptor ligands. *Curr. Top. Med. Chem.* **2003**, *3*, 445–462.
96. Bulicz, J.; Bertarelli, D. C.; Baumert, D.; Fulle, F.; Muller, C. E.; Heber, D. Synthesis and pharmacology of pyrido[2,3-d]pyrimidinediones bearing polar substituents as adenosine receptor antagonists. *Bioorg. Med. Chem.* **2006**, *14*, 2837–2849.
97. Minetti, P.; Tinti, M. O.; Carminati, P.; Castorina, M.; Di Cesare, M. A.; Di Serio, S.; Gallo, G.; Ghirardi, O.; Giorgi, F.; Giorgi, L.; Piersanti, G.; Bartoccini, F.; Tarzia, G. 2-n-Butyl-9-methyl-8-

- [1,2,3]triazol-2-yl-9H-purin-6-ylamine and analogues as A_{2A} adenosine receptor antagonists. Design, synthesis, and pharmacological characterization. *J. Med. Chem.* **2005**, *48*, 6887–6896.
98. Gatta, F.; Del Giudice, M.; Borioni, A.; Borea, P.; Dionisotti, S.; Ongini, E. Synthesis of imidazo[1,2-c]pyrazolo[4,3-e]pyrimidines, pyrazolo[4,3-e]1,2,4-triazolo[1,5-c]pyrimidines and 1,2,4-triazolo[5,1-i]purines: new potent adenosine A₂ receptor antagonists. *Eur. J. Med. Chem.* **1993**, *28*, 569–576.
99. Baraldi, P. G.; Cacciari, B.; Spalluto, G.; Bergonzoni, M.; Dionisotti, S.; Ongini, E.; Varani, K.; Borea, P. A. Design, synthesis, and biological evaluation of a second generation of pyrazolo[4,3-e]-1,2,4-triazolo[1,5-c]pyrimidines as potent and selective A_{2A} adenosine receptor antagonists. *J. Med. Chem.* **1998**, *41*, 2126–2133.
100. Baraldi, P. G.; Cacciari, B.; Spalluto, G.; Pineda de las Infantasy Villatoro, M. J.; Zocchi, C.; Dionisotti, S.; Ongini, E. Pyrazolo[4,3-e]-1,2,4-triazolo[1,5-c]pyrimidine derivatives: potent and selective A_{2A} adenosine antagonists. *J. Med. Chem.* **1996**, *39*, 1164–1171.
101. Neustadt, B. R.; Hao, J.; Lindo, N.; Greenlee, W. J.; Stamford, A. W.; Tulshian, D.; Ongini, E.; Hunter, J.; Monopoli, A.; Bertorelli, R.; Foster, C.; Arik, L.; Lachowicz, J.; Ng, K.; Feng, K. Potent, selective, and orally active adenosine A_{2A} receptor antagonists: Arylpiperazine derivatives of pyrazolo[4,3-e]-1,2,4-triazolo[1,5-c]pyrimidines. *Bioorg. Med. Chem. Lett.* **2007**, *17*, 1376–1380.
102. Silverman, L. S.; Caldwell, J. P.; Greenlee, W. J.; Kiselgof, E.; Matasi, J. J.; Tulshian, D. B.; Arik, L.; Foster, C.; Bertorelli, R.; Monopoli, A.; Ongini, E. 3H-[1,2,4]-Triazolo[5,1-i]purin-5-

amine derivatives as adenosine A_{2A} antagonists. *Bioorg. Med. Chem. Lett.* **2007**, *17*, 1659–1662.

103. Holschbach, M. H.; Bier, D.; Wutz, W.; Sihver, W.; Schuller, M.; Olsson, R. A. Derivatives of 4,6-diamino-1,2-dihydro-2-phenyl-1,2,4-triazolo[4,3-a]quinoxalin-2H-1-one: potential antagonist ligands for imaging the A_{2A} adenosine receptor by positron emission tomography (PET). *Eur. J. Med. Chem.* **2005**, *40*, 421–437.
104. Holschbach, M. H.; Bier, D.; Stusgen, S.; Wutz, W.; Sihver, W.; Coenen, H. H.; Olsson, R. A. Synthesis and evaluation of 7-amino-2-(2(3)-furyl)-5-phenylethylamino-oxazolo[5,4-d]pyrimidines as potential A_{2A} adenosine receptor antagonists for positron emission tomography (PET). *Eur. J. Med. Chem.* **2006**, *41*, 7–15.
105. Matasi, J. J.; Caldwell, J. P.; Hao, J.; Neustadt, B.; Arik, L.; Foster, C. J.; Lachowicz, J.; Tulshian, D. B. The discovery and synthesis of novel adenosine receptor (A_{2A}) antagonists. *Bioorg. Med. Chem. Lett.* **2005**, *15*, 1333–1336.
106. Vu, C. B.; Pan, D.; Peng, B.; Sha, L.; Kumaravel, G.; Jin, X.; Phadke, D.; Engber, T.; Huang, C.; Reilly, J.; Tam, S.; Petter, R. C. Studies on adenosine A_{2A} receptor antagonists: comparison of three core heterocycles. *Bioorg. Med. Chem. Lett.* **2004**, *14*, 4831–4834.
107. Dowling, J. E.; Vessels, J. T.; Haque, S.; Chang, H. X.; van Vloten, K.; Kumaravel, G.; Engber, T.; Jin, X.; Phadke, D.; Wang, J.; Ayyub, E.; Petter, R. C. Synthesis of [1,2,4]triazolo[1,5-a]pyrazines as adenosine A_{2A} receptor antagonists. *Bioorg. Med. Chem. Lett.* **2005**, *15*, 4809–4813.
108. Matasi, J. J.; Caldwell, J. P.; Zhang, H.; Fawzi, A.; Cohen-Williams, M. E.; Varty, G. B.; Tulshian, D. B. 2-(2-Furanyl)-7-phenyl[1,2,4]triazolo[1,5-c]pyrimidin-5-amine analogs:

highly potent, orally active, adenosine A_{2A} antagonists. Part 1. *Bioorg. Med. Chem. Lett.* **2005**, *15*, 3670–3674.

109. Matasi, J. J.; Caldwell, J. P.; Zhang, H.; Fawzi, A.; Higgins, G. A.; Cohen-Williams, M. E.; Varty, G. B.; Tulshian, D. B. 2-(2-Furanyl)-7-phenyl[1,2,4]triazolo[1,5-c]pyrimidin-5-amine analogs as adenosine A_{2A} antagonists: the successful reduction of hERG activity. Part 2. *Bioorg. Med. Chem. Lett.* **2005**, *15*, 3675–3678.
110. Vu, C. B.; Peng, B.; Kumaravel, G.; Smits, G.; Jin, X.; Phadke, D.; Engber, T.; Huang, C.; Reilly, J.; Tam, S.; Grant, D.; Hetu, G.; Chen, L.; Zhang, J.; Petter, R. C. Piperazine derivatives of [1,2,4]triazolo[1,5-a][1,3,5]triazine as potent and selective adenosine A_{2A} receptor antagonists. *J. Med. Chem.* **2004**, *47*, 4291–4299.
111. Vu, C. B.; Pan, D.; Peng, B.; Kumaravel, G.; Smits, G.; Jin, X.; Phadke, D.; Engber, T.; Huang, C.; Reilly, J.; Tam, S.; Grant, D.; Hetu, G.; Petter, R. C. Novel diamino derivatives of [1,2,4]triazolo[1,5-a][1,3,5]triazine as potent and selective adenosine A_{2A} receptor antagonists. *J. Med. Chem.* **2005**, *48*, 2009–2018.
112. Peng, H.; Kumaravel, G.; Yao, G.; Sha, L.; Wang, J.; Van Vlijmen, H.; Bohnert, T.; Huang, C.; Vu, C. B.; Ensinger, C. L.; Chang, H.; Engber, T. M.; Whalley, E. T.; Petter, R. C. Novel bicyclic piperazine derivatives of triazolotriazine and triazolopyrimidines as highly potent and selective adenosine A_{2A} receptor antagonists. *J. Med. Chem.* **2004**, *47*, 6218–6229.
113. Vu, C. B.; Shields, P.; Peng, B.; Kumaravel, G.; Jin, X.; Phadke, D.; Wang, J.; Engber, T.; Ayyub, E.; Petter, R. C. Triamino derivatives of triazolotriazine and triazolopyrimidine as adenosine A_{2A} receptor antagonists. *Bioorg. Med. Chem. Lett.* **2004**, *14*, 4835–4838.

114. Jaakola, V. P.; Griffith, M. T.; Hanson, M. A.; Cherezov, V.; Chien, E. Y.; Lane, J. R.; Ijzerman, A. P.; Stevens, R. C. The 2.6 angstrom crystal structure of a human A_{2A} adenosine receptor bound to an antagonist. *Science* **2008**, *322*, 1211–1217.
115. Ye, Y.; Wei, J.; Dai, X.; Gao, Q. Computational studies of the binding modes of A_{2A} adenosine receptor antagonists. *Amino Acids* **2008**, *35*, 389–396.
116. Kim, J.; Wess, J.; van Rhee, A. M.; Schoneberg, T.; Jacobson, K. A. Site-directed mutagenesis identifies residues involved in ligand recognition in the human A_{2A} adenosine receptor. *J. Biol. Chem.* **1995**, *270*, 13987–13997.
117. Neustadt, B. R.; Liu, H.; Hao, J.; Greenlee, W. J.; Stamford, A. W.; Foster, C.; Arik, L.; Lachowicz, J.; Zhang, H.; Bertorelli, R.; Fredduzzi, S.; Varty, G.; Cohen-Williams, M.; Ng, K. Potent and selective adenosine A_{2A} receptor antagonists: 1,2,4-Triazolo[1,5-c]pyrimidines. *Bioorg. Med. Chem. Lett.* **2009**, *19*, 967–97.



Development of [¹⁸F]-Labeled Pyrazolo[4,3-*e*]-1,2,4-triazolo[1,5-*c*]-pyrimidine (SCH442416) Analogs for the Imaging of Cerebral Adenosine A_{2A} Receptors with Positron Emission Tomography

Shivashankar Khanapur[†], Soumen Paul[†], Anup Shah[‡], Suresh Vatakuti[§], Michel J.B. Koole[†], Rolf Zijlma[†], Rudi A.J.O. Dierckx[†], Gert Luurtsema[†], Prabha Garg[‡], Aren van Waarde[†], Philip H. Elsinga^{*†}

[†]Department of Nuclear Medicine and Molecular Imaging, UMCG,
University of Groningen, Groningen, The Netherlands

[‡]Computer Centre, National Institute of Pharmaceutical
Education and Research, SAS Nagar, Mohali, India

[§]Department of Pharmacokinetics, Toxicology and Targeting, University of
Groningen, Groningen, The Netherlands

3

J. Med. Chem. Publication Date (Web): July 25, 2014

Abstract

Cerebral adenosine A_{2A} receptors (A_{2A}Rs) are attractive therapeutic targets for the treatment of neurodegenerative and psychiatric disorders. We developed high affinity and selective compound **8** (SCH442416) analogs as *in vivo* probes for A_{2A}Rs using PET. We observed the A_{2A}R-mediated accumulation of [¹⁸F]fluoropropyl (**[¹⁸F]-10b**) and [¹⁸F]fluoroethyl (**[¹⁸F]-10a**) derivatives of **8** in the brain. The striatum was clearly visualized in PET and *in vitro* autoradiography images of control animals and was no longer visible after pretreatment with the A_{2A}R subtype-selective antagonist KW6002. *In vitro* and *in vivo* metabolite analyses indicated the presence of hydrophilic (radio)metabolite(s), which are not expected to cross the blood-brain-barrier. **[¹⁸F]-10b** and **[¹⁸F]-10a** showed comparable striatum-to- cerebellum ratios (4.6 at 25 and 37 min postinjection, respectively) and reversible binding in rat brains. We concluded that these compounds performed equally well, but their kinetics were slightly different. These molecules are potential tools for mapping cerebral A_{2A}Rs with PET.

Introduction

Adenosine A_{2A} receptors (A_{2A}Rs) are G-protein-coupled binding sites for adenosine which stimulate adenylyl cyclase via G_S proteins and promote the formation of the second messenger, cyclic adenosine monophosphate (cAMP).¹ Adenosine activates A_{2A}Rs at nanomolar amounts and are one of the well-characterized subtype of adenosine receptors.² A_{2A}Rs are highly expressed in the basal ganglia regions of the brain, and the highest levels of A_{2A}R expression occur in the striatum, globus pallidus and substantia nigra.³⁻⁵ Lower densities of A_{2A}Rs occur in the hippocampus, cerebral cortex, amygdala, cerebellum, brainstem, and hypothalamus.⁶⁻⁹

A_{2A}R agonists are implicated in ischemia-reperfusion injury, chronic inflammation, wound healing, angiogenesis, and infectious diseases.¹⁰⁻¹² The vasodilating effect of A_{2A}R agonists (adenosine and regadenoson) has been fully characterized (see Figure 1). Adenosine and regadenoson are used as pharmacologic stress agents in (radionuclide) myocardial perfusion imaging.¹³

A_{2A}Rs mediate potential neuroprotective and neurotoxic effects in addition to modulating dopaminergic neurotransmission in the basal ganglia through the antagonistic interactions between A_{2A}Rs and dopamine D₂ receptors (D₂Rs).¹⁴⁻¹⁶ However, their role in neurodegenerative diseases such as Parkinson's disease (PD) and Alzheimer's disease (AD) is highly controversial.¹⁶ Nevertheless, based on preclinical studies, A_{2A}R antagonists have potential benefits in the treatment of neurodegenerative and psychiatric disorders such as PD, AD, neuroinflammation, ischemia, spinal cord injury, drug addiction, and other conditions.^{12, 15-18} Moreover, recent epidemiological studies have established that the regular consumption of caffeine (a xanthine derivative and AR antagonist) is associated with a lower risk for developing PD¹⁹ or AD.²⁰ Along with D₂Rs, A_{2A}R antagonists attenuate the overactivity of the indirect dopamine pathway observed during PD, restore balance between the direct and indirect output pathways, and suppress the neurodegenerative process by modulating the activity of cortico-striato-pallido-thalamocortical (CSPTC) pathways.^{15, 21, 22}

Positron emission tomography (PET) can noninvasively assess the functional status of CSPTC pathways in PD and related disorders.²³ High-affinity antagonistic radioligands that are selective for the A_{2A}Rs can be used to assess changes in A_{2A}R density during disease progression and to monitor the effects of therapy on these changes.² Moreover, they can be employed to assess the occupancy of the receptor population by therapeutic drugs in the human brain, which will allow the correlation of receptor occupancy with dose, drug / tracer plasma levels, and therapeutic effects.^{2, 12, 24, 25} We focused on A_{2A}R antagonist core structures as PET ligands (instead of A_{2A}R agonist structures) because agonist PET tracers may only bind to the high-affinity state of the receptors, resulting in a poor signal-to-noise ratio.²⁶ Moreover, the *in vivo* vulnerability to competition by endogenous adenosine may hamper the quantification of the total number of binding sites.²⁶

The design and development of novel A_{2A}R antagonist PET ligands is a key research topic because current xanthine-based tracers suffer from several disadvantages, including high nonspecific binding, low signal-to-noise ratios, and therefore, target sites in the brain are barely visible. Furthermore, the use of xanthine-based tracers suffers from a photoisomerization problem, low selectivity toward A_{2A}R.^{2, 24, 27-33} On the basis of these considerations, nonxanthine compounds were developed and evaluated in many preclinical and clinical studies for the assessment of cerebral A_{2A}Rs.¹²

A high degree of selectivity and appropriate combinations of lipophilicity, molecular weight and affinity are important in the development of ideal *in vivo* A_{2A}R PET brain tracers.³⁴ For a compound to cross the blood-brain-barrier (BBB), a relatively small molecular weight (400 to 500 Da) and moderate lipophilicity (approximate range of logP is 2 to 3.5) are optimal.³⁴⁻³⁶ High lipophilicity causes unacceptable binding to plasma proteins and lipid bilayers, resulting in high levels of nonspecific binding in the brain.³⁴ Low lipophilicity decreases the penetration of PET agents across the BBB. In addition, the tracer's affinity must balance the opposing goals of tight binding and significant washout from the brain. Furthermore, the easy and rapid (within 3 half-lives)

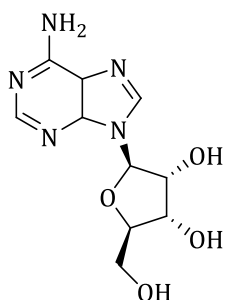
incorporation of radionuclides into the appropriate precursor molecules is necessary. Finally, the formation of lipophilic radioactive metabolites should be negligible because the presence of resulting radiometabolites in the target tissue would impede the quantification of the PET data using kinetic models.^{34, 37}

Rodent studies with nonxanthine tracer 7-(3-(4-[¹¹C]methoxyphenyl)propyl)-2-(2-furyl)pyrazolo[4,3-e]-1,2,4-triazolo[1,5-c]pyrimidine-5-amine [¹¹C]-**8** ([¹¹C]SCH442416; Figure 1)^{38, 39} and its 2-[¹⁸F]fluoroethyl derivative [¹⁸F]-**10a** ([¹⁸F]MRS5425 = [¹⁸F]FESCH in Scheme 3)^{42, 43} suggest their potential value for *in vivo* mapping of A_{2A}Rs.³⁸⁻⁴³ However, high nonspecific binding and a lower striatum (target)-to-cerebellum (nontarget) ratios (4.6 for [¹¹C]-**8** at 15 min; no target-to-nontarget data available for [¹⁸F]-**10a**) than [7-methyl-¹¹C](*E*)-8-(2,3-dimethyl-4-methoxystyryl)-1,3,7-trimethylxanthine [¹¹C]-**3** ([¹¹C]KF21213; a xanthine-based tracer, 10.5 at 60 min, Figure 1)³³ were associated with these tracers, and these compounds will require further evaluation in human subjects.^{39, 43} Furthermore, [¹¹C]-**3** (a tight binding tracer suffers from several limitations such as photoisomerization, an impaired kinetic profile, low BBB penetration, and poor water solubility.^{2, 39}

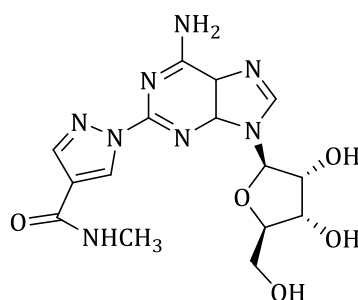
All of the A_{2A}R antagonist PET ligands that have been successfully evaluated in humans to date are [¹¹C]-labeled. The radioisotope ¹⁸F has advantages of higher specific activity and a longer physical half-life (109.8 min vs 20.4 min) than [¹¹C]ligands; these advantages allow the tracer to be distributed to remote imaging centers without cyclotron facilities and to achieve longer biodistribution and scanning times for a better assessment of the dissociation rate constant (K_{off}).^{43, 44} On the basis of above considerations, favorable docking results and because compound **8** demonstrated an appropriate lipophilicity for CNS imaging in addition to the highest A_{2A}R affinity and subtype-selectivity, the present study utilized **8** as a lead compound to develop a novel radiofluorinated A_{2A}R ligand. We designed and prepared an 7-(3-(4-(3-[¹⁸F]fluoropropoxy)phenyl)propyl)-2-(furan-2-yl)-7H-pyrazolo[4,3-e][1,2,4]triazolo[1,5-c]pyrimidin-5-amine derivative [¹⁸F]-**10b**

([¹⁸F]FPSCH in Scheme 3) and compared its pharmacokinetics and biodistribution in healthy rats with those of [¹⁸F]-**10a** and [¹¹C]-**8** to optimize the length of the fluoroalkyl chain, which could affect both A_{2A}R affinity and selectivity.

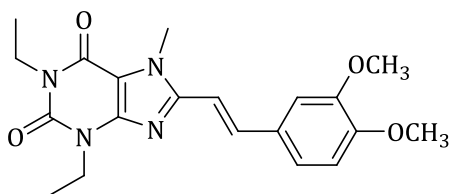
3



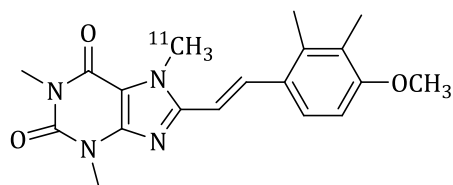
1, Adenosine



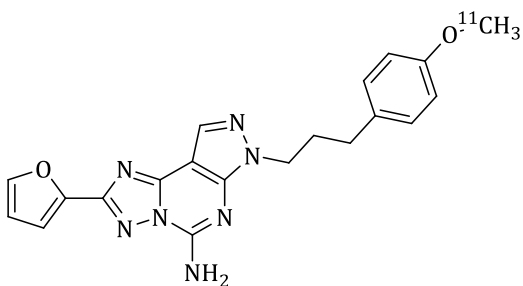
2, Regadenoson



12, KW6002



[¹¹C]-**3**, [¹¹C]KF21213



[¹¹C]-**8**, [¹¹C]SCH442416

Figure 1. Structures of some selected AR agonists, an antagonist KW6002 and A_{2A}R PET imaging agents.

Experimental Section

In Silico Docking Studies.

The coordinates of the X-ray crystal structure of human A_{2A}R in complex with the triazolotriazine **17**, a high-affinity and selective A_{2A} antagonist (Figure 2, protein data bank ID: 3PWH, <http://www.rcsb.org/pdb>), plus those of some well-known A_{2A}R antagonists, were used as a basis for ligand docking to investigate the binding properties of **10a** and **10b** (Figure 2, panel B and C). The three-dimensional (3D) structures of these molecules were drawn using the SYBYL 7.1 molecular modeling package.⁴⁵ Next, the constructed molecules were energy minimized using the Powell method for 10000 iterations with 0.05 kcal / mol as a gradient.⁴⁶ A tripos force field and Gasteiger-Hückel charges were used during minimization.⁴⁷ The GOLD 5.1 docking protocol was employed for the analysis.⁴⁸ Hydrogens were added to the crystal structure, and a grid of size 10 Å was constructed around the cocrystallized ligand. The cocrystallized ligand was removed after the preparation of the grid. The docking was then carried out to predict the binding mode of the same cocrystallized ligand, and a comparison was made with the crystallographically observed positions (n = 3). Compound **18**, a high affinity A₁R antagonist was included as a decoy compound in a pool of known A_{2A}R antagonists to further validate the docking protocol. The GOLD fitness score and the various interactions, such as hydrogen bonding / π-π interactions with important active site residues from the validated docking protocol, were selected as evaluation criteria. The docking poses were analyzed using Pymol (Delano Scientific LLC, San Carlos, CA)

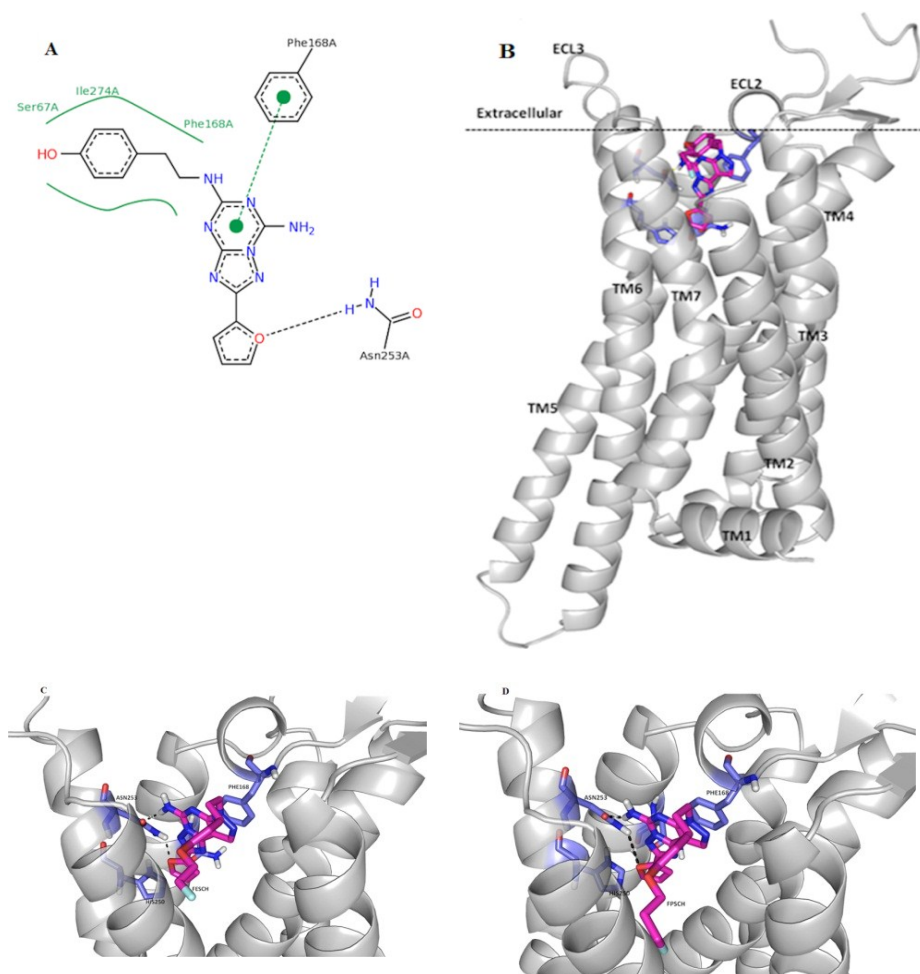


Figure 2. (A) Interaction between antagonist 17 and A_{2A}R binding site residues. (B) Docked conformation of **10b** with A_{2A}R, viewed from the membrane and extracellular (ECL) sides, showing ECL2-folded into the binding cleft. TMs 1-7 are labeled for reference. (C and D): Close-up view showing the pose for (C) **10a** and (D) **10b** in the A_{2A}R binding site residues. The residues and compounds are shown in stick models. The residues involved in ligand binding are labeled and represented as violet sticks, oxygen atoms are shown in red, nitrogen atoms are shown in navy blue and hydrogen atoms are shown in grey. The compounds are represented as purple sticks, the fluorine atom is represented in cyan, and the rest of the indicated atoms are similar to A_{2A}R residues. The dashed lines in black indicate hydrogen bonds.

Materials (Chemical Synthesis).

The compounds **8** and **12** were purchased from Axon Medchem BV (Groningen, The Netherlands). 1,3-Propanediol di-p-tosylate (**6**) and 1,2-ethanediol di-p-tosylate (**11**) were procured from Aldrich (Sigma-Aldrich, The Netherlands). Tetrabutylammonium hydroxide solution (40 % in H₂O) was purchased from Fluka (Sigma-Aldrich, The Netherlands). All other chemicals were of analytical grade and obtained from commercial suppliers such as Rathburn, Sigma, Merck and others. These chemicals were used in the syntheses without any further purification. Oxygen- or moisture-sensitive reactions were carried out under an atmosphere of dry N₂ or argon using dried glassware.

Methods for Chemical Synthesis and Molecular Characterization

Nuclear magnetic resonance spectra were recorded on a Bruker Avance 500 spectrometer [¹H NMR (500 MHz), ¹³C NMR (125 MHz)] or a Varian Oxford 400 MHz spectrometer [¹H NMR (400 MHz), ¹³C NMR (100 MHz)]. Chemical shifts are reported as δ values and coupling constants are presented in hertz (Hz). Chemical shifts for ¹³C NMR spectra are reported in ppm relative to the solvent peak.

UHPLC-HRMS was used to assess the exact molecular weight of the reference compounds ([¹⁸F]-**10a** and [¹⁸F]-**10b**) and intermediate fluorosynthons ([¹⁸F]-**5** and [¹⁸F]-**7**). The HPLC method was used to calculate the purity of the compounds. Purities of all compounds were found to be ≥ 95 %. A sample solution (100 % acetonitrile) with a concentration of approximately 0.1 mg / mL was prepared, and an injection volume of 5 μ L was used. Data were acquired as described in the *in vitro* microsomal metabolite analysis section using a 4-min gradient starting from 0.1 % formic acid in 95 % water for 1.5 min, next with an 80 % acetonitrile solution for 1 min, and finally with 0.1 % formic acid in 95 % water at a flow rate of 0.6 mL / min.

A disconnection retrosynthetic strategy was designed for the easy preparation of the **10a** and **10b** analogues.^{42, 49} Compound **8**, in dichloromethane (DCM) was demethylated using BBr₃; this yielded

the precursor **9**. This precursor without further purification was used for both the chemical and radiochemical syntheses.

Precursor **9** was characterized by ESI-HRMS m/z 376.1522 $[M + H]^+$, $C_{19}H_{17}N_7O_2 \cdot H^+$: calcd 376.1522; 1H NMR (400 MHz, Methanol- d_4): δ 8.08 (s, 1H), 7.78 (dd, $J = 1.7, 0.7$ Hz, 1H), 7.30 (dd, $J = 3.5, 0.7$ Hz, 1H), 6.92 – 6.83 (m, 2H), 6.66 (dd, $J = 3.6, 1.8$ Hz, 1H), 6.60 – 6.50 (m, 2H), 4.28 (t, $J = 6.9$ Hz, 2H), 2.47 (t, $J = 7.5$ Hz, 2H), 2.26 – 1.96 (m, 2H).

3

2-[^{19}F]-Fluoroethyl Tosylate (5).

2-Fluoroethanol **4** (1.28 g, 20 mmol) was dissolved in 20 mL of DCM at 0 °C. Tosyl chloride (4.19 g, 22 mmol) and pyridine (1.74 g, 22 mmol) were added to this solution. The reaction mixture was then allowed to warm to room temperature and stirred continuously for 3 h. After the addition of water (100 mL) and saturated ammonium chloride solution (50 mL), the mixture was extracted with DCM (3×150 mL). The combined organic fractions were washed thoroughly with brine, dried over anhydrous sodium sulfate, and concentrated *in vacuo* to generate the crude product. The crude product was then purified by silica column purification using *n*-hexane:DCM (50 % v / v) as an eluent to generate pure **5** (Scheme 1) in the form of colorless oil, R_f 0.34. The isolated yield was 51 %.

ESI-HRMS m/z 241.0309 $[M + Na]^+$, $C_9H_{11}O_3FS \cdot Na^+$, calcd 241.0310; 1H NMR (400 MHz, $CDCl_3$): δ 7.80 (d, $J = 8.3$ Hz, 2H), 7.35 (d, $J = 8.3$ Hz, 2H), 4.62 (dd, $J = 5.0, 3.2$ Hz, 1H), 4.50 (dd, $J = 5.0, 3.2$ Hz, 1H), 4.29 (dd, $J = 4.9, 3.3$ Hz, 1H), 4.22 (dd, $J = 4.9, 3.3$ Hz, 1H), 2.44 (s, 3H).

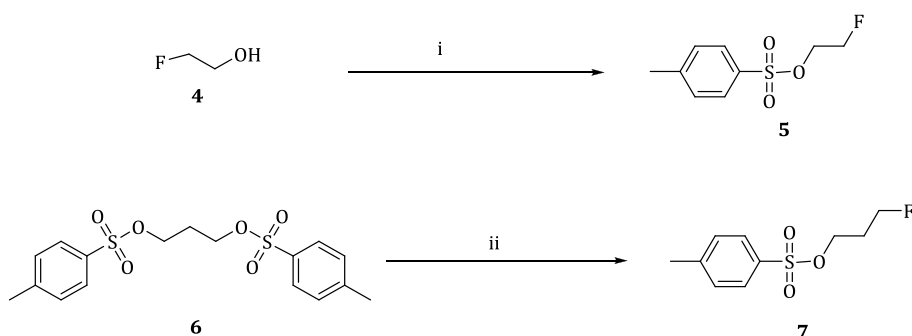
3-[^{19}F]-Fluoropropyl tosylate (7).

Tetrabutyl ammonium fluoride trihydrate (52.8 mg, 0.20 mmol) was dried azeotropically with 3×3 mL acetonitrile. During coevaporation, care should be taken to ensure that the temperature of the flask does not rise above 30 °C to prevent the decomposition of the tetrabutyl ammonium fluoride trihydrate. The contents of the flask were redissolved in a small amount of anhydrous acetonitrile, and this solution was added to a refluxing solution of 1, 3-propanediol di-p-

tosylate **6** (76.9 mg, 0.2 mmol) in acetonitrile. The reaction progress was monitored by TLC on silica plates [DCM:hexane (1.25:1 v / v)]. The refluxing was continued overnight with stirring. The obtained solution was filtered, and the filtrate was evaporated under reduced pressure. The residue was redissolved in a small amount of mobile phase and purified using silica gel column chromatography with a mixture of DCM and hexane (50 %) as the eluent to yield pure **7** (Scheme 1) in the form of a clear, slightly yellowish oil.

ESI-HRMS m/z 213.0583 [M-F]⁺, [C₁₀H₁₃O₃S-F]⁺: calcd 213.0585; high in-source fragmentation; ¹H NMR (400 MHz, CDCl₃): δ = 7.80 (d, J = 8.2, 2H), 7.35 (d, J = 8.1, 2H), 4.54 (t, J = 5.7, 1H), 4.45 (t, J = 5.6, 1H), 4.16 (t, J = 6.2, 2H), 2.45 (s, 3H), 2.14 – 1.94 (m, 2H).

Scheme 1. Synthesis of Fluoroalkyltosylates^a



Reagents and conditions: (i) tosyl chloride, pyridine, DCM, room temperature (RT), stirring 3 h; (ii) tetrabutyl ammonium fluoride trihydrate, acetonitrile, overnight reflux

7-(3-(4-(2-Fluoroethoxy)phenyl)propyl)-2-(furan-2-yl)-7H-pyrazolo[4,3-e][1,2,4]triazolo [1,5-c]pyrimidin-5-amine (10a).

The synthesis of this compound was performed according to a published procedure. The authenticity of the **10a** (Scheme 2) was confirmed by ¹H NMR, ¹³C NMR and MS data and was in agreement with the published values.⁴²

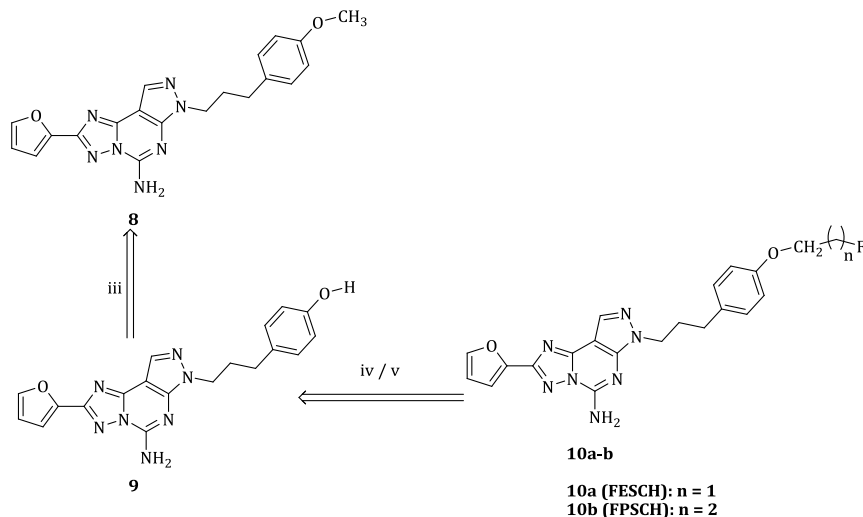
7-(3-(4-(3-Fluoropropoxy)phenyl)propyl)-2-(furan-2-yl)-7H-pyrazolo[4,3-e][1,2,4]triazolo[1,5-c]pyrimidin-5-amine (10b).

The selective fluoropropylation reaction described in the literature was slightly modified to generate authentic nonradioactive **10b** (Scheme 2).⁴⁹ Our procedure differed in the fluoroalkylating agent; we used **7** instead of 1-bromo-3-fluoropropane.

The phenol precursor **9** was dried azeotropically with 3×8 mL anhydrous toluene and then suspended in anhydrous MeOH (3 mL), and Cs₂CO₃ (110 mg, 0.34 mmol) and 3-fluoropropyltosylate **7** (79 mg, 0.34 mmol) were added. The reaction mixture was refluxed for 16 h with continuous stirring. The conversion was monitored by TLC (14 % acetonitrile in chloroform). The crude mixture was then concentrated *in vacuo*, and the crude product was redissolved and purified by preparative TLC with 14 % acetonitrile in chloroform as a mobile phase to furnish 7.9 mg of product. The product was contaminated with trace silica gel. To remove the silica gel impurities, the sample was redissolved in the mobile phase, passed through a 0.45 μm polytetrafluoroethylene (PTFE) syringe filter, and concentrated to provide 7.4 mg (25 %) of **10b** (Scheme 2) as a white solid.

ESI-HRMS *m/z* 436.1899 [M + H]⁺, C₂₂H₂₂N₇O₂F.H⁺: calcd 436.1897; ¹H NMR (500 MHz, CDCl₃): δ 8.24 (s, 1H), 7.67 (s, 1H), 7.29 (d, *J* = 5.8 Hz, 2H), 7.12 (d, *J* = 8.0 Hz, 2H), 6.83 (d, *J* = 8.1 Hz, 2H), 6.64 (s, 1H), 5.98 (s, 2H), 4.70 (t, *J* = 5.6 Hz, 1H), 4.61 (t, *J* = 5.5 Hz, 1H), 4.40 (t, *J* = 6.7 Hz, 1H), 4.08 (t, *J* = 5.9 Hz, 1H), 2.64 (t, *J* = 7.4 Hz, 2H), 2.37 – 2.04 (m, 4H) ¹³C NMR (125 MHz, CDCl₃): δ 157.08, 149.15, 147.83, 145.49, 144.87, 144.64, 133.26, 132.03, 129.38, 114.40, 112.74, 112.04, 97.26, 81.47, 80.16, 63.53, 46.97, 31.98, 31.19, 30.53, 30.38, 29.71.

Scheme 2. Disconnection Retrosynthetic Scheme for the Reference Fluoroalkylated Compound 8 Analogs (10 a and 10b)^a



^a**Reagents and conditions:** (iii) BBr₃, CH₂Cl₂, RT, 2 h; (iv) **5**, Cs₂CO₃, MeOH, reflux, 1 h; (v) **7**, Cs₂CO₃, MeOH, reflux, 16 h.

Radiochemistry

[¹⁸F]-**10a** and [¹⁸F]-**10b** were prepared by a two-pot radiosynthetic method, using the intermediate fluorosynthons [¹⁸F]-**5** and [¹⁸F]-**7** (Scheme 3, Table 2).

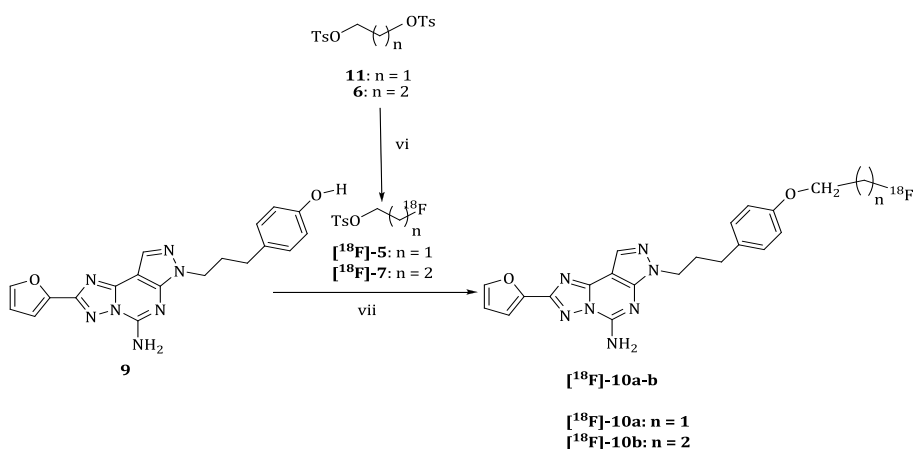
No-carrier added aqueous [¹⁸F]fluoride was produced by the irradiation of [¹⁸O]water via the ¹⁸O (p,n) ¹⁸F nuclear reaction using a Scanditronix MC-17 biomedical cyclotron. The [¹⁸F]fluoride solution from the target was trapped onto a preactivated Sep-Pak light Accel plus QMA anion-exchange cartridge to recover the ¹⁸O-enriched water. The [¹⁸F]fluoride was then eluted from the column with 1 mL of potassium carbonate solution (1 mg / mL) into a glass conical vial containing 15 mg of Kryptofix [2.2.2]. To this mixture, 1 mL of acetonitrile (Rathburn, The Netherlands) was added, and the solvents were evaporated to dryness azeotropically at 130 °C. The

[¹⁸F]KF / Kryptofix [2.2.2] complex was dried 3 times by the addition of 0.5 mL acetonitrile, and the solvent mixture was evaporated. A solution of **6** or 1,2-ethanediol di-p-tosylate **11** (4–5 mg) in acetonitrile (0.5 mL) was added to the conical vial, and the vial was heated on a heating block to 125 °C for 10 min under sealed conditions and then cooled to room temperature to generate the crude intermediate. The cooled reaction mixture was diluted with 4 mL hexane / diethyl ether (3:1), and loaded onto a Sep-Pak Silica Plus column (Waters). The cartridge was then eluted with 10 mL of hexane / diethyl ether (3:1) and the eluate captured in a counting vial was evaporated on a rotavap (Buchi HB-140) to obtain the desired pure [¹⁸F]fluorosynthon [**18F**]-**5** or [**18F**]-**7**.

Phenol precursor **9** (1.5 mg) in 0.3 mL acetonitrile and 10 µL of 40 % aqueous tetrabutylammonium hydroxide solution were added to the residual solution of 3-[¹⁸F]-fluoropropyltosylate [**18F**]-**7** or 2-[¹⁸F]-fluoroethyltosylate [**18F**]-**5**. The reaction vials were closed and maintained at 115 °C for 15 min on a heating block. After cooling to room temperature, the reaction mixture was diluted with 0.6 mL of HPLC mobile phase and injected onto a semipreparative Phenomenex Prodigy ODS C-18 RP-HPLC column (5 µm, 10×250 mm) connected to a UV-spectrometer (Waters 486 tunable absorbance detector) set at 254 nm and a Bicon Frisk-Tech radiation detector. The HPLC column was then eluted with 45 % acetonitrile and 55 % 100 mM ammonium acetate at 5 mL / min to yield [**18F**]-**10b** (t_R = 16 min); in the case of [**18F**]-**10a**, the elution solvent was 40 % acetonitrile and 60 % 100 mM CH₃COONH₄, t_R = 21 min. The collected HPLC fractions containing the products were diluted with water (25 mL) and loaded onto C-18 light Sep Pak cartridges (Waters). After trapping the radioactivity, the columns were washed with an additional 4 mL of water. The columns were dried with a flow of nitrogen and eluted with 1 mL of ethanol over a 0.22 µm Millex LG sterilization filter; the products were collected in a 25 mL sterile vial (Mallinckrodt pharmaceuticals, The Netherlands). The products were diluted with saline (4 mL), and the formulated tracers were submitted for quality control.

Independent quality control was performed on a Waters (Milford, MA) Acquity Ultraperformance LC quaternary solvent manager coupled to a tunable, dual-wavelength Ultraviolet / Visible (UV / vis) detector and a radioactivity detector (Berthold Flowstar LB 513). The radioactive product (10 μ L) was injected into a Waters 3.0 \times 50 mm i.d., 1.7 μ M Ethylene-Bridged Hybrid (BEH) shield RP18 column and eluted using 40 % acetonitrile at a flow rate of 0.8 mL / min. The instrument and column temperature were set at 254 nm and 35 $^{\circ}$ C, respectively. The retention time for [¹⁸F]**10b** was 3.2 min, and the retention time for [¹⁸F]**10a** was 1.9 min.

Scheme 3. Radiosynthesis of [¹⁸F]-**10b** and [¹⁸F]-**10a**^a



Reagents and conditions: (vi) K[¹⁸F]F-K_{2.2.2}-K₂CO₃, acetonitrile, 3, 1,2-ethanediol di-*p*-tosylate, 125 $^{\circ}$ C, 10 min; (vii) tetrabutyl ammonium hydroxide (40 % aq.), acetonitrile, sealed conditions, 115 $^{\circ}$ C, 15 min

Ligand Metabolism

In Silico Metabolite Analysis

The SMARTCyp web service (version 2.4.2) was used to predict which sites in the molecule are most vulnerable to CYP450 metabolism.⁵⁶ SMARTCyp has been shown to be valid for the metabolism of the major isoforms 1A2, 3A4, 2A6, 2B6, 2C8, 2C19 and

2E1. Additionally, it is applicable to specific models for the 2C9 (CYP2C9) and 2D6 (CYP2D6) isoforms.⁵⁰

SMARTCyp only uses the 2D structure of a compound as input, and atoms are scored based on their propensity to undergo metabolism, which is in turn calculated based on energy and accessibility factors. The energy required for oxidation at each atom is computed by fragment matching toward the SMARTS patterns. The accessibility is approximated as the relative topological distance of an atom from the center of the molecule, and the final score is computed as $\text{score} = \text{energy} - 8 * \text{accessibility}$.⁵⁰

Human Liver Microsomal Metabolite Analysis

Human liver microsomes (HLM) from 150 mixed-gender donors and a NADPH-regenerating system consisting of two solutions (NADP plus glucose-6-phosphate and glucose-6-phosphate dehydrogenase) were purchased from BD Biosciences. Dulbecco's Phosphate-Buffered Saline (DPBS), pH 7.4, was procured from Life Technologies.

Nonradioactive compounds **8** and **10b** were incubated with HLM. The metabolic reactions were initiated by the addition of NADPH. At different time points (0, 5, 15, 30, 45, 60 and 90 min), 100 μL of the solution was taken. After quenching with cold acetonitrile and centrifugation at 17250g, the supernatant solution (5 μL) was injected into an UHPLC / Q-ToF-MS. Incubations without NADPH, microsomes and test compound were conducted as negative controls to characterize the nonmetabolism related degradation of the test compound. Furthermore, verapamil was included as a positive control because it is known to be metabolized by human liver microsomes. MetaboLynx (Waters) was used to assist in the identification of metabolites.

UHPLC/Q-TOF-MS Method

Data acquisition was performed using Waters (Milford, MA) Acquity Ultraperformance LC quaternary solvent manager. The samples were injected onto a Waters 3.0 \times 50 mm internal diameter (i.d.), 1.7 μM BEH shield RP 18 column and eluted using a 6 min gradient starting

from 0.1 % formic acid in 98 % water for 5 min, then with a 100 % acetonitrile solution for 0.5 min, and finally with 0.1 % formic acid in 98 % water at a flow rate of 0.6 mL / min and a column temperature of 35 °C. The mass spectrometer was operated in electrospray positive ionization mode with an extended dynamic range and resolution mode analyzer; the machine settings were 0.5 kV capillary voltage, 45 V sampling cone, 4 V extraction cone, and 150 and 500 (°C) source and desolvation temperature, respectively. Leucine enkephalin was used as the lock mass (m/z 556.2771) at a concentration of 500 pg / μ L.

Log D_{7.4} Measurement

After tracer elution from a C-18 light Sep Pak column, 500 mL of eluate (octanol) was mixed with an equal volume of 1 M phosphate buffer (pH 7.4) and vigorously vortexed for 1 min and centrifuged (10 min, 17250g). Three 100 μ L aliquots were drawn from the corresponding n-octanol and aqueous phases. The radioactivity in each phase was counted (Compugamma 1282 CS, LKB-Wallac, Finland). The experiments were performed in triplicate for each tracer batch; the average logD_{7.4} value is reported.

***In Vitro* Ligand Stability Test**

The *in vitro* stability tests were performed by dissolving the formulated tracers in PBS, saline, rat plasma and human plasma and incubating these solutions at 37 °C. After 1 and 2 h of incubation, the solutions were analyzed by radio-TLC (R_f [**¹⁸F]-**10a** = 0.4 and [**¹⁸F]-**10b** = 0.5, 14 % acetonitrile in chloroform). The rat and human plasma samples were deproteinized by adding 3 volumes of acetonitrile and centrifuged (5 min at 17250g) before they were used for analysis. After elution with the mobile phase, the TLCs were dried and placed on phosphor storage plates, which were later scanned with a Cyclone imaging system (PerkinElmer). The percentage of conversion as a function of incubation time was calculated by ROI analysis using Optiquant (version 3.00).****

In Vivo and In Vitro Selectivity.

Nonradioactive A_{2A}R-selective **12** [1 mg / kg, 50 % dimethylacetamide (DMA): saline (v / v)] or vehicle (1 mL / kg, 50 % DMA:saline) ²⁷ were *intraperitoneally* administered 5–6 min prior to the *intravenous* injection of [¹⁸F]tracers. In the *in vitro* ARG experiments, 2 μM (0.77 mg) **12** was used as a blocking agent.

In Vitro ARG experiment.

Isolated frozen brains of young (10–12 weeks of age; 300–350 g body weight) male Sprague–Dawley rats (Harlan, The Netherlands) were cut into two halves along the sagittal symmetry plane. Each half was mounted on paper slides with its lateral side up using Tissue-Tek fixing gel (Sakura, The Netherlands). After fixing, the brain was cut sagittally into 20 μm thick cryostat sections using a Leica CM 1950 cryostat (Leica Biosystems, The Netherlands) at -15 °C. The slices were thaw-mounted onto starfrost (76×26 mm, Waldemar Knittel, Germany) adhesive precoated slides, air-dried for 30 – 40 min and stored at -80 °C until they were used (within 1 week).

The slices were brought to room temperature and preincubated for 15 min in assay buffer (50 mM Tris-HCl at pH 7.5 with 10 mM MgCl₂ and 1 % bovine serum albumin). After preincubation, the slides were placed into jars with an assay buffer containing an approximately 5 nM radioligand [[¹⁸F]-**10a**: 4.5 ± 1.5 nM (n = 3), 1.2 MBq and [¹⁸F]-**10b**: 5.1 ± 1.8 nM (n = 5), 1.02 MBq]. To test the specificity of the binding, a 2 μM compound **12**, was added to the buffer in one of the jars. The slices were incubated for 90 min at 37 °C. After incubation, the slices were washed for 5 min with ice-cold 0.01 % Triton X in PBS. They were dipped in ice-cold water for 30 s to remove buffer salts and dried under a stream of air at room temperature. After drying, the slices were placed on phosphor storage screens for 8–10 h. The screens were then read using a Cyclone imaging system (Packard Instrument Co.). Optiquant (version 3.00) was used to quantify radioactivity. Regions of interest (ROIs) were drawn manually on the striatum and cerebellum. The regional uptake of

radioactivity was measured and expressed as digital light units (DLU) / mm².

In Vivo Studies

Animals and Study Design

The animal experiments were carried out in compliance with the Law on Animal Experiments of The Netherlands. The institutional animal ethics committee approved the protocols. Male outbred Wistar-Unilever rats were obtained from Harlan (The Netherlands). The animals were housed in Macrolon cages (38×26×24 cm), maintained in a 12 h light–dark regime, and fed with standard laboratory chow (RMH-B, The Netherlands) and tap water ad libitum. After arrival, the rats were allowed to acclimatize for at least 7 days. For each tracer, the animals were divided into two groups, as follows: Group 1, vehicle-controls ([¹⁸F]-**10b** (n = 6): body weight = 295 ± 19 g and injected dose = 0.21 ± 0.11 nM; [¹⁸F]-**10a** (n = 5): body weight = 312 ± 14 g and injected dose = 1.13 ± 0.41 nM) and group 2, pretreated group ([¹⁸F]-**10b** (n = 6): body weight = 293 ± 31 g and injected dose = 0.29 ± 0.27 nM; [¹⁸F]-**10a** (n = 5): body weight = 321 ± 15 g and injected dose = 0.74 ± 0.62 nM)

Micro PET Scanning

Two animals were scanned simultaneously in each scan session (Supine position) using a Focus 220 MicroPET camera (CTI, Siemens, Munich, Germany). All animals were anesthetized with isoflurane / air (induction: 5 % isoflurane, later reduced to ≤ 2 %) and kept on electronic heating pads during the entire study period. Cannulas were placed in a femoral artery and vein for blood sampling and tracer injection (Harvard-style pump; 1 mL / min). The brain was in the field of view. A transmission scan of 515 s was made before the emission scan, using a rotating ⁵⁷Co point source. The emission data were acquired in list mode for 106 min, starting at the moment of tracer entering the body of the first rat; the second animal was injected 16 min later. PET data were corrected for attenuation, scatter, random coincidences and radioactive decay and reconstructed in 25 time frames (8×30, 3×60, 2×120, 2×180, 3×300,

5×600, 1×480 and 1×960 s) using a 2D ordered subsets expectation maximization (OSEM) algorithm (4 iterations, zoom factor, 2). The reconstructed images were smoothed with a 3D Gaussian filter [1.35 mm full width at half-maximum (fwhm)].

During the scan, arterial blood samples (volume 0.1–0.15 mL) were drawn using a standard protocol (at 0, 5, 10, 15, 20, 30, 45, 60, 75, and 90s and 2, 3, 5, 7, 10, 15, 30, 60, and 90 min after injection). After collecting 25 μ L of whole blood, plasma (25 μ L) was acquired from the remainder of the blood samples by a short centrifugation (5 min at 1,000*g*). The radioactivity in 25 μ L of plasma and whole blood was counted on a Compugamma γ -counter (1282 CS, LKB-Wallac, Turku, Finland), and the count statistics were then used as an arterial input function. The heart rates and blood oxygenation of the experimental animals were continuously monitored using pulse oximeters throughout the scanning procedure (Nonin Zevenaar, The Netherlands).

Small-animal PET Data Analysis

Time activity curves (TACs) for the frontal cortex, striatum, midbrain, cerebellum and hippocampus were determined using Inveon Research Workplace (Siemens Medical Solutions, Knoxville, TN). The summed PET data from each animal were coregistered to an MRI template of the rat brain with predefined volumes of interest (VOIs). Translation, rotation and scaling were adjusted to visually optimize the fusion of the images. The VOIs were transferred from the MRI template to the PET data, and regional TACs were generated. Standardized uptake values (SUVs) were plotted as a function of time, using body weights and injected doses.

Ex Vivo Biodistribution

After the PET-scan, the animals were sacrificed by the extirpation of the heart. Blood was collected from the animals, and plasma and a cell fraction were obtained from the sample by a short centrifugation (5 min at 1,000*g*). Several tissues were excised and weighed. The radioactivities in the tissue samples and in a sample of tracer

solution (infusate) were measured using a calibrated gamma counter. The data were expressed as the SUV.

***In Vivo* Metabolite Analysis**

Plasma samples taken at intervals of 2, 5, 10, 15, 30, 60 and 90 min were used for metabolite analysis. Protein was removed by adding 3 volumes of acetonitrile followed by centrifugation (5 min at 17250g). Samples (2.5 μ L) of the supernatant and infusate (internal standard, diluted 50 to 100 times) were loaded onto a TLC plate. After development with 15 % acetonitrile in chloroform, the plate was dried and placed on a phosphor screen which was later read by the Cyclone system. ROIs were drawn manually on the parent and metabolite spots. The concentration of the parent tracer was expressed as the percentage of total radioactivity in the acetonitrile extract. Optiquant was used for radioactivity quantification.

Statistical Analysis

All results are expressed as the mean \pm SEM. The differences between groups were examined using an unpaired two-tailed *t* test. $P < 0.05$ was considered to be statistically significant.

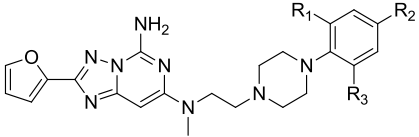
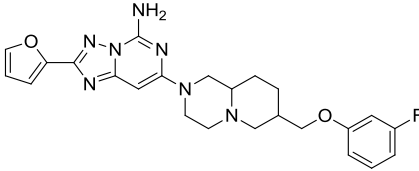
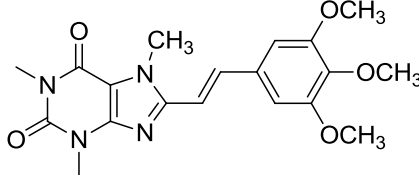
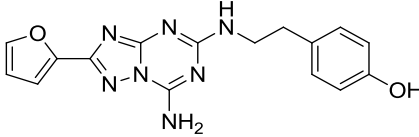
Results

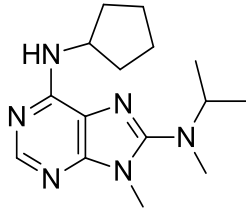
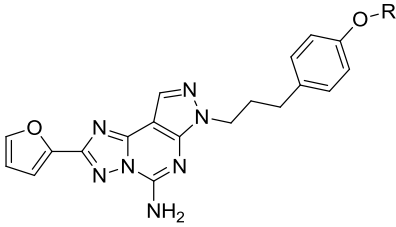
Molecular Docking

Table 1 shows the GOLD fitness scores and important interactions for the docked ligands. A molecular docking study was performed to elucidate the intermolecular interactions between the 7-(3-(4-methoxyphenyl)propyl)-2-(2-furyl)pyrazolo[4,3-e]-1,2,4-triazolo[1,5-c]pyrimidine-5-amine **8** (SCH442416, Scheme 2) derivatives and A_{2A}Rs. The major ligand binding interactions are both polar and hydrophobic in nature and occur with residues in trans-membrane domains 3, 5, 6, and 7. Residues from the second extracellular loop (ECL2) outline the upper part of the binding cavity (Figure 2B). In our study, 7-(3-(4-(2-fluoroethoxy)phenyl)propyl)-2-(furan-2-yl)-7H-pyrazolo[4,3-e][1,2,4]triazolo [1,5-c]pyrimidin-5-amine **10a** (FESCH, Scheme 2) and 7-(3-(4-(3-fluoropropoxy)phenyl)propyl)-2-(furan-2-yl)-7H-pyrazolo[4,3-

e)[1,2,4]triazolo[1,5-c]pyrimidin-5-amine **10b** (FPSCHE, Scheme 2) had binding modes that were similar to the cocrystallized 4-(2-[7-amino-2-(2-furyl)[1,2,4]triazolo[2,3-a][1,3,5]triazin-5-yl-amino]ethyl)phenol **17** (ZM241385, fifth compound in Table 1) conformation (Figure 2A), including the important hydrogen bond interactions with the active site residue Asn253 and a π - π stacking interaction with Phe168 of A_{2A}R. The exocyclic free amino group of the pyrimidine ring structure of the tricyclic core and the oxygen of the furan ring make strong H-bond interactions with Asn253 of the receptor. This finding is consistent with the results from site-directed mutagenesis studies of the A_{2A}R, which suggest that this amino acid is critical for ligand binding.⁵¹ Moreover, the π - π stacking interaction between Phe168 and His250 stabilizes the binding pose of the compound within the active site. Compound **8** derivatives, including the A_{2A}R-bound crystal structure, **17**, are oriented perpendicular to the plane of the cell membrane, with their flexible hydrocarbon side chain located in the extracellular domain. An analysis of ligand-bound crystal structure and literature evidence^{42, 52} suggests that ECL2 helps in ligand binding at the A_{2A}R. We explored the impact of structural variability at the terminal phenolic position of **8** in the GOLD docking scores. As reported previously,^{42, 52} conformational flexibility was also noted in our experiment; the terminal phenolic side chain forms a polar interaction with a crystallographic water molecule at the extracellular matrix of A_{2A}R. As expected, N⁶-cyclopentyl-N⁸-isopropyl-N^{8,9}-dimethyl-9H-purine-6,8-diamine **18** (LUF5608, sixth compound in Table 1), a high affinity A₁R antagonist and negative-control, yielded a very low docking score due to a lack of hydrogen bond formation with the active site residues of the receptor, further authenticating the findings of the docking study and indirectly confirming the specificity of **10b** and **10a** toward A_{2A}R over A₁R.

Table 1. Docking Analysis of A_{2A}R Antagonists Using GOLD software

S. No.	Compound Name	GOLD fitness Score	H-Bond (s)	π-π stacking
				
1	Where R ₁ , R ₂ = F and R ₃ = H, Piperazine derivative of Triazolopyrimidine-I (13)	69.17	Asn253 (Furan O and NH ₂)	Phe168
2	Where R ₁ , R ₂ , R ₃ = F, Piperazine derivative of Triazolopyrimidine-II (14)	59.66		Phe168 and His250
3	 Bicyclic piperazine triazolotriazine derivative (15)	65.14	Asn253 (Furan O and NH ₂), Leu267-NH ₂	Phe168 and His250
4	 KF18446 (16)	51.35	Asn253(C=O), Thr68, Ile66	Phe168
5	 ZM241385 (17)	65.69	Asn253 (Furan O), Glu167 (OH)	His250

6	 <p>LUF5608 (18)</p>	40.97	NA	Phe168
				
7	Where R = CH ₃ , 8	71.23	Asn253	Phe168 and His250
8	R = CH ₂ -CH ₂ -F, 10a	69.86	(Furan O and NH ₂)	
9	R = CH ₂ -CH ₂ -CH ₂ -F, 10b	70.6		
10	Where R = CH ₂ -F, 7-(3-(4-(1-Fluoromethoxy)phenyl)propyl)-2-(furan-2-yl)-7H-pyrazolo[4,3-e][1,2,4]triazolo[1,5-c]pyrimidin-5-amine	69.46	Asn181 (Furan O), Asn253(NH ₂)	Phe168, His250 and Trp246

Chemical and Radiochemical Synthesis

The demethylation of commercially available **8** using boron tribromide (BBr₃) resulted in a quantitative yield of 4-(3-(5-amino-2-(furan-2-yl)-7H-pyrazolo[4,3-e][1,2,4]triazolo[1,5-c]pyrimidin-7-yl)propyl)phenol, **9** (precursor of compound **8**, Scheme 2).⁴² A retrosynthetic approach was adopted for the synthesis of reference standards (**10a** and **10b**, Scheme 2), which were prepared by reacting the phenol precursor (**9**) with the appropriate fluoroalkyltosylate (**5** or **7** in Scheme 1, selective fluoroalkylation) in 35 % and 25 % yields, respectively. The two radiolabeled analogs, [¹⁸F]-**10a** and [¹⁸F]-**10b**, were synthesized by a two-step two-pot

procedure starting with the corresponding [18F]fluoroalkyl synthon ([18F]-5 or [18F]-7) made from [18F]fluoride and the appropriate ditosylate precursor (6 or 11), followed by the selective [18F]fluoroalkylation of the phenol precursor 9 (Scheme 3). Table 2 lists the decay-corrected radiochemical yields, specific radioactivities, calculated partition coefficient (clogP) and experimentally determined distribution coefficient (LogD_{7.4}) values for [18F]-10a and [18F]-10b. For both tracers, the radiochemical purity was > 98 %, and the total synthesis time, including quality control, was 114 ± 5 min (n = 18). The identities of the tracers were confirmed by spiking with authentic cold compounds in reversed-phase HPLC (RP-HPLC).

Table 2. Radiosynthesis and Lipophilicity Data

Tracer	Yield ^a and Purity (%)	Specific activity (GBq/μmol)	cLogP		LogD _{7.4} ^b
			Chemsketch 12.01	Chembiodraw ultra 12.0	
[18F]- 10a	7 ± 2 and ≥98	22.5 ± 5	2.98 ± 0.98	3.18	3.16 ± 0.03
[18F]- 10b	8 ± 2 and ≥98	136 ± 13	3.27 ± 0.98	3.41	3.41 ± 0.11

^aOverall radiochemical yields based on starting wet [18F]fluoride and corrected for decay

^bExperimental value

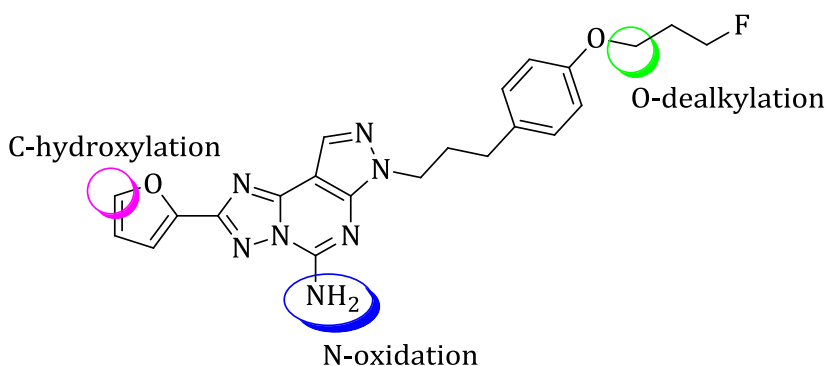
Ligand Metabolism

In Silico Metabolite Analysis

The predicted sites of metabolism are highlighted for parent compound **10b** in Scheme 4 (data not shown for **10a** and **8**). The possible metabolic routes can be ranked in the following order: C-hydroxylation > N-oxidation > O-dealkylation.

3

Scheme 4. Sites of Metabolism Predicted for **10b** by SMARTCyp Webservice^a



^aThe same predicted metabolic sites are also applicable to compounds **8** and **10a**.

Human Liver Microsomal Metabolite Analysis

Table 3 summarizes the modifications that were detected with an ultrahigh-performance liquid chromatography / quadrupole-time-of-flight-mass spectrometer (UHPLC / Q-ToF-MS) and analyzed by Metabolynx after incubating compound **8** with human liver microsomes. The relative production of the different metabolites over time is presented in Figure 3. None of these modifications and major demethylated metabolites were detected in negative control and positive control (verapamil) incubations, respectively, with human liver microsomes. Under these conditions, the m/z ratio

increased by 16, which is most likely the result of *N*-oxidation or *C*-hydroxylation. The *m/z* ratio also decreased by 14, which may be due to a demethylation reaction. Moreover, a fluorine-containing metabolite of **10b** and free fluoride was observed, indicating defluorination, similar to previously reported results for **10a**.⁴²

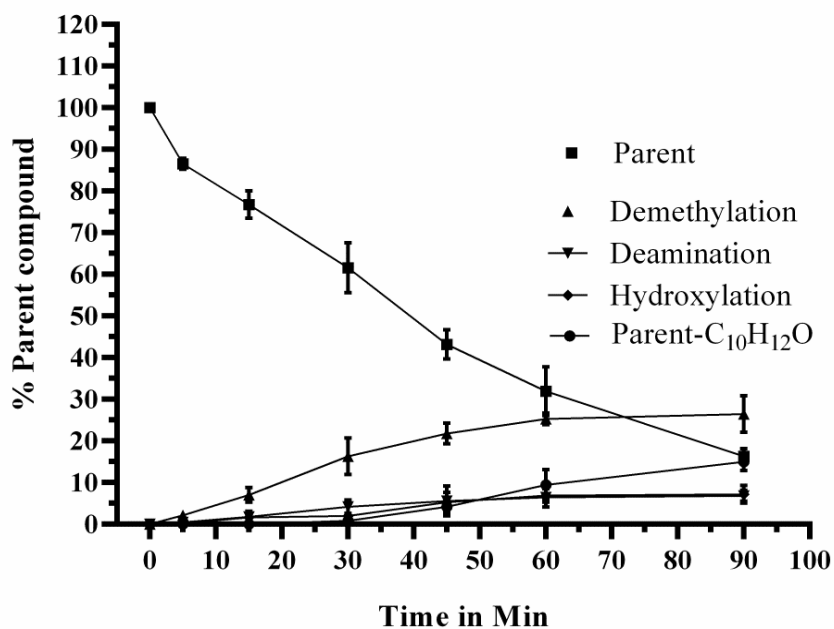
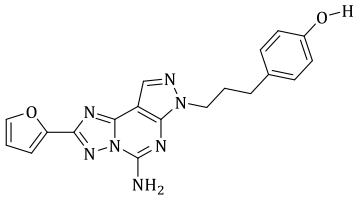
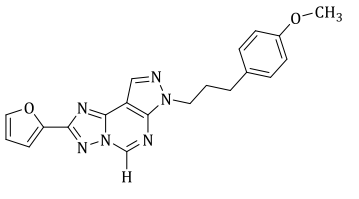
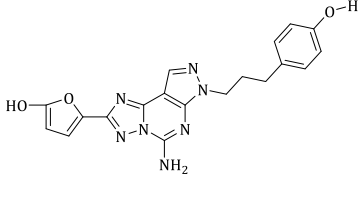
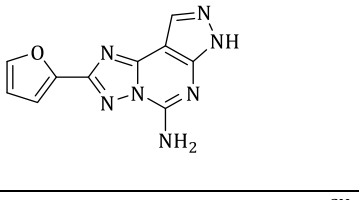
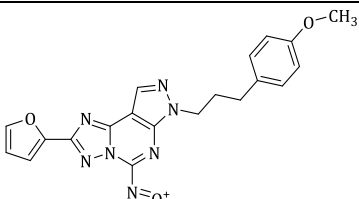


Figure 3. Relative amounts of several modifications over 90 min during incubation of (**8**) with human liver microsomes. The error bars indicate the standard deviation

Table 3. Human Liver Microsomal Metabolite Analysis

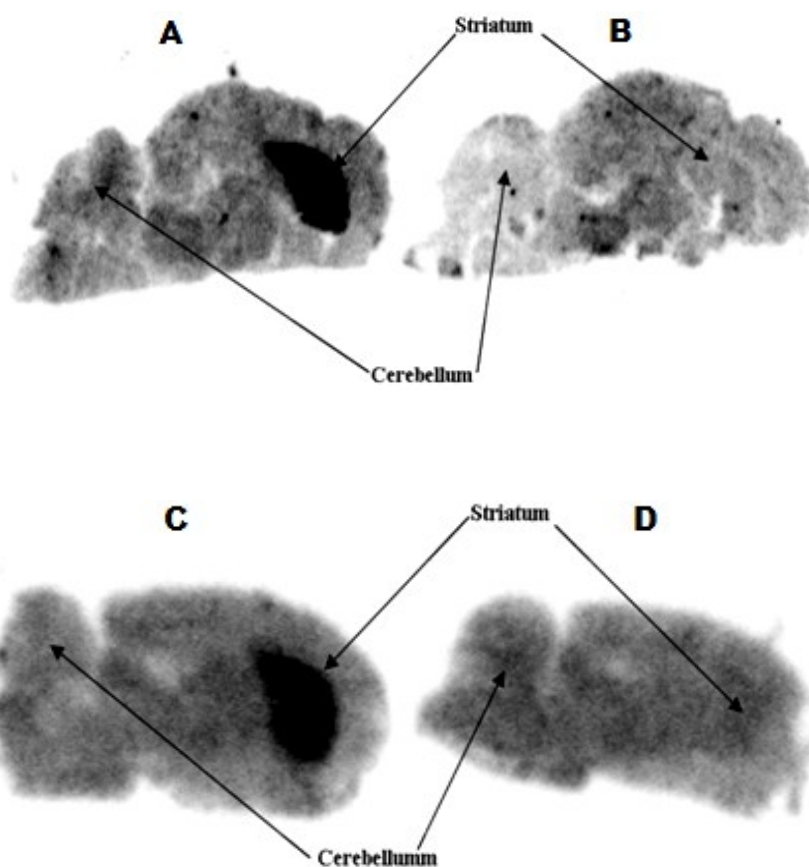
Chemical Structure	Mass modification	Rt in Min	Mass of metabolite	Proposed fragment loss or addition from / to parent
	-14.01	2.52	375.14	-CH ₂
	-15.01	2.53	376.12	-NH (Deamination)
	1.98	2.07	391.13	-CH ₂ & +O (Demethylation + C-hydroxylation)
	-148.08	1.78	241.07	-C ₁₀ H ₁₂ O (Parent-C ₁₀ H ₁₂ O)
	+15.99	2.44	405.15	+O (N-Oxidation or C-hydroxylation)

***In Vitro* Ligand Stability Test**

The *in vitro* stability of the two [18F]tracers in different solutions such as PBS, saline, rat plasma and human plasma was determined at 37 °C. After 1 and 2 h of incubation, radio-TLC analysis showed that 95-97 % of both tracers were still intact, except in the saline solution. In the saline solution, multiple spots were observed as detected by radio-TLC for both tracers, and the radioactivity corresponding to the intact tracers was only 85-90 %.

***In Vitro* Autoradiographic Experiments**

Figure 4 shows autoradiographic images of frozen rat brain sections that were incubated with [18F]-10a and [18F]-10b. In control sections, a clear difference was noted between the receptor-rich striatum and the receptor-poor cerebellum. The mean striatum-to-cerebellum ratios were 2.75 ± 0.12 ([18F]-10a) and 2.99 ± 0.16 ([18F]-10b). In the presence of an excess (2 μ M) of the A_{2A}R-specific antagonist 8-[(1*E*)-2-(2-(3,4-dimethoxyphenyl)ethenyl)-1,3-diethyl-3,7-dihydro-7-methyl-1*H*-purine-2,6-dione, **12** (KW6002 in Figure 1), the binding of the tracer to the striatum was strongly reduced and the striatum-to-cerebellum ratio decreased to unity (n = 3). Specific binding, as assessed by a blocking study, was 57–62 % and 64–67 % of the total uptake in the striatum of [18F]-10a and [18F]-10b, respectively.



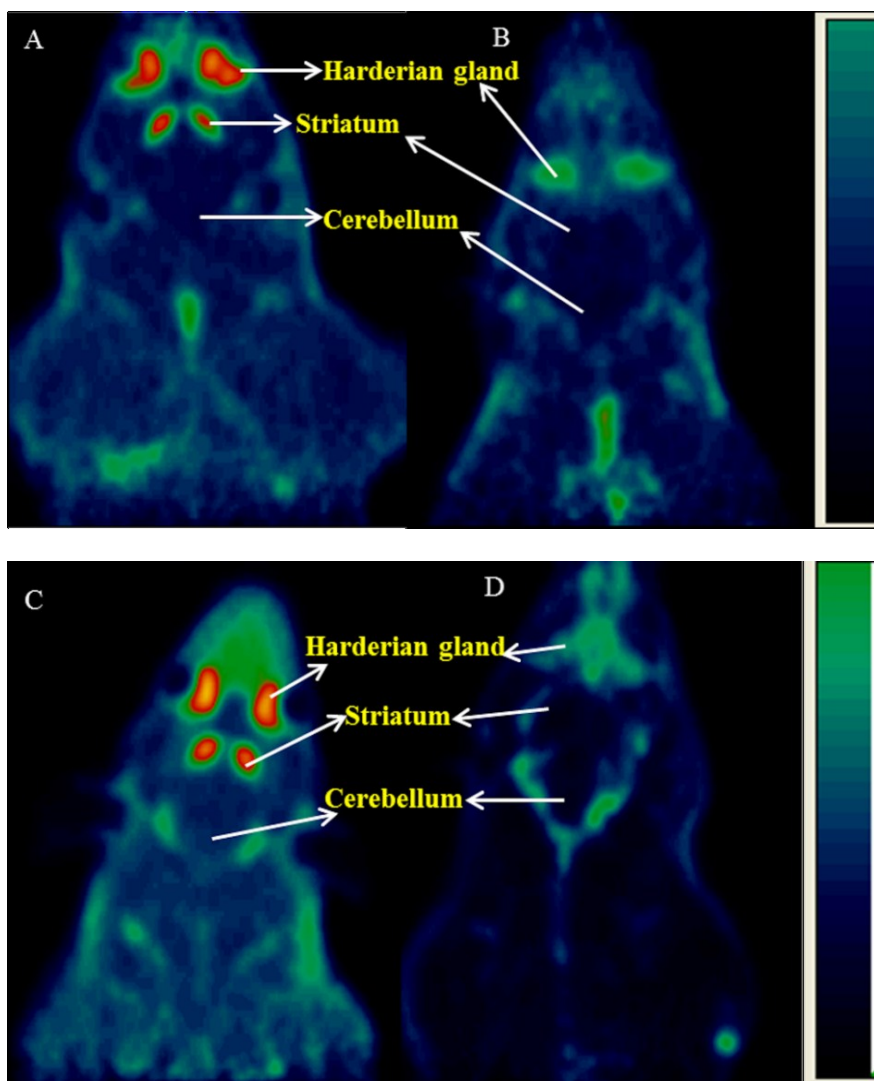
3

Figure 4. Autoradiographic images of sagittal sections of rat brains after 90 min of incubation with (A and B) [¹⁸F]-**10b** or (C and D) [¹⁸F]-**10a** in the (B and D) presence or (A and C) absence of an excess of a known A_{2A}R-selective antagonist, **12** (2 μM).

Micro PET Images

PET images acquired after injection of [¹⁸F]-**10a** and [¹⁸F]-**10b** are presented in Figure 5. The two radioligands displayed similar regional distributions that corresponded to the known regional A_{2A}R densities in the rat brain.^{3-5, 7} In order to prove specific binding, we have used vehicle-control and blocker animals (Please refer *in vivo* and *in vitro* selectivity of the experimental section for more details).

In vehicle-control animals, the striatum was clearly visualized. The extra-striatal binding of both tracers was hardly visible, but strong uptake was observed in the skull bone. When animals were pretreated with the A_{2A}R antagonist **12** (1 mg / kg), the cerebral uptake of the tracers was strongly reduced, and regional differences in tracer uptake were no longer observed.



3

Figure 5. Small-animal PET images of a coronal plane of rat brains after injections of (A and B) [¹⁸F]-**10a** or (C & D) [¹⁸F]-**10b**. The images represent the summed frames from 17 to 90 min postinjection. (A) Vehicle-control (left); (B) a compound **12**-treated animal ([¹⁸F]-**10a**) (right). (C) Vehicle-control (left); (D) a compound **12**-treated animal ([¹⁸F]-**10b**) (right). The images were normalized for body weight and injected dose.

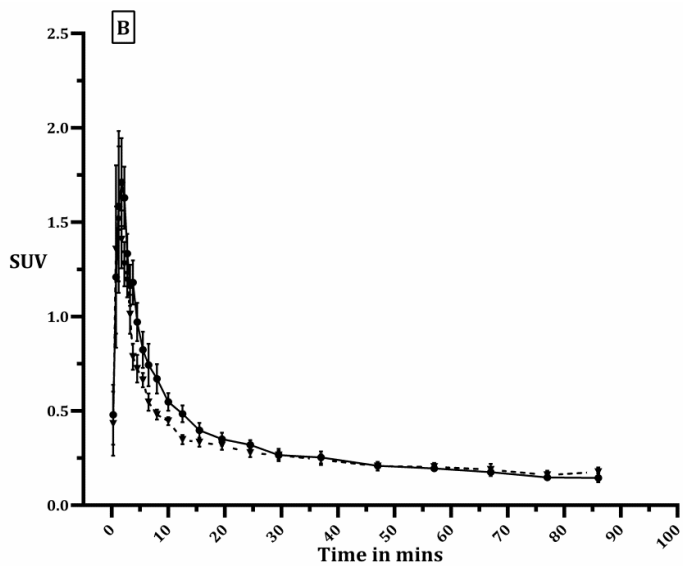
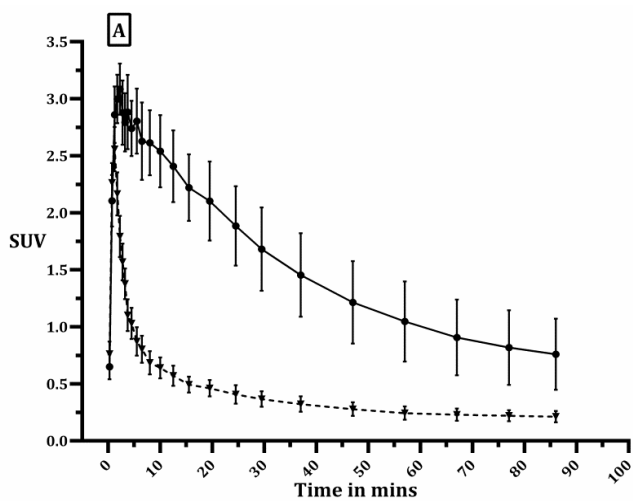
3

In Vivo Radioligand Kinetics and Metabolism

Kinetics of Radioactivity in Brain

The cerebral kinetics of radioactivity after the injection of [¹⁸F]-**10a** and [¹⁸F]-**10b** are presented in Figure 6 (panels A-D). In vehicle-treated control animals (n = 6), the uptake of radioactivity rapidly increased to a maximum (2.5 min after injection), which was followed by an exponential washout (panels A and C). In animals treated with **12** (n = 6), the cerebral uptake of ¹⁸F was strongly reduced, and the radioactivity was rapidly washed out from all brain regions (panels B and D). The difference in the striatal uptake of ¹⁸F in control and pretreated rats was statistically significant at most time points.

We estimate receptor occupancy on the basis of PET-standardized uptake values (PET-SUVs) (at the time of maximum uptake), reported A_{2A}R densities (953 fmol / mg protein in rat striatum⁵³) and injected tracer doses in nanomolar amounts. Assuming that brain tissue contains 10 % protein, we calculated that less than 2 % and 8 % of the cerebral A_{2A}R population was occupied by [¹⁸F]-**10b** and [¹⁸F]-**10a**, respectively, in both control- and blocker-treated rats.



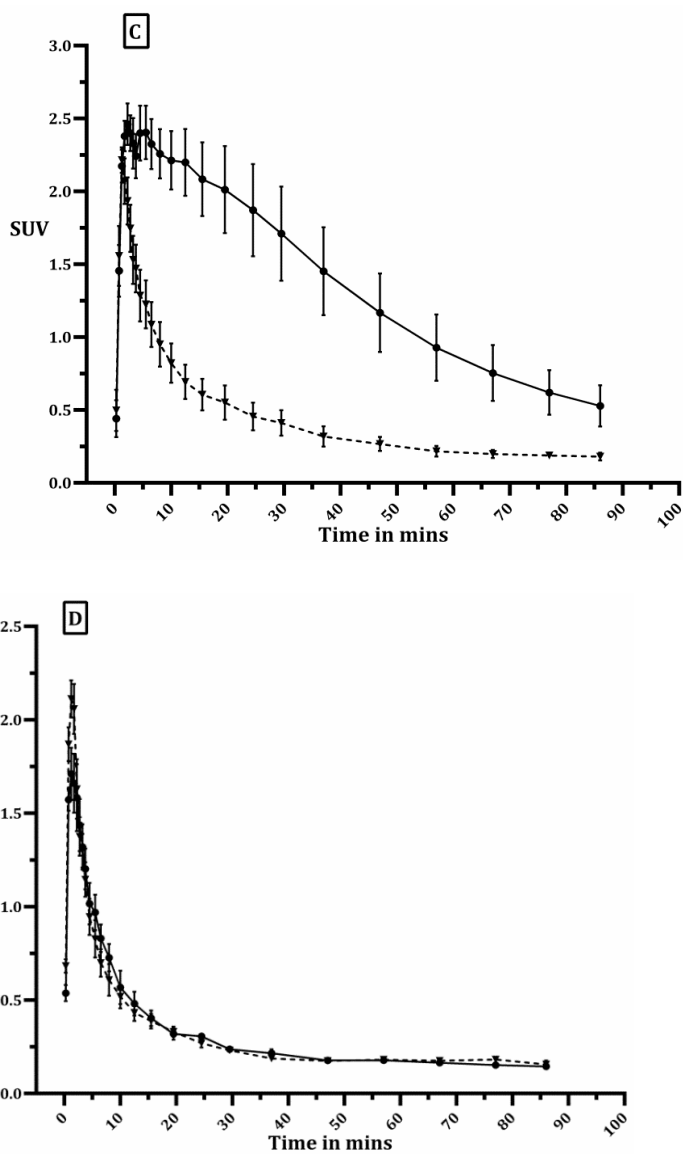


Figure 6. (A-D) Kinetics of (A & B) [18F]-10a and (C & D) [18F]-10b - derived radioactivity in the rat brain. The error bars indicate the SEM. (A and C) Vehicle-control animals (left); (B and D) compound 12-treated animals (right). ● = Striatum; ▼ = Cerebellum

Radioactivity Kinetics in Plasma

A rapid, biexponential plasma clearance was observed in all groups. Pretreatment did not significantly affect the clearance of radioactivity from the plasma compartment.

In Vivo Metabolite Analysis

An unidentified radiometabolite with a R_f value of 0–0.1 was observed in rat plasma (the R_f value of authentic [18F]-10b was 0.6). The fraction of total plasma radioactivity representing the parent compound decreased to $66 \pm 16\%$ at 60 min and $53 \pm 20\%$ at 90 min. Pretreatment with 12 did not affect the rate of tracer metabolism. The fraction of total plasma radioactivity representing [18F]-10a was $46 \pm 17\%$ at 60 min and $36 \pm 14\%$ at 90 min.

Ex Vivo Biodistribution Data

The biodistribution data for both tracers are shown in Figure 7. After pretreatment with 12, the uptake of both compounds was reduced in the A_{2A}R-rich striatum (approximately 69 % of [18F]-10b and 45 % for [18F]-10a). For [18F]-10b, the effect of the blocker was statistically significant in the frontal cortex and striatum, whereas for [18F]-10a ($n = 3$), no significant effect of the blocker was observed in any of the brain regions; however, the greatest decrease of the tracer uptake was observed in the striatum. Striatum-to-cerebellum ratios can be used as indices for the *in vivo* binding of the tracers to A_{2A}Rs. Striatum-to-cerebellum ratios of 3.5 and 2.1 were reached at 106 min postinjection for [18F]-10b ($n = 6$) and [18F]-10a ($n = 3$), respectively. The ratios of the uptake in other regions to the cerebellum were approximately equal to one. The standard uptake values in the skull bone (2.06 ± 0.58) for [18F]-10b were significantly higher than those of [18F]-10a (0.29 ± 0.05).

For both tracers, the plasma-to-blood ratio was greater than one, and the negligible binding to red blood cells in pretreated and control animals indicated that the radioligands preferentially distributed to the plasma.

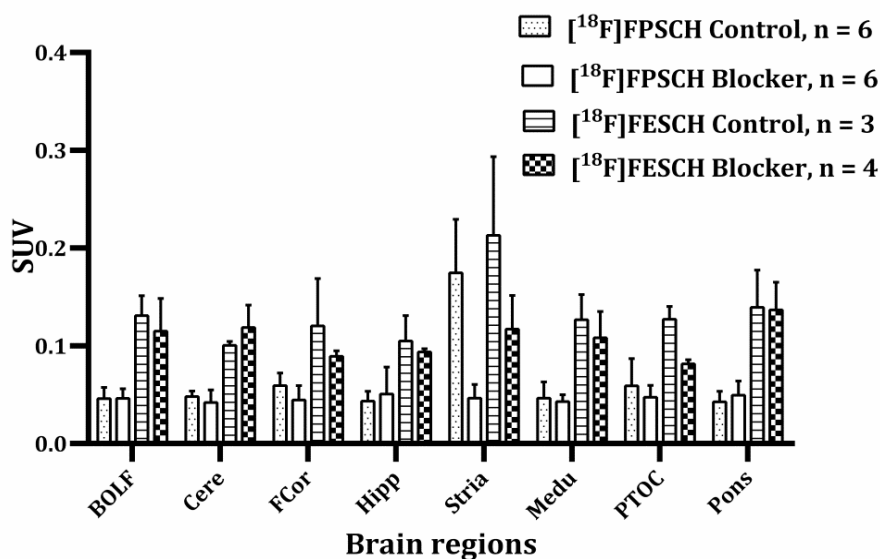


Figure 7. Cerebral biodistribution data of [18F]-10b and [18F]-10a at 106 min after injection. The error bars indicate the SEM. BOLF = Bulbus olfactorius, CERE = Cerebellum, FCor = Frontal cortex, Stria = Striatum, Hipp = Hippocampus, Medu = Medulla, PTOC = Parietal/Temporal/Occipital Cortex.

Discussion

We have evaluated [18F]-10a and [18F]-10b as PET tracers for the cerebral imaging of A_{2A}Rs; these tracers may provide many logistic advantages and can be used in centers without an on-site cyclotron. Thus, we synthesized fluorinated molecules based on a pyrazolo-triazolo-pyrimidine template (compound **8**) that is known to cross the BBB because of its appropriate lipophilicity (clogP = 2.9), molecular weight, charge, and hydrogen bonding.^{34, 38, 39} The molecular docking approach provides valuable atomic-level insight into the behavior of a small molecule in the binding site of the protein. It also provided insight into the binding mode of compound **8** derivatives to the active site of the receptor. Compound **8** and its fluoro analogs (**10a** and **10b**) had better GOLD fitness scores than

the clinically studied PET tracer (E)-8-(3,4,5-trimethoxystyryl)-1,3-dimethyl-7-[¹¹C]methylxanthine ([¹¹C]KF18446) and the A_{2A}R-bound crystal structure **17**. GOLD scores are good indicators to predict the binding orientations of compound **8** derivatives. A higher score predicts better binding orientations with the receptor residues. We have used the A₁R decoy, **18**-as negative control, to validate the quality of the GOLD scoring function.⁵⁴ Small structural changes of the phenoxy substituent appeared to be well-tolerated, and this is substantiated by our *in vivo* study. Subtype selectivity can be expected because the lead compound **8** shows a >10,000-fold selectivity for the A_{2A}R subtype compared to other AR subtypes. Moreover, the binding affinities of **8** ($K_i = 0.5$ nM) and **10a** ($K_i = 12.4$ nM) to the A_{2A}R were adequate for imaging.^{38, 42} Even though the reported K_i value of 53.6 nM for **10b**⁴⁹ is much lower than that of the lead compound **8**, the affinity data predict faster clearance than **8** and **10a** and more preferable brain kinetics for the quantitative evaluation of the ligand–receptor binding. The pyrazolo-triazolo-pyrimidine scaffold allows for the easy and quick incorporation of an [¹⁸F] label in the acidic phenol group, and this phenoxy substituent can also be used to modify the lipophilicity of the compound. Fluoroalkyl chain lengthening beyond the fluoropropyl substituent results in a higher molecular weight (MW) and lipophilicity for a compound. It has been suggested that the MW should be kept below 450 Da to facilitate brain penetration with fewer side effects such as high rapid metabolic turnover, poor absorption, and toxicity.⁵⁵ High lipophilicity causes unacceptable binding to plasma proteins, decreasing the free drug concentration available to pass the BBB, or binding to hydrophobic protein targets other than the desired one, resulting in high levels of nonspecific binding in the brain.^{34, 55} On the basis of these considerations, **10b** was selected as a novel candidate for radiolabeling to obtain the expected lipophilicity and a MW that ensures the crossing of the BBB.

Computational prediction of the sites of cytochrome *P450* (CYP450)-mediated metabolism and an *in vivo* plasma radio-TLC metabolite analysis indicated the formation of polar metabolites, which are not

expected to cross the BBB. The results obtained after incubation of **10b** with hepatic microsomes were in good agreement with a previously reported experiment and the predictions of a two-dimensional (2D) method (SMARTCyp) describing CYP450-mediated drug metabolism.^{42, 50} In contrast to the results obtained from a SMARTCyp prediction of drug metabolism (Please refer ligand metabolism module of the results section), the metabolic routes of compound **8** after incubation with human liver microsomes can be ranked in the following order: O-dealkylation > parent-C₁₀H₁₂O > N-oxidation or C-hydroxylation > deamination (Figure 3, Table 3). A stability test indicated that both **10a** and **10b** are highly stable *in vitro*. Because of the observed multiple spots as detected with radio-TLC in a saline solution, we used PBS instead of saline in the formulation of the tracers. The fraction of total plasma radioactivity representing [¹⁸F]-**10b** was 18–20 % higher than that of [¹⁸F]-**10a** at both 60 and 90 min in our *in vivo* metabolite analysis. However, stronger skull bone radioactivity uptake (i.e., stronger defluorination) was observed with [¹⁸F]-**10b** than [¹⁸F]-**10a** in both an *ex vivo* biodistribution study and a small-animal PET (microPET) image analysis. In our imaging studies (especially with [¹⁸F]-**10b**) the accurate quantitation of the radioactivity in the frontal cortex was difficult due to spillover from radiofluorine in the skull bone.

A retrosynthetic approach for **10a** and **10b** synthesis was successfully applied to avoid a cumbersome and time consuming scheme involving 8 reaction steps. In the synthesis of compound **10b**, 3-fluoropropyl tosylate **7** yielded a slightly better result than 1-bromo-3-fluoropropane (25 % vs 19 % yield) because tosylate is a better leaving group than bromide. Tracers were successfully synthesized using a two-pot two-step procedure (Scheme 3). The [¹⁸F]fluoroalkylation of phenol precursor **9** using corresponding intermediate fluorosynthons ([¹⁸F]-**5** or [¹⁸F]-**7**) yielded the desired ligands [¹⁸F]-**10a** and [¹⁸F]-**10b** at moderate yields (7–8 %) and satisfactory specific activities (Table 2). The average radiochemical yield of the [¹⁸F]-**5** or [¹⁸F]-**7** obtained was 50 ± 5 %, whereas the final fluoroalkylation conversion was approximately 25 ± 5 %.

Purification by HPLC and solid phase extraction provided a decay-corrected radiochemical yield of 7-8 %. The long evaporation step of the captured eluate [14 mL of hexane / ether (3:1)] during the purification of the [18F]-5 or [18F]-7 and the losses that occurred during the other manipulations of the synthesis accounted for the moderate radiochemical yields of the synthesized tracers [18F]-10a and [18F]-10b. The purification of the [18F]-5 or [18F]-7 by RP-HPLC and C-18 light Sep-Pak columns may improve the radiochemical yield. Our radiosynthetic procedure for [18F]-10a is much faster (by 15–20 min) than the existing procedure.⁴² The applied radiolabeling approach is versatile; we can quickly adopt the same procedure for the radiosynthesis of both compounds [18F]-10a and [18F]-10b. The radiochemical purities were also adequate and amounted to more than 98 % of the total radioactivity as determined by UHPLC quality control.

In vitro autoradiography (ARG) confirmed the selectivity of [18F]-10a and [18F]-10b for A_{2A}Rs. The tracer binding pattern, especially in the striatum and other parts of the brain, was comparable with *ex vivo* biodistribution readings. The regional distribution of radioactivity in the rat brain after the injection of [18F]-10a and [18F]-10b also suggests that these tracers are capable of measuring regional A_{2A}R densities. After pretreatment with a subtype-selective xanthine antagonist, **12**, the tracer uptake in the striatum was greatly suppressed, and regional differences were no longer present. In the biodistribution and PET studies, the uptake of [18F]-10b in the cerebellum and frontal cortex (areas lacking A_{2A}Rs) was also decreased after pretreatment with **12**. The most logical explanation for the specific binding in the cerebellum is that the endothelium and blood vessels express A_{2A}Rs, even if the brain tissue does not.^{12, 56} Taking into account the findings that pretreatment with **12** reduces the distribution volume of candidate reference tissues such as the cerebellum, we choose not to quantify the blocking effect using a (simplified) reference tissue model, 2-tissue compartment model, and Logan analysis.

The striatal uptake of both [18F]-ligands was clearly visualized using PET scans; both tracers reached a striatum-to-cerebellum ratio of

approximately 4.6, which is similar to the experiments with [^{11}C]-**8** result (4.6 ± 0.27).³⁹ However, the maximum ratio for [^{18}F]-**10b** was reached at a later time point (37 min) than that of [^{18}F]-**10a** (25 min) and [^{11}C]-**8** (15 min), most likely because of the higher lipophilicity of [^{18}F]-**10b** (Figure 8). Lipophilicity may prolong the circulating half-life of a tracer, resulting in extended availability for binding to A_{2A}Rs. After the maximum had been reached, the concentration of [^{18}F]-**10a** in the brain remained fairly stable until 30 min after injection (similar to [^{11}C]-**8**), whereas the concentration of [^{18}F]-**10b** showed a somewhat stronger washout. The cerebral kinetics of both radioligands were compatible with the duration of a PET scan (Figure 8).

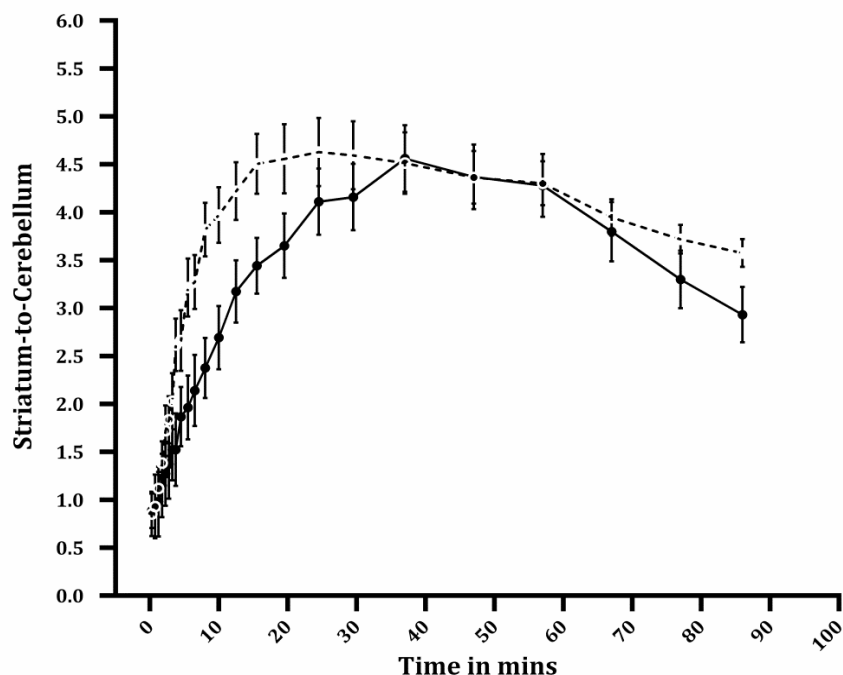


Figure 8. Striatum-to-cerebellum ratios of [^{18}F]-**10b** and [^{18}F]-**10a** as a function of time. The solid and broken lines represent [^{18}F]-**10b** and [^{18}F]-**10a**, respectively. The error bars indicate the SEM.

Conclusion

[¹⁸F]-10b and [¹⁸F]-10a could be prepared using a two-step procedure. Both radioligands showed a distribution in the rat brain, corresponding to the regional A_{2A}R densities known from *in vitro* ARG and binding assays. Experimental LogD_{7.4} values, plasma metabolite analysis and small-animal PET data analysis results suggest that these radiopharmaceuticals are potentially useful for mapping cerebral A_{2A}Rs. The molecular docking studies, similar target-to-nontarget ratios in *ex vivo* brain biodistribution and kinetic analysis, distribution patterns and only slightly different kinetics suggest that small increases in the length of the fluoroalkyl chain do not result in impaired pharmacokinetics and metabolic stability.

Acknowledgments

This project was supported by De Cock Stichting and ZonMW (No. 91111007, UPLC-MS-TOF). We thank Jurgen Sijbesma, MA Khayum and Marianne Schepers for their technical assistance

References

1. Ralevic, V.; Burnstock, G. Receptors for purines and pyrimidines. *Pharmacol. Rev.* **1998**, *50*, 413–492.
2. Khanapur, S.; van Waarde, A.; Ishiwata, K.; Leenders, K. L.; Dierckx, R. A.; Elsinga, P. H. Adenosine A_{2A} receptor antagonists as Positron Emission Tomography (PET) tracers. *Curr. Med. Chem.* **2014**, *21*, 312–328.
3. Martinez-Mir, M. I.; Probst, A.; Palacios, J. M. Adenosine A₂ receptors: Selective localization in the human basal ganglia and alterations with disease. *Neuroscience* **1991**, *42*, 697–706.
4. Ji, X. D.; Stiles, G. L.; van Galen, P. J.; Jacobson, K. A. Characterization of human striatal A₂-adenosine receptors using radioligand binding and photoaffinity labeling. *J. Recept. Res.* **1992**, *12*, 149–169.
5. Parkinson, F. E.; Fredholm, B. B. Autoradiographic evidence for G-protein coupled A₂-receptors in rat neostriatum using [3H]-CGS 21680 as a ligand. *Naunyn-Schmiedeberg's Arch. Pharmacol.* **1990**, *342*, 85–89.
6. Lindstrom, K.; Ongini, E.; Fredholm, B. B. The selective adenosine A_{2A} receptor antagonist SCH 58261 discriminates between two different binding sites for [3H]-CGS 21680 in the rat brain. *Naunyn-Schmiedeberg's Arch. Pharmacol.* **1996**, *354*, 539–541.
7. Ongini, E.; Fredholm, B. B. Pharmacology of adenosine A_{2A} receptors. *Trends Pharmacol. Sci.* **1996**, *17*, 364–372.
8. Fredholm, B. B.; Ijzerman, A. P.; Jacobson, K. A.; Linden, J.; Muller, C. E. International Union of Basic and Clinical Pharmacology. LXXXI. Nomenclature and classification of

- adenosine receptors: An update. *Pharmacol. Rev.* **2011**, *63*, 1–34.
9. Cunha, R. A.; Johansson, B.; Constantino, M. D.; Sebastiao, A. M.; Fredholm, B. B. Evidence for high-affinity binding sites for the adenosine A_{2A} receptor agonist [3H] CGS 21680 in the rat hippocampus and cerebral cortex that are different from striatal A_{2A} receptors. *Naunyn-Schmiedeberg's Arch. Pharmacol.* **1996**, *353*, 261–271.
 10. Feoktistov, I.; Biaggioni, I.; Cronstein, B. N. Adenosine receptors in wound healing, fibrosis and angiogenesis. *Handb. Exp. Pharmacol.* **2009**, *193*, 383–397.
 11. Blackburn, M. R.; Vance, C. O.; Morschl, E.; Wilson, C. N. Adenosine receptors and inflammation. *Handb. Exp. Pharmacol.* **2009**, *193*, 215–269.
 12. de Lera Ruiz, M.; Lim, Y. H.; Zheng, J. Adenosine A_{2A} receptor as a drug discovery target. *J. Med. Chem.* **2014**, *57*, 3623–3650.
 13. Jacobson, K. A. Introduction to adenosine receptors as therapeutic targets. *Handb. Exp. Pharmacol.* **2009**, *193*, 1–24.
 14. Armentero, M. T.; Pinna, A.; Ferré, S.; Lanciego, J. L.; Müller, C. E.; Franco, R. Past, present and future of A_{2A} adenosine receptor antagonists in the therapy of Parkinson's disease. *Pharmacol. Ther.* **2011**, *132*, 280–299.
 15. Morelli, M.; Carta, A. R.; Jenner, P. Adenosine A_{2A} receptors and Parkinson's disease. *Handb. Exp. Pharmacol.* **2009**, *193*, 589–615.
 16. Popoli, P.; Pepponi, R. Potential therapeutic relevance of adenosine A_{2B} and A_{2A} receptors in the central nervous system *CNS Neurol. Disord.: Drug Targets* **2012**, *11*, 664–674.

17. Ribeiro, J. A.; Sebastião, A. M.; de Mendonça, A. Adenosine receptors in the nervous system: Pathophysiological implications. *Prog. Neurobiol.* **2002**, *68*, 377–392.
18. Jacobson, K. A.; Gao, Z. G. Adenosine receptors as therapeutic targets. *Nat. Rev. Drug. Discovery* **2006**, *5*, 247–264.
19. Palacios, N.; Gao, X.; McCullough, M. L.; Schwarzschild, M. A.; Shah, R.; Gapstur, S.; Ascherio, A. Caffeine and risk of Parkinson's disease in a large cohort of men and women. *Mov. Disord.* **2012**, *27*, 1276–1282.
20. Cao, C.; Loewenstein, D. A.; Lin, X.; Zhang, C.; Wang, L.; Duara, R.; Wu, Y.; Giannini, A.; Bai, G.; Cai, J.; Greig, M.; Schofield, E.; Ashok, R.; Small, B.; Potter, H.; Arendash, G. W. High blood caffeine levels in MCI linked to lack of progression to dementia. *J. Alzheimer's Dis.* **2012**, *30*, 559–572.
21. Parent, A.; Hazrati, L. N. Functional anatomy of the basal ganglia. I. The cortico-basal ganglia-thalamo-cortical loop. *Brain Res. Rev.* **1995**, *20*, 91–127.
22. Hamani, C.; Saint-Cyr, J. A.; Fraser, J.; Kaplitt, M.; Lozano, A. M. The subthalamic nucleus in the context of movement disorders. *Brain* **2004**, *127*, 4–20.
23. Asanuma, K.; Tang, C.; Ma, Y.; Dhawan, V.; Mattis, P.; Edwards, C.; Kaplitt, M. G.; Feigin, A.; Eidelberg, D. Network modulation in the treatment of Parkinson's disease. *Brain* **2006**, *129*, 2667–2678.
24. Bauer, A.; Ishiwata, K. Adenosine receptor ligands and PET imaging of the CNS. *Handb. Exp. Pharmacol.* **2009**, *193*, 617–642.
25. Holschbach, M. H.; Olsson, R. A. Applications of adenosine receptor ligands in medical imaging by positron emission tomography. *Curr. Pharm. Des.* **2002**, *8*, 2345–2352.

26. Narendran, R.; Hwang, D. R.; Slifstein, M.; Talbot, P. S.; Erritzoe, D.; Huang, Y.; Cooper, T. B.; Martinez, D.; Kegeles, L. S.; Abi-Dargham, A.; Laruelle, M. *In vivo* vulnerability to competition by endogenous dopamine: Comparison of the D2 receptor agonist radiotracer (-)-N-[11C]propyl-norapomorphine ([11C]NPA) with the D₂ receptor antagonist radiotracer [11C]-raclopride. *Synapse* **2004**, *52*, 188–208.
27. Hirani, E.; Gillies, J.; Karasawa, A.; Shimada, J.; Kase, H.; Opacka-Juffry, J.; Osman, S.; Luthra, S. K.; Hume, S. P.; Brooks, D. J. Evaluation of [4-O-methyl-(11)C]KW-6002 as a potential PET ligand for mapping central adenosine A_{2A} receptors in rats. *Synapse* **2001**, *42*, 164–176.
28. Ishiwata, K.; Noguchi, J.; Toyama, H.; Sakiyama, Y.; Koike, N.; Ishii, S.; Oda, K.; Endo, K.; Suzuki, F.; Senda, M. Synthesis and preliminary evaluation of [11C]KF17837, a selective adenosine A_{2A} antagonist. *Appl. Radiat. Isot.* **1996**, *47*, 507–511.
29. Ishiwata, K.; Ogi, N.; Shimada, J.; Nonaka, H.; Tanaka, A.; Suzuki, F.; Senda, M. Further characterization of a CNS adenosine A_{2A} receptor ligand [11C]KF18446 with *in vitro* autoradiography and *in vivo* tissue uptake. *Ann. Nucl. Med.* **2000**, *14*, 81–89.
30. Marian, T.; Boros, I.; Lengyel, Z.; Balkay, L.; Horvath, G.; Emri, M.; Sarkadi, E.; Szentmiklosi, A. J.; Fekete, I.; Tron, L. Preparation and primary evaluation of [11C]CSC as a possible tracer for mapping adenosine A_{2A} receptors by PET. *Appl. Radiat. Isot.* **1999**, *50*, 887–893.
31. Noguchi, J.; Ishiwata, K.; Wakabayashi, S.; Nariai, T.; Shumiya, S.; Ishii, S.; Toyama, H.; Endo, K.; Suzuki, F.; Senda, M. Evaluation of carbon-11-labeled KF17837: A potential CNS adenosine A_{2A} receptor ligand. *J. Nucl. Med.* **1998**, *39*, 498–503.

32. Stone-Elander, S.; Thorell, J.; Eriksson, L.; Fredholm, B. B.; Ingvar, M. *In vivo* biodistribution of [N-11C-methyl]KF 17837 using 3-D-PET: Evaluation as a ligand for the study of adenosine A_{2A} receptors. *Nucl. Med. Biol.* **1997**, *24*, 187–191.
33. Wang, W. F.; Ishiwata, K.; Nonaka, H.; Ishii, S.; Kiyosawa, M.; Shimada, J.; Suzuki, F.; Senda, M. Carbon-11-labeled KF21213: A highly selective ligand for mapping CNS adenosine A_{2A} receptors with positron emission tomography. *Nucl. Med. Biol.* **2000**, *27*, 541–546.
34. Fujita, M.; Innis, R. B. *In vivo* molecular imaging: Ligand development and research applications. In *Neuropsychopharmacology: The Fifth Generation Of Progress*; Davis, K. , Charney, D. , Coyle, J., Nemeroff, C. , Eds.; Lippincott, Williams, & Wilkins: Philadelphia, PA, 2002; pp 411–425.
35. Leopoldo, M.; Lacivita, E.; De Giorgio, P.; Contino, M.; Berardi, F.; Perrone, R. Design, synthesis, and binding affinities of potential positron emission tomography (PET) ligands with optimal lipophilicity for brain imaging of the dopamine D₃ receptor. Part II. *Bioorg. Med. Chem.* **2009**, *17*, 758–766.
36. Pike, V. W. PET radiotracers: Crossing the blood-brain barrier and surviving metabolism. *Trends Pharmacol. Sci.* **2009**, *30*, 431–440.
37. Amini, N.; Nakao, R.; Schou, M.; Halldin, C. Identification of PET radiometabolites by cytochrome P₄₅₀, UHPLC/Q-ToF-MS and fast radio-LC: Applied to the PET radioligands [11C]flumazenil, [18F]FE-PE2I, and [11C]PBR28. *Anal. Bioanal. Chem.* **2013**, *405*, 1303–1310.
38. Todde, S.; Moresco, R. M.; Simonelli, P.; Baraldi, P. G.; Cacciari, B.; Spalluto, G.; Varani, K.; Monopoli, A.; Matarrese, M.; Carpinelli, A.; Magni, F.; Kienle, M. G.; Fazio, F. Design, radiosynthesis, and biodistribution of a new potent and

- selective ligand for *in vivo* imaging of the adenosine A_{2A} receptor system using positron emission tomography. *J. Med. Chem.* **2000**, *43*, 4359–4362.
39. Moresco, R. M.; Todde, S.; Belloli, S.; Simonelli, P.; Panzacchi, A.; Rigamonti, M.; Galli-Kienle, M.; Fazio, F. *In vivo* imaging of adenosine A_{2A} receptors in rat and primate brain using [11C]SCH442416. *Eur. J. Nucl. Med. Mol. Imaging* **2005**, *32*, 405–413.
40. Mihara, T.; Noda, A.; Arai, H.; Mihara, K.; Iwashita, A.; Murakami, Y.; Matsuya, T.; Miyoshi, S.; Nishimura, S.; Matsuoka, N. Brain adenosine A_{2A} receptor occupancy by a novel A₁/A_{2A} receptor antagonist, ASP5854, in Rhesus monkeys: Relationship to anticataleptic effect. *J. Nucl. Med.* **2008**, *49*, 1183–1188.
41. Matsuya, T.; Takuma, K.; Sato, K.; Asai, M.; Murakami, Y.; Miyoshi, S.; Noda, A.; Nagai, T.; Mizoguchi, H.; Nishimura, S.; Yamada, K. Synergistic effects of adenosine A_{2A} antagonist and L-DOPA on rotational behaviors in 6-hydroxydopamine-induced hemi-Parkinsonian mouse model. *J. Pharmacol. Sci.* **2007**, *103*, 329–332.
42. Shinkre, B. A.; Kumar, T. S.; Gao, Z. G.; Deflorian, F.; Jacobson, K. A.; Trenkle, W. C. Synthesis and evaluation of 1,2,4-triazolo[1,5-c]pyrimidine derivatives as A_{2A} receptor-selective antagonists. *Bioorg. Med. Chem. Lett.* **2010**, *20*, 5690–5694.
43. Bhattacharjee, A. K.; Lang, L.; Jacobson, O.; Shinkre, B.; Ma, Y.; Niu, G.; Trenkle, W. C.; Jacobson, K. A.; Chen, X.; Kiesewetter, D. O. Striatal adenosine A_{2A} receptor-mediated positron emission tomographic imaging in 6-hydroxydopamine-lesioned rats using [(18)F]-MRS5425. *Nucl. Med. Biol.* **2011**, *38*, 897–906.

44. Elsinga, P. H.; van Waarde, A.; Jaeggi, K. A.; Schreiber, G.; Helderdoorn, M.; Vaalburg, W. Synthesis and evaluation of (S)-4-(3-(2'-[11C]isopropylamino)-2-hydroxypropoxy)-2H-benzimidazol-2-one ((S)-[11C]CGP 12388) and (S)-4-(3-((1'-[18F]fluoroisopropyl)amino)-2-hydroxypropoxy)-2H-benzimidazol-2-one ((S)-[18F]fluoro-CGP 12388) for visualization of beta-adrenoceptors with positron emission tomography. *J. Med. Chem.* **1997**, *40*, 3829–3835.
45. *Sybyl*, version 7.1; Tripos Associates Inc.: St. Louis, MO 2005.
46. Sherali, H. D.; Ulular, O. Conjugate gradient methods using quasi-Newton updates with inexact line searches. *Journal of Mathematical Analysis and Applications* **1990**, *150*, 359–377.
47. Gasteiger, J.; Marsili, M. Iterative partial equalization of orbital electronegativity : A rapid access to atomic charges. *Tetrahedron* **1980**, *36*, 3219–3228.
48. Verdonk, M. L.; Cole, J. C.; Hartshorn, M. J.; Murray, C. W.; Taylor, R. D. Improved protein-ligand docking using GOLD. *Proteins* **2003**, *52*, 609–623
49. Kumar, T. S.; Mishra, S.; Deflorian, F.; Yoo, L. S.; Phan, K.; Kecskes, M.; Szabo, A.; Shinkre, B.; Gao, Z. G.; Trenkle, W.; Jacobson, K. A. Molecular probes for the A_{2A} adenosine receptor based on a pyrazolo[4,3-e][1,2,4]triazolo[1,5-c]pyrimidin-5-amine scaffold. *Bioorg. Med. Chem. Lett.* **2011**, *21*, 2740–2745.
50. Rydberg, P.; Gloriam, D. E.; Zaretski, J.; Breneman, C.; Olsen, L. SMARTCyp: A 2D method for prediction of cytochrome P₄₅₀-mediated drug metabolism. *ACS Med. Chem. Lett.* **2010**, *1*, 96–100.
51. DalBen, D.; Lambertucci, C.; Marucci, G.; Volpini, R.; Cristalli, G. Adenosine receptor modeling: What does the A_{2A} crystal structure tell us?. *Curr. Top. Med. Chem.* **2010**, *10*, 993–1018.

52. Jaakola, V. P.; Griffith, M. T.; Hanson, M. A.; Cherezov, V.; Chien, E. Y.; Lane, J. R.; Ijzerman, A. P.; Stevens, R. C. The 2.6 angstrom crystal structure of a human A_{2A} adenosine receptor bound to an antagonist. *Science* **2008**, *322*, 1211–1217.
53. Alfaro, T. M.; Vigia, E.; Oliveira, C. R.; Cunha, R. A. Effect of free radicals on adenosine A_{2A} and dopamine D2 receptors in the striatum of young adult and aged rats. *Neurochem. Int.* **2004**, *45*, 733–738.
54. Graves, A. P.; Brenk, R.; Shoichet, B. K. Decoys for docking. *J. Med. Chem.* **2005**, *48*, 3714–3728.
55. Pajouhesh, H.; Lenz, G. R. Medicinal chemical properties of successful central nervous system drugs. *NeuroRx* **2005**, *2*, 541–553.
56. Fredholm, B. B.; Cunha, R. A.; Svenningsson, P. Pharmacology of adenosine A_{2A} receptors and therapeutic applications. *Curr. Top. Med. Chem.* **2003**, *3*, 413–426.



**Synthesis and Preclinical Evaluation of
[¹¹C]Preladenant as a PET Tracer for the
Imaging of Cerebral Adenosine A_{2A} Receptors**

Shivashankar Khanapur[†], Xiaoyun Zhou[†], Anja P. Huizing, Rolf Zijlma, Rudi A.J.O. Dierckx, Aren van Waarde, Erik F.J. de Vries, Philip H. Elsinga*

Department of Nuclear Medicine and Molecular Imaging, UMCG,
University of Groningen, Groningen, The Netherlands

4

[†] These authors contributed equally

Under revision in *J. Med. Chem.*

Abstract

2-(2-Furanyl)-7-[2-[4-[4-(2-[¹¹C]methoxyethoxy)phenyl]-1-piperazinyl]ethyl]7*H*-pyrazolo[4,3-*e*][1,2,4]triazolo[1,5-*c*]pyrimidine-5-amine [¹¹C]-**3** ([¹¹C]Preladenant) was developed as a new PET ligand for mapping cerebral adenosine A_{2A} receptors (A_{2A}Rs). The tracer was synthesized in high specific activity and purity. Tissue distribution was studied by PET, *ex-vivo* biodistribution and *in vitro* autoradiography. Regional brain uptake of [¹¹C]-**3** was consistent with known A_{2A}Rs distribution, with highest uptake in striatum. PET showed that [¹¹C]-**3** has favorable brain kinetics. The results indicate that [¹¹C]-**3** exhibits suitable characteristics as an A_{2A}R PET tracer.

Introduction

Adenosine A_{2A} receptors (A_{2A}Rs) are G-protein coupled receptors that are mainly expressed on the dendritic spines of striatopallidal GABAergic neurons in the brain.¹ A_{2A}Rs are involved in many neuropsychiatric disorders, such as Parkinson's disease (PD), Huntington's disease, Alzheimer's disease, drug addiction, alcohol abuse, epilepsy seizures, sleep disorders and schizophrenia.² A_{2A}Rs play an important role in regulation of striatal dopaminergic transmission in the basal ganglia through antagonistic interactions between postsynaptic A_{2A} and dopamine D₂ receptors (D₂Rs).¹ In addition, A_{2A}Rs may play a role in the regulation of excitatory glutamatergic neurotransmission because of their ability to form functional heterodimers with D₂Rs, metabotropic glutamate receptor 5, cannabinoid receptor type 1 and adenosine A₁ receptors (A₁Rs).^{3, 4} A number of studies have suggested that blockade of A_{2A}Rs reduces overactivity of the indirect dopamine pathway observed during PD.⁵ Thus, inhibition of A_{2A}R-mediated signaling can alleviate motor deficits⁶⁻⁸ without provoking marked levodopa-induced dyskinesia.^{9, 10} To gain a better understanding of the involvement of A_{2A}Rs in disease conditions, noninvasive imaging of the density and occupancy of these receptors could provide valuable information.

Positron Emission Tomography (PET) is a noninvasive imaging technique that allows monitoring of physiological processes in living subjects. Therefore, PET could be applied to study changes in the distribution and expression of A_{2A}Rs in pathological conditions *in vivo*. Several ¹¹C and ¹⁸F labeled ligands have been evaluated as PET tracers for A_{2A}Rs.¹¹⁻¹⁶ Till now, (E)-8-(3,4,5-trimethoxystyryl)-1,3-dimethyl-7-[¹¹C]methylxanthine [**[¹¹C]-1**] ([¹¹C]TMSX) and 7-(3-(4-[¹¹C]methoxyphenyl)propyl)-2-(2-furyl)pyrazolo[4,3-e]-1,2,4-triazolo[1,5-c]pyrimidine-5-amine [**[¹¹C]-2**] ([¹¹C]SCH442416) are the best characterized tracers for mapping cerebral A_{2A}Rs (Figure 1).^{17, 18} However, low binding potentials, high nonspecific binding and consequently low target-to-nontarget ratios (e.g. striatum-to-cerebellum ratio at 15 min: 1.2 and 2.2 for [**[¹¹C]-1**] and [**[¹¹C]-2**]

respectively) are important disadvantages of these tracers (Figure 1).^{11, 13} Therefore, new radioligands with a high degree of selectivity, high enough affinity to image receptors but not so high as to compromise receptor quantification.¹⁹ and good pharmacokinetic properties are required for mapping A_{2A}Rs in the living brain. 2-(2-Furanyl)-7-[2-[4-[4-(2-methoxyethoxy)phenyl]-1-piperazinyl]ethyl]7*H*-pyrazolo[4,3-*e*][1,2,4]triazolo[1,5-*c*]pyrimidine-5-amine **3** (Preladenant) is an A_{2A}R antagonist, which readily crosses the blood-brain-barrier, shows a high affinity ($K_i = 1.1$ nM, human A_{2A}Rs) and selectivity (> 1000 fold selective for A_{2A}Rs over adenosine A₁, A_{2B}, and A₃ receptors) towards A_{2A}Rs.²⁰ It exhibited an adequate safety, tolerability and clinical efficacy profile in preclinical and Phase I and II clinical trials. However, it failed to demonstrate clinical efficacy in Phase III and hence its clinical evaluation as treatment of Parkinson's disease was stopped. Yet, the properties of **3** could still make it a potential PET tracer for *in vivo* imaging of A_{2A}Rs, because treatment efficacy is not an issue for the development of radiotracers. Furthermore, easy and quick incorporation of a radionuclide by [¹¹C]methylation of the 2-(4-(4-(2-(5-amino-2-(furan-2-yl)-7*H*-pyrazolo[4,3-*e*][1,2,4]triazolo[1,5-*c*]pyrimidin-7-yl)ethyl)piperazin-1-yl)phenoxy)ethoxymethane **4** (O-desmethyl preladenant precursor) molecule seems to be possible. In addition, large expenses in the radiotracer development process can be avoided, because the toxicity and metabolic profile of preladenant are known. In this paper, we report the synthesis and *in vivo* evaluation of 2-(2-Furanyl)-7-[2-[4-[4-(2-[¹¹C]methoxyethoxy)phenyl]-1-piperazinyl]ethyl]7*H*-pyrazolo[4,3-*e*][1,2,4]triazolo[1,5-*c*]pyrimidine-5-amine [¹¹C]-**3** ([¹¹C]preladenant) as PET tracer for imaging of A_{2A}Rs in the brain in rats.

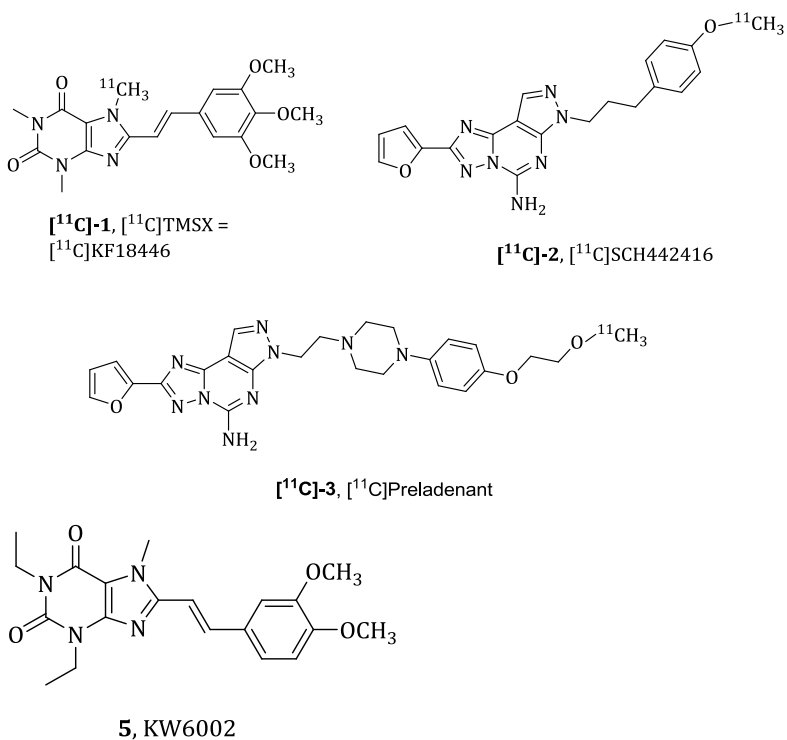


Figure 1. Structures of the best characterized A_{2A}R PET imaging agents, [¹¹C]-3 and an antagonist

Experimental Section

General

Compound **3** (Preladenant) was purchased from Chemscene, LLC (USA). Silicon tetrachloride and sodium iodide were procured from Sigma-Aldrich (the Netherlands). Compound **5** was purchased from Axon Medchem BV (The Netherlands). All other chemicals were of analytical grade and obtained from commercial suppliers. All were used without further purification.

¹H and ¹³C NMR spectra were recorded on a Varian Oxford 400 MHz spectrometer (400 MHz, 100.59 MHz, respectively), Chemical shifts are reported as δ values and coupling constants in hertz (Hz).

Chemical shifts for ^1H and ^{13}C NMR were reported in ppm relative to the tetramethylsilane peak. ESI-HRMS was used to assess the exact molecular weight of O-desmethylpreladenant **4**

Synthesis of O-Desmethylpreladenant (**2**), (Scheme 1)

Compound **3** (0.1 g, 0.2 mmol) and sodium iodide (0.54 g, 3.6 mmol) were dissolved in a mixture of dichloromethane (8 mL) and acetonitrile (8 mL). To this mixture, silicon tetrachloride (0.4 mL, 3.6 mmol) was added and the reaction mixture was stirred continuously at room temperature for 17 h. The reaction was quenched by pouring the reaction mixture into water (8 mL). The suspension was basified to $\text{pH} \geq 10$ by the addition of 20 % sodium hydroxide solution (2 mL). This two-layer system was stirred vigorously for another 2 h. The organic layer was then removed and the aqueous phase was filtered. The crude product (residue) was purified by washing it with water (5×8 mL) and then with acetone (3×3 mL) to get **4** (0.08 g, 0.163 mmol, 82 %) as a white solid. RP-HPLC using Phenomenex prodigy ODS (3) C-18 HPLC column ($5 \mu\text{m}$, 10×250 mm) was used to check the purity of precursor **4**. The product was eluted with a mobile phase, consisting of 0.1 M ammonium acetate / acetonitrile (60 : 40 v / v), at a flow rate of 4 mL / min. The purity of precursor **4** was typically 98 %.

$^1\text{H-NMR}$ (400 MHz, $\text{DMSO-}d_6$): δ 8.21 (s, 1H), 8.11 (bs, 2H, NH_2), 7.98 (s, 1H), 7.26 (d, $J = 3.4$, 1H), 6.90-6.80 (m, 4H), 6.77 (dd, $J = 3.3$, 1.7, 1H), 4.84 (t, $J = 5.5$, 1H), 4.46 (t, $J = 6.7$, 2H), 3.92 (t, $J = 5.1$, 2H), 3.70 (dd, $J = 10.3$, 5.2, 2H), 3.05-2.95 (m, 4H), 2.92-2.83 (m, 2H), 2.68-2.56 (m, 4H).

$^{13}\text{C-NMR}$ (100 MHz, $\text{DMSO-}d_6$): δ 155.8, 152.7, 149.1, 149.1, 146.7, 145.9, 145.8, 145.5, 131.9, 96.1, 117.7, 115.4, 112.7, 112.6, 70.2, 60.1, 57.0, 53.1, 49.9, 44.8.

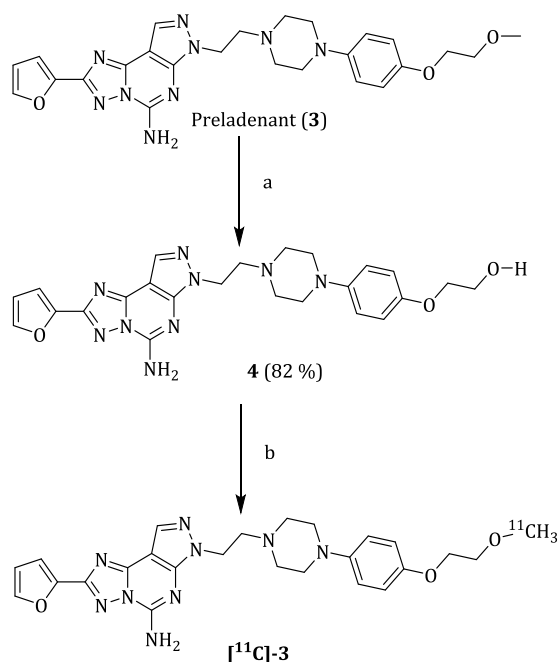
ESI-HRMS m/z 490.2309 $[\text{M}+\text{H}]^+$, $\text{C}_{24}\text{H}_{27}\text{N}_9\text{O}_3 \cdot \text{H}^+$: Calcd. 490.2315

Radiochemistry, (Scheme 1)

[¹¹C]Methane was produced via the ¹⁴N (p, α) ¹¹C nuclear reaction by irradiating a nitrogen / hydrogen gas mixture using a Scanditronix MC17 cyclotron. [¹¹C]CH₃I was prepared based on a gas-phase synthesis involving the reaction of [¹¹C]CH₄ with I₂.²¹ [¹¹C]CH₃I was trapped in a conical vial containing 1 mg **4** and 10 mg potassium hydroxide in 0.3 mL DMSO at room temperature. After trapping of [¹¹C]CH₃I was complete, the reaction mixture was heated at 40 °C for 3 min. Subsequently, the mixture was neutralized with 0.2 mL 1M HCl, filtered [0.45 μm Polytetrafluoroethylene syringe filter], diluted with 0.5 mL HPLC eluent and purified by RP-HPLC using Phenomenex prodigy ODS (3) C-18 HPLC column (5 μm, 10 × 250 mm). The mixture was eluted with a mobile phase, consisting of 0.1 M ammonium acetate / acetonitrile (60 : 40 v / v), at a flow rate of 4 mL / min. The radioactive product with a retention time of approximately 11 min was collected and diluted with water (90 mL). The product was trapped on a C18 light SepPak cartridge (Waters). The cartridge was washed twice with 8 mL water. The cartridge was eluted with 1 mL ethanol, 4 mL PBS and the eluent was sterilized over a 0.22 μm Millex LG sterilization filter. Then, the formulated tracer was submitted to quality control (QC).

QC was performed by UHPLC, consisting of a Waters (Milford, MA) Acquity Ultrapformance LC quaternary solvent manager coupled to a tunable, dual-wavelength UV detector operated at 254 nm and a radioactivity detector (Berthold Flowstar LB 513). The radioactive product (10 μL) was injected onto an Ethylene Bridged Hybrid (BEH) shield RP-18 column (3.0 × 50 mm, 1.7 μm) and eluted with acetonitrile / water pH 2 (25 : 75, v / v) at a flow rate of 0.6 mL / min. The column temperature was set at 35 °C.

Scheme 1. Synthesis of Precursor (4) and Radiosynthesis of [¹¹C]-3^a



4

^a**Reagents and conditions:** (a) SiCl₄ / NaI, CH₂Cl₂ / CH₃CN, 1 / 1, rt, 17 h; (b) [¹¹C]CH₃I, KOH, DMSO, 40 °C, 3 min.

Distribution Constant (log D_{7.4})

An aliquot of 10 μL of formulated [¹¹C]-3 was added to a mixture of *n*-octanol / PBS (1 mL, 1 : 1 v / v). The tubes were vortexed for 1 min, followed by 30 min of shaking in a water bath at 37 °C. 200 μL aliquots were drawn from the *n*-octanol and aqueous phases. The radioactivity in each phase was counted by a gamma-counter (Compugamma 1282 CS, LKB-Wallac, Turku, Finland). The

experiments were performed in quadruplicate and repeated for three independent tracer productions. The average LogD_{7.4} value and the standard deviation are reported.

***In vitro* Autoradiography**

Brains were taken from young (10–11 weeks of age; 300–350 g body weight) male Wistar rats (Harlan, The Netherlands) and cut into halves along the sagittal symmetry plane. Sagittal sections of 20 μm thickness were cut at -18 °C with Leica CM 1950 microtome (Leica Biosystems, The Netherlands) and thaw-mounted onto starfrost adhesive pre-coated slides (76 × 26 mm, Waldemar Knittel, Germany). Brain sections were air-dried at room temperature for 45 min and stored at -80 °C until further use (within 1 week).

On the day of the experiment, the sections were allowed to warm to room temperature for 5–10 min and then pre-incubated with incubation buffer (50 mM Tris-HCl, 10 mM MgCl₂, 0.1 % bovine serum albumin, pH 7.4 at 25 °C) for 15 min at room temperature. After the incubation buffer was removed, sections were placed into jars containing incubation buffer (70 mL, 37 °C) and [¹¹C]-**3** at a concentration of 12.5 ± 3.0 nM (n = 3). Nonspecific binding was determined by placing sections into jars containing same amounts of incubation buffer and tracer, but in addition of 2 μM **5**. The slides were incubated for 60 min at 37 °C, then washed twice with ice-cold PBS (70 mL, 5 min + 3 min) and dipped for 15 s into ice-cold sterile water (70 mL) and dried with an air flow at room temperature. The slices were then exposed to phosphor storage screens for 3 h. The screens were read by a Cyclone Storage Phosphor System (Packard Instruments Co). Quantification of plate readings was performed with Optiquant (version 3.00). Regions of interest (ROIs) were drawn manually around the striatum and cerebellum. Regional uptake of radioactivity was measured and expressed as digital light units/mm².

In Vivo Studies

Animals

The protocol was approved by the Institutional Animal Care and Use Committee of the University of Groningen (DEC 6698B). Male outbred Wistar-Unilever rats (Hsd / Cpb:WU, 10–12 weeks old, 300–400 grams) were purchased from Harlan (The Netherlands). The animals were housed in Macrolon cages (38 × 26 × 24 cm) at a 12 h light-dark cycle and were fed with standard laboratory chow (RMH-B, The Netherlands) and water ad libitum. After arrival from the supplier, the rats were allowed to acclimatize for at least seven days. Prior to PET imaging, animals were anesthetized with isoflurane in medical air (5 % isoflurane for induction, 1.5–2.5 % isoflurane for maintenance) and kept on electronic heating pads to maintain their body temperature during the study. A cannula was placed in the femoral vein for tracer injection with a Harvard-style pump at a speed of 1 mL / min. 7–10 min prior to tracer injection, vehicle (50 % dimethylacetamide in saline) or an A_{2A} antagonist **5** (1 mg / kg) in a solution of 50 % dimethylacetamide in saline (1 mg / mL) was injected *intraperitoneally*. Heart rate and blood oxygenation level of animals were monitored throughout the scanning procedure, using pulse oximeters (Zevenaar, The Netherlands).

4

PET Acquisition

PET imaging was performed using a Focus 220 MicroPET camera (Preclinical solutions, Siemens Healthcare Molecular Imaging, USA Inc.). Two animals were scanned simultaneously (supine position) using a 60 min scan protocol. The brains of both animals were placed in the center of the field of view. A transmission scan of 515 s using a ⁵⁷Co point source was performed before the emission scan. The emission scan was started at the moment the tracer (107.3 ± 32.3 MBq, 4.70 ± 1.29 nmol) entered the body.

PET Data Processing

List mode emission data were separated in 21 time frames (6 × 10, 4 × 30, 2 × 60, 1 × 120, 1 × 180, 4 × 300, 3 × 600 s). The data were

reconstructed per time frame using an iterative reconstruction algorithm (attenuation-weighted 2-dimensional ordered-subset expectation maximization, 4 iterations, 16 subsets; zoom factor 2, image matrix 256). After cropping, the final datasets consisted of 95 slices with a slice thickness of 0.8 mm and an in-plane image matrix of 128×128 pixels of size 0.47 mm. Datasets were fully corrected for random coincidences, scatter, and attenuation.

Time frames of each PET scan were summed and co-registered to a magnetic resonance imaging (MRI) template of a rat brain with predefined volumes of interest (VOIs). The VOIs were transferred from the MRI template to the PET data, and regional time-activity curves (TACs, Bq / cm²) were generated for whole brain, total cortex, frontal cortex, occipital cortex, parietal cortex, striatum, midbrain, thalamus hippocampus and cerebellum using Inveon Research Workplace software (Siemens Medical Solutions, Knoxville, TN). TACs were corrected for body weight (g) and injected dose (MBq). SUVs were plotted as a function of time.

***Ex Vivo* Biodistribution**

After the PET scan, animals were sacrificed by extirpation of the heart. Blood was collected and processed by centrifugation for 5 min at 1000 *g* to obtain the plasma and red blood cell fractions. Several brain regions and peripheral tissues were excised and weighed. Radioactivity of tissue samples and in a sample of tracer solution (infusate) was measured using a calibrated gamma counter. The data was expressed as SUV.

Statistical Analysis

All results are expressed as mean \pm SD. Differences between groups were examined using an unpaired two-tailed *t* test. $p < 0.05$ was considered statistically significant.

Results and Discussion

Chemistry

Selective O-demethylation (Scheme 1) of commercially available [¹¹C]-**3** with the silicon tetrachloride / sodium iodide complex yielded **4** in a chemical yield of 82 %. Reversed phase-high performance liquid chromatography (RP-HPLC) demonstrated that the purity of **4** was always >98 %; no signal was detected at the retention time of **3**. This retro-synthetic approach was adopted to avoid a cumbersome multi-step approach for the synthesis of the precursor **4**. The identity of compound **4** was confirmed by ¹H and ¹³C NMR and electrospray ionization high-resolution mass spectrometry (ESI-HRMS). The silicon tetrachloride / sodium iodide complex is a selective ether cleaving reagent, which is able to cleave the terminal methyl ether, leaving the phenyl ether intact. Other ether cleaving reagents, including BBr₃ and AlI₃, showed poor selectivity, resulting in the formation of a mixture of terminal alcohol and phenol analogues as products.

4

Radiochemistry

[¹¹C]-**3** was prepared by reaction of precursor **4** with [¹¹C]CH₃I in the presence of potassium hydroxide using a Zymark robotic system (Scheme 1). The resulting radiolabeled product [¹¹C]-**3** was purified by RP-HPLC, followed by a solid-phase extraction procedure for formulation. The average decay corrected radiochemical yield, based on the starting activity of [¹¹C]CH₃I, was 35 ± 10 % (n = 12). The radiolabelling procedure proved reliable, as no failures were observed in 22 productions. The total synthesis time, including purification and formulation, was about 45 min. Quality control by ultra-high performance liquid chromatography (UHPLC) showed that [¹¹C]-**3** always had a radiochemical purity > 98 % and a specific activity of 47 ± 20 GBq / μmol. Tracer identity was confirmed by RP-HPLC coelution with the authentic reference compound **3**. In addition, the identity of the product was confirmed after radioactive decay by UHPLC / Q-ToF-MS; the observed mass of the product (m/z 504.2478) was in agreement with the calculated mass of

prelادنانت (504.2471). Although theoretically alkylation could have occurred at either the amine or alcohol functionalities in precursor **4**, a fragment with m/z 236.1761 proved that the labeled product was indeed methyl ether **1** and not the N-methylated product (see Scheme 1 Figure 2). Potassium hydroxide was used as a base in the radiosynthesis to deprotonate the hydroxyl group of precursor **4** and thus to increase its reactivity towards [¹¹C]CH₃I. For the successful formation of product [¹¹C]-**3**, a low reaction temperature (40 °C) and anhydrous reaction conditions are crucial. Reaction temperatures above 40 °C resulted in low yields; temperatures above 130 °C yielded the N-methylated by-product (Figure 2). Moisture in the reaction mixture also resulted in the formation of the N-methylated compound (Figure 2), low yield or failure of the tracer synthesis. To determine tracer stability, the formulated tracer (> 98 % radiochemical purity) was stored at room temperature and re-analyzed by UHPLC 45 min after the first analysis. The radiochemical purity of formulated [¹¹C]-**3** was not affected by storage at room temperature for 45 min, indicating that the shelf-life of the tracer is at least 45 min and thus sufficient for a tracer labeled with ¹¹C (half-life 20.4 min).

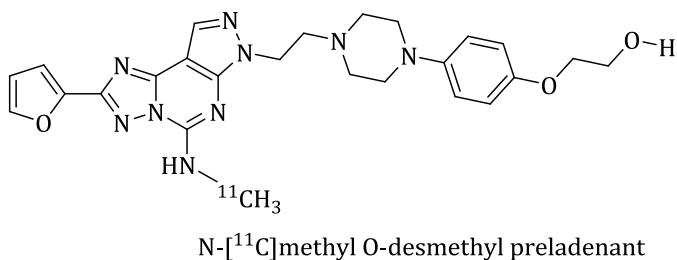


Figure 2. Structure of a radiosynthetic by-product

The distribution coefficient ($\text{LogD}_{7.4}$) of [¹¹C]-**3** at pH 7.4 was found to be 2.27 ± 0.22 ($n = 6$), demonstrating that the tracer is lipophilic enough to penetrate the blood-brain-barrier.

***In Vitro* Autoradiography**

Autoradiographic images of sagittal rat brain sections incubated with [¹¹C]-3 for 60 min are shown in Figure 3. High tracer uptake was observed in striatum, whereas low uptake was found in all other brain regions. Incubation of the brain sections with [¹¹C]-3 in the presence of an excess of the A_{2A}R antagonist (E)-1,3-diethyl-8-(3,4-dimethoxystyryl)-7-methyl-3,7-dihydro-1H-purine-2,6-dione **5** (KW6002, 2 μM) resulted in a strong reduction in tracer uptake in striatum to a level comparable to that in other brain regions. Striatum-to-cerebellum uptake ratios in brain sections incubated with [¹¹C]-3 in the absence or presence of 2 μM KW6002 were 5.1 ± 0.5 (n = 3) and 1.0 ± 0.2 (n = 3), respectively (*P* < 0.001). *In vitro* autoradiography studies confirmed that the [¹¹C]-3 binding pattern is in agreement with the known A_{2A}R distribution in the brain^{22, 23} and that [¹¹C]-3 binding in striatum (with high levels of A_{2A}R expression) can be effectively blocked by an A_{2A}R antagonist, indicating that the PET tracer specifically binds to A_{2A}Rs.

4

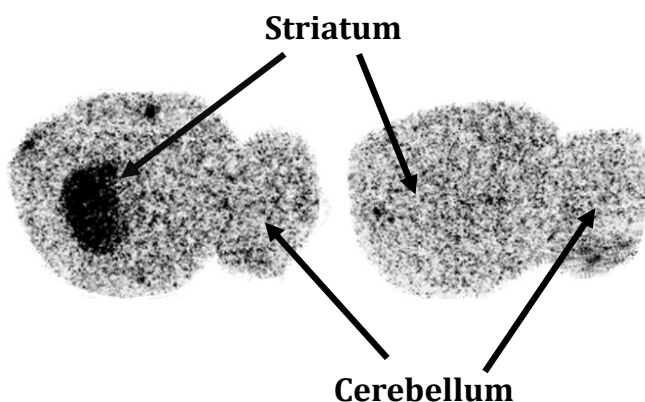


Figure 3. *In vitro* autoradiograms of sagittal rat brain sections after 60 min of incubation with [¹¹C]-3. Left: vehicle-control brain section, Right: coincubated with 2 μM **5**

Ex-Vivo Biodistribution

Ex-vivo biodistribution data of [¹¹C]-**3** in various brain regions is presented in Table 1. The distribution of the PET tracer is in accordance with known regional A_{2A}R densities, with high tracer uptake in striatum and low uptake in all extra-striatal brain regions.^{22, 23} In control animals, the average striatum (standardized uptake value (SUV) = 3.0 ± 0.5) to cerebellum (SUV = 0.36 ± 0.10) tracer uptake ratio was 8.7 ± 2.4 at around 75 min post-injection. Pretreatment with 1 mg / kg of the subtype-selective A_{2A}R antagonist **5** significantly reduced the tracer uptake in striatum by 82 % (SUV_{striatum, compound 5} = 0.55 ± 0.22; P < 0.001). As a consequence, the striatum-to-cerebellum uptake ratio decreased to 1.6 ± 0.4. No statistically significant difference in tracer uptake between control and compound **5**-pretreated rats was observed in any other brain region or in any peripheral organ (Supplementary table 1).

Table 1. Ex Vivo Biodistribution Data of [¹¹C]Preladenant in Rat Brain, 76 min After Injection

Tissue	Vehicle-control animals	Compound 5-pretreated	Difference vs Control (<i>p</i>)
Bulbus olfactorius	0.31 ± 0.03	0.30 ± 0.10	NS
Cerebellum	0.36 ± 0.09	0.35 ± 0.13	NS
Frontal cortex	0.35 ± 0.05	0.32 ± 0.11	NS
Hippocampus	0.30 ± 0.03	0.35 ± 0.13	NS
Medulla	0.33 ± 0.05	0.34 ± 0.12	NS
Parietal/Temporal/ Occipital cortex	0.45 ± 0.05	0.35 ± 0.12	NS
Pons	0.31 ± 0.01	0.36 ± 0.12	NS
Hypothalamus and Thalamus	0.37 ± 0.09	0.35 ± 0.14	NS
Striatum	3.01 ± 0.51	0.54 ± 0.24	< 0.001

SUV values (mean ± S.D.) are listed, NS = not significant

Table 2. *Ex Vivo* Biodistribution Data of [¹¹C]Preladenant in Peripheral Organs, 76 min After Injection

Tissue	Vehicle-control animals	Compound 5-pretreated
Whole blood	0.44 ± 0.20	0.28 ± 0.15
Plasma	0.45 ± 0.22	0.29 ± 0.15
Red blood cells	0.26 ± 0.03	0.23 ± 0.12
Heart	0.82 ± 0.09	0.69 ± 0.38
Lung	1.05 ± 0.40	1.08 ± 0.59
Thymus	0.66 ± 0.07	0.57 ± 0.32
Duodenum	3.82 ± 2.12	2.42 ± 0.58
Ileum	0.86 ± 0.40	0.84 ± 0.49
Pancreas	1.18 ± 0.21	1.12 ± 0.65
Spleen	1.10 ± 0.11	1.07 ± 0.63
Liver	3.27 ± 1.66	3.32 ± 1.84
Fatty tissue	0.67 ± 0.07	0.49 ± 0.34
Adrenal gland	2.29 ± 1.03	1.90 ± 0.99
Kidney	1.52 ± 0.56	1.36 ± 0.78
Muscle	0.55 ± 0.21	0.37 ± 0.21
Bone	0.44 ± 0.28	0.28 ± 0.14

SUV values (mean ± S.D.) are listed.

PET Imaging

Small animal PET images acquired 30-60 min after injection of [¹¹C]-**3** are presented in Figure 4. [¹¹C]-**3** showed a regional distribution in rat brain that corresponds to regional A_{2A}R densities.^{22, 23} Tracer uptake in striatum was clearly visible in vehicle-treated animals (Figure 4, left), whereas extra-striatal binding of the tracer was virtually absent.

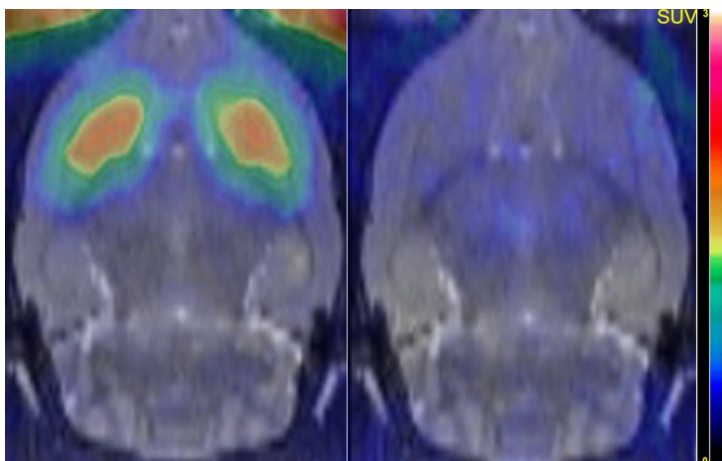
Tracer kinetics of [¹¹C]-**3** in several selected brain regions are presented in Figure 5A. The first peak of the cerebral [¹¹C]-**3** uptake appears approximately 1 min after tracer administration. The washout of [¹¹C]-**3** from rat brain was best fitted by a two-exponential decay in the cerebellum. In this region, half-life values were approximately 1 min and 50 min for the faster component

($t_{1/2\alpha}$ - distribution phase) and slower component ($t_{1/2\beta}$ - elimination phase), respectively (Figure 5A). In contrast, [¹¹C]-3 uptake in the striatum, a brain region with high A_{2A}R density, remains high throughout the scan. Striatal tracer uptake peaks at 22.5 min with an SUV of 2.2 ± 0.2 and subsequently slowly decreases to SUV 1.9 ± 0.2 at 60 min post-injection. Thalamus and frontal cortex presented a slightly higher tracer uptake (not statistically different; Figure 5A) compared with cerebellum. This may be due to a spill-over of striatal tracer uptake into surrounding tissues, as *ex vivo* biodistribution data did not show any statistically significant difference in tracer uptake in all extra-striatal brain regions including thalamus and frontal cortex.

When animals were pretreated with the A_{2A}R antagonist 5 (1 mg/kg), uptake of [¹¹C]-3 in striatum was significantly reduced ($p < 0.001$) from 4.5 min after tracer injection until the end of the scan (Figure 5B). Consequently, the striata were no longer visible in the PET images (Figure 4, right), as pretreatment with the A_{2A}R antagonist had decreased the striatum-to-cerebellum of [¹¹C]prelabeled uptake ratio at 60 min from 6.5 ± 0.1 to 1.4 ± 0.1 . 5 pretreatment did not affect tracer kinetics in cerebellum (Figure 5B), occipital cortex, hippocampus and midbrain (data not shown for these regions).

Comparison of brain SUVs obtained from *ex-vivo* biodistribution studies with SUVs from PET analysis (50–60 min post-injection) showed a 60 % higher average striatal [¹¹C]-3 uptake obtained from biodistribution studies than from PET analysis ($P = 0.0006$). This discrepancy may result from an underestimation of the PET signal, due to partial volume effects, as the size of the rat striatum is of the same order of magnitude as the spatial resolution of the PET camera used (Full width at half maximum spatial resolution 1.74 mm at 5 mm of radial offset; 2.07–2.88 mm when two animals scanned simultaneously).²⁴ In contrast, [¹¹C]-3 uptake in frontal cortex as determined by PET was 28 % higher than the values obtained in biodistribution studies ($p = 0.001$). Tracer uptake in frontal cortex

was overestimated by PET, because of “spill in” activity into this brain region from the adjacent striatum and harderian glands.²⁵ In other brain regions, tracer uptake determined by PET and *ex-vivo* biodistribution was comparable, indicating that partial-volume effect was negligible in these regions.



4

Figure 4. PET images of a coronal plane of a rat brain 30–60 min after i.v. injection of [¹¹C]-3 (cropped images). PET images are superimposed on a brain MRI template. Left: vehicle-control rat, hot spots inside the brain represent striatum. Right: rat treated with 5 (1 mg / kg) prior to tracer injection (blocking). Hot spots outside the brain are the harderian glands. The images were normalized for body weights and injected doses

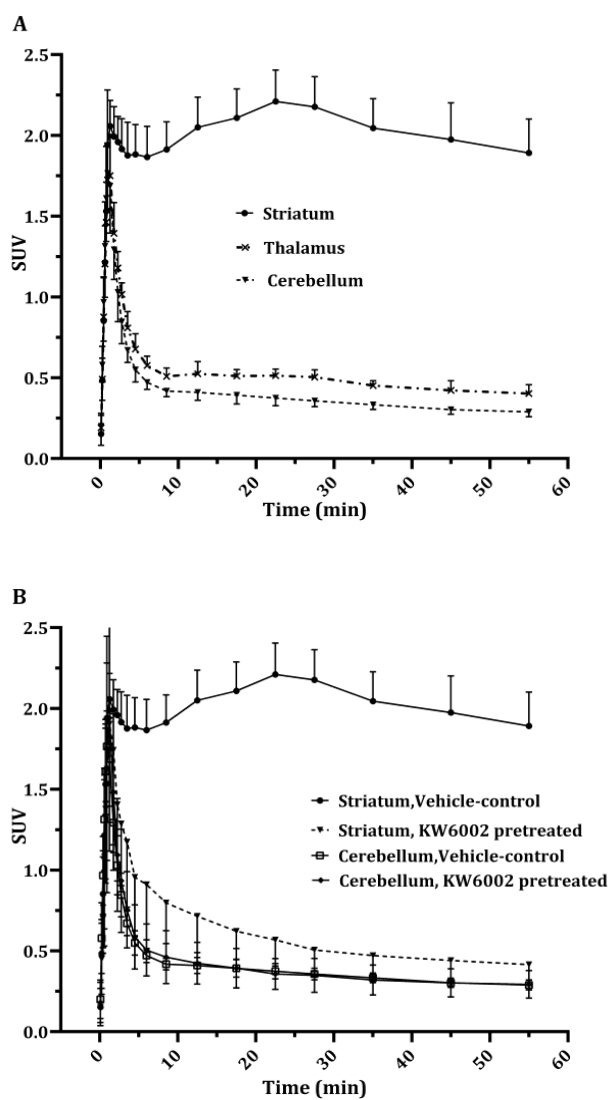


Figure 5. (A): Time activity curves of [¹¹C]-3 in striatum, thalamus and cerebellum of vehicle-control rats (n = 6). (B) Uptake kinetics of [¹¹C]-3 in striatum and in cerebellum of vehicle (n = 6) and compound 5 (n = 6) pretreated rats, respectively. Error bars indicate standard deviation.

Conclusion

[¹¹C]-**3** was successfully synthesized in high radiochemical yield. [¹¹C]-**3** had a high specific activity and chemical and radiochemical purity. The tracer entered the brain quickly and displayed a regional distribution and specific uptake that is in agreement with known A_{2A}R expression in the brain. The high specific binding in striatum and the low nonspecific binding in other brain regions indicate that [¹¹C]-**3** is a suitable PET radioligand for mapping A_{2A}Rs in rat brain. However, further validation of [¹¹C]-**3** in nonhuman primates and human volunteers is warranted to assess the value of this new PET tracer.

Acknowledgment

We thank Chantal Kwizera, Jurgen Sijbesma, Mohammed Khayum and Marianne Schepers for their technical assistance.

References

1. Schiffmann, S. N.; Fisone, G.; Moresco, R.; Cunha, R. A.; Ferre, S. Adenosine A_{2A} receptors and basal ganglia physiology. *Prog. Neurobiol.* **2007**, *83*, 277–292.
2. de Lera Ruiz, M.; Lim, Y. H.; Zheng, J. Adenosine A_{2A} receptor as a drug discovery target. *J. Med. Chem.* **2014**, *57*, 3623–3650.
3. Schwarzschild, M. A.; Agnati, L.; Fuxe, K.; Chen, J. F.; Morelli, M. Targeting adenosine A_{2A} receptors in Parkinson's disease. *Trends Neurosci.* **2006**, *29*, 647–654.
4. Ferre, S.; Quiroz, C.; Orru, M.; Guitart, X.; Navarro, G.; Cortes, A.; Casado, V.; Canela, E. I.; Lluís, C.; Franco, R. Adenosine A_{2A} receptors and A_{2A} receptor heteromers as key players in striatal function. *Front. Neuroanat.* **2011**, *5*, 36.
5. Morelli, M.; Carta, A. R.; Jenner, P. Adenosine A_{2A} receptors and Parkinson's disease. *Handb. Exp. Pharmacol.* **2009**, (193), 589–615.
6. LeWitt, P. A.; Guttman, M.; Tetrud, J. W.; Tuite, P. J.; Mori, A.; Chaikin, P.; Sussman, N. M.; 6002-US-005 Study Group Adenosine A_{2A} receptor antagonist istradefylline (KW-6002) reduces "off" time in Parkinson's disease: a double-blind, randomized, multicenter clinical trial (6002-US-005). *Ann. Neurol.* **2008**, *63*, 295–302.
7. Hauser, R. A.; Cantillon, M.; Pourcher, E.; Micheli, F.; Mok, V.; Onofrij, M.; Huyck, S.; Wolski, K. Preladenant in patients with Parkinson's disease and motor fluctuations: a phase 2, double-blind, randomised trial. *Lancet Neurol.* **2011**, *10*, 221–229.
8. Hauser, R. A.; Olanow, C. W.; Kieburtz, K. D.; Neale, A.; Resburg, C.; Meya, U.; Bankak, S. I. A phase 2, placebo-controlled, randomized, double-blind trial of tozadenant (Syn-115) in patients with Parkinson's disease with wearing-off fluctuations on levodopa. *J. Neurol. Sci.* **2013**, *333*, e119.
9. Hodgson, R. A.; Bertorelli, R.; Varty, G. B.; Lachowicz, J. E.; Forlani, A.; Fredduzzi, S.; Cohen-Williams, M. E.; Higgins, G.

- A.; Impagnatiello, F.; Nicolussi, E.; Parra, L. E.; Foster, C.; Zhai, Y.; Neustadt, B. R.; Stamford, A. W.; Parker, E. M.; Reggiani, A.; Hunter, J. C. Characterization of the potent and highly selective A_{2A} receptor antagonists preladenant and SCH 412348 [7-[2-[4-2,4-difluorophenyl]-1-piperazinyl]ethyl]-2-(2-furanyl)-7H-pyrazolo[4,3-e][1,2,4]triazolo[1,5-c]pyrimidin-5-amine] in rodent models of movement disorders and depression. *J. Pharmacol. Exp. Ther.* **2009**, *330*, 294–303.
10. Hauser, R. A.; Shulman, L. M.; Trugman, J. M.; Roberts, J. W.; Mori, A.; Ballerini, R.; Sussman, N. M.; Istradefylline 6002-US-013 Study Group Study of istradefylline in patients with Parkinson's disease on levodopa with motor fluctuations. *Mov. Disord.* **2008**, *23*, 2177–2185.
11. Moresco, R. M.; Todde, S.; Belloli, S.; Simonelli, P.; Panzacchi, A.; Rigamonti, M.; Galli-Kienle, M.; Fazio, F. In vivo imaging of adenosine A_{2A} receptors in rat and primate brain using [11C]SCH442416. *Eur. J. Nucl. Med. Mol. Imaging* **2005**, *32*, 405–413.
12. Hirani, E.; Gillies, J.; Karasawa, A.; Shimada, J.; Kase, H.; Opacka-Juffry, J.; Osman, S.; Luthra, S. K.; Hume, S. P.; Brooks, D. J. Evaluation of [4-O-methyl-(11)C]KW-6002 as a potential PET ligand for mapping central adenosine A_{2A} receptors in rats. *Synapse* **2001**, *42*, 164–176.
13. Ishiwata, K.; Noguchi, J.; Wakabayashi, S.; Shimada, J.; Ogi, N.; Nariai, T.; Tanaka, A.; Endo, K.; Suzuki, F.; Senda, M. 11C-labeled KF18446: a potential central nervous system adenosine A_{2A} receptor ligand. *J. Nucl. Med.* **2000**, *41*, 345–354.
14. Stone-Elander, S.; Thorell, J.; Eriksson, L.; Fredholm, B. B.; Ingvar, M. *In vivo* biodistribution of [N-11C-methyl]KF 17837 using 3-D-PET: Evaluation as a ligand for the study of adenosine A_{2A} receptors. *Nucl. Med. Biol.* **1997**, *24*, 187–191.
15. Noguchi, J.; Ishiwata, K.; Wakabayashi, S.; Nariai, T.; Shumiya, S.; Ishii, S.; Toyama, H.; Endo, K.; Suzuki, F.; Senda, M. Evaluation of carbon-11-labeled KF17837: a potential CNS

- adenosine A_{2A} receptor ligand. *J. Nucl. Med.* **1998**, *39*, 498–503.
16. Bhattacharjee, A. K.; Lang, L.; Jacobson, O.; Shinkre, B.; Ma, Y.; Niu, G.; Trenkle, W. C.; Jacobson, K. A.; Chen, X.; Kiesewetter, D. O. Striatal adenosine A_{2A} receptor-mediated positron emission tomographic imaging in 6-hydroxydopamine-lesioned rats using [(18)F]-MRS5425. *Nucl. Med. Biol.* **2011**, *38*, 897–906.
17. Mishina, M.; Ishiwata, K.; Naganawa, M.; Kimura, Y.; Kitamura, S.; Suzuki, M.; Hashimoto, M.; Ishibashi, K.; Oda, K.; Sakata, M.; Hamamoto, M.; Kobayashi, S.; Katayama, Y.; Ishii, K. Adenosine A_{2A} Receptors Measured with [11C]TMSX PET in the Striata of Parkinson's Disease Patients. *PLoS ONE* **2011**, *6*, e17338.
18. Ramlackhansingh, A. F.; Bose, S. K.; Ahmed, I.; Turkheimer, F. E.; Pavese, N.; Brooks, D. J. Adenosine 2A receptor availability in dyskinetic and nondyskinetic patients with Parkinson disease. *Neurology* **2011**, *76*, 1811–1816.
19. Fujita, M.; Innis, R. B. *In vivo* molecular imaging: Ligand development and research applications. In *Neuropsychopharmacology: The Fifth Generation Of Progress*; Davis, K. , Charney, D. , Coyle, J., Nemeroff, C. , Eds.; Lippincott, Williams, & Wilkins: Philadelphia, PA, 2002; pp 411–425.20. Neustadt, B. R.; Hao, J.; Lindo, N.; Greenlee, W. J.; Stamford, A. W.; Tulshian, D.; Ongini, E.; Hunter, J.; Monopoli, A.; Bertorelli, R.; Foster, C.; Arik, L.; Lachowicz, J.; Ng, K.; Feng, K. Potent, selective, and orally active adenosine A_{2A} receptor antagonists: Arylpiperazine derivatives of pyrazolo[4,3-e]-1,2,4-triazolo[1,5-c]pyrimidines. *Bioorg. Med. Chem. Lett.* **2007**, *17*, 1376–1380.
20. Neustadt, B. R.; Hao, J.; Lindo, N.; Greenlee, W. J.; Stamford, A. W.; Tulshian, D.; Ongini, E.; Hunter, J.; Monopoli, A.; Bertorelli, R.; Foster, C.; Arik, L.; Lachowicz, J.; Ng, K.; Feng, K. Potent, selective, and orally active adenosine A_{2A} receptor antagonists: Arylpiperazine derivatives of pyrazolo[4,3-e]-

- 1,2,4-triazolo[1,5-c]pyrimidines. *Bioorg. Med. Chem. Lett.* **2007**, *17*, 1376–1380.
21. Larsen, P.; Ulin, J.; Dahlstrøm, K.; Jensen, M. Synthesis of [11C]iodomethane by iodination of [11C]methane. *Applied Radiation and Isotopes* **1997**, *48*, 153–157.
22. Martinez-Mir, M. I.; Probst, A.; Palacios, J. M. Adenosine A2 receptors: selective localization in the human basal ganglia and alterations with disease. *Neuroscience* **1991**, *42*, 697–706.
23. Parkinson, F. E.; Fredholm, B. B. Autoradiographic evidence for G-protein coupled A2-receptors in rat neostriatum using [3H]-CGS 21680 as a ligand. *Naunyn Schmiedebergs Arch. Pharmacol.* **1990**, *342*, 85–89.
24. Goertzen, A. L.; Bao, Q.; Bergeron, M.; Blankemeyer, E.; Blinder, S.; Canadas, M.; Chatziioannou, A. F.; Dinelle, K.; Elhami, E.; Jans, H. S.; Lage, E.; Lecomte, R.; Sossi, V.; Surti, S.; Tai, Y. C.; Vaquero, J. J.; Vicente, E.; Williams, D. A.; Laforest, R. NEMA NU 4-2008 comparison of preclinical PET imaging systems. *J. Nucl. Med.* **2012**, *53*, 1300–1309.
25. Lehnert, W.; Gregoire, M. C.; Reilhac, A.; Meikle, S. R. Characterisation of partial volume effect and region-based correction in small animal positron emission tomography (PET) of the rat brain. *NeuroImage* **2012**, *60*, 2144–2157.



**Small Animal PET to Study Adenosine A₁
and A_{2A} Receptor Agonist-Induced
Changes of Blood Brain Barrier Permeability**

Shivashankar Khanapur, Soumen Paul, Siddesh Hartimath, Jurgen W
Sijbesma, Rudi A.J.O. Dierckx, Aren van Waarde, Philip H Elsinga

†Department of Nuclear Medicine and Molecular Imaging, UMCG,
University of Groningen, Groningen, The Netherlands

5

Abstract

Adenosine and adenosine analogs may modulate blood brain barrier (BBB) permeability in mice and rats through stimulation of adenosine A₁ and A_{2A} receptors (A₁R and A_{2A}R). We performed a PET-study to determine whether changes of BBB permeability after administration of A₁ or A_{2A}R agonists can be assessed by examining changes of the cerebral *in vivo* kinetics of a hydrophilic radioligand. To validate the outcome of the PET assay, Evans blue was used as marker of BBB disruption. **Methods:** MicroPET scans combined with arterial blood sampling were performed in three groups of isoflurane-anesthetized Wistar rats: (1) controls treated with only physiological saline 1 mL / kg; (2) pretreated with the A₁R agonist cyclopentyladenosine (CPA), dose 0.26 mg / kg; (3) pretreated with the A_{2A} agonist Rapiscan (regadenoson), dose 0.05 mg / kg. We used the hydrophilic CXCR₄ antagonist N-[¹¹C]methyl-AMD3465 (clogP = -0.86) as the imaging probe for these studies. In addition to the above treatment groups, osmotic barrier opening was investigated with the help of a visual tracer Evans blue and mannitol. **Results:** Administration of CPA and Rapiscan resulted in a strong (> 50 %) and moderate (< 10 %) reduction of heart rate, respectively. We failed to observe BBB opening, as judged by tracer distribution volumes (V_T) calculated from a Logan plot. Pretreatment of animals with CPA and Rapiscan did not significantly increase V_T of N-[¹¹C]methyl-AMD3465. No indication of BBB permeability in A₁ or A_{2A}R agonist-treated and mannitol-treated animals was found based on Evans blue capillary leakage into the brain tissue. In addition, no visual presence of Evans blue in the brain was found. **Conclusion:** BBB opening could not be accomplished by any technique and was therefore also not detected by PET. The radioligand N-[¹¹C]methyl-AMD3465 failed to enter the rodent brain after pretreatment of rats with an A₁ or A_{2A} agonist.

Introduction

The blood-brain-barrier (BBB) is composed of endothelial cells¹ which line the microvasculature of the brain and are connected by tight junctions. These cells are functionally placed between brain and periphery. The BBB is divided into three sections: 1) the actual BBB, 2) blood-cerebrospinal fluid barrier, and 3) arachnoid barrier.² All three sections are involved in protection of the central nervous system by limiting the entry of toxic substances into the brain. Lipophilic molecules may pass the barrier in different ways. Small molecules can enter via i) ion channels ii) dissolving in the hydrophobic cell membrane followed by barrier passage via passive diffusion, and iii) facilitated transport. Such transporters may be either carrier-mediated or receptor-mediated.³ Other transporters, like P-glycoprotein (P-gp), multidrug resistance-associated protein (MRP) and breast cancer resistance protein (BCRP), are actually limiting substance entry into the brain by actively pumping molecules back to the blood after they have entered the brain by passive diffusion. The efficiency of the BBB is proven by the fact that more than 98 % of all molecules with molecular weight greater than 500 Da do not enter the brain. With increasing prevalence of brain disorders there is an increasing demand for CNS drugs, but potentially important diagnostic and therapeutic agents fail to cross the barrier because of its neuroprotective role. Thus, there is a need to modulate BBB permeability and facilitate the entry of therapeutic drugs into the CNS.

Adenosine receptors (ARs) are G-protein coupled receptors and play several roles in mammalian physiology, including modulation of immune responses. ARs can be divided in the A₁R, A_{2A}R, A_{2B}R and A₃R subtypes. Adenosine analogs can modulate BBB permeability in mice and rats through stimulation of A₁R and A_{2A}R receptors.⁴ Activation of A₁R and A_{2A}R on brain endothelial cells causes cytoskeletal remodeling and changes of cell size and shape. Such stimulation appears to result in temporary opening of the tight

junctions between the endothelial cells, allowing short-term entry of large molecules, like dextran or antibodies, into the brain.⁴

Thus far, no PET studies have been performed to assess changes of BBB permeability after administration of A₁R or A_{2A}R agonists. A PET assay for measurement of tight junction opening could employ a hydrophilic compound labeled with a positron emitter. Under normal conditions, such a compound will not enter the brain, but remains in the vascular compartment. After administration of a permeability-modulating drug [like the A₁R agonist cyclopentyl adenosine (CPA) or the A_{2A} agonist Rapiscan (regadenoson)], the hydrophilic tracer (in this case N-[¹¹C]methyl-AMD3465) (Figure 1) may enter the brain resulting in a detectable PET signal.

Materials and Methods

General

N⁶-Cyclopentyl adenosine (CPA), Evans blue and mannitol were purchased from Sigma (Sigma-Aldrich, The Netherlands). Rapiscan was procured from IDB Holland BV. All other chemicals were of analytical grade and obtained from commercial suppliers like Rathburn, Acros, Merck etc.

Radiochemical Synthesis

[¹¹C]Methane was produced via the ¹⁴N (p, α) ¹¹C nuclear reaction by irradiating a nitrogen / hydrogen gas mixture using a Scanditronix MC17 biomedical cyclotron. [¹¹C]CH₃I was prepared based on a gas-phase synthesis involving [¹¹C]CH₄ and I₂.⁵ [¹¹C]Methyl triflate was formed by on-line passing the [¹¹C]methyl iodide through a column of silver triflate at 200–220 °C. [¹¹C]Methyl triflate was then transferred and trapped into a conical vial which contained 0.4 mg of N-desmethyl-trifluoroacetyl-AMD3465 in 300 μL dry acetone at 0 °C. After trapping of [¹¹C]methyl triflate, the reaction mixture was heated at 80 °C for 4–5 min to evaporate acetone. Subsequently, 300 μL of methanol and 100 μL of NaOH (1M) was added and the

reaction mixture was again heated at 80 °C for another 5 min to hydrolyze the trifluoroacetyl protective group (Figure 1). During these steps the needle vent was kept open. The resulting mixture was neutralized with phosphoric acid (16 µL), diluted with 0.6 mL HPLC eluent and purified by HPLC using a Zorbax SB C₁₈ (250x 7.8 mm) column and sodium phosphate buffer (pH 2.0) / EtOH (95 / 5 v / v) as the eluent at a flow of 4 mL / min. The radioactive product with a retention time of 12 ± 1 min was collected, neutralized with 1M NaOH (~400 µL) and passed over a Millex 0.22 µm GV filter (Millipore, Ireland) to yield a sterile solution of N-[¹¹C]methyl-AMD3465. Later, the formulated tracer was submitted for HPLC quality control using a Jupiter C₁₈ column (300 x 7.8 mm, Phenomenex) and water (pH 2.0 with HClO₄) / acetonitrile (90 / 10) as an eluent at a flow rate 1 mL / min. Retention time was 8 ± 1 min.

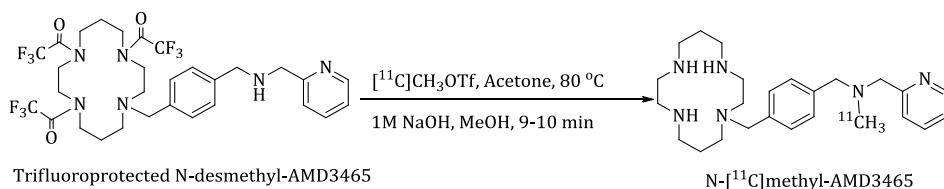


Figure 1. Radiosynthesis of N-[¹¹C]methyl-AMD3465

Distribution Coefficient (Log D_{7.4}) Measurement

After tracer elution from a C-18 light Sep Pak column, 500 mL of eluate (octanol) was mixed with an equal volume of 1M phosphate buffer pH 7.4 and vigorously vortexed for 1 min followed by centrifugation (10 min, 17,250g). Three 100 µL aliquots were drawn from the corresponding n-octanol and aqueous phases. The radioactivity in each phase was counted (Compugamma 1282 CS, LKB-Wallac, Finland). For every tracer batch, experiments were performed in triplicate; the average LogD_{7.4} value is reported.

In Vivo Studies

Animals and Study Design

The animal experiments were carried out by licensed investigators in compliance with the Law on Animal Experiments of The Netherlands. The Committee on Animal Ethics of the University of Groningen approved the protocol. Male outbred Wistar-Unilever rats were obtained from Harlan (The Netherlands). The animals were housed in Macrolon cages (38 × 26 × 24cm) maintained at a 12 h light-dark regime and were fed standard laboratory chow (RMH-B, The Netherlands) and tap water ad libitum. After arrival, the rats were allowed to acclimatize for at least seven days. Body weights and injected doses in the different pretreatment groups are listed in Table 1.

Table 1. Animal Data^o

Group	Body weight (g)	Injected dose (MBq)
Control (n = 5)	340 ± 28	20 ± 12
CPA 0.26 mg / kg (n = 4)	312 ± 31	25.7 ± 5.5
Rapiscan 0.05 mg / kg (n = 3)	315 ± 36	14 ± 4

^omean ± SD

Small-Animal PET Scanning

Two animals were scanned simultaneously in each scan session (supine position), using a Focus 220 MicroPET camera (CTI, Siemens, Munich, Germany). All animals were anesthetized with isoflurane / air (induction: 5 % isoflurane, later reduced to ≤2 %). Cannulas were placed in a femoral artery and vein for blood sampling and tracer injection (Harvard-style pump; 1 mL / min), respectively. A transmission scan of 515 s was made before the emission scan, using a rotating ⁵⁷Co point source, in order to correct the subsequently acquired N-[¹¹C]methyl-AMD3465 images for attenuation and scatter. Rats were under anesthesia for 30–40 min before tracer injection (time required for cannulation and

transmission scan). Emission data were acquired in list mode for 76 min (brain in the field of view). Data acquisition was started at the moment of tracer entering the body of the first rat; whereas the second animal was injected 16 min later. Scanning was then continued for another 60 min. The animal that was injected last was also anesthetized at a later moment. Thus, the duration of anesthesia was similar in all study groups.

PET data were corrected for attenuation, scatter, random coincidences and radioactive decay and reconstructed in 23 time frames (8×30 , 3×60 , 2×120 , 2×180 , 3×300 , 1×480 , 3×600 and 1×960 s) using a 2D ordered subsets expectation maximization (OSEM) algorithm, provided by Siemens (4 iterations, 16 subsets and zoom factor 2). The final datasets consisted of 95 slices, with a slice thickness of 0.8 mm and an in-plane image matrix of 128×128 pixels of size 1.1 mm. Reconstructed images were smoothed with a 3D Gaussian filter [1.35 mm full width at half-maximum (FWHM)]

During the scan, arterial blood samples (volume 0.1–0.15 mL) were drawn using a standard protocol i.e., at 0, 5, 10, 15, 20, 30, 45, 60, 75, 90 s and 2, 3, 5, 7, 10, 15, 30, 60, 90 min after injection. After collecting 25 μ L whole blood, plasma (25 μ L) was acquired from the remainder of the blood samples by short centrifugation (5 min at 1000g). Radioactivity in 25 μ L plasma and whole blood was counted and used as an arterial input function. Heart rate, stroke volume and blood oxygenation of the experimental animals were continuously monitored throughout the scanning procedure, using pulse oximeters (Nonin Pulse Sense, Zevenaar, The Netherlands).

Small-Animal PET Data Analysis

Time activity curve (TAC) for whole brain was determined using Inveon Research Workplace software (Siemens Medical Solutions, Knoxville, TN). The summed PET data of each animal were coregistered to a MRI template of the rat brain with predefined volumes of interest (VOIs). Translation, rotation and scaling were adjusted to visually optimize the image fusion. The VOIs were

transferred from the MRI template to the PET data, and regional TACs were generated. Standardized uptake values measured by PET (PET-SUVs) were plotted as a function of time, using body weights and injected doses [tissue activity concentration (MBq / mL)] / [(injected dose (MBq) / body weight (g))]. Kinetic analysis was performed by fitting 1- and 2-tissue compartment models (TCM) to the PET data, using data (without metabolite-correction) from arterial plasma samples and uncorrected data from whole blood samples as input function while cerebral blood volume was fixed to 0.036.⁷ Quality of the fits was evaluated using the Akaike Information Criterion (AIC). Graphical analysis of the PET data was performed using a Logan plot; the fit started at 9min post injection.⁸ Distribution volume (V_T) and binding potential (k_3 / k_4) were evaluated as quantitative endpoints of 1TCM, 2TCM and Logan plot.

Ex Vivo Biodistribution

After the PET-scan, the animals were terminated by extirpation of the heart. Blood was collected, and plasma and a cell fraction were obtained from the sample by short centrifugation (5 min at 1000g). Several tissues were excised and weighed. Radioactivity in tissue samples and in a sample of tracer solution (infusate) was measured using a calibrated gamma counter. The data was expressed as dimensionless SUV.

Evaluation of BBB Permeability

Permeability of the BBB for Evans blue dye was evaluated in accordance with a published method.⁹ Three groups of rats were studied to assess permeability of the BBB for Evans blue.

Group 1: Negative control (n = 2): Received Evans blue solution (2 % in normal saline, 4 mL / kg body weight, *i.p.*) only in combination with *i.v.* saline.

Group 2: Pretreatment group (n = 4): Received Evans blue solution (as group 1), at 30 min after treatment with either CPA (A₁R agonist,

0.25 mg / kg, *i.p.*, n = 2) or Lexiscan (A_{2A}R agonist, 0.05 mg / kg, *i.v.*, n = 2).

Group 3: Positive control (n = 2): Received Evans blue solution (as group 1), but a cannula was placed in a carotid artery before Evans blue administration. After 30 min a hyperosmotic solution of mannitol was infused through this cannula (25 % w / v mannitol, infusion rate 0.25 mL / s / kg).

In all animals, the brain was perfused with PBS 90 min after the Evans blue administration. Brain tissue was removed, and divided in left and right hemispheres. One hemisphere was frozen for later analysis; the other was homogenized in 1100 μ L of PBS, sonicated and centrifuged. Trichloroacetic acid (0.5 mL, 50 %) was added to the supernatant which was then incubated overnight at 4 °C and again centrifuged. The Evans blue concentration in the deproteinized supernatant was measured quantitatively with a spectrophotometer set at 610 nm.

Statistical Tests

All results are expressed as mean \pm SEM. Differences between groups were analyzed using 1-way ANOVA. A probability smaller than 0.05 was considered statistically significant.

Results

Chemical and Radiochemical Synthesis

The decay-corrected radiochemical yield of the tracer was 60 ± 2 % (n = 12) and the total synthesis time was less than 50 min including the HPLC purification. The radiochemical purity was > 99 % and the specific radioactivity 30 ± 5 GBq / μ mol. Tracer identity was confirmed by spiking with authentic cold compounds in reversed phase-HPLC.

LogD_{7.4} Measurement

LogD_{7.4} values of N-[¹¹C]methyl-AMD3465 was found to be -0.86 ± 0.09 (n = 3).

Small-Animal PET Images

Small animal PET images were acquired after injection of N-[¹¹C]methyl-AMD3465. The brain was visualized, neither in control animals, nor in animals pretreated with CPA or Rapsican. The brain appeared like a black hole in all PET images.

Kinetics of Radioactivity in Brain

Cerebral kinetics of radioactivity after injection of N-[¹¹C]methyl-AMD3465 is presented in Figure 2. In control animals (n = 3) and CPA (n = 3) or Rapsican (n = 2) pretreated animals, uptake of radioactivity rapidly increased to a maximum (i.e., 1.5 min after injection) which was followed by an exponential washout. The increase of brain uptake (PET-SUV) of N-[¹¹C]methyl-AMD3465 after CPA treatment was statistically significant whereas same is not true in case of Rapsican pretreatment.

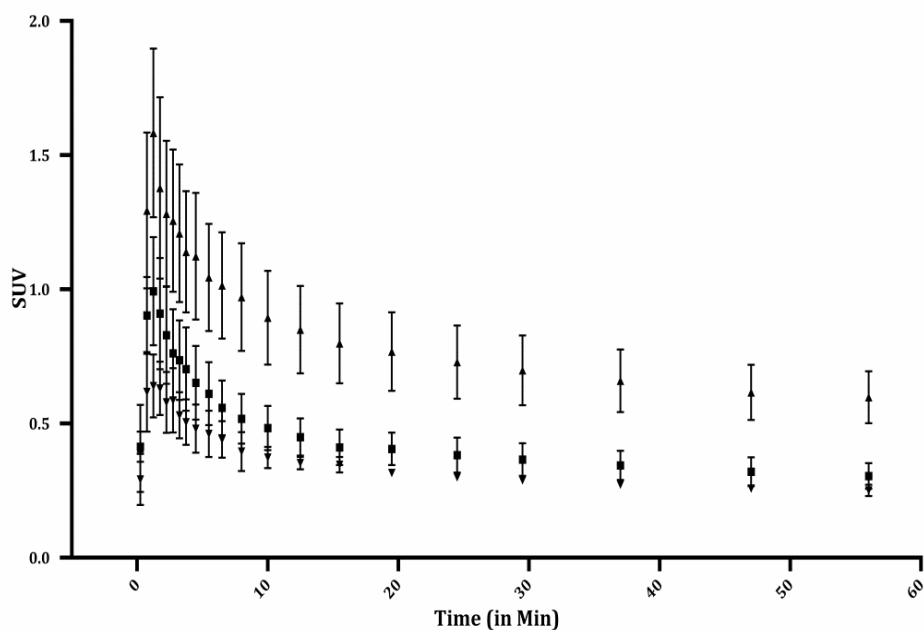


Figure 2. Whole brain time activity curve of CPA(▲), Control(■) and Rapiscan treated(▼) animals.

Kinetics of Radioactivity in Plasma

Plasma kinetics of radioactivity after injection of N-[¹¹C]methyl-AMD3465 is presented in Figure 3. A rapid, bi-exponential plasma clearance was observed in all groups. CPA, Rapiscan and control animals treatment did not significantly affect the clearance of radioactivity from the plasma compartment, although plasma levels of radioactivity appeared to be higher in animals pretreated with CPA and Rapiscan.

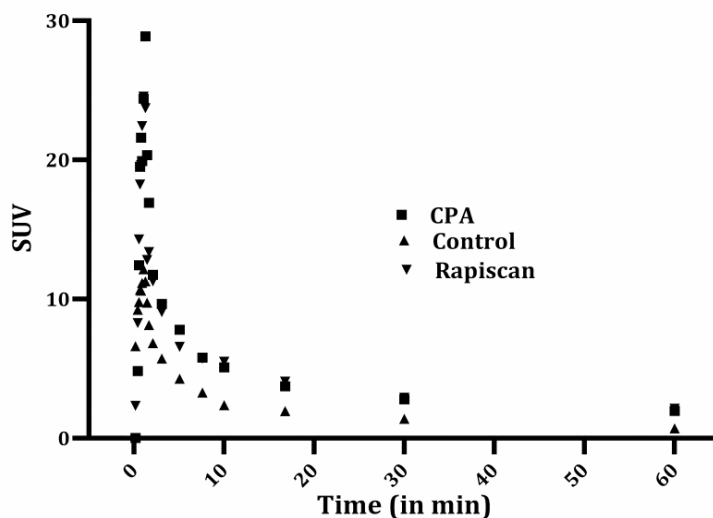


Figure 3. Kinetics of N-[^{11}C]methyl-AMD3465 radioactivity in rat plasma

5

Graphical Analysis of PET Data

Tracer V_T was calculated using a Logan plot, time-activity curve from a ROI drawn around the entire brain, and radioactivity counts from arterial blood samples. The Logan plot approached linearity within 9 min after injection. There was no increase in V_T of N-[^{11}C]methyl-AMD3465 after pretreatment of animals with CPA or Rapiscan compared to controls (Table 2). PET data for whole brain radioactivity was suitable for Logan analysis but not Patlak analysis indicating reversibility of tracer binding.

When a 2TCM was fitted to time-activity curve from a ROI drawn around the entire brain, using radioactivity counts from arterial blood samples as input function, the ratio of k_3 / k_4 , a measure of tracer binding potential, for N-[^{11}C]CH₃-AMD3465 remained unaltered after pretreatment with the A₁R or A_{2A}R agonist (Table 2).

Table 2. Results from Graphical Analysis and Compartment Modeling of PET Data (ROI Drawn Around Entire Brain) of N-[¹¹C]methyl-AMD3465

Group	V _T (Logan)	V _T (2TCM)	BP _{ND} (k ₃ / k ₄) (2TCM)
Control (n = 3)	0.21 ± 0.11	0.25 ± 0.13	1.92 ± 0.71
CPA (n = 3)	0.10 ± 0.03	0.17 ± 0.03	1.84 ± 0.22
Rapiscan (n = 2)	0.23 ± 0.19	0.23 ± 0.20	1.74 ± 0.31

Biodistribution Data

Biodistribution data of N-[¹¹C]methyl-AMD3465, acquired 80 min after injection is presented in Figure 4. Pretreatment of animals with CPA and Rapiscan, did not result in significant increase of N-[¹¹C]methyl-AMD3465 uptake in brain areas and peripheral organs

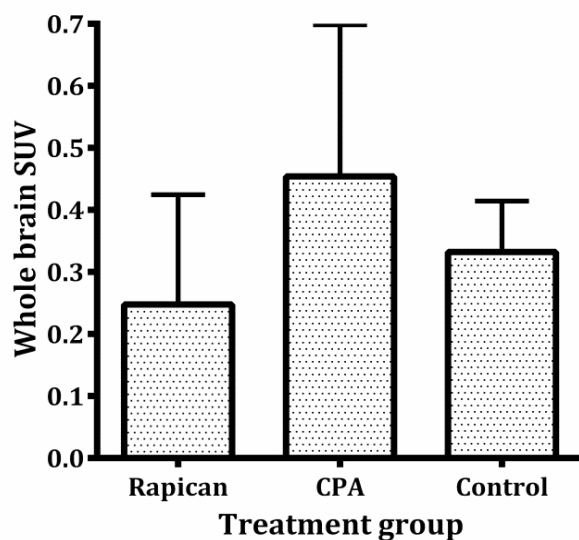


Figure 4. Brain biodistribution of N-[¹¹C]methyl-AMD3465, 80 min

after injection in different treatment groups

Evans Blue Assay Result

Brain extracts from Evans Blue treated rats were quantitatively measured by spectrophotometer at 610 nm in all pretreatment animals. No trace of BBB opening was seen in both adenosine agonist-treated and mannitol-treated animals. Furthermore, no visual presence of Evans blue was found in brain tissues.

Physiological Response

After *i.p.* administration of the A₁ agonist CPA a very strong decline of heart rate was observed within 5 min (from 340 to about 100) whereas after *i.v.* injection of the A_{2A} agonist Rapiscan, we noticed a slight decline (from 340 to 320). The pulse oximeter readings showed that the drop in heart rate was accompanied by an increase in cardiac stroke volume.

5

Discussion

This project aimed to answer the question whether transient opening of the BBB after treatment of animals with adenosine receptor agonists can be detected with hydrophilic radiotracers and PET. Such tracers do not pass the normal intact barrier, but may pass after tight junction opening.

As initial attempt, we used N-[¹¹C]methyl-AMD3465 (CXCR₄ antagonist tracer). The logP of N-[¹¹C]methyl-AMD3465 is -0.86 ± 0.09 and therefore this radioligand is not able to cross the BBB by passive diffusion. The preliminary PET data and images showed no differences in brain uptake between animals treated with adenosine receptor agonists and untreated controls. A biodistribution study, performed at 80 min after tracer injection, also did not indicate any increases of radioactivity in the brain of pretreated animals. The kinetic modeling approach indicated that neither the partition coefficient (K_1 / k_2) nor the binding potential (k_3 / k_4) of N-

[¹¹C]methyl-AMD3465 were affected by the treatment. However, plasma levels of the tracer were different in the 3 pretreatment groups, causing a discrepancy between biodistribution and compartment modeling data

According to Carman et al., ⁴ transient BBB opening should occur after treatment of animals with an A₁R or A_{2A}R agonist and should persist for several hours. In our experiments, the agonists were administered properly as proven by strong physiological responses of the rats (decline of heart rate, increase of stroke volume). After pretreatment of animals with Rapiscan, the brain TAC appeared to rise less rapidly to a maximum than in untreated rats. This suggests that cerebral blood flow is reduced after A_{2A} agonist treatment, which may in fact be the case since we noted a decline of heart rate. However, in CPA treated animals where a much stronger decline of heart rate occurred, the brain TAC rose even more rapidly to a maximum than in control rats. Thus, the relationship between heart rate and brain TAC is not very clear

We could not detect any BBB opening with PET. We failed to observe hydrophilic tracer uptake in rat brain after pretreatment with A₁ and A_{2A} agonists. This negative finding could be related to different underlying mechanisms:

1. Hydrophilic tracers may be rapidly cleared from the circulation (i.e., within 5 or 10 min after injection) whereas opening of the barrier may occur only later, after a prolonged interval (e.g., more than 20 min after agonist administration). Thus the barrier would open at a moment when the bulk of the injected tracer has already been cleared from the circulation.
2. Because of certain physiological conditions of the animals during the scanning procedure (anesthesia, acidosis, hypercapnia or hypothermia) the BBB may not have opened after pretreatment with an A₁R or A_{2A}R agonist. In the published study describing barrier opening ⁴ animals were

only anesthetized at the end of the experiment for the purpose of euthanasia.

The Evans blue assay of BBB permeability was performed to assess whether the negative outcome of the PET assay was due to inappropriate tracer kinetics (mechanism 1) or failure of the experimental animals to respond to the adenosinergic stimulus (mechanism 2). No evidence for BBB opening was found in our Evans blue experiments, which indicates that in our anesthetized animals the BBB may not have opened at all, in contrast to the awake animals which were treated with AR agonists in the literature.⁴

Conclusion

In a preliminary microPET study with the hydrophilic ligand N-[¹¹C]methyl-AMD3465, we could not demonstrate BBB opening after adenosine receptor stimulation. The tracer did not enter the brain after pretreatment of rats with A₁ or A_{2A} agonists. We also did not detect Evans blue leakage by spectrophotometric analysis, indicating failure of BBB opening. The cause of this negative finding remains to be clarified.

References

1. Abbott, N. J.; Dolman, D. E.; Drndarski, S.; Fredriksson, S. M. An improved in vitro blood-brain barrier model: rat brain endothelial cells co-cultured with astrocytes. *Methods Mol. Biol.* **2012**, *814*, 415–430.
2. Abbott, N. J. Blood-brain barrier structure and function and the challenges for CNS drug delivery. *J. Inherit. Metab. Dis.* **2013**, *36*, 437–449.
3. Wong, A. D.; Ye, M.; Levy, A. F.; Rothstein, J. D.; Bergles, D. E.; Searson, P. C. The blood-brain barrier: an engineering perspective. *Front. Neuroeng* **2013**, *6*, 7.
4. Carman, A. J.; Mills, J. H.; Krenz, A.; Kim, D. G.; Bynoe, M. S. Adenosine receptor signaling modulates permeability of the blood-brain barrier. *J. Neurosci.* **2011**, *31*, 13272–13280.
5. Larsen, P.; Ulin, J.; Dahlstrøm, K.; Jensen, M. Synthesis of [11C]iodomethane by iodination of [11C]methane. *Appl. Radiat. Isot.* **1997**, *48*, 153–157.
6. Roman, V.; Keijser, J. N.; Luiten, P. G.; Meerlo, P. Repetitive stimulation of adenosine A₁ receptors *in vivo*: changes in receptor numbers, G-proteins and A₁ receptor agonist-induced hypothermia. *Brain Res.* **2008**, *1191*, 69–74.
7. Julien-Dolbec, C.; Tropres, I.; Montigon, O.; Reutenauer, H.; Ziegler, A.; Decorps, M.; Payen, J. F. Regional response of cerebral blood volume to graded hypoxic hypoxia in rat brain. *Br. J. Anaesth.* **2002**, *89*, 287–293.
8. Logan, J. Graphical analysis of PET data applied to reversible and irreversible tracers. *Nucl. Med. Biol.* **2000**, *27*, 661–670.
9. Manaenko, A.; Chen, H.; Kammer, J.; Zhang, J. H.; Tang, J. Comparison evans blue injection routes: intravenous *versus* intraperitoneal, for measurement of blood-brain barrier in a mice hemorrhage model. *J. Neurosci. Methods* **2011**, *195*, 206–210.



**Small-Animal PET Study of Adenosine A₁ Receptors
in Rat Brain: Blocking Receptors and
Rising Extracellular Adenosine**

Soumen Paul[†], **Shivashankar Khanapur[†]**, Anna A. Rybczynska[†], Chantal Kwizera[†], Jurgen W.A. Sijbesma[†], Kiichi Ishiwata[‡], Antoon T.M. Willemsen[†], Philip H. Elsinga^{†,§}, Rudi A.J.O. Dierckx^{†,§} and Aren van Waarde[†]

[†] Nuclear Medicine and Molecular Imaging, UMCG,
University of Groningen, Groningen, The Netherlands

[‡] Positron Medical Center, Tokyo Metropolitan
Institute of Gerontology, Tokyo, Japan

[§] Department of Nuclear Medicine, University Hospital Ghent, Ghent,
Belgium

6

J Nucl Med 2011; 52:1293–1300

Abstract

Activation of adenosine A₁ receptors (A₁R) in the brain causes sedation, reduces anxiety, inhibits seizures, and promotes neuroprotection. Cerebral A₁R can be visualized using 8-dicyclopropylmethyl-1-[¹¹C]-methyl-3-propyl-xanthine ([¹¹C]MPDX) and PET. This study aims to test whether [¹¹C]MPDX can be used for quantitative studies of cerebral A₁R in rodents. **Methods:** [¹¹C]MPDX was injected (*intravenously*) into isoflurane-anesthetized male Wistar rats (300 g). A dynamic scan of the central nervous system was obtained, using a small-animal PET camera. A cannula in a femoral artery was used for blood sampling. Three groups of animals were studied: group 1, controls (saline-treated); group 2, animals pretreated with the A₁R antagonist 8-cyclopentyl-1,3-dipropylxanthine (DPCPX, 1 mg, *intraperitoneally*); and group 3, animals pretreated (*intraperitoneally*) with a 20 % solution of ethanol in saline (2 mL) plus the adenosine kinase inhibitor 4-amino-5-(3-bromophenyl)-7-(6-morpholino-pyridin-3-yl)pyrido [2,3-d] pyrimidine dihydrochloride (ABT-702, 1 mg). DPCPX is known to occupy cerebral A₁R, whereas ethanol and ABT-702 increase extracellular adenosine. **Results:** In groups 1 and 3, the brain was clearly visualized. High uptake of [¹¹C]MPDX was noted in striatum, hippocampus, and cerebellum. In group 2, tracer uptake was strongly suppressed and regional differences were abolished. The treatment of group 3 resulted in an unexpected 40–45 % increase of the cerebral uptake of radioactivity as indicated by increases of PET standardized uptake value, distribution volume from Logan plot, nondisplaceable binding potential from 2- tissue-compartment model fit, and standardized uptake value from a biodistribution study performed after the PET scan. The partition coefficient of the tracer (K_1 / k_2 from the model fit) was not altered under the study conditions. **Conclusion:** [¹¹C]MPDX shows a regional distribution in rat brain consistent with binding to A₁R. Tracer binding is blocked by the selective A₁R antagonist DPCPX. Pretreatment of animals with ethanol and adenosine kinase inhibitor increases [¹¹C]MPDX uptake. This increase may reflect an increased availability of A₁R after acute exposure to ethanol.

Introduction

The adenosine receptor (AR) family consists of the A₁, A_{2A}, A_{2B} and A₃ subtypes. A₁ and A₃R inhibit, whereas A_{2A} and A_{2B} stimulate, production of the second messenger, 3',5'-cyclic adenosine monophosphate. A₁R and A_{2A}R are activated by nanomolar concentrations of adenosine, whereas A_{2B} and A₃R become activated only when adenosine levels rise into the micromolar range because of inflammation, hypoxia, or ischemia.¹⁻³

A₁Rs are highly expressed and extensively distributed in various regions of the human brain such as the hippocampus, cerebral cortex, thalamic nuclei, and basal ganglia.^{4,5} In the central nervous system, adenosine acts as an endogenous modulator of neurotransmission,⁶ a neuroprotectant⁷, and an anticonvulsant.⁸ Its neuroprotective action is mediated *via* A₁R and may be associated with inhibition of the release of excitatory neurotransmitters, hyperpolarization of neurons, and inhibition of Ca²⁺ channels.⁹ Adenosine acts also as an analgesic, by affecting nociceptive afferent and transmission neurons *via* A₁R.¹⁰ A₁R agonists usually stimulate¹¹, whereas A₁R antagonists diminish, sleep.¹² Thus, such compounds may be therapeutically useful. Yet, A₁R agonists have failed to undergo successful clinical development because of dose-limiting cardiovascular side effects.

Adenosine kinase inhibitors (AKIs) represent an alternative treatment strategy. Adenosine kinase (AK) catalyzes a phosphorylation reaction, converting adenosine to adenosine monophosphate.^{13,14} The inhibition of AK decreases the cellular reuptake of adenosine, resulting in increased local adenosine concentrations.¹⁴ The feasibility of raising adenosine availability in the central nervous system by inhibiting AK has been demonstrated in hippocampal and spinal cord slices¹⁵ and by *in vivo* studies on extracellular adenosine in rat striatum, which was increased up to 10-fold.¹⁶

The psychoactive drug ethanol also raises extracellular levels of adenosine in the brain (up to 4-fold¹⁷) by augmenting the rate of

adenosine formation¹⁸ and inhibiting adenosine uptake via nucleoside transporters.¹⁸⁻²⁰ The anxiolytic, sedating, and motor-impairing effects of ethanol are related to its interaction with adenosinergic signaling.

PET with a radiolabeled A₁R ligand may allow study of the involvement of A₁R in the pathophysiology of disease, the response of the A₁R population to therapy, and assessment of the occupancy of A₁R by therapeutic drugs. Several positron emitting A₁R ligands have been prepared for this purpose, but only 2 have been widely used: 8-dicyclopropylmethyl-1-[¹¹C]-methyl-3-propylxanthine²¹ ([¹¹C]MPDX) and [¹⁸F]-8-cyclopentyl-3-(3-fluoropropyl)-1-propylxanthine.⁵ Both ligands bind with high affinity and selectivity to A₁R *in vivo* (K_i and K_d values, 3.0 and 4.4 nM, respectively).

Because small-animal PET studies with [¹¹C]MPDX had not been performed previously, we tested this ligand for quantitative small-animal PET studies in rodents with the intention of later using this technique for the assessment of changes of A₁R density in rodent models of human disease. In addition, we examined the impact of raised levels of extracellular adenosine on the cerebral binding of [¹¹C]MPDX.

6

Materials and Methods

Chemicals

Ethanol and triethylamine were purchased from Merck. The adenosine A₁ antagonist 1,3-dipropyl-8-cyclopentylxanthine (DPCPX) was a product of Sigma, and the potent nonnucleoside 4-amino-5-(3-bromophenyl)-7-(6-morpholino-pyridin-3-yl)pyrido[2,3-d]pyrimidine dihydrochloride (ABT-702) was obtained from Tocris. Stock solutions of DPCPX and ABT-702 were prepared in dimethyl sulfoxide. The radioligand [¹¹C]MPDX was prepared by reaction of [¹¹C]methyl iodide with the appropriate 1-N-desmethyl precursor. Briefly, [¹¹C]methyl iodide was trapped in 0.3 mL of N,N-dimethylformamide containing 1 mg of 1-N-desmethyl precursor and 5 μL of NaOH and was heated at 120 °C for 5 min.

After 1.0 mL of 0.1 M HCl had been added, the solution was loaded onto a high-performance liquid chromatography column (Econosphere, C₁₈, 5 μm [Altech]; 10 × 250 mm) and eluted with a mixture of 0.1 M NaH₂PO₄ and ethanol (70 / 30) at a flow rate of 4 mL / min. The fractions containing [¹¹C]MPDX were collected. Retention time of [¹¹C]MPDX was 14 min. The decay-corrected radiochemical yield was 35 % ± 5 % (based on [¹¹C]methyl iodide), the specific radioactivity was greater than 11 TBq / mmol at the moment of injection, and the radiochemical purity was greater than 98 %.

Animal Model

The animal experiments were performed by licensed investigators in compliance with the Law on Animal Experiments of The Netherlands. The protocol was approved by the Committee on Animal Ethics of the University of Groningen. Male Wistar rats were maintained at a 12-h light/12-h dark regime and were fed standard laboratory chow *ad libitum* (body weights are provided in Table 1).

Table 1. Animal Data

Group	Body wt (g)	Injected dose		ROI size (cm ³)
		MBq	nmol	
Control (n = 5)	299 ± 8	24 ± 10	2.2 ± 0.9	1.02 ± 0.02
DPCPX (n = 5)	314 ± 18	26 ± 14	2.4 ± 1.3	1.02 ± 0.04
EtOH+ABT702 (n = 5)	302 ± 16	34 ± 11	3.1 ± 1.0	1.02 ± 0.03
Metabolite analysis (n = 6)	314 ± 14	20 ± 12	1.8 ± 1.1	–

Data are mean ± SD

Small-Animal PET Scanning

In most experiments, 2 rats were scanned simultaneously, using a Focus 220 microPET camera (Siemens-Concorde). Animals were anesthetized with a mixture of isoflurane / air (inhalation anesthesia, 5 % ratio during induction, later reduced to <2 %). A cannula was placed in a femoral artery for blood sampling. Rats were under anesthesia for 30 – 40 min before tracer injection (time required for cannulation and transmission scan). The tracer ([¹¹C]MPDX) was injected through the penile vein (injected dose is

given in Table 1). A list-mode protocol was used (76 min, brain in the field of view). Scanning was started during injection of radioactivity in the lower rat; the upper animal was injected 16 min later. The animal that was injected last was also anesthetized at a later moment. Thus, the duration of anesthesia was similar in all study groups. A series of blood samples (14 samples; volume, 0.10 – 0.15 mL) was drawn, initially in rapid succession (every 15 s) and later at longer intervals (≤ 30 min). Plasma was acquired from these samples by short centrifugation (Eppendorf centrifuge, 5 min at 13000 rpm). Radioactivity in 25 μ L of plasma was counted and used as an arterial input function.

For examination of the specificity of tracer binding, 5 animals were pretreated by *intraperitoneal* injection of DPCPX (1 mg, in 0.3 mL of dimethyl sulfoxide, 15 – 20 min before injection of the tracer). For examination of the impact of raised levels of extracellular adenosine on [¹¹C]MPDX binding, 5 other rats received ethanol (2 mL of a 20 % solution in saline *intraperitoneally*) and the AKI ABT-702 (1 mg, in 0.3 mL of dimethyl sulfoxide *intraperitoneally*). Both ethanol and ABT-702 were administered 15 – 20 min before injection of [¹¹C]MPDX. Control animals (n = 5) received saline only. The ethanol dose that we administered corresponds to substantial consumption of alcohol in humans (about six 0.33-L bottles of normal beer containing 5 % alcohol).

List-mode data were reframed into a dynamic sequence of 8×30 , 3×60 , 2×120 , 2×180 , 3×300 , 1×480 , 2×600 , and 1×960 s frames. The data were reconstructed per time frame using an iterative reconstruction algorithm (attenuation-weighted 2-dimensional ordered-subset expectation maximization, provided by Siemens; 4 iterations, 16 subsets; zoom factor, 2). The final datasets consisted of 95 slices, with a slice thickness of 0.8 mm and an in plane image matrix of 128×128 pixels of size 1×1 mm. Datasets were fully corrected for random coincidences, scatter, and attenuation. A separate transmission scan (duration, 515 s) was acquired for attenuation correction. That scan was made before the

emission scan. Images were smoothed with a gaussian filter (1.35 mm in both directions).

Small-Animal PET Data Analysis

Three-dimensional regions of interest (ROIs) were manually drawn around the entire brain. Time-activity curves and volumes (cm³) for the ROIs were calculated, using standard software (AsiPro, version 6.2.5.0; Siemens-Concorde). PET standardized uptake values (SUVs) for brain radioactivity were calculated, using measured body weights and injected doses and assuming a specific gravity of 1 g/mL for brain tissue and blood plasma.

Dynamic PET data were analyzed using plasma radioactivity from arterial blood samples as an input function and a graphical method according to Logan.²² Because [¹¹C]MPDX proved to be rapidly cleared but slowly metabolized, no metabolite correction of the input function was performed. The error introduced by this procedure (overestimation of the true plasma input) is 10.0 % and identical in all study groups; thus, we concluded that metabolite correction could be omitted. Software routines for MatLab 7 (The MathWorks), written by Dr. Antoon T.M. Willemsen (University Medical Center Groningen), were used for curve fitting. The Logan fit was started at 10 min. The cerebral distribution volume (V_T) of the tracer was estimated from the Logan plot. The dynamic PET data were also analyzed using the same input function and software routines, a 2-tissue compartment model (2TCM), and a fixed blood volume of 3.6 %. The partition coefficient (K_1 / k_2) and nondisplaceable binding potential (BP_{ND}) (k_3 / k_4) of [¹¹C]MPDX were estimated from the model fit. Similar methods were used previously by Kimura *et al.*²³ for quantification of A₁R in the human brain. However, A₁Rs are significantly expressed in rat cerebellum, in contrast to human cerebellum, in which A₁R density is negligible. Therefore, the cerebellum cannot be used as a reference region in small-animal PET studies of the rodent brain.

Biodistribution Studies

After the scanning period, the anesthetized animals were sacrificed. Blood was collected, and plasma and a cell fraction were obtained from the blood sample by short centrifugation (5 min at 1,000*g*). Several brain areas and peripheral tissues (Table 2) were excised. All tissue samples were weighed. The radioactivity in tissue samples was measured using a γ -counter, applying a decay correction. The results were expressed as dimensionless SUVs. The parameter SUV is defined as tissue activity concentration (MBq / g) \times body weight (g) / injected dose (MBq).

Table 2. Biodistribution Data of [11C]MPDX, 80 Min After Injection

Tissue	Control (n = 5)	DPCPX- treated (n = 5)	Diff. vs control	EtOH / ABT702- treated (n = 5)	Diff. vs control
Amygdala	0.75 ± 0.09	0.27 ± 0.05	< 0.0001	1.12 ± 0.12	<0.0005
Bulbus olfactorious	0.64 ± 0.18	0.34 ± 0.07	< 0.01	0.75 ± 0.27	NS
Cerebellum	1.34 ± 0.29	0.46 ± 0.09	0.0001	2.16 ± 0.42	< 0.01
Cingulate	0.88 ± 0.16	0.35 ± 0.08	0.0001	1.13 ± 0.23	0.06
Entorhinal	0.89 ± 0.10	0.37 ± 0.04	< 0.0001	1.27 ± 0.25	< 0.01
Frontal	0.89 ± 0.20	0.30 ± 0.08	0.0002	1.16 ± 0.26	NS
Hippocamp- us	1.09 ± 0.14	0.31 ± 0.08	< 0.0001	1.47 ± 0.24	0.01
Medulla	0.75 ± 0.18	0.42 ± 0.11	0.01	1.51 ± 0.29	< 0.001
Parietal, temporal and occipital cortex	0.97 ± 0.20	0.34 ± 0.07	0.0001	1.40 ± 0.48	NS
Pons	0.89 ± 0.21	0.44 ± 0.14	< 0.01	1.45 ± 0.30	< 0.01
Striatum	1.01 ± 0.13	0.31 ± 0.07	< 0.0001	1.18 ± 0.31	NS
Bone	0.24 ± 0.04	0.22 ± 0.09	NS	0.24 ± 0.09	NS
Colon	0.83 ± 0.21	0.61 ± 0.19	NS	0.71 ± 0.06	NS
Duodenum	1.12 ± 0.33	0.95 ± 0.57	NS	1.19 ± 0.17	NS
Fat	1.95 ± 1.15	1.52 ± 0.19	NS	1.06 ± 0.24	NS

Heart	0.69 ± 0.14	0.66 ± 0.08	NS	0.85 ± 0.17	NS
Ileum	1.52 ± 0.52	1.19 ± 0.41	NS	1.38 ± 0.43	NS
Kidney	1.09 ± 0.18	1.26 ± 0.07	0.08	1.50 ± 0.50	NS
Liver	2.94 ± 0.40	4.43 ± 1.03	< 0.02	3.63 ± 0.68	NS
Lung	0.70 ± 0.09	0.73 ± 0.07	NS	0.88 ± 0.07	< 0.01
Muscle	0.40 ± 0.09	0.48 ± 0.07	NS	0.53 ± 0.07	< 0.05
Pancreas	0.98 ± 0.18	1.01 ± 0.23	NS	1.48 ± 0.22	< 0.005
Plasma	0.77 ± 0.06	0.73 ± 0.13	NS	0.71 ± 0.13	NS
Red cells	0.34 ± 0.04	0.38 ± 0.09	NS	0.44 ± 0.07	< 0.02
Spleen	0.95 ± 0.14	0.65 ± 0.06	< 0.005	1.06 ± 0.26	NS
Trachea	0.73 ± 0.15	0.81 ± 0.31	NS	0.85 ± 0.23	NS

SUV values (mean ± S.D.) are listed, Diff. = Difference NS = not significant.

Metabolite Analysis

A separate group of animals (n = 6) was used for metabolite analysis. In these rats, a small-animal PET scan was obtained and a biodistribution study was performed, but a smaller series of arterial blood samples was drawn (at intervals of 5, 10, 20, 40, and 60 min after tracer injection, volume increasing from 0.3 to 0.7 mL). Plasma was acquired by short centrifugation (Eppendorf centrifuge, 5 min at 13000 rpm). Protein was removed by mixing plasma with an equivalent volume of 20 % trichloroacetic acid in acetonitrile, followed again by short centrifugation. The protein free supernatant was injected into a high-performance liquid chromatography system (stationary phase, μ Bondapak, 7.8 × 300 mm [Waters]; mobile phase, 3 % triethylamine and phosphate, pH 2.0: acetonitrile, 60:40

v/v, with a flow rate of 2 mL / min). The retention time of authentic [11C]MPDX (and nonradioactive MPDX) was about 11 min. Two radioactive metabolites eluted at shorter retention times (6 and 8 min, respectively). This reversed-phase system is a slightly modified version of a published analytic procedure.²⁴ One-milliliter samples of the eluate were collected at 0.5-min intervals. Radioactivity in these samples was determined with a γ -counter and was automatically corrected for decay.

Statistical Tests

Differences between groups were analyzed using 1-way ANOVA. A probability smaller than 0.05 was considered statistically significant.

Results

Small-Animal PET Images

Small-animal PET images acquired after injection of [11C]MPDX are presented in Figure 1. In saline-treated control animals, the brain was clearly visualized. High tracer uptake was observed in the hippocampus, cerebellum, and striatum (left panel) in addition to some areas of the cortex (image not shown). After pretreatment of rats with DPCPX, cerebral uptake of the tracer was strongly reduced, and regional differences in tracer uptake were no longer apparent (middle panel). When animals were pretreated with ethanol and the AKI ABT-702, a global increase of tracer uptake was noted, compared with the control group (right panel).

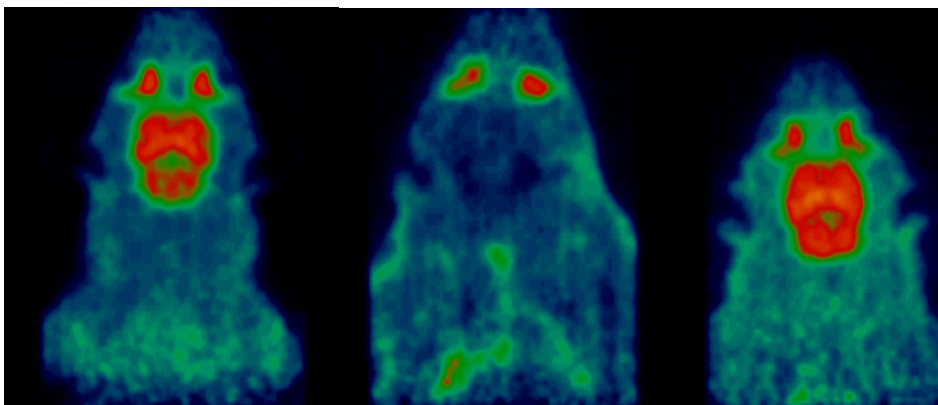


FIGURE 1. Small-animal PET images of rat brain acquired after injection of [¹¹C]MPDX (summed frames from 2 min to end of scan, SUV maximum set to 3): untreated control animal (left), animal pretreated with DPCPX (middle), and animal pretreated with ethanol and ABT-702 (right)

Kinetics of Radioactivity in Brain and Plasma

Cerebral kinetics of [¹¹C]MPDX-derived radioactivity (PET SUV in the whole brain as a function of time) are presented in Figure 2. In saline-treated control animals, uptake of the tracer rapidly increased to a maximum, which was already reached between 7 and 12 min, and was followed by washout. In animals pretreated with DPCPX, only a rapid washout of tracer was observed, and the cerebral uptake of ¹¹C was strongly reduced. In rats pretreated with ABT-702 and ethanol, cerebral uptake of radioactivity was significantly increased, compared with the control group. Maximal tracer uptake now occurred after 13–20 min and was followed by washout. On the basis of SUVs measured with small-animal PET, A₁R densities reported in the literature (e.g., 5003 fmol of protein per milligram in rat hippocampus²⁵), injected masses of the tracer (Table 1), and assuming that cerebral tissue contains 10 % protein, we estimate that less than 5 % of the A₁R population in the rat brain was occupied by [¹¹C]MPDX under the conditions of our study. Kinetics of radioactivity in rat plasma after injection of [¹¹C]MPDX are presented in Figure 2. A rapid, biexponential clearance was

observed in all groups. Treatment of animals with DPCPX or a combination of ethanol and AKI (ABT-702) did not significantly affect tracer clearance from the plasma compartment. Areas under the curve (percentage of control) were 100.0 ± 8.4 , 95.5 ± 6.6 , and 96.0 ± 7.5 for the baseline, ethanol and ABT-702, and DPCPX groups, respectively (mean \pm SEM).

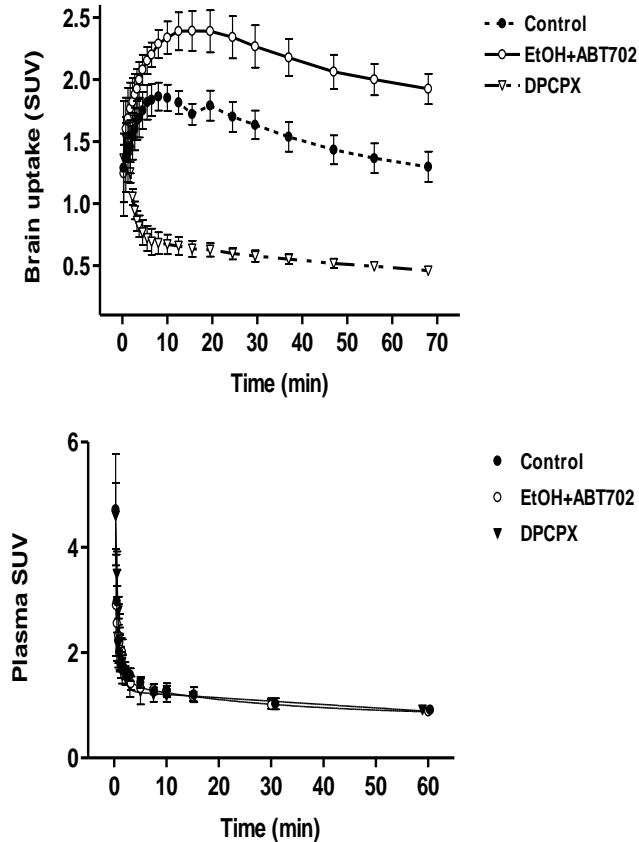


Figure 2. Kinetics of [¹¹C]MPDX –derived radioactivity in rat brain (left) and plasma (right). Error bars indicate SEM. Plasma data are not corrected for metabolites. ● = control group; ○ = Ethanol and ABT-702 –treated animals; ▽ = animals pretreated with DPCPX

Metabolite Analysis

The appearance of radiolabeled metabolites in rat plasma after injection of [11C]MPDX was studied in 2 untreated control animals, 2 rats treated with ethanol and ABT-702, and 2 rats pretreated with DPCPX. Injected [11C]MPDX was found to be hardly metabolized. The fraction of parent compound decreased from almost 100 % at time zero to 82 %–84 % at 60 min (Figure 3). Pretreatment did not affect the rate of tracer metabolism

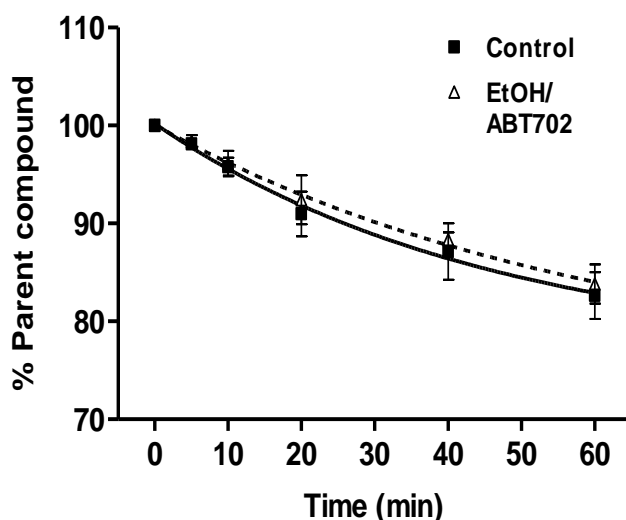


Figure 3. Fraction of plasma radioactivity representing parent [11C]MPDX. Error bars indicate SEM

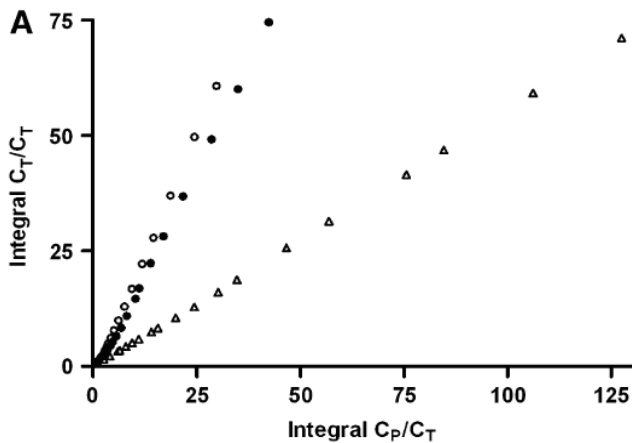
Biodistribution Data

Biodistribution data of ¹¹C, acquired 80 min after injection of [11C]MPDX, are presented in Table 2. Pretreatment of animals with DPCPX resulted in a highly significant reduction of tracer uptake in all studied brain areas. Among peripheral organs, a significant reduction of tracer uptake was observed only in the spleen. DPCPX treatment caused a significant increase of the amount of radioactivity in the liver. Renal uptake of the tracer appeared to be increased as well, but the change was relatively small and this trend did not reach statistical significance. Treatment of rats with ethanol and ABT-702 increased uptake of radioactivity in the brain. This

increase was statistically significant in the amygdala, cerebellum, entorhinal cortex, hippocampus, medulla, and pons. In other brain areas, an increase was also noted but this trend did not reach statistical significance because of a relatively large individual variance in the study groups. Outside the brain, increases of tracer uptake were noted in lungs, skeletal muscle, pancreas, and red blood cells after treatment of animals with ethanol and ABT-702.

Graphical Analysis of PET Data

V_T of tracer was calculated using a Logan plot (Figure 4), time-activity curves from an ROI drawn around the entire brain, and radioactivity counts from arterial blood samples. V_T of tracer was significantly decreased (by 63 %) after pretreatment of animals with DPCPX and significantly increased (by 39 %) after pretreatment with ethanol and ABT-702 (Table 3).



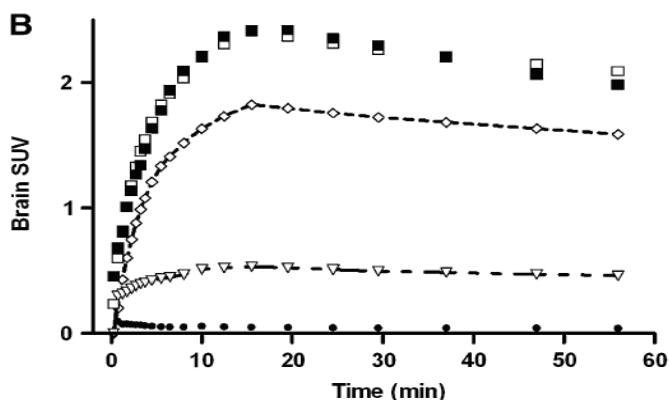


Figure 4. Logan plots (A) of control, ethanol and ABT-702-treated, and DPCPX-treated rats and 2TCM fit (B) for animal pretreated with ethanol and ABT-702. (A) ● = 5 control group; ○ = ethanol and ABT-702-treated animals; △ = animals pretreated with DPCPX. (B) ■ = measured activity in brain; □ = fitted activity in brain, ◇ = specific binding in brain; ▽ = nondisplaceable binding in brain and tracer in plasma; ◆ = tracer in plasma

6

Table 3. Results from Graphical Analysis and Compartment Modeling of PET Data (ROI Drawn Around Entire Brain)

Parameter	V_T (Logan plot)	K_1 / k_2 (2TCM)	$BP_{ND} (k_3 / k_4)$ (2TCM)	V_T (2TCM)
Control rats	1.52 ± 0.18	0.62 ± 0.17	1.52 ± 0.10	1.56 ± 0.37
DPCPX pretreated	0.57 ± 0.05 ($p < 0.0001$)	0.58 ± 0.07 (NS)	0.00 ($p < 0.0001$)	0.58 ± 0.07 ($p < 0.0001$)
EtOH / ABT702-pretreated	2.12 ± 0.25 ($p < 0.005$)	0.68 ± 0.17 (NS)	2.34 ± 0.64 ($p < 0.05$)	2.21 ± 0.44 ($p < 0.05$)

Mean \pm S.D. P values relate to the effect of pretreatment compared to untreated controls.

NS = not significant

Compartment Modeling of PET Data

A 2TCM was fitted to time–activity curves from an ROI drawn around the entire brain, using radioactivity counts from arterial blood samples as an input function. A 1-tissuecompartment model could not be fitted to the time–activity curves of control and ethanol and ABT-702–treated animals at all, in contrast to a 2TCM. Thus, the 2TCM was clearly superior. The partition coefficient of [¹¹C]MPDX (ratio K_1 / k_2 from the model fit) was not significantly affected by any of the treatments, in contrast to BP_{ND} (Table 3). BP_{ND} was reduced to zero after treatment of animals with DPCPX and significantly increased (by 54 %) after treatment with ethanol and ABT-702. V_T calculated from the 2TCM fit corresponded closely to V_T acquired by graphical (Logan) analysis of the PET data, although the intraindividual variability was greater. V_T (from the model fit) was significantly reduced (by 63 %) after pretreatment of animals with DPCPX and significantly increased (by 42 %) after treatment with ethanol and ABT-702.

Discussion

Specificity of [¹¹C]MPDX Binding

The regional distribution of radioactivity in the rat brain after injection of [¹¹C]MPDX (Figure 1, left) suggests that this tracer is capable of visualizing regional A₁R densities. Further evidence for specific *in vivo* binding of [¹¹C]MPDX was obtained by pretreating animals with the subtype-selective antagonist DPCPX. In pretreated animals, the brain uptake of radioactivity after injection of [¹¹C]MPDX was strongly suppressed, and regional differences were no longer evident (Figure 1, middle; Figure 2, left). A biodistribution study, performed at 80 min after tracer injection, confirmed that uptake of radioactivity was reduced by DPCPX to a low value that was homogeneous throughout the brain (Table 2). The greatest declines were observed in the hippocampus (72 %), striatum (69 %), cerebellum (66 %), frontal cortex (66 %), parietal cortex (65 %), and amygdala (64 %). Outside the brain, a reduction of [¹¹C]MPDX uptake was observed only in the spleen, possibly reflecting specific binding of the tracer to A₁R, because A₁Rs are involved in splenic

contraction.²⁶ DPCPX caused a significant increase of the levels of radioactivity in rat liver and tended to increase renal activity levels as well (Table 2), indicating that after blocking of the receptor compartment, a greater fraction of the injected dose is taken up by organs involved in tracer excretion.

To further test the origin of the PET signal, we plotted the specific binding of [¹¹C]MPDX in various brain areas (uptake in saline-treated control animals minus uptake in animals pretreated with DPCPX, Table 2) against regional A₁R numbers, known from autoradiography.²⁷⁻²⁹ The regions plotted were the amygdala, cerebellum, cingulate, entorhinal, and frontal cortices; hippocampus; medulla; parietal-temporal-occipital cortex; pons; and striatum. Receptor density in the hippocampus (main target region) was set to 100 %, to allow the use of data from several published studies. An excellent correlation was observed between literature values for A₁R density and [¹¹C]MPDX uptake at 80 min after injection (Figure 5).

Data analysis of the cerebral time-activity curves in saline- and DPCPX-treated animals also confirmed specific binding of [¹¹C]MPDX to cerebral A₁R. Tracer V_T in the entire brain—calculated either by graphical analysis or by kinetic modeling of the PET data—showed a decline (>60 %) similar to that of tracer SUV measured after 80 min (Table 3). In contrast, BP_{ND} of [¹¹C]MPDX estimated by fitting a 2TCM was reduced to zero after pretreatment of animals with DPCPX (Table 3), suggesting that specific binding of [¹¹C]MPDX is absent in DPCPX-treated animals.

Effect of Ethanol and Inhibition of Adenosine Kinase

Acute administration of ethanol is known to result in strong increases of extracellular adenosine both in cell culture and in the rat brain *in vivo*, which can be assessed by microdialysis.¹⁷ Two different mechanisms may underlie this effect of ethanol. First, ethanol is metabolized to acetate and acetyl-coA before entering the tricarboxylic acid cycle. Increased flux through acetyl coA-synthetase leads to increased production of adenosine from adenosine monophosphate *via* 5'-nucleotidase and stimulation of cellular

adenosine release.¹⁸ Second, ethanol blocks nucleoside transporters in cellular membranes, particularly the type 1 equilibrative nucleoside transporter.^{19,20,30,31} Increased binding of adenosine to cerebral A₁R is believed to be an important factor underlying the motor incoordination³²⁻³⁵ and sleep-promoting³⁶ effects of ethanol.

The co-administration of an AKI (e.g., ABT-702) with ethanol leads to even stronger increases of extracellular adenosine, because phosphorylation of adenosine by the enzyme AK is normally the primary route of adenosine metabolism. Inhibition of AK decreases the rate of adenosine inactivation and locally enhances extracellular adenosine concentrations—not at baseline but rather under conditions of increased formation of adenosine. Orally administered AKIs are known to raise regional concentrations of endogenous adenosine in the brain,^{15,16} and for this reason, these compounds have therapeutic potential as analgesic, antiinflammatory, and antiepileptic agents.^{14,37}

Because both ethanol administration and AK inhibition are known to increase the levels of extracellular adenosine, we expected to observe a decreased binding of the PET tracer [11C]MPDX in the rat brain after acute treatment of rats with ethanol and ABT-702. Competition of adenosine for tracer binding to A₁R is likely to occur, because the affinities of adenosine and [11C]MPDX for cerebral A₁R are in the same (nanomolar) range.³⁸ However, in ethanol and ABT-702-pretreated animals, we observed a paradoxical increase rather than a decrease of cerebral tracer binding. Statistically significant increases occurred in PET SUV (Figures 1 and 2), SUV from an ex vivo biodistribution study (Table 2), and tracer V_T (Table 3). Kinetic modeling was performed to gain more insight into the mechanisms underlying the paradoxical increase of cerebral radioactivity induced by ethanol and ABT-702. Fitting of a 2TCM to the cerebral time-activity curves of control and treated animals indicated that the partition coefficient of the tracer (K_1 / k_2) was not affected by treatment, in contrast to BP_{ND}, which showed a significant increase (Table 3). The fit data, and also our data on tracer clearance (Figure

2) and metabolism (Figure 3), suggest that tracer delivery is not changed by treatment. Increases of the apparent A₁R densities (on average, 35 %; maximally, 55 %) in the brain of rats and mice have been reported, both after acute^{32,39} and after chronic^{39,40} administration of ethanol, using *ex vivo* binding assays. Such changes could cause increased cerebral binding of [¹¹C]MPDX after treatment of rodents with ethanol and ABT-702. However, further studies are necessary to identify the mechanism underlying increased binding of the A₁R ligand under these conditions.

Conclusion

Our data suggest that regional A₁R densities in rat brain can be assessed using the tracer [¹¹C]MPDX and small-animal PET. In the brain of untreated control animals, the highest levels of tracer uptake were observed in target regions with a high density of A₁R, such as the hippocampus, striatum, cerebellum, and cerebral cortex (Figure 1). Pretreatment of animals with the specific A₁R antagonist DPCPX resulted in a strong suppression of tracer uptake in the central nervous system and an abolishment of the regional differences (Figure 1; Table 2). Specific binding of the tracer in various brain regions corresponded closely to regional A₁R densities known from autoradiography (Figure 5). Tracer binding can be quantified both by graphical analysis (Logan plot, calculation of V_T) and by kinetic modeling (BP_{ND} or V_T from 2TCM, Table 3). The PET data did not provide evidence for increased competition of endogenous adenosine after acute treatment of animals with ethanol and ABT-702, but a globally increased binding of [¹¹C]MPDX was noted in the rat brain (Figures 1 and 2; Tables 2 and 3), which may correspond to increases of apparent A₁R density reported in the literature. Further studies are necessary to elucidate the mechanisms underlying the enhanced [¹¹C]MPDX binding after treatment of animals with ethanol and ABT-702.

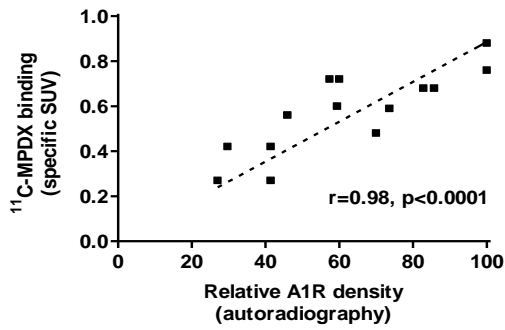


FIGURE 5. Correlation between specific *in vivo* binding of [¹¹C]MPDX and regional A₁R density as known from autoradiography

References

1. Collis MG, Hourani SM. Adenosine receptor subtypes. *Trends Pharmacol Sci* **1993**, *14*(10), 360–366.
2. Fredholm BB, Abbracchio MP, Burnstock G, Daly JW, Harden TK, Jacobson KA et al. Nomenclature and classification of purinoceptors. *Pharmacol Rev* **1994**, *46*(2), 143–156.
3. Haas HL, Selbach O. Functions of neuronal adenosine receptors. *Naunyn-Schmiedebergs Arch Pharmacol* **2000**, *362*(4-5), 375–381.
4. Fastbom J, Pazos A, Probst A, Palacios JM. Adenosine A1 receptors in the human brain: a quantitative autoradiographic study. *Neuroscience* **1987**, *22*(3), 827–839.
5. Bauer A, Holschbach MH, Meyer PT, Boy C, Herzog H, Olsson RA et al. In vivo imaging of adenosine A₁ receptors in the human brain with [18F]CPFPX and positron emission tomography. *Neuroimage* **2003**, *19*(4), 1760–1769.
6. Williams M. Adenosine - a selective neuromodulator in the mammalian CNS? *Trends Neurosci* **1984**, *7*(5), 164–168.
7. Fredholm BB. Adenosine and neuroprotection. *Int Rev Neurobiol* **1997**, *40*, 259–280.
8. Young D, Dragunow M. Status epilepticus may be caused by loss of adenosine anticonvulsant mechanisms. *Neuroscience* **1994**, *58*(2), 245–261.
9. Dunwiddie TV, Masino SA. The role and regulation of adenosine in the central nervous system. *Annu Rev Neurosci* **2001**, *24*, 31–55.
10. Sawynok J, Reid A, Poon A. Peripheral antinociceptive effect of an adenosine kinase inhibitor, with augmentation by an adenosine deaminase inhibitor, in the rat formalin test. *Pain* **1998**, *74*(1), 75–81.
11. Portas CM, Thakkar M, Rainnie DG, Greene RW, McCarley RW. Role of adenosine in behavioral state modulation: a microdialysis study in the freely moving cat. *Neuroscience* **1997**, *79*(1), 225–235.

12. Lin AS, Uhde TW, Slate SO, McCann UD. Effects of intravenous caffeine administered to healthy males during sleep. *Depress Anxiety* **1997**, *5(1)*, 21–28.
13. Arch JR, Newsholme EA. The control of the metabolism and the hormonal role of adenosine. *Essays Biochem* **1978**, *14*, 82-123.
14. McGaraughty S, Cowart M, Jarvis MF. Recent developments in the discovery of novel adenosine kinase inhibitors: mechanism of action and therapeutic potential. *CNS Drug Rev* **2001**, *7(4)*, 415–432.
15. Golembiowska K, White TD, Sawynok J. Adenosine kinase inhibitors augment release of adenosine from spinal cord slices. *Eur J Pharmacol* **1996**, *307(2)*, 157–162.
16. Britton DR, Mikusa J, Lee CH, Jarvis MF, Williams M, Kowaluk EA. Site and event specific increase of striatal adenosine release by adenosine kinase inhibition in rats. *Neurosci Lett* **1999**, *266(2)*, 93–96.
17. Sharma R, Engemann SC, Sahota P, Thakkar MM. Effects of ethanol on extracellular levels of adenosine in the basal forebrain: an in vivo microdialysis study in freely behaving rats. *Alcohol Clin Exp Res* **2010**, *34(5)*, 813–818.
18. Nagy LE. Ethanol metabolism and inhibition of nucleoside uptake lead to increased extracellular adenosine in hepatocytes. *Am J Physiol* **1992**, *262(5 Pt 1)*, C1175–C1180.
19. Nagy LE, Diamond I, Casso DJ, Franklin C, Gordon AS. Ethanol increases extracellular adenosine by inhibiting adenosine uptake via the nucleoside transporter. *J Biol Chem* **1990**, *265(4)*, 1946–1951.
20. Krauss SW, Ghirnikar RB, Diamond I, Gordon AS. Inhibition of adenosine uptake by ethanol is specific for one class of nucleoside transporters. *Mol Pharmacol* **1993**, *44(5)*, 1021–1026.
21. Fukumitsu N, Ishii K, Kimura Y, Oda K, Sasaki T, Mori Y et al. Imaging of adenosine A1 receptors in the human brain by positron emission tomography with [11C]MPDX. *Ann Nucl Med* **2003**, *17(6)*, 511–515.

22. Logan J. Graphical analysis of PET data applied to reversible and irreversible tracers. *Nucl Med Biol* **2000**, *27(7)*, 661–670.
23. Kimura Y, Ishii K, Fukumitsu N, et al. Quantitative analysis of adenosine A₁ receptors in human brain using positron emission tomography and [1-methyl-¹¹C] 8-dicyclopropylmethyl-1-methyl-3-propylxanthine. *Nucl Med Biol* **2004**, *31*, 975–981.
24. Furuta R, Ishiwata K, Kiyosawa M, Ishii S, Saito N, Shimada J et al. Carbon-11-labeled KF15372: a potential central nervous system adenosine A₁ receptor ligand. *J Nucl Med* **1996**, *37(7)*, 1203–1207.
25. Elmenhorst D, Basheer R, McCarley RW, Bauer A. Sleep deprivation increases A₁ adenosine receptor density in the rat brain. *Brain Res.* **2009**, *1258*, 53–58.
26. Fozard JR, Milavec-Krizman M. Contraction of the rat isolated spleen mediated by adenosine A₁ receptor activation. *Br J Pharmacol* **1993**, *109(4)*, 1059–1063.
27. Fastbom J, Pazos A, Palacios JM. The distribution of adenosine A₁ receptors and 5'-nucleotidase in the brain of some commonly used experimental animals. *Neuroscience* **1987**, *22(3)*, 813–826.
28. Kanai Y, Araki T, Kato H, Kogure K. Autoradiographic distribution of neurotransmitter and second messenger system receptors in animal brains. *Behav Brain Res* **1994**, *65(1)*, 67–73.
29. Daval JL, Werck MC, Nehlig A, Pereira de Vasconcelos A. Quantitative autoradiographic study of the postnatal development of adenosine A₁ receptors and their coupling to G proteins in the rat brain. *Neuroscience* **1991**, *40(3)*, 841–851.
30. Choi DS, Cascini MG, Mailliard W, Young H, Paredes P, McMahan T et al. The type 1 equilibrative nucleoside transporter regulates ethanol intoxication and preference. *Nat Neurosci* **2004**, *7(8)*, 855–861.
31. King AE, Ackley MA, Cass CE, Young JD, Baldwin SA. Nucleoside transporters: from scavengers to novel therapeutic targets. *Trends Pharmacol Sci* **2006**, *27(8)*, 416–425.

32. Clark M, Dar MS. *In vitro* autoradiographic evidence for adenosine modulation of ethanol-induced motor disturbances in rats. *Alcohol Alcohol Suppl* **1991**, 1203–206.
33. Phan TA, Gray AM, Nyce JW. Intrastratial adenosine A₁ receptor antisense oligodeoxynucleotide blocks ethanol-induced motor incoordination. *Eur J Pharmacol* **1997**, 323(2–3), R5–R7.
34. Dar MS, Mustafa SJ. Acute ethanol/cannabinoid-induced ataxia and its antagonism by oral/systemic/intracerebellar A₁ adenosine receptor antisense in mice. *Brain Res* **2002**, 957(1), 53–60.
35. Connole L, Harkin A, Maginn M. Adenosine A₁ receptor blockade mimics caffeine's attenuation of ethanol-induced motor incoordination. *Basic Clin Pharmacol Toxicol* **2004**, 95(6), 299–304.
36. Thakkar MM, Engemann SC, Sharma R, Sahota P. Role of wake-promoting basal forebrain and adenosinergic mechanisms in sleep-promoting effects of ethanol. *Alcohol Clin Exp Res* **2010**, 34(6), 997–1005.
37. Kowaluk EA, Jarvis MF. Therapeutic potential of adenosine kinase inhibitors. *Expert Opin Investig Drugs* **2000**, 9(3), 551–564.
38. Noguchi J, Ishiwata K, Furuta R, Simada J, Kiyosawa M, Ishii S et al. Evaluation of carbon-11 labeled KF15372 and its ethyl and methyl derivatives as a potential CNS adenosine A₁ receptor ligand. *Nucl Med Biol* **1997**, 24(1), 53–59.
39. Jarvis MF, Becker HC. Single and repeated episodes of ethanol withdrawal increase adenosine A₁, but not A_{2A}, receptor density in mouse brain. *Brain Res* **1998**, 786(1–2), 80–88.
40. Daly JW, Shi D, Wong V, Nikodijevic O. Chronic effects of ethanol on central adenosine function of mice. *Brain Res* **1994**, 650(1), 153–15.



Summary

7

Adenosine is an endogenous ligand with several functions in the central nervous system (CNS), such as inhibition of neuronal activity in many signaling pathways. The adenosine receptor (AR) family consists of the A_1 , A_{2A} , A_{2B} and A_3 subtypes (A_1R , A_{2AR} , A_{2BR} and A_3R , respectively). A_1R and A_3R inhibit whereas A_{2AR} and A_{2BR} stimulate production of the secondary messenger, cAMP. Neuromodulator adenosine A_1 receptors (A_1R) stimulation may result in neuroprotection and suppression of neuroinflammation.

A_{2AR} s are a pharmacological target of potential interest because of their role in neurodegenerative and psychiatric disorders. Even though they mediate potential neuroprotective and neurotoxic effects, the pharmacology of A_{2AR} s and their role in neurodegenerative disorders is not fully understood. Preclinical and epidemiological studies suggest their potential role in PD, AD, neuroinflammation, ischemia, spinal cord injury and drug addiction.

Positron Emission Tomography (PET) is a noninvasive nuclear medicine imaging technique capable of measuring biochemical and physiological processes *in vivo* in a quantitative manner. The use of radiolabelled A_1R and A_{2AR} antagonists as PET tracers in healthy rats and in animal models of disease is the main subject of this thesis. Several ligands for PET imaging of A_1R and A_{2AR} have been prepared.

This thesis begins with a general introduction about adenosine, its role in health and disease, sources, regulation and fate of extracellular adenosine, a description of the principles of PET imaging, current radioligands for both A_1R s and A_{2AR} s and their detailed biological evaluation in rodents, nonhuman primates and humans (Chapter 1 & 2). Furthermore, potential lead structures for the development of new A_{2AR} antagonists and PET tracers were discussed (Chapter 2).

The first part of this thesis concerns the development of subtype-selective radioligands with high affinity for mapping cerebral A_{2AR} s. We aimed to develop PET probes for A_{2AR} s with larger striatum /

cerebellum ratios, better *in vivo* pharmacokinetic profile and higher absolute brain uptake than the previously reported ligands [^{11}C]SCH442416 or [^{18}F]FESCH ([^{18}F]fluoroethyl SCH442416).

Chapter 3 describes the selection, synthesis, radiolabelling, *in vitro* ARG and pre-clinical *in vivo* evaluation of two fluorinated $A_{2A}R$ ligands, [^{18}F]FPSCH ([^{18}F]fluoropropyl SCH442416) and [^{18}F]FESCH in healthy rats. Such ligands can provide logistic advantages over C-11 labeled tracers, and be distributed to remote centers without an expensive on-site cyclotron. A systematic comparison was made between these homologs of SCH442416 compound. A dynamic PET scan with arterial blood sampling was made in anesthetized healthy rats that were either vehicle-treated or pretreated with the $A_{2A}R$ antagonist KW6002. *Ex vivo* biodistribution analysis and *in vitro* autoradiography (ARG) were used to acquire information on the regional distribution of radioactivity. *In vitro* microsomal and *in vivo* plasma metabolite analyses were performed using ultra-high-performance liquid chromatography / quadrupole-time-of-flight-mass spectrometry and radio-TLC.

A retrosynthetic approach was adopted for the synthesis of nonradioactive fluorinated SCH442416 analogues. A two-pot, two-step radioactive synthesis could be used to prepare [^{18}F]FPSCH and [^{18}F]FESCH. $A_{2A}R$ -mediated accumulation of both tracers was observed in the rat brain. *In vitro* and *in vivo* metabolite analysis indicated the presence of hydrophilic radiometabolite(s) which are not expected to cross the blood-brain-barrier. Judged by similar target-to-nontarget ratios in *ex vivo* biodistribution analysis and microPET, both radiotracers performed equally well with slightly different kinetics. This study also suggested that lengthening of the fluoroalkyl chain (from methyl and ethyl groups to propyl group) do not result in impaired pharmacokinetics and metabolic stability of a SCH442416 analogue and thus provides a means to optimize the properties.

Chapter 4 explains the synthesis and preclinical evaluation of [^{11}C]preladenant as a potential PET tracer for imaging cerebral

A_{2A}Rs. Retrosynthetic approach was adopted to get the O-desmethyl precursor. [¹¹C]preladenant was developed as a new PET ligand for mapping cerebral adenosine A_{2A} receptors (A_{2A}Rs) in high specific activity and purity. Tracer tissue distribution was studied by PET, *ex vivo* biodistribution and *in vitro* autoradiography. All these studies suggested that [¹¹C]preladenant regional uptake was consistent with known A_{2A}Rs distribution, with highest uptake in striatum. Because of its high target (striatum)-to-nontarget (cerebellum) ratios in the rat brain, [¹¹C]preladenant exhibits suitable characteristics as a A_{2A}R PET tracer.

The second part of this thesis describes studies aiming to evaluate the potential of PET imaging for detecting and monitoring physiological and biochemical changes after different AR-related pharmacological challenges.

In chapter 5, we investigated whether transient opening of the blood-brain barrier after treatment of animals with (nonradioactive) adenosine A₁ and A_{2A} receptor agonists can be detected with hydrophilic radiotracers and PET. Such tracers do not pass the intact barrier, but may pass after BBB opening. For our initial pilot study, the CXCR₄ antagonist [¹¹C]CH₃-AMD3465 was exploited as a hydrophilic PET tracer. Cerebral uptake (SUV) and distribution volume (V_T) of this tracer were not increased after pretreatment of animals with the A₁R agonist CPA or the A_{2A}R agonist Rapiscan. Further studies are necessary to determine whether this negative finding is due to inappropriate kinetics of the used tracers or to lack of blood-brain barrier opening in anesthetized rats. Spectrophotometric analysis of brain extracts suggested no Evans blue leakage indicating BBB did not open during the time course of our PET study.

In chapter 6, we evaluated [¹¹C]-MPDX for visualization of A₁R in healthy rat brain. High and specific radioactivity uptake was noted in striatum, hippocampus, and cerebellum which corresponded closely to regional A₁R densities known from autoradiography. Raising extracellular adenosine levels [with a 20 % solution of ethanol in

saline (2 mL) and 1 mg of the adenosine kinase inhibitor 4-amino-5-(3-bromophenyl)-7-(6-morpholino-pyridin3-yl) pyrido [2,3-d] pyrimidine dihydrochloride (ABT-702)] did not result in measurable competition of adenosine with [¹¹C]-MPDX for binding to A₁R, but rather a globally increased cerebral binding of [¹¹C]-MPDX was noted (by 40 % to 45 %). Kinetic modeling suggested that this increase is not related to altered blood flow or altered blood-brain barrier passage of the radioligand, but rather to increased binding at the receptor level. Thus, competition of endogenous adenosine with [¹¹C]MPDX for binding to A₁R could not be detected.



Future Perspectives

8

Since potent [^{11}C]- and [^{18}F]-labelled $\text{A}_{2\text{A}}$ antagonists have been developed; several lines of research can be further pursued regarding cerebral $\text{A}_{2\text{A}}\text{R}$ imaging.

1. Preclinical evaluation of recently developed nonxanthine $\text{A}_{2\text{A}}\text{R}$ PET tracers.
 - a. Animal models of Parkinson's disease (including modulation of glutamatergic-adenosinergic function)
 - b. Animal models of Huntington's disease
 - c. Animal models of neuroinflammation
2. Human studies with established radioligands for $\text{A}_{2\text{A}}\text{R}$.
 - a. Multiple sclerosis
 - b. Parkinson's dementia
3. PET studies of $\text{A}_{2\text{A}}\text{R}$ occupancy by therapeutic drugs (drug discovery studies)

Evaluation of [^{11}C]SCH442416, [^{18}F]FESCH, [^{11}C]SCH420814 and [^{18}F]MNI444 in Various Animal Models

Preclinical studies with [^{11}C]SCH442416^{1,2} and [^{11}C]SCH420814 (our unpublished data) and their [^{18}F]fluoroethyl derivatives ([^{18}F]MRS5425 = [^{18}F]FESCH³ and [^{18}F]MNI-444⁴)¹⁻⁴ suggest their potential use for *in vivo* mapping of cerebral $\text{A}_{2\text{A}}\text{R}$ s. Because of preferable brain kinetics in the rat and monkey brain, [^{11}C]SCH442416 and [^{18}F]FESCH may be better tracers than [^{11}C]SCH420814 and [^{18}F]MNI444 (Human application of these tracers could be a potential problem because of their very slow tracer kinetics). However, it is too early to rule out [^{11}C]SCH420814 and [^{18}F]MNI444 and will require further evaluation in various animal models and human subjects before drawing any conclusions.

6-Hydroxydopamine Rat Model of PD (Including Modulation of Glutaminergic-Adenosinergic Function)

Tracer uptake can be examined in a rat model of PD (unilateral 6-hydroxydopamine lesion) to evaluate their ability to measure changes in receptor densities. Because of the larger size of their brains, rats are more suitable for microPET imaging than mice. The hydroxydopamine lesion results in selective losses of dopaminergic neurons located in the substantia nigra, in contrast to other animal models, which are less dopamine-specific. The neurotoxin 6-hydroxydopamine is injected into the striatum, using a stereotactic procedure. Injection of the toxic drug into the striatum leads to neuronal death in the substantia nigra after three to four days, via retrograde transport. This interval provides a time window for therapeutic interventions. The severity of the lesion can be tested by quantifying amphetamine-induced rotation behavior at 11 or 12 days after 6-OHDA injection.

After the behavioral test, animals can be scanned with a nonxanthine $A_{2A}R$ ligand. During this scan, blood samples are drawn from an arterial cannula to acquire an arterial input function. Regional distribution volume of the tracer in rat brain can be calculated from a Logan plot and also from a 2-tissue compartment model. After the scan, animals can be terminated and their brains isolated for *ex vivo* biodistribution and immunohistochemical analysis. Even though the 6-OHDA model is the most widely used animal model of Parkinson's disease, it lacks specific disease related properties such as progressive, age dependent effects and Lewy bodies of PD. Transgenic rat models (with mutations in the alpha-synuclein and LRRK₂ genes) could provide a research tool for studying processes like progressive loss / damage of dopaminergic neurons and formation of Lewy bodies.⁵ The best characterized tracer could be used to image $A_{2A}R$ changes in both the 6-OHDA and transgenic rat models for PD.

In PD, excessive glutaminergic outflow causes progressive degeneration of dopaminergic neurons. Synergistic interaction

between $A_{2A}R$ and metabotropic glutamate subtype 5 (mGlu5) takes place at striatal glutaminergic terminals where these receptors are co-localized. Both receptors act synergistically to increase dopamine- and cAMP-regulated phosphoprotein of 32kDa (DARPP-32). Simultaneous blockade of A_{2A} and mGlu5 receptors showed high efficacy in reversing PD symptoms in rodents.^{6, 7} Modulation of adenosinergic and metabotropic glutaminergic receptor function in a 6-OHDA rat model of PD could be studied by *in vivo* microPET imaging. PET tracers for $A_{2A}R$ and the nonradioactive highly selective mGlu5 receptor antagonist, 3-((2-Methyl-4-thiazolyl)ethynyl)pyridine (MTEP) can be used to study the impact of therapy on mGlu5 receptor and $A_{2A}R$ expression. In the study, an anti-mGlu5R antibody could be used in western blotting, immunohistochemical and immunocytochemical applications, to quantify mGlu5 receptor expression in tissue samples.

Quinolinic Acid or 3-Nitropropionic Acid Rat Model of Huntington's Disease

Huntington's disease (HD) is a progressive hereditary neurodegenerative disease caused by neuronal loss in the striatum and cortex, especially GABAergic medium spiny neurons. These changes result in motor (Chorea), cognitive and psychiatric abnormalities. Glutamate excitotoxicity and mitochondrial dysfunction have been suggested as factors triggering neurodegeneration in HD.⁸ Animal models of HD used were based on each of these problems. Intra-striatal injection of quinolinic acid (for glutamate excitotoxicity) or administration of 3-nitropropionic acid (3-NP, for mitochondrial dysfunction) resembles electrophysiological, histological, motor and other behavioral symptoms of human HD.⁹ Striatal expression of enkephalin and $A_{2A}R$ s was decreased even before motor symptoms appeared. Such specific changes could be related to a direct or indirect effect of mutated huntingtin on $A_{2A}R$ s, such as that seen in striatal cells overexpressing mutant protein.⁹

The brain uptake of radiolabeled $A_{2A}R$ ligands can be examined to assess changes of $A_{2A}R$ expression in rodent models of HD with microPET.

Neuroinflammation

Neuroinflammation, characterized by the presence of activated microglia and astrocytes, is an important feature of many neurological disorders like Parkinson, Alzheimer, and Huntington disease, multiple sclerosis and encephalitis as measured in the post-mortem brain and by noninvasive imaging methods.¹⁰ It has been suggested that stable levels of microglia activation in PD represent a marker of ongoing disease activity, activated microglia promoting disease progression. If true, measurements of activated microglia with PET could be used for monitoring of disease progression and the impact of therapeutic intervention.¹¹ If activated microglia cells are indeed a key factor in progression of PD, treatment with $A_{2A}R$ antagonists may reduce microglia activation and slow down the disease progression. In the human brain, upregulation of $A_{2A}R$ s may be related to suppression of neuroinflammation,¹² and neuroprotection. A recent article reported that higher cerebrospinal fluid levels of caffeine (a nonsubtype-selective AR antagonist) are associated with a more favorable outcome after severe traumatic brain injury.¹³ $A_{2A}R$ s are expressed not only on neurons but also on glia, where they play an important role in regulation of immune response by controlling neurotoxic and proinflammatory molecules, glial cell proliferation, and cAMP production.¹⁴

8

The herpes simplex virus neuroinflammation model of rodent encephalitis may be suitable for microPET studies of $A_{2A}R$ expression. This model could assess regional changes of the binding of $A_{2A}R$ PET ligands as a consequence of active virus and activated microglia.

Evaluation of Best Characterized Tracer in Human Studies

Besides the preclinical studies in rodents proposed above, PET studies in humans are required and could be focused on the role of $A_{2A}R$ in disorders of the brain. Till date, the only clinically applicable nonxanthine PET tracer for $A_{2A}R$ is [^{11}C]SCH442416. Other $A_{2A}R$ tracers have only been evaluated in rodents and nonhuman primates; promising results suggest their potential use for *in vivo* mapping of human cerebral $A_{2A}R$ s.

Multiple Sclerosis

$A_{2A}R$ densities appear to be altered in MS patients. Upregulation of $A_{2A}R$ in lymphocytes isolated from the blood of MS patients was noted.¹⁵ Recently, a study was published using the A_{2A} antagonist tracer [^{11}C]TMSX and Magnetic Resonance diffusion tensor imaging in 8 patients with secondary progressive multiple sclerosis (SPMS) and 7 healthy controls. Distribution volume (V_T) was significantly increased in the supraventricular normal-appearing white matter (NAWM) of MS patients as compared to controls. Ability of [^{11}C]TMSX-PET to detect the diffuse brain changes in NAWM could complement the conventional MRI, where diffuse alterations are more difficult to identify.¹⁵ Similar studies could be performed using the superior tracer [^{11}C]SCH442416 and be extended to other neurodegenerative diseases with an inflammatory component. This study may show that $A_{2A}R$ s are increased in the brain of SPMS patients, and that [^{11}C]SCH442416-PET provides a novel approach to learn about central nervous system pathology in SPMS *in vivo*.

Parkinson's Dementia

$A_{2A}R$ s, concentrated in the striatum, modulate dopaminergic activity and glutamate release in the brain. Adenosine activity through $A_{2A}R$ s can eventually give rise to neurotoxicity, neuronal damage and cell death.¹⁶ $A_{2A}R$ functioning is related to neurodegeneration in Parkinson's disease.¹⁷ PD patients with dementia show increased $A_{2A}R$ expression in hippocampus and cerebral cortex.¹⁸ In addition;

animal models indicate that blocking of $A_{2A}Rs$ was associated with prevention of memory impairments.¹⁹ On the basis of these considerations, cerebral $A_{2A}Rs$ in Parkinson's dementia patients could be examined with PET, using the best characterized tracer of the moment. Key objectives of the proposed research could be:

1. Are there any differences in uptake of radioactivity after injection of an $A_{2A}R$ tracer between Parkinson patients with dementia as compared to PD patients without dementia or aged-matched healthy volunteers?
2. Are changes of $A_{2A}Rs$ related to cognitive or memory performance in the mentioned subject groups?

Cognitive testing can be performed to evaluate the relationship between $A_{2A}Rs$ expression and cognitive function in Parkinson's patients. [^{11}C]SCH442416, [^{11}C]SCH420814 or [^{18}F]MNI444 could be employed to gain a better understanding of the involvement of $A_{2A}Rs$ in PD and PD-associated dementia.

PET Studies of $A_{2A}R$ Occupancy by Therapeutic Drugs

Dose-dependent occupancy of $A_{2A}Rs$ by nonradioactive $A_{2A}R$ antagonists can be assessed in the brain of rhesus monkeys or humans using [^{11}C]SCH442416 and PET, in order to correlate receptor occupancy and therapeutic effect. If a drug crosses the BBB and displaces receptor-bound [^{11}C]SCH442416 in a dose-dependent fashion then we can estimate the receptor occupancy of a drug in the brain. [^{11}C]SCH442416 might be an excellent tool for measurement of the $A_{2A}R$ occupancy of various drugs (both xanthines and nonxanthines) and hence aid in the drug discovery process.

References

1. Todde, S.; Moresco, R. M.; Simonelli, P.; Baraldi, P. G.; Cacciari, B.; Spalluto, G.; Varani, K.; Monopoli, A.; Matarrese, M.; Carpinelli, A.; Magni, F.; Kienle, M. G.; Fazio, F. Design, radiosynthesis, and biodistribution of a new potent and selective ligand for *in vivo* imaging of the adenosine A_{2A} receptor system using positron emission tomography. *J. Med. Chem.* **2000**, *43*, 4359–4362.
2. Moresco, R. M.; Todde, S.; Belloli, S.; Simonelli, P.; Panzacchi, A.; Rigamonti, M.; Galli-Kienle, M.; Fazio, F. *In vivo* imaging of adenosine A_{2A} receptors in rat and primate brain using [¹¹C]SCH442416. *Eur. J. Nucl. Med. Mol. Imaging* **2005**, *32*, 405–413.
3. Bhattacharjee, A. K.; Lang, L.; Jacobson, O.; Shinkre, B.; Ma, Y.; Niu, G.; Trenkle, W. C.; Jacobson, K. A.; Chen, X.; Kiesewetter, D. O. Striatal adenosine A_{2A} receptor-mediated positron emission tomographic imaging in 6-hydroxydopamine-lesioned rats using [(¹⁸F)]-MRS5425. *Nucl. Med. Biol.* **2011**, *38*, 897–906.
4. Barret, O.; Hannestad, J.; Alagille, D.; Vala, C.; Tavares, A.; Papin, C.; Morley, T.; Fowles, K.; Lee, H.; Seibyl, J.; Tytgat, D.; Laruelle, M.; Tamagnan, G. Adenosine 2A Receptor Occupancy by Tozadenant and Preladenant in Rhesus Monkeys. *J. Nucl. Med.* **2014**, jnumed.114.142067 published ahead of print July 31, 2014 (10.2967/jnumed.114.142067).
5. Blandini, F.; Armentero, M. Animal models of Parkinson's disease. *FEBS Journal* **2012**, *279*, 1156–1166.
6. Coccurello, R.; Breyse, N.; Amalric, M. Simultaneous blockade of adenosine A_{2A} and metabotropic glutamate mGlu₅ receptors increase their efficacy in reversing Parkinsonian deficits in rats. *Neuropsychopharmacology* **2004**, *29*, 1451–1461.
7. Kachroo, A.; Orlando, L. R.; Grandy, D. K.; Chen, J. F.; Young, A. B.; Schwarzschild, M. A. Interactions between metabotropic

- glutamate 5 and adenosine A2A receptors in normal and parkinsonian mice. *J. Neurosci.* **2005**, *25*, 10414–10419.
8. Damiano, M.; Galvan, L.; Déglon, N.; Brouillet, E. Mitochondria in Huntington's disease. *Biochimica et Biophysica Acta (BBA) - Molecular Basis of Disease* **2010**, *1802*, 52-61.
 9. Blum, D.; Hourez, R.; Galas, M. C.; Popoli, P.; Schiffmann, S. N. Adenosine receptors and Huntington's disease: implications for pathogenesis and therapeutics. *Lancet Neurol.* **2003**, *2*, 366–374.
 10. Doorduyn, J. Herpes viruses and neuroinflammation: PET imaging and implication in schizophrenia, University Medical Center, University of Groningen, Groningen, 2010.
 11. Doorduyn, J.; de Vries, E. F.; Dierckx, R. A.; Klein, H. C. PET imaging of the peripheral benzodiazepine receptor: monitoring disease progression and therapy response in neurodegenerative disorders. *Curr. Pharm. Des.* **2008**, *14*, 3297–3315.
 12. Rebola, N.; Simoes, A. P.; Canas, P. M.; Tome, A. R.; Andrade, G. M.; Barry, C. E.; Agostinho, P. M.; Lynch, M. A.; Cunha, R. A. Adenosine A2A receptors control neuroinflammation and consequent hippocampal neuronal dysfunction. *J. Neurochem.* **2011**, *117*, 100–111.
 13. Sachse, K. T.; Jackson, E. K.; Wisniewski, S. R.; Gillespie, D. G.; Puccio, A. M.; Clark, R. S. B.; Dixon, C. E.; Kochanek, P. M. Increases in cerebrospinal fluid caffeine concentration are associated with favorable outcome after severe traumatic brain injury in humans. *J. Cereb. Blood Flow Metab.* **2007**, *28*, 395–401.
 14. Nakajima, K.; Kohsaka, S. Microglia: neuroprotective and neurotrophic cells in the central nervous system. *Curr. Drug Targets Cardiovasc. Haematol. Disord.* **2004**, *4*, 65–84.
 15. Rissanen, E.; Virta, J. R.; Paavilainen, T.; Tuisku, J.; Helin, S.; Luoto, P.; Parkkola, R.; Rinne, J. O.; Airas, L. Adenosine A2A receptors in secondary progressive multiple sclerosis: a [¹¹C]TMSX brain PET study. *J. Cereb. Blood Flow Metab.* **2013**, *33*, 1394–1401.

16. de Mendonca, A.; Sebastiao, A. M.; Ribeiro, J. A. Adenosine: does it have a neuroprotective role after all? *Brain Res. Brain Res. Rev.* **2000**, *33*, 258–274.
17. Barrachina, M.; Mairena Martan; Ciruela, F.; Ferrer, I. Epigenetic Modulation of Adenosine A2A Receptor: A Putative Therapeutical Tool for the Treatment of Parkinson's Disease. In 2011.
18. Angulo, E.; Casado, V.; Mallol, J.; Canela, E. I.; Vinals, F.; Ferrer, I.; Lluís, C.; Franco, R. A1 adenosine receptors accumulate in neurodegenerative structures in Alzheimer disease and mediate both amyloid precursor protein processing and tau phosphorylation and translocation. *Brain Pathol.* **2003**, *13*, 440–451.
19. Canas, P. M.; Porciuncula, L. O.; Cunha, G. M.; Silva, C. G.; Machado, N. J.; Oliveira, J. M.; Oliveira, C. R.; Cunha, R. A. Adenosine A2A receptor blockade prevents synaptotoxicity and memory dysfunction caused by beta-amyloid peptides via p38 mitogen-activated protein kinase pathway. *J. Neurosci.* **2009**, *29*, 14741–14751.



Samenvatting

9

Adenosine is een endogeen ligand met verschillende functies binnen het centraal zenuwstelsel, zoals remming van neuronale activiteit in vele signaaltransductieroutes. De adenosine receptor (AR) familie bestaat uit A_1 , A_{2A} , A_{2B} en A_3 subtypes (A_1R , A_{2AR} , A_{2BR} en A_3R). A_1R en A_3R remmen de productie van de second messenger cAMP terwijl A_{2AR} en A_{2BR} deze productie juist stimuleren. Stimulering van de adenosine A_1 receptoren (A_1R) kunnen resulteren in neuroprotectie en onderdrukking van neuroinflammatie.

A_{2AR} s zijn vanuit farmacologisch gezichtpunt interessant vanwege de rol in neurodegeneratieve en psychiatrische ziekten. Hoewel ze neuroprotectieve en neurotoxische effecten beïnvloeden, zijn veel zaken met betrekking tot de farmacologie van A_{2AR} s en hun rol in neurodegeneratieve ziekten nog niet goed onderzocht. Preklinische en epidemiologische studies geven aan dat A_{2AR} s mogelijk een rol spelen in de ziekten van Parkinson, Alzheimer, neuroinflammatie, ischemie, dwarslaesies en verslaving aan medicijnen.

Positron Emissie Tomografie (PET) is een niet-invasieve nucleair geneeskundige afbeeldingstechniek die in staat is om biochemische en fysiologische processen *in vivo* te meten op kwantitatieve wijze. Het gebruik van radioactief gemerkte A_1R en A_{2AR} antagonisten als PET-radioliganden in gezonde ratten en in dieren met een bepaalde ziekte is het onderwerp van dit proefschrift. Verschillende liganden voor het afbeelden van A_1R en A_{2AR} met behulp van PET zijn onderzocht.

Het proefschrift begint met een algemene inleiding over adenosine, en de rol onder normale omstandigheden en bij ziektes, over de regulering van extracellulair adenosine, een beschrijving van de principes van PET, reeds gebruikte radioliganden voor A_1R s en A_{2AR} s en hun biologische evaluatie in knaagdieren, primaten en de mens (Hoofdstuk 1 & 2). Verder worden mogelijke nieuwe chemische structuren voorgesteld voor de ontwikkeling van nieuwe A_{2AR} antagonisten en PET radioliganden (Hoofdstuk 2).

Het eerste deel van dit proefschrift houdt zich bezig met de ontwikkeling van subtype-selectieve radioliganden met hoge affiniteit om $A_{2A}R$ s in de hersenen af te beelden. Ons doel was om PET-radioliganden voor $A_{2A}R$ s te ontwikkelen om hogere striatum / cerebellum ratios, een betere *in vivo* farmacokinetisch profiel en een hogere absolute hersenopname te bereiken dan de reeds beschreven radioliganden [^{11}C]SCH442416 of [^{18}F]FESCH ([^{18}F]fluorethyl SCH442416).

Hoofdstuk 3 beschrijft de selectie, synthese, radiolabelling, *in vitro* autoradiografie en preklinische *in vivo* evaluatie van twee gefluorineerde $A_{2A}R$ liganden, [^{18}F]FPSCH ([^{18}F]fluorpropyl SCH442416) en [^{18}F]FESCH in gezonde ratten. Deze liganden hebben logistieke voordelen ten opzichte van C-11 gemerkte radioliganden, en kunnen getransporteerd worden naar ziekenhuizen die niet in het bezit zijn van een duur cyclotron. Een systematische vergelijking tussen deze twee homologen van SCH442416 is uitgevoerd. Een dynamische PET studie is beschreven waarbij ook arterieel bloed werd geanalyseerd bij gezonde ratten. Naast een controle groep werd een andere groep voorbehandeld met de $A_{2A}R$ antagonist KW6002. *Ex vivo* biodistributie studies en *in vitro* autoradiografie (ARG) werden gebruikt om informatie te krijgen over de regionale verdeling van de radioactiviteit in de hersenen. Analyse van metabolieten met microsomen (*in vitro*) en in plasma (*in vivo*) werd uitgevoerd met behulp van de zogenaamde ultra-high-performance vloeistof chromatografie / quadrupole-time-of-flight-mass spectrometry en radio-TLC.

9

Een retrosynthetische benadering werd gekozen voor de bereiding van gefluorineerde SCH442416 analogen. The radioactive labeling van [^{18}F]FPSCH en [^{18}F]FESCH werd gedaan in twee reactiestappen. De opname van beide radioliganden in het rattenbrein weerspiegelde de aanwezigheid van $A_{2A}R$. Resultaten van *in vitro* en *in vivo* metabolieten analyse wezen op de aanwezigheid van een of meerdere hydrofiele radiometabolieten die waarschijnlijk niet de bloed-hersen-barriere (BHB) passeren. Afgaande op vergelijkbare

target-to-non-target ratios gevonden bij de *ex vivo* biodistributie en microPET, presteren beide radioliganden even goed waarbij kleine verschillen werden gevonden in de kinetiek. Uit deze studie werd ook duidelijk dat verlenging van de fluoralkyl keten (van methyl en ethyl naar propyl groep) geen nadelig effect heeft op de farmacokinetiek en metabole stabiliteit van de SCH442416 analoga en daardoor mogelijkheden biedt om eigenschappen van deze radioliganden te optimaliseren.

In hoofdstuk 4 wordt de synthese en preklinische evaluatie beschreven van [¹¹C]preladienant als mogelijke PET tracer het afbeelden van A_{2A}Rs in de hersenen. Er werd opnieuw gekozen voor een retrosynthetische aanpak om de O-desmethyl precursor te maken. [¹¹C]Preladienant werd verkregen met hoge specifieke activiteit en zuiverheid. De regionale verdeling van het radioligand werd bestudeerd met PET, *ex vivo* biodistributie en *in vitro* autoradiografie. Al deze studies geven aan dat de regionale opname van [¹¹C]preladienant goed overeen kwam met de verdeling van A_{2A}Rs zoals die bekend is in de literatuur. Vanwege de hoge striatum-cerebellum ratio in het rattebrein kan geconcludeerd worden dat [¹¹C]preladienant een geschikte radioligand kan zijn om A_{2A}R met PET te meten.

In het tweede deel van dit proefschrift worden studies beschreven om de mogelijkheden te onderzoeken of met PET fysiologische en biochemische veranderingen kunnen worden gemeten door AR farmacologisch te beïnvloeden.

In hoofdstuk 5 onderzochten we of de tijdelijke opening van de BHB door middel van behandeling niet-radioactieve adenosine A₁ and A_{2A} receptor agonisten kon worden gemeten door gebruik te maken van hydrofiele PET-radioliganden. Hydrofiele liganden passeren normaliter niet de BHB maar zouden dit wel kunnen bij tijdelijke opening van de BHB. In deze verkennende studie werd de CXCR₄ antagonist [¹¹C]CH₃-AMD3465 gebruikt als hydrofiel PET-radioligand. De opname in de hersenen en het distributie volume (V_T) van dit radioligand nam echter niet toe na behandeling van de

ratten met de A₁R agonist CPA of de A_{2A}R agonist Rapiscan. Meer studies zijn nodig om te bepalen of dit negatieve resultaat te wijten is aan de farmacokinetische eigenschappen van de PET-radioligand of dat de opening van de BHB onvoldoende is geweest. Spectrofotometrische analyse van de kleurstof Evans Blue hersenextracten gaven aan dat de BHB niet geopend was tijdens de PET studie.

In hoofdstuk 6 onderzochten we of [¹¹C]-MPDX geschikt is om A₁R in het rattenbrein af te beelden. De opname van radioactiviteit was hoog en receptor-specifiek in striatum, hippocampus, en cerebellum. Deze hersengebieden hebben relatief hoge expressie van A₁R zoals is bepaald met ARG. Wij lieten ook de concentratie van extracellulair adenosine toenemen [door middel van toediening van 20 % oplossing van ethanol in fysiologisch zout (2 mL) met 1 mg van de adenosine kinase inhibitor 4-amino-5-(3-bromophenyl)-7-(6-morpholino-pyridin3-yl) pyrido [2,3-d] pyrimidine dihydrochloride (ABT-702)]. Wij waren echter niet in staat om competitie van deze toegenomen concentratie van adenosine met [¹¹C]-MPDX voor binding aan A₁R te meten. Er werd juist een toename van binding van [¹¹C]-MPDX (40 % to 45 %) in de hersenen gemeten. Kinetische analyse resultaten lieten zien dat deze toename niet het gevolg was van een veranderde doorbloeding of BHB-passage maar wel van verhoogde binding aan de receptor.



Acknowledgements

The satisfaction and euphoria that accompany the successful completion of any task would be incomplete without hard work and mentioning the people who make it possible, whose constant guidance, help, support and encouragement serve as a beam of light and crown my efforts with success.

First and foremost, I offer my earnest and heartfelt gratitude to my primary promoter and supervisor, **Prof. Philip Elsinga**, head of radiochemistry, Department of Nuclear Medicine and Molecular Imaging, UMC, Groningen. Philip, your tolerance in every step, keen interest, regular observations, kind co-operation, boundless enthusiasm, encouragement, stimulative and constructive criticism throughout this work has brought up this dissertation work into its current shape. You helped to me realize radiochemistry easy. You encouraged me to come up with my own solutions and gave me enough independence to be a responsible researcher while on the other hand you were very helpful with many things. Your way of supervision kept my motivation high for the whole period of my PhD project. Further, I am also grateful to you for your generous help with the Dutch summary of this thesis. Words fail to express my real feeling regarding your cool attitude at hard times.

It is indeed great pleasure to express my deep sense of gratitude and humble thanks to my co-promoter **Dr. Aren van Waarde**. Aren, your support, criticism, motivation, guidance and unflinching encouragements were instrumental towards the completion of this thesis. You have been a delightful source of knowledge for me by sending me all news in the field of adenosine receptors and lending me a hand in the in vivo studies of this thesis. I am deeply thankful to you for the hours you spent on reading, discussing and correcting my manuscripts and this thesis. Apart from research, personally I feel that you take care of your students like a guardian who imbibes positive thinking. I could always knock your door without prior appointments and get instant solutions for my queries.

It would be untruthful on my part if I fail to thank my second promoter **Prof. Rudi Dierckx**, Head of the Department on Nuclear Medicine and

Molecular imaging, for providing me with an opportunity to work in a multinational and stimulating environment. My sincere acknowledgment for your suggestions and help during these years.

I would also extend my acknowledgments to **Dr. Erik de Vries**. Erik, thank you for every single suggestion, comment and question raised on our [^{11}C]Preladenant paper and on Monday morning meetings that helped me to be more critical towards my project and for being available every time when I needed your help.

I would also like to thank members of the reading committee **Prof. Filip de Vos**, **Prof. Jan Booij** and **Prof. K.L. Leenders**, for their willingness to read and approve this thesis.

My gratitude continues to **Dr. Gert Luurtsema** and **Marianne Schepers** for their fruitful collaboration on the liver microsomal metabolite and MS analyses. I would like to express my thanks to **Dr. Michel Koole**, for his association with my Journal of Medicinal Chemistry paper and forthcoming pharmacokinetic modelling paper. I also thank **Dr. Janine Doorduyn** for her kind support and help. I would also like to thank **Dr. Prabha Garg** and **Anup Shah** (Computer Center, NIPER, Mohali, India) for their fruitful collaboration over the years. We could easily observe that our collaborative data really added value to the chapter 3 of this thesis.

Dear **Chantal Kwizera** and **Tushar Tomar**, thank you very much for being my paranymphs. Chantal, you are so kind, very helpful, wonderful teacher and colleague in the lab. Words cannot express all my gratitude to you. Tushar, you were my great house-mate. Thanks for your help, support and nice chats.

I also thank **Klaas-Willem Sietsma**, **Remko Koning**, **Hans Pol**, **Hilde, Janet, Jitze Medema**, **Handrikus**, **Johan R. de Jong**, **Antoon T.M. Willemsen**, **Michel** and **Rolf Zijlma**, for the friendly banter and all your invaluable technical help. My special thanks goes to **Bram Mass** and **Jurgen Sijbesma**. Bram, you are an ideal human being and a good friend. Thanks for your technical assistance, support and nice

conversations. Thanks to Jurgen, for his help in the *in vivo* studies that are part of this thesis. Jurgen, you are one of the most helpful people in NGMB. Thanks for teaching surgical and injection techniques and for helping with the set up for the animal experiment.

It's my pleasure to thank the help provided by **Annie van Zanten**, and **Annegrit Wijker** with regard to solving financial problems during my PhD period. **Sarita**, I would like to thank you for solving administrative issues and making all the arrangements in the PhD defense process.

I would like to thank GUIDE, especially, **Riekje, Mathilde** and **Maaike** for their great assistance with all the papers, organizing my extension and for the financial support to attend conferences.

I gratefully acknowledge all the people from the central animal facility (CDP) for their help and advices. A special mention goes to **Miriam, Annemieke** and **Michel**.

I am very much gratified by the broad base of support and help that I received from my fellow colleagues at NGMB. Thanks to **Ines, Anna, David, Daniele, Zilin, Nathalie, Merhsima, Anniek, Heli, Alex, Ewelina, Reza, Nisha, Andrea** and many others. I would like to express my special thanks to friends and colleagues of "Adenosine Team" (**Soumen Paul, Xiaoyun Zhou, and Anja Huizing**). You people made my stay at department more enjoyable and memorable. I am extremely thankful to all my colleagues in the room LM 64.00.04 for making it the loudest, noisiest and funniest room on LM floor. A special mention goes to **Khayum, William Jan Kuik, Vladimir** and **Soumen Paul**. I had a nice conversation on football World Cup 2014 matches and various other interesting topics with **Reind Hoekman, Carlos Amaro, Bas Schipanboord** and of course with Khayum.

Mohammad Abdul Khayum, thanks for your "ever ready to help" attitude and great discussions. **Siddu**, I will never forget all the instants, experiments, days and nights in the lab together as well as the fun we shared. Thanks for your help, your understanding and our interesting debates and meetings.

Outside the lab, I know a big Indian community, which made my stay in Groningen more memorable and pleasant one with different festival celebrations, dance nights, dinners and nice trips. My special thanks go to **Shodan-Chaitanya, Suresh Vatakuti, Tushar-Jasmine, Laxmi Krishnappa, Gaurav-Neha Malviya, Pramod-Meena, Ganesh ram-Subha, Raaj-shirisha, Akshay-Spoorthi, Rajender Baddam-Shilpa, Rajasunath Gondi-Sai Sree, Kiran Katta-Shruthi, Gaurav Kanojia, Vikram Rao Bollineni, Yamini, Gopi Krishnan, Aditya Gottumukkala, Ashoka Vardhana Reddy, Kushi, Rama Kataria, Shivakumar Giriya-pura, Gopi, Sasanka-Divya, Venkatesh-Nisha, Sunil-Smitha, Jai-Ruchi, Prabhat-Aashita, Soumen-Soutri, Goutham Tinku, Pranov, Praneeth, Justin Joseph, Milon Mondal, Milind Pore, Sai Sreekanth, Sanjeev Kumar, Sarita Adepu, Vineet Mahajan, Eswar Reddy, Appu Venkat, Kiran Matcha, Pravin Patil, Suresh babu** and many others. My gratitude continues to **ZICS** and **GCC** members. I would like to thank **Hedy Vrakking, Frans, Chaitanya Shodan** and **Siddesh** for attending my wedding at Sirwar, Karnataka, India.

I never missed my family while I was in Netherlands, thanks to you, **Vinod uncle, Meena Aunty, Vinesh, Nawina, Vinay, Frans, Hedy Vrakking, Hans Van Seventer, Joann van Seventer-Keltie, Shivashankar-Rashmi Hemberal**. You all are really my family in Netherlands.

I would also extend my gratitude to all my International friends including Pakistani and Bangladeshi friends. A special mention goes to **Muhammad Shafique, Afsal, Sulman, Atta Ur Rehman, Ali, Hasan Mahmud Rana-Mithila** and **Aatique**.

It is indeed great pleasure to express my deep sense of gratitude and humble thanks to my beloved teachers **Dr. R.H. Udipi, Dr. K.M.K. Swamy** and **N. Srinivasulu**, Raichur, India. I am very grateful to each of you for your guidance, love, contribution, suggestions, and every single word you said to me. You are all a real source of inspiration! I happily acknowledge my friends in India **Manoj Kumar Yadava, Bhagya, Pradeep Narayanaswamy, Umashankar, Veeresh Babu, Sawan**

Kumar, Shakeer, H.K. Mallikarjun, Sarvagna, Vahid and all my other friends who have always been with me in my happiness, sorrow and excitements. I thank them all. A special mention goes to **Manoj** and **Shivakrishna** for making aesthetic graphics for the cover page. Manoj-Bhagya, Pradeep, Umashankar you have always been there when I needed you most and all of you have supported and motivated me.

It will be less how much ever I try to express my feelings towards my **late grandfather and grandmother, parents, brothers, sisters** and **all my family members**. It is not fair to thank them but I can only seek their valuable love, affection and support throughout my life, which I think will lead me to my destiny. My most important acknowledgement is to my brother-in laws, **Basavaraj Turukundoni** and **Shivaputra Hosamani**. Special thanks are due to my **in-laws** for their love and for accepting me as their son-in-law. Lastly, and most importantly, I wish to thank my best-half, **Ananya**. Thanks for your understanding, endless love and for being my strength and happiness during my journey of PhD. It is indeed a difficult task to acknowledge the services of all those who have extended their valuable assistance directly or indirectly. I would like to sincerely thank all of them.

Shivashankar Khanapur

